Novel group 13 reagents for the activation of small molecules

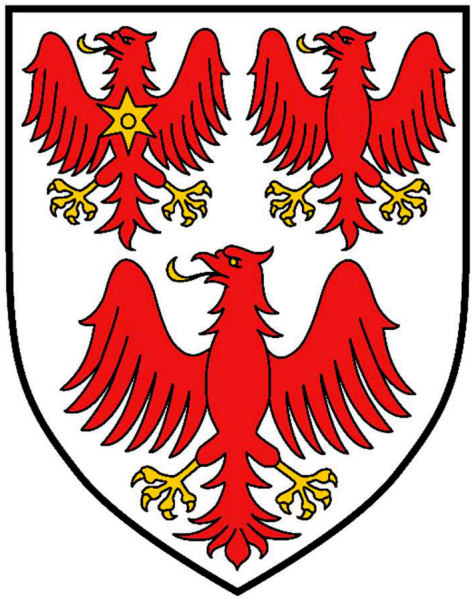

Andreas Heilmann

The Queen's College, Oxford

A thesis submitted in partial fulfilment of the requirements for the degree of Doctor of Philosophy

January 2023

Acknowledgements

I am immensely grateful to Prof. Simon Aldridge for his never-ending support and encouragement over the last eight years. As an undergrad he introduced me to the wonderful world of main group chemistry, and his insights and enthusiasm for the field have shaped me as a chemist. I was very fortunate to have had the opportunity to join his lab as a project student, and later as a Part II and DPhil. His dedicated supervision throughout all this time has been a major factor in ultimately making this thesis a success. I am particularly grateful for having learned his approach to problem solving, which to me is an invaluable life-skill.

I would also like to thank Prof. Jose Goicoechea for his encouragement and sustained interest throughout this project.

During my time as a Part II and DPhil student I have had the pleasure to work with many brilliant people in the Aldridge group, all of which have made my time there very enjoyable. A special thank you goes to all those who have contributed directly to this thesis. A massive thank you goes to Agamemnon Crumpton, who has spent many hours calculating unsusal reaction mechanism for this project, teaching me DFT, and has been a great friend inside and outside the lab. A massive thank you also goes to Dr. Jamie Hicks for supervising me as a Part II student and at the beginning of my DPhil, for teaching me how to do research successfully, for solving and teaching me how to solve crystal structures, and for his efforts to make this project a success. Another big thank you goes to Dr. Petra Vasko for teaching me the rigorous way of doing things and calculating several reaction mechanisms. I also want to thank Dr. Matthew Roy and Liam Griffin for collaborating on the CO homologation project, and my Part II student Artemis Saddington for laying the foundations of the gallium imide chemistry. Major thanks are owed to Dr. Alexa Caise and Xiongfei Zheng for many helpful discussions. Furthermore, I would like to thank all remaining members of the Aldridge group past and present, Dr. Anna Booth, Dr. Huan Do, Dr. Yin Kai Loh, Dr. Mathias Ellwanger, Dr. Josef Boronski, Dr. Malte

Fischer, Dr. Caitilin McManus, Dr. Andrey Protchenko, Dr. Marcel Schropp, Simon Thölke, Aisling Roper, Lewis Wales, and all others, for providing a stimulating work environment. In addition I would like to thank the members of the Goicoechea group, especially Dr. Oliver Townrow, for helpful discussions.

Thanks are also owed to Dr. Amber Thompson and Dr. Kirsten Christensen for help diagnosing weird crystallography problems, enabling me work at the diamond light source, and helping me collect good data on precious crystals despite nearly burnt out X-ray tubes. Furthermore, thanks are owed to the NMR service.

Finally I would like to thank my friend Dr. Natasha Smith, my brother Leonard and my parents for encouraging me throughout this project and keeping me sane.

Abstract

This thesis examines the activation of small molecules by aluminyl compounds, as well as by aluminium imides, derived from them, and related gallium compounds.

Chapter 3 details the reactions of nucleophilic aluminyl and gallyl reagents, K_2[**NON**M]$_2$ (M = Al, Ga; **NON** = 4,5-bis(2,6-diisopropylanilido)-2,7-di-tert-butyl-9,9-dimethyl-xanthene) with a range of organoazides. Depending on steric bulk, reaction with one or two equivalents per metal centre is observed, affording terminal metal imides or metallo-tetrazenes respectively. These imides are shown to be highly reactive species, as exemplified by their reactions with H_2, solvent molecules (such as toluene or THF) or intramolecular C(sp^3)–H bonds.

Chapter 4 describes the reactivity of the aluminium imide K_2[**NON**Al(NDipp)]$_2$ (Dipp = 2,6-^{i}Pr$_2$C$_6$H$_3$) towards a range of unsaturated oxygen-containing substrates. The reaction of this imide with CO_2 yields DippNCO and the carbonate complex K_2[**NON**Al(CO_3)]$_2$ under dilute conditions. The reaction with N_2O yields DippN_3 and the *cis*-hyponitrite complex K_2[**NON**Al(ONNO)]$_2$, while the reaction with benzaldehyde leads to the formation of the hemi-aminal complex K[**NON**AlN(Dipp)OCHPh]; subsequent reaction with CO_2 then leads to the liberation of the imine PhCHNDipp and K_2[**NON**Al(CO_3)]$_2$. Thus, it is demonstrated that K_2[**NON**Al(NDipp)]$_2$ can act as a transfer reagent for the $[NDipp]^{2-}$ fragment. Experimental and computational investigations reveal that these reactions likely proceed via a series of cycloaddition and cycloreversion reactions, and that depending on conditions alternative products may be obtained.

Chapter 5 details the reactions of a range of group 13 imides with CO, as well as the reactions of boryl- and silyl- substituted group 13 imides with N_2O. The reaction of K_2[**NON**Al(NDipp)]$_2$ with CO leads to the uptake of two molecules of CO and affords K_2[**NON**Al{C(=NDipp)CO_2}]$_2$, a product that is derived via a combination of C–O bond cleavage and C–C bond formation steps. The analogous reactions with silyl- or boryl-

substituted imides instead lead to the formation of heterocarboxylate-cyanide complexes, K_2[**NON**M(O_2CR)(CN)]$_2$, or siloxy-cyanide complexes, K_2[**NON**M($OSiR_3$)(CN)]$_2$, depending on the nature of the group 13 metal and the imido substituent. Heteroatom substituted aluminium imides react readily with N_2O affording the corresponding organoazides and the aluminium hyponitrite complex K_2[**NON**Al(ONNO)]$_2$. K[**NON**Ga($NSiPh_3$)] however reacts only slowly with N_2O at elevated temperatures, ultimately leading to the formation of siloxy-azide complex K[**NON**Ga($OSiPh_3$)(N_3)]. Thus, the heteroatom substituted group 13 imides act either as a source of a $[NR]^{2-}$, as in the conversion of N_2O to RN_3, or as a source of the nitride ion, $[N]^{3-}$, facilitating the conversion of CO to $[CN]^-$.

Chapter 6 describes the reactivity of aluminyl reagents towards CO. The four-electron reduction of CO affords compounds featuring topologically linear $[C_4O_4]^{4-}$ chains, which can undergo selective chain growth to afford a branched $[C_6O_6]^{4-}$ chain, thus demonstrating solution state chain branching via C–O cleavage for the first time. Thermal isomerisation of the $[C_4O_4]^{4-}$ fragment can be observed at elevated temperatures in the presence of additional potassium ions. Under more reducing conditions a compound featuring a linear $[C_4O_4]^{6-}$ fragment can be obtained, while a salt metathesis reaction allows access to a compound featuring a cyclic $[C_4O_4]^{2-}$ unit. The mechanism for CO homologation proceeds via initial coordination of CO, followed by C–C coupling and carbene dimerisation. In the initial coordination complexes, CO primarily acts as a Z type ligand, reflecting the highly electron-rich nature of the aluminyl reagents.

Abbreviations

Throughout this thesis the following abbreviations will be used:

Ar	–	aryl
br	–	broad
cAAC	–	cyclic alkyl amino carbene
calc.	–	calculated
COT	–	1,3,5,7-cyclooctatetraene
Cp*	–	pentamethylcyclopentadienyl
Cp^{3t}	–	tri-tert-butylcyclopentadienyl
crypt	–	2.2.2-cryptand
d	–	doublet
DFT	–	density functional theory
Dipp	–	2,6-di-iso-propylphenyl
equiv.	–	equivalents
Et	–	ethyl
FLP	–	frustrated Lewis pair
HOMO	–	highest occupied molecular orbital
^{i}Pr	–	iso-propyl
IR	–	infra red
$^{n}J_{XY}$	–	coupling constant
L	–	general ligand
LUMO	–	lowest unoccupied molecular orbital
m	–	meta
m	–	multiplet
MAO	–	methylaluminoxane
Me	–	methyl
Mes	–	2,4,6-trimethylphenyl
NHC	–	*N*-heterocyclic carbene
NMR	–	nuclear magnetic resonance
NON	–	4,5-bis(2,6-diisopropylanilido)-2,7-di-tert-butyl-9,9-dimethylxanthene
o	–	ortho
OTf	–	triflate
p	–	para
Ph	–	phenyl
ppm	–	parts per million
q	–	quartet
s	–	singlet
t	–	triplet
^{t}Bu	–	tert-butyl
THF	–	tetrahydrofuran
Trip	–	2,4,6-tri-iso-propylphenyl
X	–	general anion

Table of Contents

Chapter 1. Introduction

1.1 Main group chemistry

Over the last quarter of the twentieth century our understanding of heavier main group compounds has been majorly advanced, and today main group chemistry is a thriving field of research. It was long believed that the chemistry of main group elements was confined to only one or two stable oxidation states, and the so-called double bond rule further stated that no multiple bonding involving the heavier *p*-block elements was possible.[1] The isolation of Lappert's stannylene,[2] West's disilene,[3] and Yoshifuji's diphosphene,[4] were major break-troughs and challenged these notions. Since then, a large number of low oxidation state main group compounds have been isolated, using bulky ligands to stabilise such species kinetically. Furthermore, it has been realised that many such compounds can undergo reactions with small molecules under mild conditions. This led Power in 2010 to draw parallels between the reactivity of main group species and transition metals.[5] Several classes of compound were considered to show "transition metal like" reactivity towards small molecules. These include species featuring multiple bonds involving the heavier main group elements,[6] carbenes and their heavier analogues,[7] and frustrated Lewis pairs.[8] In all cases the reactivity arises due to the availability of empty and filled orbitals, capable of synergistically activating molecules in a push-pull fashion.[5] Within this sphere the low valent chemistry of aluminium has recently received much attention.

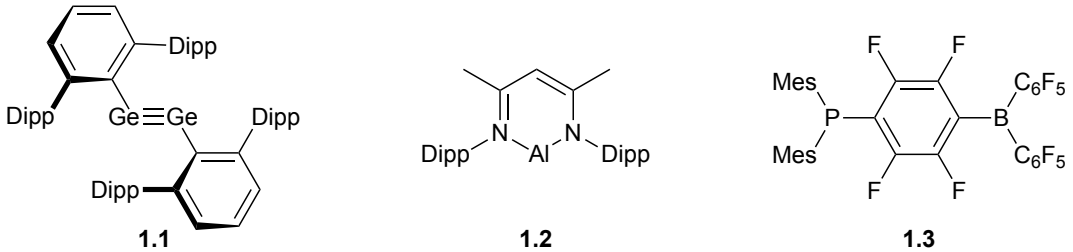

Figure 1.1: Selected reactive main group compounds

1.2 The chemistry of aluminium

Aluminium is the most abundant metal in the Earth's crust.[9] It finds applications in its elemental form as a construction material, due to its low cost, low density, mechanical and electrical properties, and resistance to oxidation.[10] In its compounds, aluminium is almost universally encountered in the +III oxidation state, although a growing number of low valent aluminium compounds have been reported, primarily in the +I oxidation state.[11] Aluminium halide, alkyl, and hydride compounds are widely used in synthesis, both in a laboratory setting and on an industrial scale. Industrially relevant compounds include $AlCl_3$, which is used as a catalyst in Friedel-Crafts chemistry,[12] aluminium alkyls, which are used as activators in Ziegler-Natta chemistry,[13] and aluminium oxide, which is used as an inert catalyst support.[14] Applications of such compounds generally draw on the high Lewis acidity of aluminium(III) species, which results from the high charge and small size of Al^{3+} ion.[11,15] Furthermore, due to the low electronegativity of aluminium, Al–E bonds are usually very polar, and by implication highly reactive.[16]

1.3 Low oxidation state aluminium chemistry

Over the last three decades the low oxidation state chemistry of aluminium has been of sustained interest, with a surge in interest in recent years.[11,17–22] Although Al(I) and Al(II) species are typically thermodynamically unstable with respect to disproportionation to Al(0) and Al(III), an ever increasing number of aluminium compounds in oxidation states as low as 0 has been isolated. Key to stabilising species in the lower oxidation states, is the use of sterically bulky ligands, to prevent aggregation processes via which disproportionation reactions occur.[19,23] Thus, a number of compounds featuring aluminium in the +II oxidation state have been isolated, invariably featuring Al–Al bonds.[17] The +I oxidation state is, however, by far the most common sub-valent state and has been the focal point of much research.

1.4 Aluminium(I) chemistry

The first aluminium(I) compounds to be investigated were the simple binary halides, AlX (X = Cl, Br, I). These can be generated at high temperatures and low pressures, in an entropy-driven process.[24–26] Synthetically useful metastable solutions of aluminium(I) halides can be obtained by co-condensing the species generated at high temperatures with mixtures of donor and non-donor solvents. This methodology, however, requires specialised equipment. That being said, in the presence of strong donors such as NEt_3, tetrameric species of the form $[AlX{\cdot}NEt_3]_4$ (X = Br, I) could be obtained, which were structurally characterised.[25,26]

Historically, the first well defined molecular aluminium(I) compound, $(Cp^*Al)_4$, was reported by Schnöckel in 1991.[27] This compound was initially prepared from AlCl and $MgCp^*_2$, however as our understanding of the low oxidation state aluminium chemistry has evolved, several alternative syntheses have been developed that circumvent the need for AlCl. These include the reduction of $(Cp^*AlCl_2)_2$, Lewis base induced disproportionation of $(Cp^*AlBr)_2$, and reductive elimination of Cp*H from Cp^*_2AlH (Scheme 1.1).[27–30] $(Cp^*Al)_4$ adopts a tetrameric structure in the solid state, featuring a tetrahedral $[Al_4]^{4+}$ core, with each vertex being capped by an η^5-bound Cp^{*-} ligand. In solution and in the gas phase $(Cp^*Al)_4$ is in equilibrium with monomeric Cp*Al (Scheme 1.1). As demonstrated by NMR spectroscopy, this equilibrium can be shifted towards the monomer at higher temperatures, or by employing larger cyclopentadienyl ligands.[31] Tetrameric structures featuring tetrahedral $[Al_4]^{4+}$ cores have also been observed for other aluminium(I) compounds of the type $(RAl)_4$ (R = $C(SiMe_3)_3$, $Si(SiMe_3)_3$, $Si(CMe_3)_3$, DippNSiMe$_3$), which do not feature cyclopentadienyl ligands.[32–35]

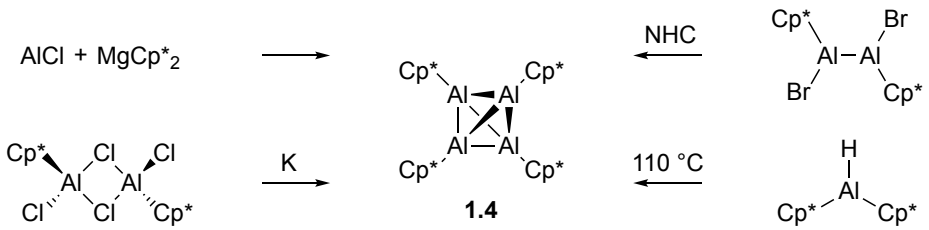

Scheme 1.1: Syntheses of $[Cp^*Al]_4$

The first example of a monomeric aluminium(I) compound, {HC(MeCNDipp)$_2$}Al (NacnacAl), was reported by Roesky in 2000.[36] This compound is stabilised by a bulky bidentate beta-diketiminate ligand, and can be prepared via reduction of the corresponding di-iodide. Single crystal X-ray diffraction experiments reveal an essentially planar AlN_2C_3 ring, and a two coordinate aluminium centre. Unlike the cyclopentadienyl stabilised systems, only one other variant of Roesky's system exists, in which the Me groups of the backbone have been replaced by ^{t}Bu groups.[37]

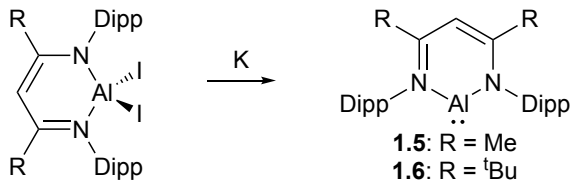

Scheme 1.2: Syntheses of Nacnac-supported aluminium(I) compounds.

In 2003 Power reported the synthesis of the first barrelene type dialumane.[38] This compound was obtained via the reduction of a terphenyl stabilised aluminium diiodide in the presence of toluene. It is proposed that this reaction generates a transient dialumene, which undergoes a [4+2] cycloaddition with the solvent.[38,39] The reactivity of such systems was not further elaborated until 2013, when it was shown that the reaction with the solvent is reversible and that barrelene type dialumanes can act as sources of dialumenes or monomeric alumylenes.[40–43]

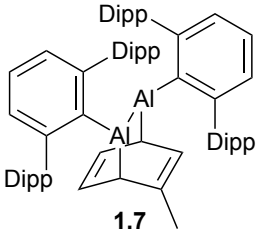

Figure 1.2: The first barrelene type dialumane.

The isolation of the first dialumene was reported by Inoue in 2017.[44,45] This was achieved by the reduction of an NHC stabilised aluminium diiodide bearing either a bulky silyl or aryl substituent.

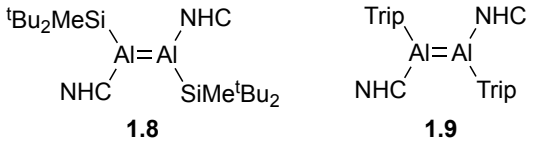

1.8 **1.9**

Figure 1.3: The first dialumenes.

In 2018 our group reported the synthesis of the first aluminyl complex, $[AlX_2]^-$.[46] These are formally anionic complexes, featuring aluminium in the +I oxidation state. This discovery sparked active research in this area, and to date several other examples of aluminyl complexes have been isolated. Their chemistry is discussed below.

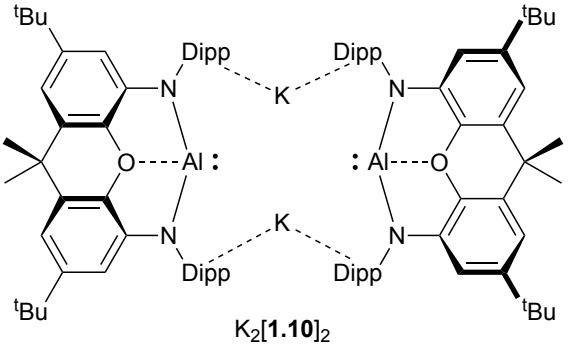

K_2[**1.10**]$_2$

Figure 1.4: The first aluminyl complex.

The first isolable monomeric cyclopentadienyl-stabilised aluminylene, $Cp^{3t}Al$, was reported by Braunschweig in 2019.[47] This compound employs the very bulky 1,2,4-tri-tert-butylcyclopentadienyl ligand, and was prepared via Lewis base induced cleavage of the mixed valence Lewis acid–base adduct $Cp^{3t}AlAlBr_2Cp^*$, **1.11**.

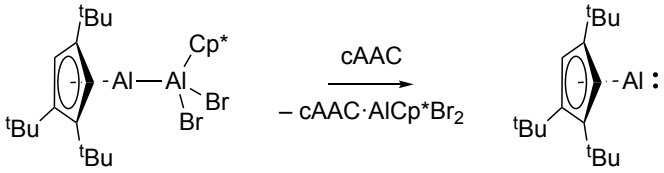

1.11 **1.12**

Scheme 1.3: Synthesis of the first alumylene.

Also in 2019, Braunschweig reported the stabilisation of the parent AlH unit by coordination of two cAAC ligands.[48] The Al–C bond lengths determined by single crystal X-ray diffraction are indicative of a covalently bound aluminium(III) centre, however calculations suggest that this compound is best described by two resonance structure. The major resonance structure describes the compound as an aluminium(I) compound stabilised by two carbenes, while the

minor resonance structure describes it as an aluminium(III) compound bound to two reduced cAAC anions, and possessing singlet diradical character. The latter accounts for roughly one third to the overall electronic character of this compound.

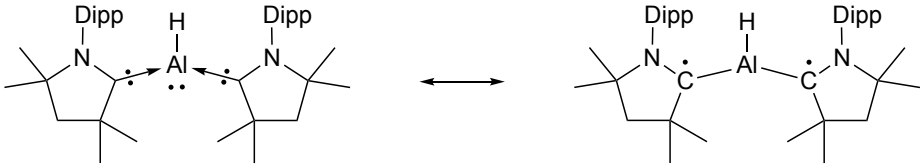

1.13

Figure 1.5: Resonance structures of cAAC stabilised aluminium(I) hydride **1.13**.

The latest breakthrough in this field was reported by Power in 2021, who reported the synthesis of the first one-coordinate alumylene, which was stabilised by an extremely bulky terphenyl ligand, involving ^{i}Pr groups in the 3- and 5-position of the central phenyl ring.[49]

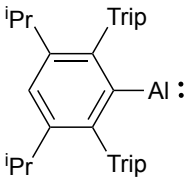

1.14

Figure 1.6: The first one coordinate alumylene.

1.5 Reactivity of neutral aluminium(I) complexes

The reactivity of neutral aluminium(I) complexes is a highly topical area of chemistry and has been reviewed regularly.[11,17–22] $(Cp^*Al)_4$ has been primarily investigated as a source of monomeric Cp*Al. The latter is isolobal with CO, and has been used extensively as a ligand in transition metal complexes.[19] The reactivity of this compound towards small molecules is, however, less well established. NacnacAl can be considered a heavy carbene analogue owing to the presence of a σ-symmetry lone pair and formally empty *p*-orbital on the aluminium centre.[36] Its reactivity towards a wide variety of substrates has been explored, and vibrant research into NacnacAl continues to this day.[20–22,50] While the primary modes of reactivity are oxidative addition and cycloaddition of unsaturated molecules, other modes of reactivity (such as oxidation reactions) have also been explored. Recent highlights include the homologation of

CO,[51–53] reduction of benzene and SF_6,[54,55] and oxidative addition of robust C–F and C–O bonds.[56–58]

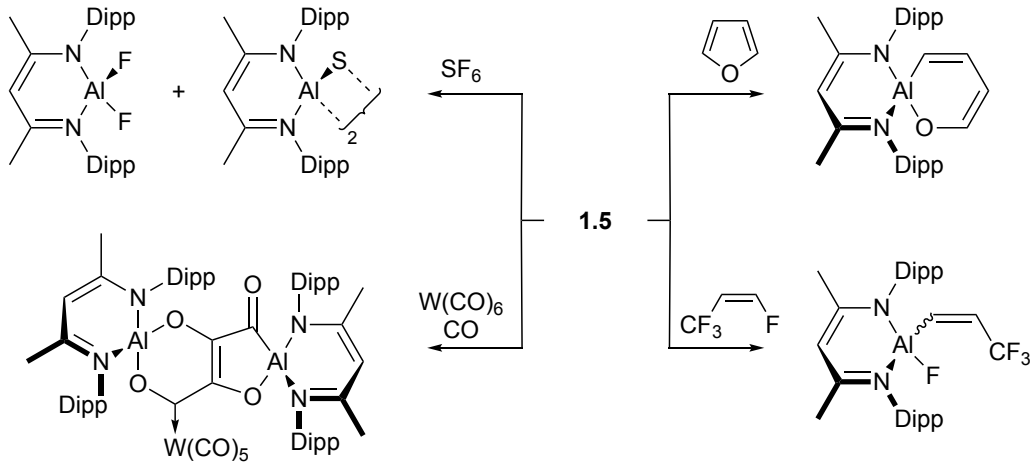

Scheme 1.4: Selected reactions of NacnacAl, **1.5**.

1.6 Anionic group 13 compounds

Group 13 compounds commonly react as Lewis acids. Anionic low valent group 13 reagents have been targeted as a means of accessing complementary nucleophilic reactivity for these elements. N-heterocyclic carbenes are remarkably stable carbene compounds, primarily due to the stabilisation by two amido substituents.[59] Diazabutadiene ligands were also found to stabilise the heavier group 14 compounds,[60] and indeed have allowed the isolation of the first gallyl anion by Schmidbaur in 1999,[61] and the first boryl anion by Yamashita and Nozaki in 2006.[62] In 2014 Mountford and Aldridge reported the isolation of the first thallyl anion,[63] which was supported by two boryl ligands. The first example of an indyl anion was reported by Coles in 2018 using a different diamido ligand,[64] and in the same year Goicoechea and Aldridge reported the first example of an aluminyl anion.[46]

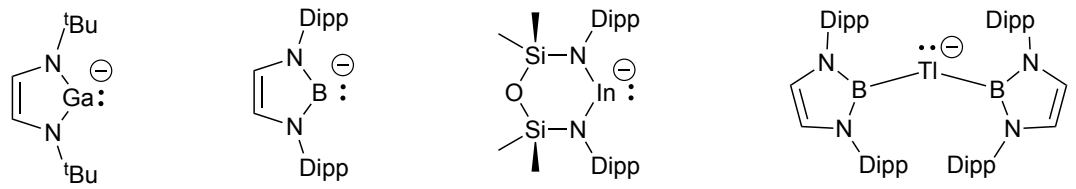

1.15 **1.16** **1.17** **1.18**

Figure 1.7: The first examples of low valent group 13 anions of the elements B, Ga In and Tl.

Although gallyl reagents have been known for a number of years, little is known about their reactivity towards small molecules. Their primary mode of reactivity is the reaction with metal electrophiles to form new M–Ga bonds. This chemistry has been comprehensively reviewed.[65,66] Similarly boryl anions have been used extensively as ligands for a number of main group and transition metal species, and have been shown to be exceptional sigma donors. Furthermore, boryl reagents are strong nucleophiles, and have been demonstrated to react with small molecules, as well as organic electrophiles. This chemistry has also been reviewed extensively.[67–69]

1.7 Aluminyl chemistry

1.7.1 Synthesis of aluminyl compounds

The first aluminyl species was reported in 2018 by our group.[46] Reduction of aluminium(III) precursor **NON**AlI with excess KC_8 in toluene affords aluminyl K_2[**NON**Al_2], K_2[**1.10**]$_2$, in high yields. This species is stabilised by a bulky xanthene-based dianionic diamido-ligand [**NON**]$^{2-}$. When the reaction is carried out under less reducing conditions, such as when sodium metal is used as a reductant, the aluminium(II) dimer [**NON**Al]$_2$, **1.20**, is obtained.[70] Attempts to further reduce this Al(II) species to the aluminyl compound were unsuccessful, indicating that the dimer is not an intermediate in the formation of K_2[**1.10**]$_2$.

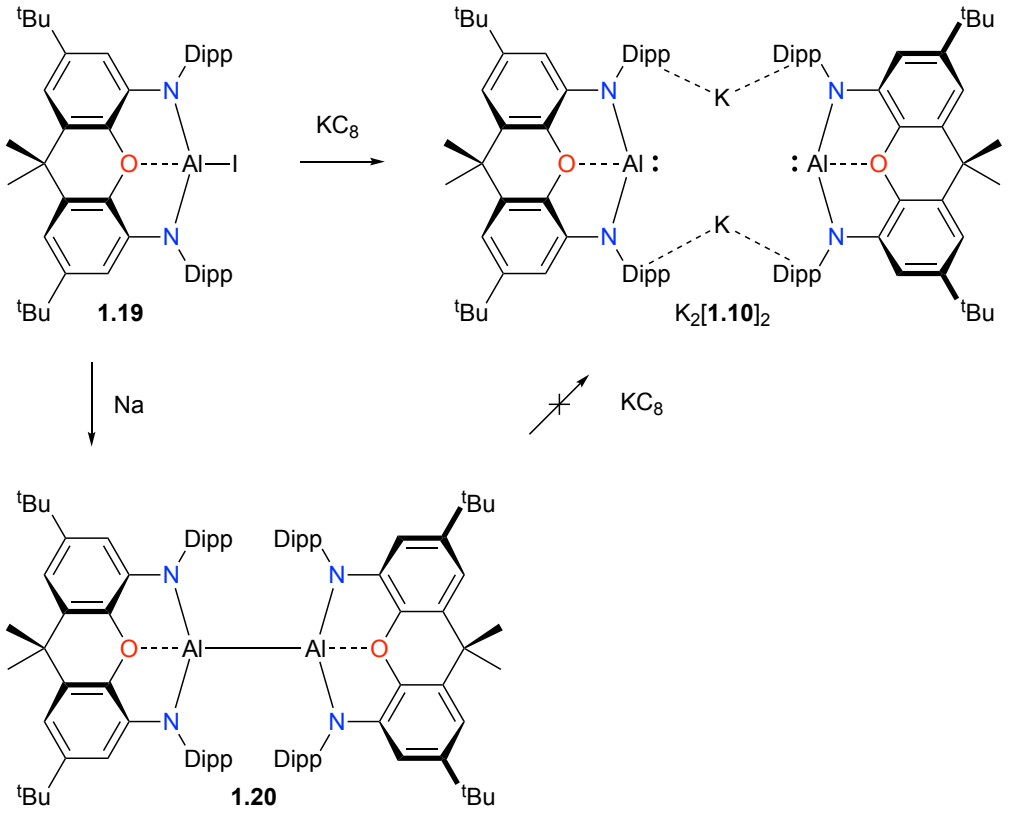

Scheme 1.5: Reduction chemisty of (NON)AlI.

The molecular structure of aluminyl complex K_2[**1.10**]$_2$ was determined by single crystal X-ray diffraction experiments.[46] In the solid state K_2[**1.10**]$_2$ adopts a dimeric structure, in which two anionic [**NON**Al]$^-$ units are bridged by K^+ counter-ions. The Al···Al and Al···K separations are >6.6 Å and >3.8 Å indicating that no significant covalent bonds exist between the metals. Furthermore, the Al···O interaction with the xanthene backbone is >2.2 Å, which is significantly longer than the sum of the respective covalent radii (1.87 Å). DOSY NMR measurements suggest that the dimeric structure is retained in benzene solution. The gallium analogue of K_2[**NON**Al]$_2$, gallyl complex K_2[**NON**Ga]$_2$, K_2[**1.21**]$_2$, can be prepared via the reduction of **NON**GaI with potassium naphthalenide in THF. K_2[**1.21**]$_2$ adopts a near identical structure to K_2[**1.10**]$_2$ in the solid state.[46]

K_2[**1.10**]$_2$ reacts with 2.2.2 cryptand to yield the monomeric aluminyl [K(crypt)][**NON**Al], [K(crypt)][**1.10**].[71] In the solid state, this complex has no close Al···Al or Al···K interactions. As such this complex can be described as genuine 'naked' monomeric aluminyl complex. The structures of the [**NON**Al]$^-$ ion in [K(crypt)][**1.10**] and K_2[**1.10**]$_2$ exhibit near identical

geometries, and bonding parameters, indicating that the potassium ions in the dimer do not strongly influence the electronic structure of the anionic component.

Following the initial discovery, a number other aluminyl species have been reported. These have been stabilised by a number of different ligands, including diamido,[72–74] alkyl amido,[75,76] and dialkyl ligand sets.[77] These are summarised in Figure 1.8.

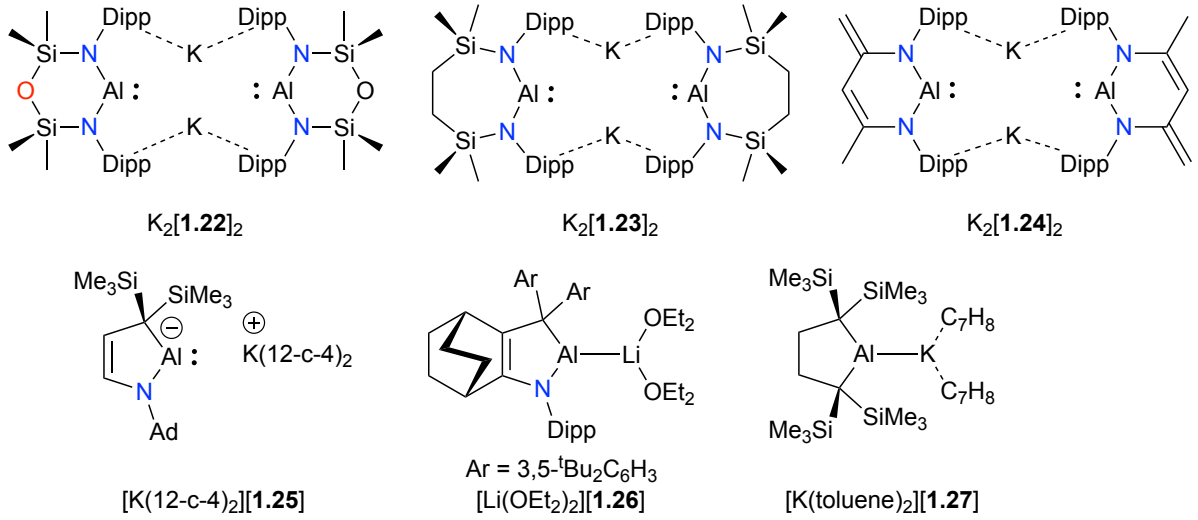

Figure 1.8: Representative examples of aluminyl complexes.

K_2[**1.22**]$_2$ and K_2[**1.23**]$_2$ are obtained via the potassium reduction of the corresponding aluminium iodide precursors.[72,73] Structurally they resemble compounds K_2[**1.10**]$_2$, forming potassium bridged dimers in the solid state. The N–Al–N bond angle for K_2[**1.23**]$_2$ (108.8(1)°) is wider than that of K_2[**1.22**]$_2$ (103.9(1)°) but considerably narrower than the corresponding angle in K_2[**1.10**]$_2$ (128.1(1)°). Similarly [$Li(OEt_2)_2$][**1.26**] is obtained via lithium reduction of the corresponding iodide;[76] [$K(12\text{-}c\text{-}4)_2$][**1.25**] and [$K(C_7H_8)_2$][**1.27**] are obtained via reductions of the corresponding aluminium(II) dimers.[75,77] In the solid state [$Li(OEt_2)_2$][**1.26**] features a very long Al–Li bond, with a bond length of 2.710(6), while [$K(12\text{-}c\text{-}4)_2$][**1.25**] features no interactions between aluminium and potassium. In contrast, K_2[**1.24**]$_2$ was obtained via a backbone deprotonation reaction of NacnacAl with KHMDS.[74]

1.7.2 Electronic structure of aluminyl compounds

The electronic structure of the anions [**1.10**]$^-$, [**1.22**]$^-$, [**1.23**]$^-$, [**1.25**]$^-$, and [**1.27**]$^-$ in the absence of interactions with counter-ions was investigated using DFT methods at the PBE0 D3BJ/def2-

TZVP level of theory.[78] It was found that for all ions the HOMO corresponds to an aluminium-centred lone pair. The chemically important empty *p*-orbital on aluminium corresponds to the LUMO for [**1.27**]$^-$, the LUMO+1 for [**1.25**]$^-$, and the LUMO+3 for [**1.10**]$^-$, [**1.22**]$^-$, and [**1.23**]$^-$. The relative energies of these orbitals are shown in Figure 1.9.

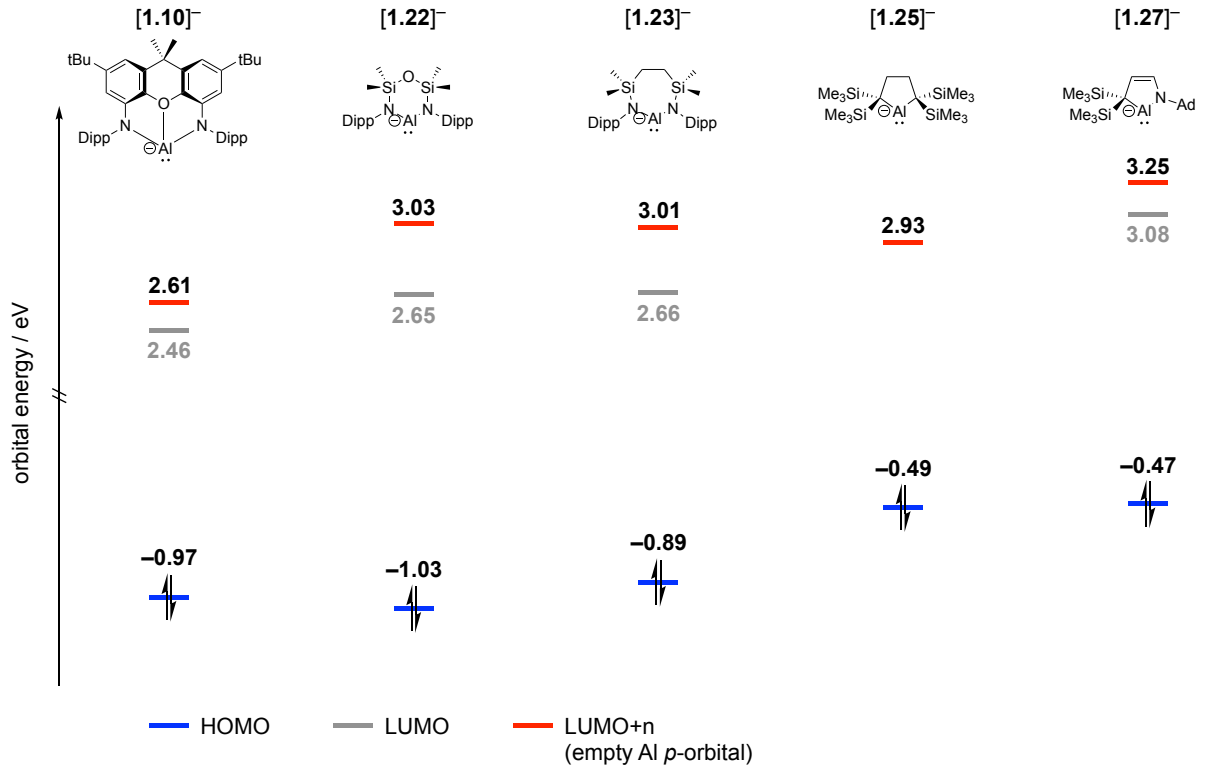

Figure 1.9: Energy level diagram for free aluminyl anions.

The observed trends for the HOMO and LUMO+n orbital energies generally follow the trends expected based on the coordination geometry and substitution pattern around the aluminium centre.[59] The HOMO energies for the dialkyl and alkyl-amido substituted aluminyl systems are higher compared to the diamido systems, on account of the less electronegative α-substituents. However, despite possessing one nitrogen substituent and a more narrow angle at aluminium [**1.27**]$^-$ has a marginally higher energy HOMO than [**1.26**]$^-$. Among the diamido aluminyls, [**1.22**]$^-$ has a slightly lower energy than [**1.23**]$^-$, in line with a wider angle at aluminium. Unexpectedly, the energy of the HOMO of [**1.10**]$^-$ falls in between the former two, despite a significantly wider angle at aluminium and an additional weak donor interaction with the oxygen atom of the xanthene backbone. Considering the empty *p*-orbitals on aluminium,

that of [**1.27**]$^-$ exhibits the highest energy, followed by [**1.22**]$^-$ and [**1.23**]$^-$. These orbital energies are elevated relative to the dialkyl-substituted aluminyl [**1.25**]$^-$ and reflect on the π-donating nature of the amido substituents, which imparts antibonding character to the vacant *p*-orbital on aluminium. Interestingly however, the energy of the corresponding orbital for diamido aluminyl [**1.10**]$^-$ is found to be the lowest out of the systems considered. This implies that the empty *p*-orbital on aluminium features very little antibonding character, both with respect to potential N-to-Al π-donation and the weak interaction of aluminium with the oxygen atom of the xanthene backbone. In this regard [**1.10**]$^-$ is unique among the nitrogen substituted systems. The reason for the lack of N-to-Al π-donation is geometric in nature; due to the constraints of the ligand, the lone pairs on the nitrogen atoms do not align with the vacant *p*-orbital on aluminium, resulting in poor orbital overlap. The same is not true for the remaining nitrogen containing systems.

1.8 Reactivity of aluminyl compounds

1.8.1 Nucleophilic substitutions

Unlike previous generations of low valent aluminium compounds, aluminyl reagents possess pronounced nucluophilicity, undergoing substitution reactions with a wide range of organic and inorganic electrophiles. For example, aluminyl reagents react with MeI, MeOTf, $PhCH_2Cl$, MeOPh, with formation of new Al–C bond.[77,79–82] The fact that even relatively poor leaving groups such as PhO^- can be used is a testament to the high nucleophilicity of the aluminyl species.

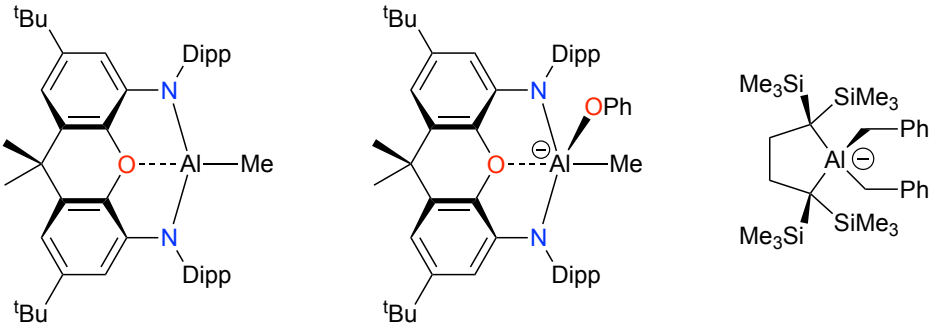

1.28 **[1.29]**$^-$ **[1.30]**$^-$

Figure 1.10: Products obtained from the reaction of aluminyl compounds with electrophiles.

Aluminyl reagents also possess reactivity that goes beyond their use as nucleophiles. This is exemplified by their reactions with organic carbonyl compounds, which lead to products arising from deprotonation, hydroalumination or reduction reactions.[83]

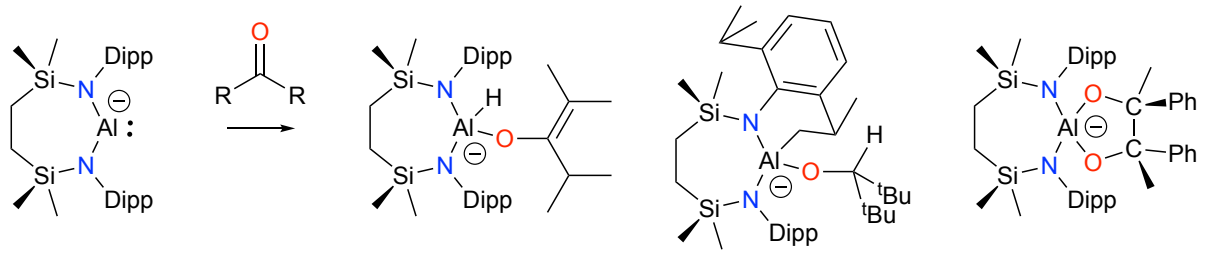

Scheme 1.6: Reactions of K_2[**1.22**]$_2$ with ketones.

Reactions with organic Lewis acids also lead to varied reaction outcomes. The reactions with boranes lead to reduction,[75] bond activation[84] or the formation of Lewis base adducts.[79] The latter was achieved using triphenylborane. When the analogous reaction is carried out with the trityl cation, nucleophilic attack of the *para*-position of one of the phenyl rings was observed.[79]

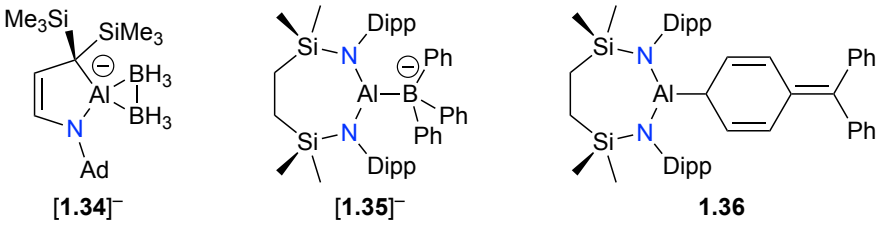

Figure 1.11: Products obtained from the reaction of aluminyl compounds with boranes and trityl cations.

Furthermore, aluminyl compounds have been reacted with a range of metal electrophiles, leading to the formation of Al–M bonded complexes. This has been successful for metals including M = Mg, Ca, Y, Ti , Cu, Ag, Au, and Zn.[70,73,85–89] Changing the counter-ions allows a means for controlling the polarity of the Al–M bond, and hence their reactivity. For more electronegative metals the $Al^{\delta+}$–$M^{\delta-}$ bond is polarised towards M, imparting nucleophilic character onto the metal. This was demonstrated in the reactions of such species with CO_2 or carbodiimides, leading to products featuring M–C bonds, rather than Al–C bonds.[70,87–89]

1.8.2 Oxidative addition reactions

A wide range of oxidative addition reactions have been reported for aluminyl species, mimicking the reactivity of Roesky's NacnacAl system. Examples of substrates undergoing bond activation of this sort includes compounds featuring a number of E–H bonds (E = H, C, Si, N, P, O) as well as C–E (E = C, O, F, Br) bonds.[74,75,77,79–81]

The reactions of aluminyl reagents with mono- and di- alkylated arenes leads to the C–H activation in the *meta*-position and benzylic positions while no evidence for activation of C–H bonds in the *ortho*- or *para*-position relative to any substituent was obtained.[80,81] These reactions proceed in an S_NAr-like fashion, via nucleophilic attack of aluminium at the aromatic ring. The regioselectivity is governed by the stability of the resulting transition state.

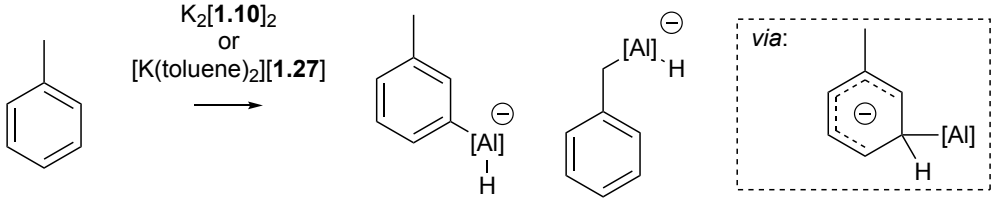

Scheme 1.7: *meta*-selective C–H activation of toluene.

1.8.3 Reactions with unsaturated carbon compounds

The reactions of low valent aluminium compounds with unsaturated carbon-containing substrates is well established. Aluminyl reagents mimic some of the reactions observed for the NacnacAl system, but show diverging reactivity as well. The reaction of [K(crypt)][**NON**Al] with benzene for example leads to the insertion of the aluminium centre into a C=C bond, affording a seven membered ring.[71]

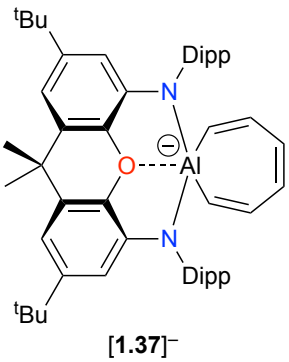

[**1.37**]⁻

Figure 1.12: Benzene C–C activation product [K(crypt)][**1.37**].

The reactions of aluminyl reagents with alkenes and alkynes have been shown to afford products featuring a AlC_2 three membered rings, via formal [2+1] cycloadditions, while the reactions of with naphthalene or anthracene lead to formal [4+1] cycloadditions.[71,90,91] Finally, the reactions with COT have been reported. In these cases reduction to $[COT]^{2-}$ was observed.[72,73]

1.8.4 Oxidation reactions

Aluminyl reagents are nucleophilic and strongly reducing. Due to these properties they react readily with a range of reducing agents and allow rational access to species that are otherwise difficult to synthesise, including heavier carbonyl analogues, and related species with the potential for multiple bonding.

1.8.4.1 Group 14 oxidants

An example of the oxidation of an aluminyl complex with a group 14 reagent involves the reaction of aluminyl $[Li(OEt_2)_2]$[**1.26**] with a diazomethane.[92] This leads initially to the formation of an AlN_2 three membered ring, which upon gentle warming loses N_2 to afford a compound a short Al–C bond. The HOMO of [**1.39**]$^-$ corresponds to a π-symmetry bonding orbital with significant contributions from both Al and C; a detailed theoretical analysis of the bonding was however not provided.

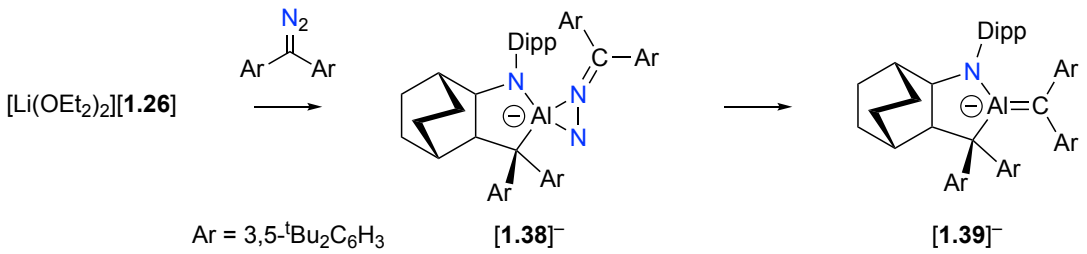

Scheme 1.8: Synthesis of a complex featuring an Al=C double bond.

1.8.4.2 Group 15 oxidants

The reactions of aluminyl reagents with azides have been described.[93,94] These are detailed in chapter 3. Furthermore, the reactions of aluminyl reagents with P_4 have been reported. The reaction with K_2[**NON**Al]$_2$ leads to either two- or four-electron reduction of the P_4 unit,

depending on the stoichiometry of the reaction.[95] The structures of the products are shown below (Scheme 1.9). Furthermore, the reactivity of [K(12-c-4)$_2$][**1.27**] with P_4 has been reported.[96] The 8:1 reaction leads to the complete cleavage of the P_4 cage and formation of an dialuminyl phosphide.

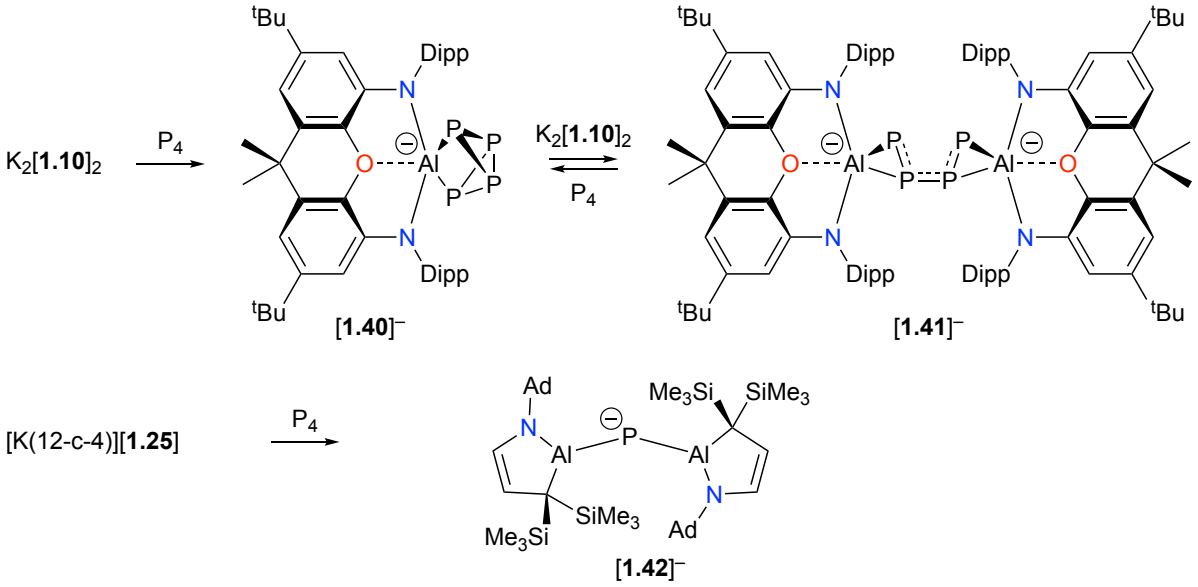

Scheme 1.9: Activation of white phosphorus by aluminyl complexes.

1.8.4.3 Group 16 oxidants

The reactions of aluminyl K$_2$[**NON**Al]$_2$ with CO_2 and PhNCO lead to the formation of carbonate and carbamate complexes respectively.[97] These reactions are proposed to proceed via the corresponding oxides. In order to isolate the oxide intermediates, the aluminyl reagents were reacted with N_2O. In the case of K$_2$[**NON**Al]$_2$, this leads to the formation of the *cis*-hyponitrite complex K$_2$[**NON**Al(ONNO)]$_2$ if the reaction is carried out in benzene or toluene. When this reaction is carried out in THF at temperatures < 0 °C, the THF-stabilised oxide K$_2$[**NON**Al(THF)O]$_2$ can be isolated. This oxide is found to be highly reactive, decomposing in solution within hours at room temperature. It undergoes reactions with N_2O, CO_2, and PhNCO to afford the previously observed products, showing that the (presumably even more reactive) non THF-ligated oxide is a viable intermediate. Furthermore, the oxide itself was shown to activate H_2 by 1,2-addition at room temperature.

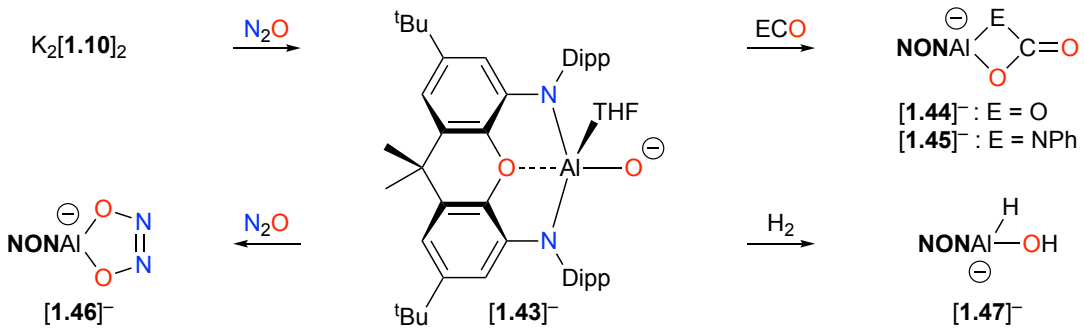

Scheme 1.10: Synthesis and reactivity of a terminal aluminium oxide.

Similarly, the reactions of aluminyl K_2[**1.22**]$_2$ with CO_2 and N_2O have been reported.[98] The reaction with CO_2 also leads to the formation of a carbonate complex. The reaction with N_2O however affords an aluminium oxide. Carrying out the reaction in the presence of 2.2.2-cryptand leads to formation of a *cis*-hyponitrite complex, while addition of sequestering agents to the isolated oxide, invariably led to the activation of the ligand.

The reaction of K_2[**1.22**]$_2$ with CS_2 leads to the formation of trithiocarbonate or ethene-tetrasulfide complexes depending on the stoichiometry of the reaction.[99] Formation of the ethene-tetrasulfide complex is proposed to proceed via dimerization of two carbene fragments, obtained from the κ^2-S,S binding of CS_2. Analogous chemistry for oxygenated species is reported in chapter 5. Formation of the trithiocarbonate is proposed to proceed via an aluminium sulphide.

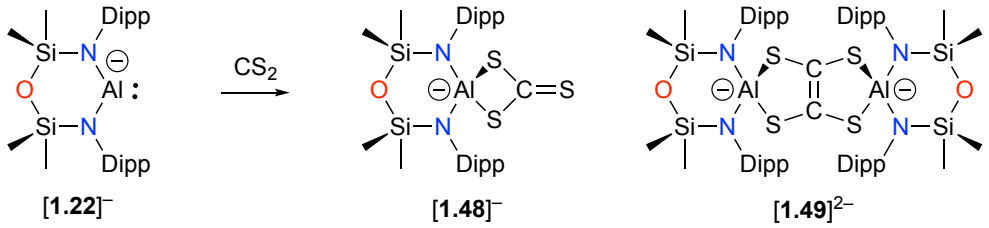

Scheme 1.11: Reactions of K_2[**1.22**]$_2$ with CS_2.

Subsequently, the reaction of K_2[**1.22**]$_2$ with elemental sulphur was investigated.[100] The direct combination of the reagents leads to the formation of the tetrasulfide complex, which upon treatment with triphenylphosphine afforded the target aluminium sulphide. The reaction with 2.2.2-cryptand then affords a terminal aluminium sulphide species.

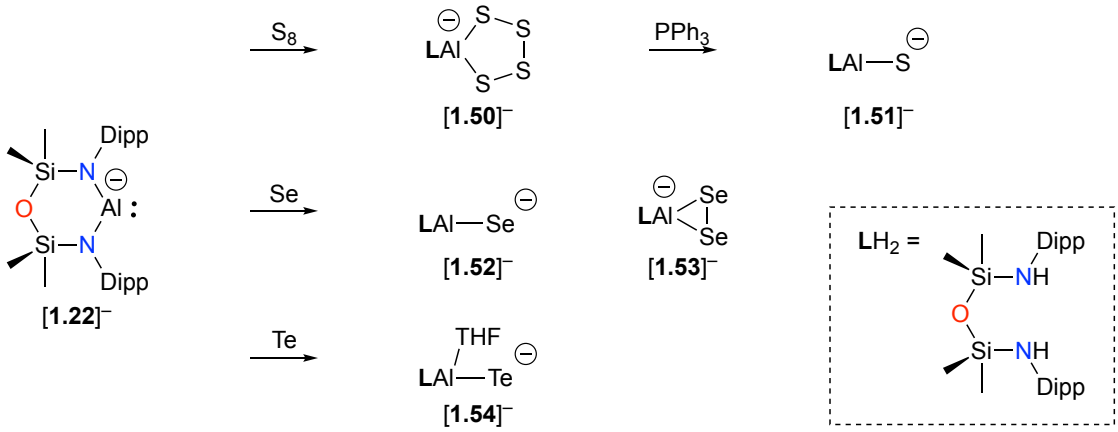

Scheme 1.12: Oxidation of K_2[**1.22**]$_2$ with the heavier chalogens.

In addition, the reaction of K_2[**1.22**]$_2$ with selenium was investigated. In this case, a selenide could be obtained.[100] Repeating the reaction in the presence of 2.2.2-cryptand and leads to the formation of a diselenide (Scheme 1.12).[101] Finally, the telluride could be prepared from K_2[**1.22**]$_2$ and elemental tellurium in the presence of catalytic tri-n-butylphosphine in THF. This reaction affords the THF-stabilised aluminium telluride.[102]

With the complete series of aluminium chalcogenides complete, their electronic structure of the anions [(O{SiMe$_2$NDipp}$_2$)Al(E)]$^-$ (E = O–Te) was investigated by DFT calculations.[100] As for the [**NON**AlO]$^-$, the HOMO and HOMO-1 correspond to a pair of orthogonal *p*-orbitals primarily centred at E, with the HOMO-1 constituting the potential π-bonding interaction. The bonding situation in each system was analysed by NBO and AIM methods. It is found that the bond orders increase down the group, which can be shown to arise due to an increasing contribution of the π-bond. This is somewhat counterintuitive, as the π-orbital overlap is expected to decrease with increasing size of the atoms. The observed trend is therefore attributed to the decreasing difference in electronegativity.

The heavier oxide analogues are shown to undergo reactivity reminiscent of that of the oxide. The crypt-sequestered sulphide and selenides react with CO_2 via [2+2] addition to yield the corresponding sulfido and selenocarbonates.[100] The corresponding reaction of the unsequestered telluride in THF leads to the double insertion of CO_2 to afford a tellurodicarbonate.[102] Monitoring the reaction of a mixture using labelled $^{13}CO_2$ by $^{13}C\{^1H\}$

NMR spectroscopy, reveals the formation of an intermediate, proposed to the tellurocarbonate. In further studies, the reactions of the selenide and sulphide with benzaldehyde and benzophenone were investigated.[100] In the case of benzaldehyde, insertion of two molecules into the Al–E bond is observed, while the analogous reaction with benzophenone reacts in a 1:1 ratio. Presumably these reactions are driven by the formation of Al–O bonds and to some extent controlled by sterics.

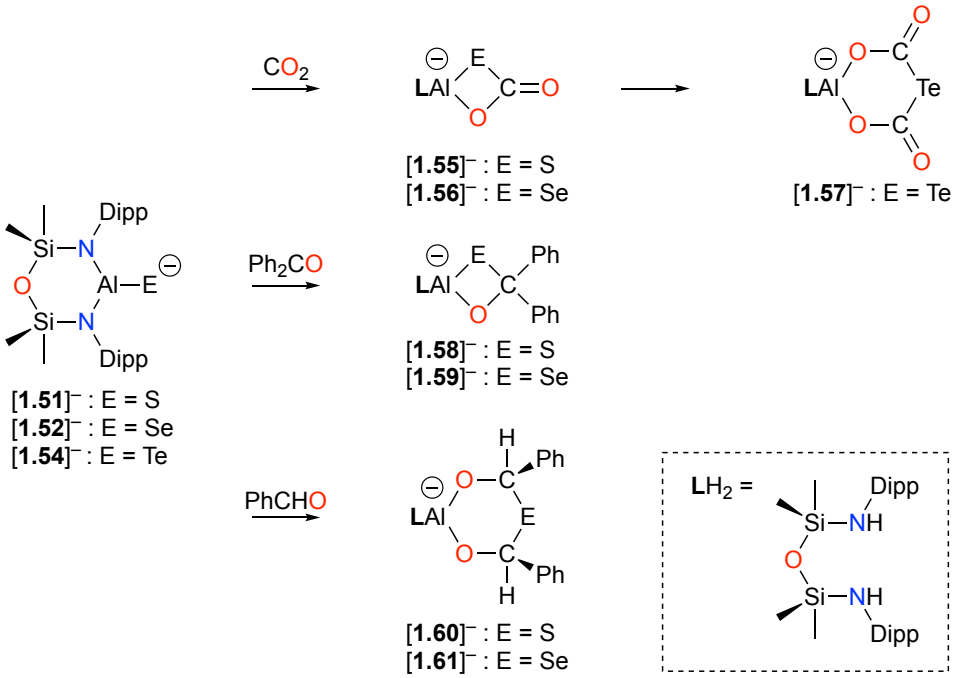

Scheme 1.13: Reactivity of aluminium chalcogenides with carbonyl compounds.

1.9 References

[1] E. Lansing, B. S. Kenneth Pitzer, *The Thermodynamic and Physical Properties of the Elements*, Cornell University Press, **1947**.

[2] P. J. Davidson, M. F. Lappert, *J. Chem. Soc. Chem. Commun.,* **1973**, 317a–317a.

[3] R. West, M. J. Fink, J. Michl, *Science,* **1981**, *214*, 1343–1344.

[4] M. Yoshifuji, I. Shima, N. Inamoto, K. Hirotsu, T. Higuchi, *J. Am. Chem. Soc.,* **1981**, *103*, 4587–4589.

[5] P. P. Power, *Nature*, **2010**, *463*, 171–177.

[6] R. C. Fischer, P. P. Power, *Chem. Rev.,* **2010**, *110*, 3877–3923.

[7] T. Chu, G. I. Nikonov, *Chem. Rev.*, **2018**, *118*, *7*, 3608–3680.

[8] D. W. Stephan, G. Rker, D. W. Stephan, G. Erker, *Angew. Chem.*, **2015**, *127*, 6498–6541.

[9] W. M. Haynes, D. R. Lide, T. J. Bruno, Eds. , *CRC Handbook of Chemistry and Physics*, CRC Press, **2016**.

[10] J. Emsley, *Nature's Building Blocks*, Oxford University Press, Oxford, **2011**.

[11] C. Weetman, H. Xu, S. Inoue, Recent Developments in Low-Valent Aluminum Chemistry. In Encyclopedia of Inorganic and Bioinorganic Chemistry, R.A. Scott (Ed.), **2023**.
[12] G. A. Olah, V. P. Reddy, G. K. S. Prakash, in *Kirk-Othmer Encyclopedia of Chemical Technology*, John Wiley & Sons, Inc., Hoboken, NJ, USA, **2000**.
[13] R. Mülhaupt, *Macromol. Chem. Phys.*, **2003**, *204*, 289–327.
[14] M. Trueba, S. P. Trasatti, *Eur. J. Inorg. Chem.*, **2005**, *2005*, 3393–3403.
[15] R. D. Shannon, *Acta Crystallogr., Sect. A: Found. Adv.*, **1976**, *32*, 751–767.
[16] L. Pauling, *J. Am. Chem. Soc.*, **1932**, *54*, 3570–3582.
[17] P. Bag, C. atherine Weetman, S. Inoue, *Angew. Chem.*, **2018**, *130*, 14594–14613.
[18] K. Hobson, C. J. Carmalt, C. Bakewell, *Chem. Sci.*, **2020**, *11*, 6942-6956.
[19] G. Linti, H. Schnöckel, *Coord. Chem. Rev.*, **2000**, *206–207*, 285–319.
[20] H. W. Roesky, S. Shravan Kumar, *Chem. Commun.*, **2005**, 4027-4038.
[21] M. Zhong, S. Sinhababu, H. W. Roesky, *Dalton Trans.*, **2020**, *49*, 1351–1364.
[22] Y. Liu, J. Li, X. Ma, Z. Yang, H. W. Roesky, *Coord. Chem. Rev.*, **2018**, *374*, 387–415.
[23] A. Ecker, E. Weckert, H. Schnöckel, *Nature*, **1997**, *387*, 379–381.
[24] M. Tacke, H. Schnöckel, *Inorg. Chem.*, **1989**, *28*, 2895–2896.
[25] A. Ecker, H. Schnöckel, *Z. Anorg. Allg. Chem.*, **1996**, *622*, 149–152.
[26] M. Mocker, C. Robl, H. Schnöckel, *Angew. Chem. Int. Ed.,* **1994**, *33*, 1754–1755.
[27] S. Schulz, H. W. Roesky, H. J. Koch, G. M. Sheldrick, D. Stalke, A. Kuhn, *Angew. Chem. Int. Ed.,* **1993**, *32*, 1729–1731.
[28] C. Dohmeier, D. Loos, H. Schnöckel, *Angew. Chem. Int. Ed.,* **1996**, *35*, 129–149.
[29] A. Hofmann, A. Lamprecht, J. O. C. Jiménez-Halla, T. Tröster, R. D. Dewhurst, C. Lenczyk, H. Braunschweig, *Chem. Eur. J.*, **2018**, *24*, 11795–11802.
[30] C. Ganesamoorthy, S. Loerke, C. Gemel, P. Jerabek, M. Winter, G. Frenking, R. A. Fischer, *Chem. Commun.*, **2013**, *49*, 2858–2860.
[31] H. Sitzmann, M. F. Lappert, C. Dohmeier, C. Üffing, H. Schnöckel, *J. Organomet. Chem.*, **1998**, *561*, 203–208.
[32] C. Schnitter, H. W. Roesky, C. Röpken, R. Herbst-Irmer, H.-G. Schmidt, M. Noltemeyer, *Angew. Chem. Int. Ed.*, **1998**, *37*, 14.
[33] A. Purath, H. Schnöckel, *J. Organomet. Chem.*, **1999**, *579*, 373–375.
[34] A. Purath, G. Dohmeier, A. Ecker, H. Schnöckel, K. Amelunxen, T. Passler, N. Wiberg, *Organometallics*, **1998**, *17*, 1894–1896.
[35] M. Schiefer, N. D. Reddy, H. W. Roesky, D. Vidovic, *Organometallics*, **2003**, *22*, 3637–3638.
[36] C. Cui, H. W. Roesky, H.-G. Schmidt, M. Noltemeyer, H. Hao, F. Cimpoesu, *Angew. Chem. Int. Ed.*, **2000**, *39*, 4274–4276.
[37] X. Li, X. Cheng, H. Song, C. Cui, *Organometallics*, **2007**, *26*, 1039–1043.
[38] R. J. Wright, A. D. Phillips, P. P. Power, *J. Am. Chem. Soc.*, **2003**, *125*, 10784–10785.
[39] C. Cui, X. Li, C. Wang, J. Zhang, J. Cheng, X. Zhu, *Angew. Chem. Int. Ed.*, **2006**, *45*, 2245–2247.
[40] T. Agou, K. Nagata, N. Tokitoh, *Angew. Chem. Int. Ed.*, **2013**, *52*, 10818–10821.
[41] T. Agou, K. Nagata, T. Sasamori, N. Tokitoh, *Chem. Asian. J.*, **2014**, *9*, 3099–3101.
[42] T. Agou, K. Nagata, T. Sasamori, N. Tokitoh, *P., S., and Si.*, **2016**, *191*, 588–590.
[43] K. Nagata, T. Agou, T. Sasamori, N. Tokitoh, *Chem. Let.*, **2015**, *44*, 1610–1612.
[44] C. Weetman, A. Porzelt, P. Bag, F. Hanusch, S. Inoue, *Chem. Sci.*, **2020**, *11*, 4817–4827.
[45] P. Bag, A. Porzelt, P. J. Altmann, S. Inoue, *J. Am. Chem. Soc.*, **2017**, *139*, 14384–14387.
[46] J. Hicks, P. Vasko, J. M. Goicoechea, S. Aldridge, *Nature*, **2018**, *557*, 92–95.

[47] A. Hofmann, T. Tröster, T. Kupfer, H. Braunschweig, *Chem. Sci.*, **2019**, *10*, 3421–3428.
[48] S. K. Mellerup, Y. Cui, F. Fantuzzi, P. Schmid, J. T. Goettel, G. Bélanger-Chabot, M. Arrowsmith, I. Krummenacher, Q. Ye, V. Engel, B. Engels, H. Braunschweig, *J. Am. Chem. Soc.*, **2019**, *141*, 16954–16960.
[49] J. D. Queen, A. Lehmann, J. C. Fettinger, H. M. Tuononen, P. P. Power, *J. Am. Chem. Soc.*, **2020**, *142*, 20554–20559.
[50] T. Chu, I. Korobkov, G. I. Nikonov, *J. Am. Chem. Soc.*, **2014**, *136*, 9195–9202.
[51] R. Y. Kong, M. R. Crimmin, *J. Am. Chem. Soc.*, **2018**, *140*, 13614–13617.
[52] R. Y. Kong, M. Batuecas, M. R. Crimmin, *Chem. Sci.*, **2021**, *12*, 14845–14854.
[53] M. Batuecas, R. Y. Kong, A. J. P. White, M. R. Crimmin, *Angew. Chem. Int. Ed.*, **2022**, *61*, e202202241.
[54] D. J. Sheldon, M. R. Crimmin, *Chemical Communications* **2021**, *57*, 7096–7099.
[55] S. Brand, H. Elsen, J. Langer, W. A. Donaubauer, F. Hampel, S. Harder, *Angew. Chem. Int. Ed.*, **2018**, *57*, 14169–14173.
[56] M. R. Crimmin, M. J. Butler, A. J. P. White, *Chem. Commun.*, **2015**, *51*, 15994–15996.
[57] C. Bakewell, A. J. P. White, M. R. Crimmin, *Angew. Chem. Int. Ed.*, **2018**, *57*, 6638–6642.
[58] F. Rekhroukh, W. Chen, R. K. Brown, A. J. P. White, M. R. Crimmin, *Chem. Sci.*, **2020**, *11*, 7842–7849.
[59] D. Bourissou, O. Guerret, F. P. Gabbaï, G. Bertrand, *Chem. Rev.*, **2000**, *100*, 39–92.
[60] M. Asay, C. Jones, M. Driess, *Chem. Rev.*, **2011**, *111*, *2*, 354–396.
[61] E. S. Schmidt, A. Jockisch, H. Schmidbaur, *J. Am. Chem. Soc.*, **1999**, *121*, 9758–9759.
[62] Y. Segawa, M. Yamashita, K. Nozaki, *Science,* **2006**, *314*, 113–115.
[63] A. v. Protchenko, D. Dange, J. R. Harmer, C. Y. Tang, A. D. Schwarz, M. J. Kelly, N. Phillips, R. Tirfoin, K. H. Birjkumar, C. Jones, N. Kaltsoyannis, P. Mountford, S. Aldridge, *Nat. Chem.*, **2014**, *6*, 315–319.
[64] R. J. Schwamm, M. D. Anker, M. Lein, M. P. Coles, C. M. Fitchett, *Angew. Chem. Int. Ed.*, **2018**, *57*, 5885–5887.
[65] C. Jones, D. P. Mills, R. P. Rose, A. Stasch, W. D. Woodul, *J. Organomet. Chem.*, **2010**, *695*, 2410–2417.
[66] R. Baker, C. Jones, *Coord. Chem. Rev.*, **2005**, *249*, 1857–1869.
[67] M. Yamashita, *Bull. Chem. Soc. Jpn.*, **2011**, *84*, 983–999.
[68] W. Lu, H. Hu, Y. Li, R. Ganguly, R. Kinjo, *J. Am. Chem. Soc.*, **2016**, *138*, 6650–6661.
[69] M. D. Anions, L. Weber, *Eur. J. Inorg. Chem.*, **2017**, *2017*, 3461–3488.
[70] M. M. D. Roy, J. Hicks, P. Vasko, A. Heilmann, A. M. Baston, J. M. Goicoechea, S. Aldridge, *Angew. Chem. Int. Ed.*, **2021**, *60*, 22301–22306.
[71] J. Hicks, P. Vasko, J. M. Goicoechea, S. Aldridge, *J. Am. Chem. Soc.*, **2019**, *141*, 11000–11003.
[72] R. J. Schwamm, M. D. Anker, M. Lein, M. P. Coles, *Angew. Chem. Int. Ed.*, **2019**, *58*, 1489–1493.
[73] R. J. Schwamm, M. P. Coles, M. S. Hill, M. F. Mahon, C. L. McMullin, N. A. Rajabi, A. S. S. Wilson, *Angew. Chem. Int. Ed.*, **2020**, *59*, 3928–3932.
[74] S. Grams, J. Eyselein, J. Langer, C. Färber, S. Harder, *Angew. Chem. Int. Ed.*, **2020**, *59*, 15982–15986.
[75] K. Koshino, R. Kinjo, *J. Am. Chem. Soc.*, **2020**, *142*, 9057–9062.
[76] C. Yan, R. Kinjo, C Yan, R. Kinjo, *Angew. Chem. Int. Ed.*, **2022**, *61*, e202211800.
[77] S. Kurumada, S. Takamori, M. Yamashita, *Nat. Chem.*, **2019**, *12*, 36–39.
[78] J. Hicks, P. Vasko, J. M. Goicoechea, S. Aldridge, *Angew. Chem. Int. Ed.*, **2021**, *60*, 1702–1713.

[79] R. J. Schwamm, M. S. Hill, H. Liu, M. F. Mahon, C. L. McMullin, N. A. Rajabi, *Chem. Eur. J.*, **2021**, *27*, 14971–14980.
[80] S. Kurumada, K. Sugita, R. Nakano, M. Yamashita, *Angew. Chem. Int. Ed.*, **2020**, *59*, 20381–20384.
[81] J. Hicks, P. Vasko, A. Heilmann, J. M. Goicoechea, S. Aldridge, *Angew. Chem. Int. Ed.*, **2020**, *59*, 20376–20380.
[82] M. J. Evans, M. D. Anker, M. P. Coles, *Inorg. Chem.*, **2021**, *60*, 4772–4778.
[83] H.-Y. Liu, M. S. Hill, M. F. Mahon, *Chem. Commun.*, **2022**, *58*, 6938–6941.
[84] S. Kurumada, M. Yamashita, *J. Am. Chem. Soc.*, **2022**, *144*, 4327–4332.
[85] K. Sugita, M. Yamashita, *Chem. Eur. J.*, **2020**, *26*, 4520–4523.
[86] K. Sugita, M. Yamashita, *Organometallics*, **2020**, *39*, 2125–2129.
[87] J. Hicks, A. Mansikkamäki, P. Vasko, J. M. Goicoechea, S. Aldridge, *Nat. Chem.*, **2019**, *11*, 237–241.
[88] C. McManus, J. Hicks, X. Cui, L. Zhao, G. Frenking, J. M. Goicoechea, S. Aldridge, *Chem. Sci.*, **2021**, *12*, 13458–13468.
[89] H.-Y. Liu, S. E. Neale, M. S. Hill, M. F. Mahon, C. L. McMullin, *Dalton Trans.*, **2022**, *51*, 3913–3924.
[90] K. Sugita, R. Nakano, M. Yamashita, *Chem. Eur. J.*, **2020**, *26*, 2174–2177.
[91] M. J. Evans, S. E. Neale, M. D. Anker, C. L. McMullin, M. P. Coles, *Angew. Chem. Int. Ed.*, **2022**, *61*, e202117396.
[92] C. Yan, R. Kinjo, *Angew. Chem. Int. Ed.*, **2022**, *61*, e202211800.
[93] A. Heilmann, J. Hicks, P. Vasko, J. M. Goicoechea, S. Aldridge, *Angew. Chem. Int. Ed.*, **2020**, *59*, 4897–4901.
[94] M. D. Anker, R. J. Schwamm, M. P. Coles, *Chem. Commun.*, **2020**, *56*, 2288–2291.
[95] M. M. D. Roy, A. Heilmann, M. A. Ellwanger, S. Aldridge, *Angew. Chem. Int. Ed.*, **2021**, *60*, 26550–26554.
[96] K. Koshino, R. Kinjo, *Organometallics*, **2020**, *39*, 4183–4186.
[97] J. Hicks, A. Heilmann, P. Vasko, J. M. Goicoechea, S. Aldridge, *Angew. Chem. Int. Ed.*, **2019**, *58*, 17265–17268.
[98] M. D. Anker, M. P. Coles, *Angew. Chem. Int. Ed.*, **2019**, *58*, 18261–18265.
[99] M. D. Anker, C. L. McMullin, N. A. Rajabi, M. P. Coles, *Angew. Chem. Int. Ed.*, **2020**, *59*, 12806–12810.
[100] M. J. Evans, M. D. Anker, C. L. McMullin, S. E. Neale, N. A. Rajabi, M. P. Coles, *Chem. Sci.*, **2022**, *13*, 4635–4646.
[101] M. D. Anker, M. P. Coles, *Angew. Chem. Int. Ed.*, **2019**, *131*, 13586–13589.
[102] M. J. Evans, M. D. Anker, C. L. McMullin, N. A. Rajabi, M. P. Coles, *Chem. Commun.*, **2021**, *57*, 2673–2676.

Chapter 2. Experimental methods

2.1 Synthetic methods

2.1.1 Handling of air sensitive compounds

The majority of the compounds discussed in this thesis are highly sensitive to air and moisture and were therefore handled under an atmosphere of purified nitrogen or argon using standard Schlenk line and glovebox techniques.[1,2] The Schenk line was connected to an argon supply and a vacuum pump, maintaining a pressure of ca. 2×10^{-2} mbar in the system. All glassware was dried at 200 °C overnight and flame dried prior to use. Air was removed from the vessels by evacuating (to ca. 5×10^{-2} mbar) and refilling with argon at least three times. Solids were added in a glovebox, and liquids were added using cannulae or syringes.

2.1.2 Handling of gases

Different methods were used to introduce gases into reactions. In most cases gases were introduced by degassing solutions using two freeze–pump–thaw cycles, before filling the headspace of the reaction vessel with the chosen gas. This allows for the addition of stoichiometric amounts of gases, by controlling the pressure of the gas, and the volume of the reaction vessel. When small amounts of gas were required, these were measured using a syringe and injected into the solution before quickly sealing the reaction vessel.

2.2 Analytic methods

2.2.1 NMR spectroscopy

NMR spectra were measured on a Bruker Avance III HD Nanobay 400 MHz NMR spectrometer equipped with a 9.4T magnet, a Bruker Avance III 500 MHz NMR spectrometer equipped with a 11.75T magnet, a Bruker Avance 500 MHz NMR spectrometer equipped with a 11.75T magnet and a ^{13}C detect cryoprobe, or a Bruker NEO 600 MHz NMR spectrometer equipped with a 14.1 T magnet and broadband helium cryoprobe. ^{1}H and ^{13}C NMR spectra were referenced internally to residual protio-solvent (^{1}H) or solvent (^{13}C) resonances and are

reported relative to tetramethylsilane (δ = 0 ppm). ^{11}B spectra were referenced externally against $BF_3 \cdot OEt_2$ (δ = 0 ppm). ^{1}H–^{1}H and ^{13}C–^{1}H correlation experiments were carried out to aid assignments. NMR samples were prepared in 5 mm Wilmad 507-PP tubes fitted with J. Young Teflon valves under an inert atmosphere. C_6D_6 was dried over K or CaH_2, distilled, and stored over a K mirror. THF-d_8 was dried over CaH_2 or molten K, distilled under reduced pressure, and stored over 4 Å molecular sieves. Both solvents were degassed using the freeze-pump-thaw method prior to use.

2.2.2 Infrared spectroscopy

Infrared spectra were measured using a Nicolet 500 FT-IR spectrometer. Samples were prepared in an inert atmosphere as a Nujol mull between KBr discs, and sealed in an air-tight cell.

2.2.3 Elemental analysis

Elemental analyses were carried out by Elemental Microanalysis Ltd, Okehampton, Devon, UK, or by London Metropolitan University, UK.

2.2.4 Single-crystal X-ray diffraction

Single-crystal X-ray diffraction data were collected using an Oxford Diffraction Supernova dual source diffractometer equipped with a 135 mm Atlas CCD area detector. Crystals were selected under Paratone-N oil, mounted on Micromount loops and quench-cooled using an Oxford Cryosystems open flow N_2 cooling device.[3] Data were collected at 150 K using mirror monochromated Cu Kα radiation (λ = 1.5418 Å; Oxford Diffraction Supernova). Crystals of K[**4.4**]$\cdot C_6H_6$ were very small and weakly diffracting, therefore data were collected at 100 K using synchrotron radiation (λ = 0.6998 Å) at beamline I19-1 at the Diamond Light Source. Data collected were processed using the CrysAlisPro package, including unit cell parameter refinement and inter-frame scaling (which was carried out using SCALE3 ABSPACK within CrysAlisPro).[4] Equivalent reflections were merged and diffraction patterns processed with the CrysAlisPro suite.[4] Structures were subsequently solved using SHELXT 2014[5] and refined

on F^2 and against all independent reflections by full-matrix least-squares using the SHELXL 2014 package[6] and the graphical interface Olex2.[7] Distances and angles were calculated using the full covariance matrix. A small fraction of the structures was solved by Dr. Jamie Hicks, using the graphical interface X-seed,[8] the remainder was solved and refined by the author.

2.3 Computational methods

The computational work described in this thesis was carried out either by Mr. Agamemnon Crumpton, Dr. Petra Vasko, or myself. All computational work reported here was carried out at the Density Functional Theory (DFT) level, using ORCA (Revisions 5.0.1 and 5.02)[9–11] or Gaussian16 (Revision C.01).[12] The exchange correlation functionals B3LYP[13–16] and PBE0[17–19] were employed in conjunction with the Def2-SVP[20,21] and Def2-TZVP basis sets.[20,21] Most calculations include either a D3(BJ)[22,23] or D4[24] dispersion correction. Alternatively, the r2scan-3c[25] composite method was used. Some calculations (where specified) include a CPCM solvation model.[26]

NBO analyses were performed using the NBO7 programme.[27] For computational efficiency calculations were typically carried out on model systems, including some of the following simplifications: replacement of ^{t}Bu or ^{i}Pr groups with Me groups and/or omission of counter-ions.

2.4 Preparation of starting materials

Unless stated otherwise all reagents were obtained from commercial sources, and were used without further purification. Et_2O and THF were distilled from sodium and benzophenone and stored over potassium and sodium mirrors respectively. Acetonitrile, benzene, n-pentane, n-hexane, and toluene were dried using a MBraun solvent purification system, degassed by sparging with argon, and stored over 3 Å molecular sieves, sodium or potassium mirror. A solution of 12-crown-4 in toluene was dried over 3 Å molecular sieves. 2.2.2-cryptand was purified by sublimation.

NONAlI,[28] K_2[**NON**Al]$_2$,[28] **NON**GaI,[28] (CHNDipp)$_2BN_3$,[29] Ph_3CN_3,[30] K_2[**NON**Al(CO_3)]$_2$,[31] $Ag_2[C_4O_4]$[32] were prepared according to literature procedures.

Synthesis of K_2[NONGa]$_2$

K_2[**NON**Ga]$_2$ was prepared according to a modified literature procedure.[28] To a solution of **NON**GaI (500 mg, 0.57 mmol) in THF (20 mL) at –50 °C was added dropwise a precooled solution of potassium naphthalenide (160 mg, 0.9 equiv.) with constant stirring. After standing overnight, the mixture was filtered, and volatiles were removed, affording K_2[**NON**Ga]$_2$ as a yellow powder. Yield (402 mg, 89 %). NMR data match the literature values.[28]

Syntheses of Ph_3SiN_3, ^{t}BuPh$_2$SiN$_3$, ^{i}Pr$_3$SiN$_3$

A mixture of Ph_3SiCl (400 mg, 1.4 mmol) and NaN_3 (175 mg, 2.7 mmol) was suspended in acetonitrile (20 mL) and heated at 318 K for 1 d. Volatiles were removed in vacuo, and the residue extracted with hexane (40 mL), and the filtrate concentrated to ca 5 mL. Upon storing at –30 °C overnight, Ph_3SiN_3 was obtained as while crystals. Yield 350 mg, 85 %. NMR data match the literature values.[33]

^{t}BuPh$_2$SiN$_3$ was prepared in an analogous fashion. In this case, the reaction mixture was extracted with pentane, filtered, and volatiles were removed to afford ^{t}BuPh$_2$SiN$_3$ as a sticky, colourless oil. Due to the oily nature of the product the yield was difficult to define precisely, and samples were used without further purification. ^{1}H NMR (400 MHz, C_6D_6): δ 1.04 (s, 9H, ^{t}Bu), 7.09–7.17 (m, 6H, Ar-C*H*), 7.60–7.65 (m, 4H, Ar-C*H*).

^{i}Pr$_3$SiN$_3$ was prepared in a similar fashion to ^{t}BuPh$_2$SiN$_3$. ^{i}Pr$_3$SiN$_3$ is a colourless, air-sensitive liquid. Therefore the yield was difficult to define precisely, and samples were used without further purification. ^{1}H NMR (400 MHz, C_6D_6): δ 0.95 (s). No further resonances were observed in the ^{1}H NMR spectrum or could be located in a ^{1}H–^{1}H COSY NMR spectrum.

2.5 References

[1] R. E. Dodd, P. L. Robinson, *Experimental Inorganic Chemistry. A Guide to Laboratory Practice*, Elsevier, Amsterdam.

[2] R. J. Errington, *Advanced Practical Inorganic and Metalorganic Chemistry*, Blackie Academic and Professional, London.

[3] J. Cosier, A. M. Glazer, *J. Appl. Cryst.*, **1986**, *19*, 105-107.

[4] CrysAlisPro, Agilent Technologies, Version 1.171.39.46.

[5] Sheldrick, G. M. *Acta Crystallogr., Sect. A: Found. Adv.,* **2015**, *71*, 3–8.

[6] Sheldrick, G. M. *Acta Crystallogr., Sect. C: Struct. Chem.,* **2015**, *71*, 3–8.

[7] O. V. Dolomanov, L. J. Bourhis, R. J. Gildea, J. A. K. Howard, H. Puschmann, *J. Appl. Cryst.*, **2009**, *42*, 339-341.

[8] L. J. Barbour, *J. Supramol. Chem.*, **2001**, 1189–1191.

[9] F. Neese, The ORCA program system, *Wiley Interdiscip. Rev.: Comput. Mol. Sci.*, **2012**, *2*, 73–78.

[10] F. Neese, Software update: the ORCA program system, version 4.0, *Wiley Interdiscip. Rev.: Comput. Mol. Sci.*, **2017**, *8*, e1327.

[11] F. Neese, F. Wennmohs, U. Becker, C. Riplinger, The ORCA quantum chemistry program package, *J. Chem. Phys.*, **2020**, *152*, 224108.

[12] Gaussian 16, Revision C.01, M. J. Frisch, G. W. Trucks, H. B. Schlegel, G. E. Scuseria, M. A. Robb, J. R. Cheeseman, G. Scalmani, V. Barone, G. A. Petersson, H. Nakatsuji, X. Li, M. Caricato, A. V. Marenich, J. Bloino, B. G. Janesko, R. Gomperts, B. Mennucci, H. P. Hratchian, J. V. Ortiz, A. F. Izmaylov, J. L. Sonnenberg, D. Williams- Young, F. Ding, F. Lipparini, F. Egidi, J. Goings, B. Peng, A. Petrone, T. Henderson, D. Ranasinghe, V. G. Zakrzewski, J. Gao, N. Rega, G. Zheng, W. Liang, M. Hada, M. Ehara, K. Toyota, R. Fukuda, J. Hasegawa, M. Ishida, T. Nakajima, Y. Honda, O. Kitao, H. Nakai, T. Vreven, K. Throssell, J. A. Montgomery, Jr., J. E. Peralta, F. Ogliaro, M. J. Bearpark, J. J. Heyd, E. N. Brothers, K. N. Kudin, V. N. Staroverov, T. A. Keith, R. Kobayashi, J. Normand, K. Raghavachari, A. P. Rendell, J. C. Burant, S. S. Iyengar, J. Tomasi, M. Cossi, J. M. Millam, M. Klene, C. Adamo, R. Cammi, J. W. Ochterski, R. L. Martin, K. Morokuma, O. Farkas, J. B. Foresman, and D. J. Fox, Gaussian, Inc., Wallingford CT, 2019.

[13] A. D. Becke, *J. Chem. Phys.* **1993**, *98*, 5648–5652.

[14] C. Lee, W. Yang, R. G. Parr, *Phys. Rev. B*, **1988**, *37*, 785–789.

[15] S. H. Vosko, L. Wilk, M. Nusair, *Can. J. Phys.*, **1980**, *58*, 1200–1211.

[16] P. J. Stephens, F. J. Devlin, C. F. Chabalowski, M. J. Frisch, *J. Phys. Chem.*, **1994**, *98*, 11623–11627.

[17] J. P. Perdew, K. Burke, and M. Ernzerhof, *Phys. Rev. Lett.*, **1996**, *77*, 3865–3868.

[18] J. P. Perdew, K. Burke, and M. Ernzerhof, *Phys. Rev. Lett.*, **1996**, *78*, 1396.

[19] C. Adamo and V. Barone, *J. Chem. Phys.*, **1999**, *110*, 6158–6170.

[20] A. Schaefer, C. Huber, R. Ahlrichs, *J. Chem. Phys.* **1994**, *100*, 5829–5835.

[21] A. Schaefer, H. Horn, R. Ahlrichs, *J. Chem. Phys.* **1992**, *97*, 2571–2577.

[22] S. Grimme, J. Antony, S. Ehrlich, H. Krieg, *J. Chem. Phys.*, **2010**, *132*, 154104–154119.

[23] S. Grimme, S. Ehrlich and L. Goerigk, *J. Comput. Chem.* **2011**, *32*, 1456–1465.

[24] E. Caldeweyher, S. Ehlert, A. Hansen, H. Neugebauer, S. Spicher, C. Bannwarth, S. Grimme, *J. Chem. Phys.*, **2019,** *150*, 154122.

[25] S. Grimme, A. Hansen, S. Ehlert, J.-M. Mewes, *J. Chem. Phys.*, **2021**, *154*, 064103.

[26] V. Barone, M. Cossi, *J. Phys. Chem.*, **1998**, *102*, 1995–2001.

[27] NBO 7.0. E. D. Glendening, J. K. Badenhoop, A. E. Reed, J. E. Carpenter, J. A. Bohmann, C. M. Morales, P. Karafiloglou, C. R. Landis, F. Weinhold, Theoretical Chemistry Institute, University of Wisconsin, Madison, WI, **2018**.
[28] J. Hicks, P. Vasko, J. M. Goicoechea, S. Aldridge, *Nature*, **2018**, *557*, 92–95.
[29] H. Braunschweig, M. A. Celik, T. Dellermann, G. Frenking, K. Hammond, F. Hupp, H. Kelch, I. Krummenacher, F. Lindl, L. Mailänder, J. H. Müssig, A. Ruppert, *Chem. Eur. J.* **2017**, *23*, 8006.
[30] A. Hinz, R. Labbow, F. Reiß, A. Schulz, K. Sievert, A. Villinger, *Struct. Chem.*, **2015**, *26*, 1641–1650.
[31] J. Hicks, A. Heilmann, P. Vasko, J. M. Goicoechea, S. Aldridge, *Angew. Chem. Int. Ed.* **2019**, *58*, 17265–17268.
[32] J. T. Hill-Cousins, I. Pop, G. Pileio, G. Stevanato, P. Håkansson, S. S. Roy, M. H. Levitt, L. J. Brown, R. C. D. Brown, *Org. Let.*, **2015**, *17*, 2150–2153.
[33] D. Tofan, M.Temprado, S. Majumdar, C. D. Hoff, C. C. Cummins, *Inorg. Chem.* **2013**, *52*, 8851–8864

Chapter 3. Synthesis of terminal aluminium imides

3.1 Introduction

Group 13 imides are of sustained interest from a fundamental perspective, in the context of potential multiple bonding, and have possible applications as hydrogen storage materials[1–3] or as precursors to group 13 nitride semiconductors.[4] While the chemistry of group 13 imides is well developed, monomeric systems are rare.[5–9] This is due to the high polarity of M–N bonds (and the relative weakness of the π interactions), which results in a significant thermodynamic driving force for oligomerisation. Early syntheses of group 13 imides proceeded via the stepwise thermal elimination of H_2 or other small organic molecules from amine adducts, affording amides, imines, and nitrides in the process.[10]

The degree of aggregation of imide complexes was found to be controlled by the size of the substituents placed on the group 13 metal and on nitrogen (Scheme 3.1).[11,12] The use of small substituents leads to higher aggregates, with cage structures,[9,13–17] while with larger substituents trimeric and dimeric imines could be isolated.[12,17–22] These typically adopt cyclic structures, and for certain examples, degradation via ligand activation was also observed.[11] Monomeric systems ultimately could not be obtained, due to the harsh reaction conditions, and the decrease in steric shielding brought about by each successive elimination.

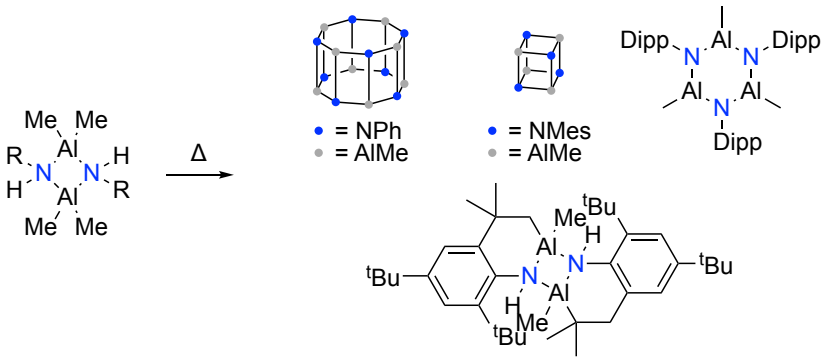

Scheme 3.1: Selected iminoalane oligomers obtained via thermolysis.

With the more recent isolation of suitable low valent group 13 precursors, the synthesis of imides via reactions with azides or other nitrene transfer reagents became a viable option. The

advantages of this approach arise from the significantly milder reaction conditions, which allow for the kinetic trapping of less stable species. Nonetheless, steric protection remains of utmost importance in order to minimise the possibilities for aggregation.

The reaction of a low valent group 13 precursor with azides commonly leads to the formation of metallotetrazenes.[23–28] Transient imides are formed, which undergo a [2+3] cycloaddition with a second equivalent of azide. Alternatively, transient imides have been shown to undergo intramolecular C–H activation,[29] oligomerisation,[19,30] or activation of the N–Si bond of a second equivalent of the azide (Figure 3.1).[24,31]

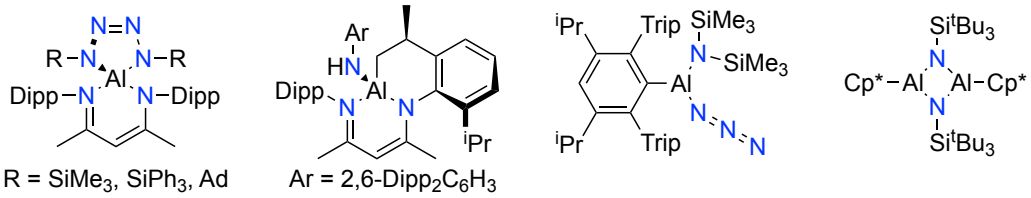

Figure 3.1: Selected products obtained from the reaction of aluminium(I) precursors with azides.

To date, nine examples of monomeric group 13 imides have been reported (Figure 3.2), however at the outset of this project only one crystallographically characterised example of a monomeric aluminium imide was known.[23,31–36]

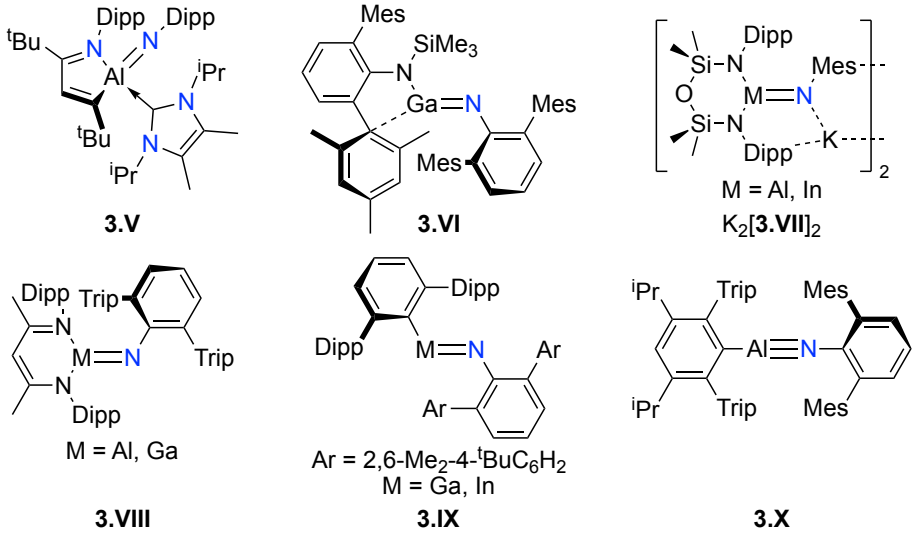

Figure 3.2: Stable group 13 imides.

All known literature examples were synthesised via the reaction of a low valent precursor with an azide, with the exception of **3.V** which is the product of a ring contraction reaction.[32] These

compounds feature short M–N_{imide} bonds and adopt a (*trans*) bent structure, except **3.X** which is linear.[31] DFT calculations suggest, that these compounds feature very polar bonds, with some degree of multiple bond character. However, the contributions of the π bonds to the overall bond energies have been calculated to be relatively low.[31,37,38]

It has previously been shown that the oxidation of aluminyl compounds with N_2O and the heavier chalcogens leads to the formation of terminal aluminium chalcogenide complexes.[39-42] Therefore we proposed at the outset that this chemistry could be extended to imides. Here the reactivity of aluminyl and gallyl reagents, K_2[**NON**M]$_2$ (M = Al, Ga), towards a range of azides is investigated, with the aim of synthesising aluminium and gallium imides.

3.2 Results and discussion

3.2.1 Synthesis

Addition of excess Me_3SiN_3 to a benzene solution of K_2[**NON**Al]$_2$ lead to rapid gas evolution and a colour change from orange to colourless. A ^{1}H NMR spectrum of the reaction mixture reveals essentially clean conversion to a single new product with signals at δ_H = 0.29 and –0.39 ppm integrating to 9H each, consistent with the uptake of two equivalents of Me_3SiN_3 per aluminium centre.

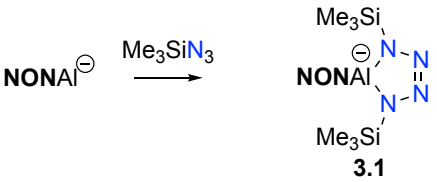

3.1

Scheme 3.2: Reaction of K_2[**NON**Al]$_2$ with excess Me_3SiN_3. Counter-ions omitted and species shown as monomeric for clarity.

Crystals suitable for single crystal X-ray diffraction were obtained upon standing overnight. The molecular structure thus obtained revealed the product to be the tetrazene complex K[**NON**Al{N_4($SiMe_3$)$_2$}], K[**3.1**]. This reaction is proposed to proceed via a transient aluminium imide which subsequently undergoes a [2+3] cycloaddition to afford the product K[**3.1**].

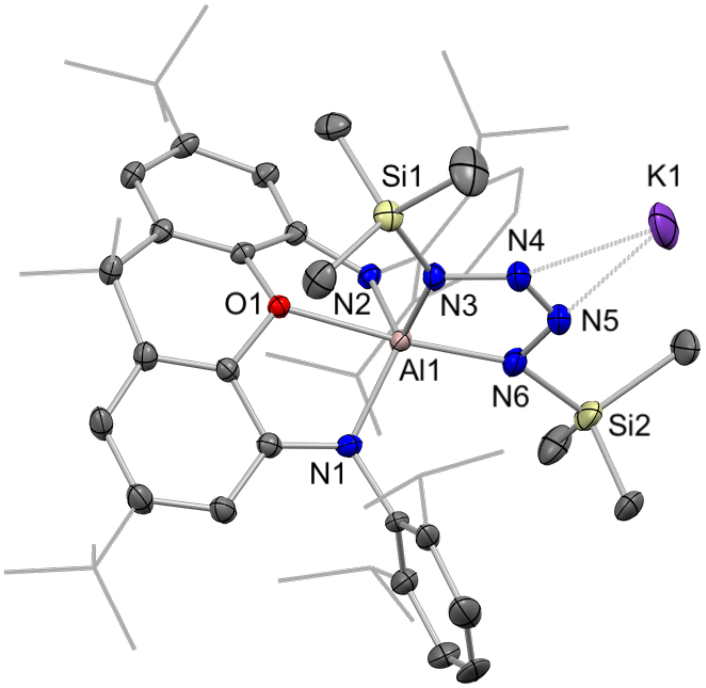

Figure 3.3: Molecular structure of K[**3.1**] as determined by X-ray crystallography. Thermal ellipsoids drawn at 30% probability, H atoms omitted, and selected groups shown in wireframe format for clarity. Key bond lengths (Å): Al1–N3 1.8862(15), Al1–N6 1.8997(15), N3–N4 1.381(2), N4–N5 1.267(3), N5–N6 1.392(3), Si1–N3 1.7441(16), Si2–N6 1.7521(16), K1–N4 2.6177(16), K1–N5 2.7972(19).

In the solid state K[**3.1**] adopts a polymeric structure, in which K^+ ions bridge between the tetrazene N atoms and the xanthene backbone. The Al1–N3 and Al1–N6 bond lengths (1.8862(15), 1.8997(15) Å) fall in the usual range for Al–N_{amido} single bonds (1.762–1.990 Å).[43] Within the planar tetrazene unit, some degree of delocalisation is observed. The outer N–N bond lengths (1.381(2), 1.392(3) Å) are somewhat short for single bonds (1.371–1.479 Å), while the central bond (1.267(3) Å) is slightly long for a double bond (1.216–1.264 Å).[44] The K1–N4 distance (2.6177(16) Å) is a shorter than the sum of covalent radii (2.74 Å).[45]

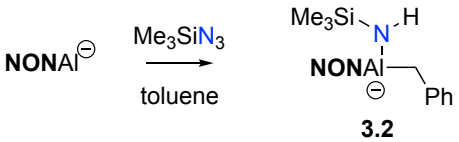

3.2

Scheme 3.3: Reaction of K_2[**NON**Al]$_2$ with 1 equivalent of Me_3SiN_3 in toluene.

In an attempt to isolate the putative imide intermediate, K_2[**NON**Al]$_2$ was reacted with 1 equivalent of Me_3SiN_3 per aluminium centre in benzene. This leads to the formation of a complex mixture of unidentified products, from which crystals of

K_6[**NON**Al(CH_2Ph)($NHSiMe_3$)]$_6$, K_6[**3.2**]$_6$ were obtained. K_6[**3.2**]$_6$ arises from the reaction of a transient imide with residual toluene (carried through from the synthesis of the aluminyl starting material). Repeating this reaction in toluene at –78 °C and warming to room temperature allows for the isolation of K_6[**3.2**]$_6$ in 23% isolated yield.

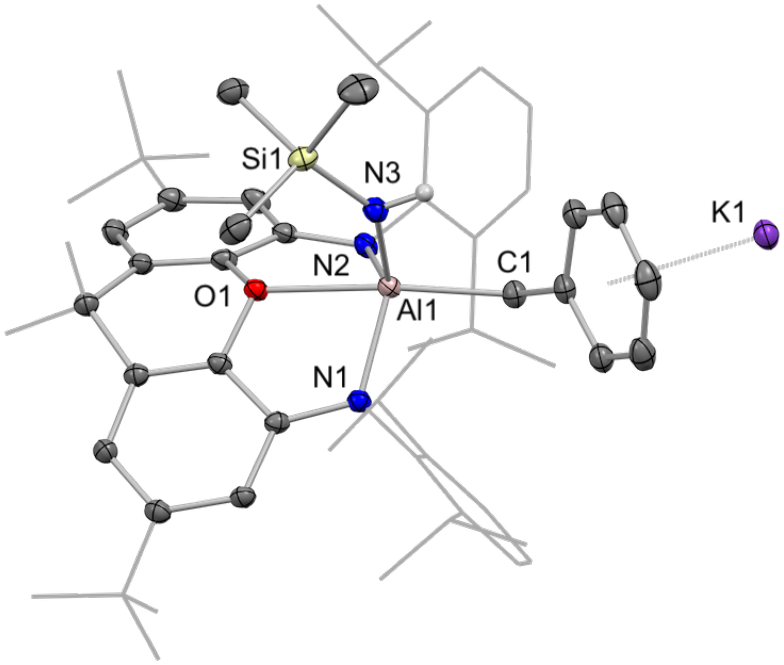

Figure 3.4: Molecular structure of K[**3.2**] as determined by X-ray crystallography. Thermal ellipsoids drawn at 30% probability, H atoms except N–H omitted, and selected groups shown in wireframe format for clarity. Key bond lengths (Å): Al1–N3 1.829(2), Al1–C1 2.052(3), N3–Si1 1.711(2).

In the solid state K_6[**3.2**]$_6$ adopts a hexameric structure, in which K^+ ions bridge between the aryl ring of the benzyl group and the xanthene backbone. The Al1–N3 (1.829(2) Å) and Al1–C1 (2.052(3) Å) distances fall within the ranges expected for Al−N_{amido} (1.871(56) Å) and Al−C (1.992(51) Å) and single bonds.[39]

At this point it seemed unlikely that the transient imide could be isolated in conjunction with this imide substituent. Therefore different organo-azides were employed in the reaction with the aluminyl starting material, to change the steric and electronic properties of the imide substituent. Initially aryl substituents were investigated, as they are less σ-donating than silyl groups, and a wide variety of aryl azides with different steric profiles are readily accessible.

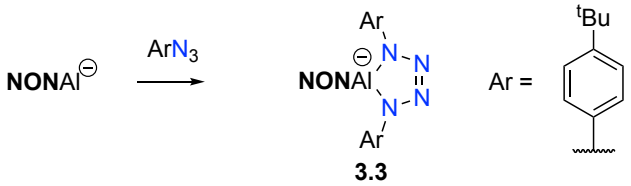

3.3

Scheme 3.4: Reaction of K_2[**NON**Al]$_2$ with excess 4-^{t}Bu$C_6H_4N_3$. Counter-ions omitted and species shown as monomeric for clarity.

The reaction of aluminyl with excess 4-^{t}Bu$C_6H_4N_3$ leads to the formation of a related tetrazene complex K_2[**NON**Al{N_4($C_6H_4{}^t$Bu)$_2$}]$_2$, K_2[**3.3**]$_2$ as the only major product. This species can be detected by ^{1}H NMR spectroscopy; in addition to the resonances associated with the NON ligand, signals integrating to 8 H are observed in the aromatic region. Even though only two ^{t}Bu signals appear in the ^{1}H NMR spectrum, ^{1}H-^{13}C correlation experiments and ^{13}C{^{1}H} data confirm the presence of three inequivalent ^{t}Bu environments, corresponding to the resonances at δ_C = 31.9, 31.7, 31.5 ppm. Crystals suitable for single crystal X-ray diffraction were obtained and the molecular structure thus obtained confirms the formulation as a tetrazene compound.

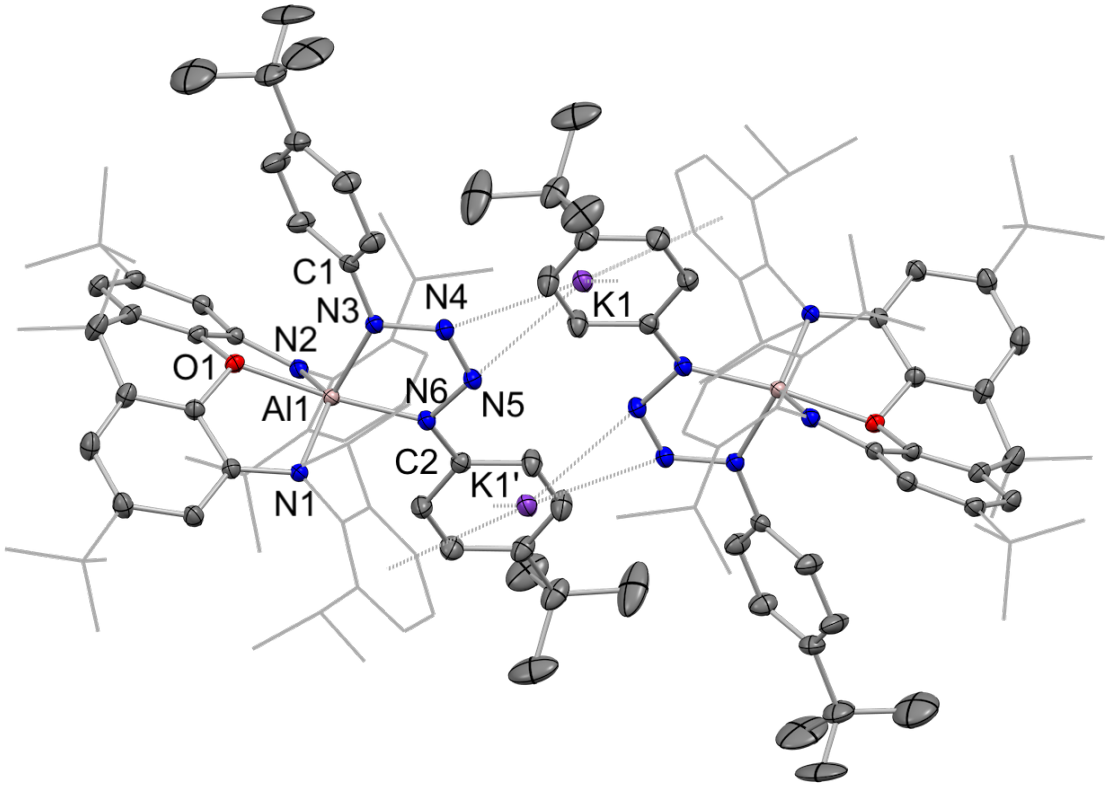

Figure 3.5: Molecular structure of K_2[**3.3**]$_2$ as determined by X-ray crystallography. Thermal ellipsoids drawn at 30% probability, H atoms omitted, and selected groups shown in wireframe format for clarity. Key bond lengths (Å): Al1−N3 1.8970(14), Al1−N6 1.9221(15), N3−N4 1.366(2), N4−N5 1.280(2), N5−N6 1.3904(19), N3−C1 1.418(2), N6−C2 1.405(2), N4−K1 2.8379(15), N5−K1 2.8758(15), N5−K1' 2.8697(16).

Unlike K[**3.1**], K[**3.3**] adopts a centrosymmetric dimeric structure in the solid state. Two formally anionic [**3.3**]$^-$ units are bridged by K^+ counter-ions. The tetrazene unit, including the aryl groups, is non planar, presumably to accommodate an interaction with the second K^+ ion. The Al–N (1.8970(14), 1.9221(15) Å) and N–N bond lengths (1.366(2), 1.280(2), 1.3904(19) Å) are similar to those of K[**3.3**], the K–N distances are however somewhat longer.

Attempts to perform this reaction stoichiometrically, lead to the formation of a mixture of two major products, alongside small amounts of K_2[**3.3**]$_2$. The major constituent of the two features a singlet ^{1}H NMR resonance at δ_H = 2.98 ppm, suggesting the presence of a N–H moiety, and therefore implies that the targeted imide was not stable.

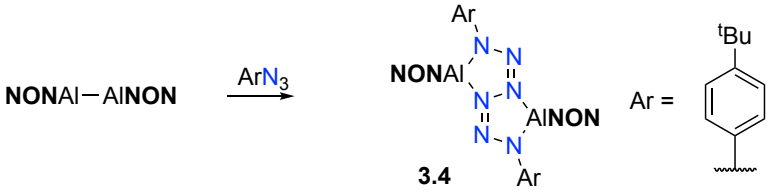

Scheme 3.5: Proposed origin of **3.4**.

On one occasion a crystal of the hexazine compound (**NON**Al)$_2${N$_6$(C$_6$H$_4$^{t}Bu)$_2$} **3.4** was obtained. This likely arises from the reaction of the [**NON**Al]$_2$ impurity in the aluminyl starting material with the azide. Analogous compounds have been obtained from the reaction of Mg(I) dimers with organoazides.

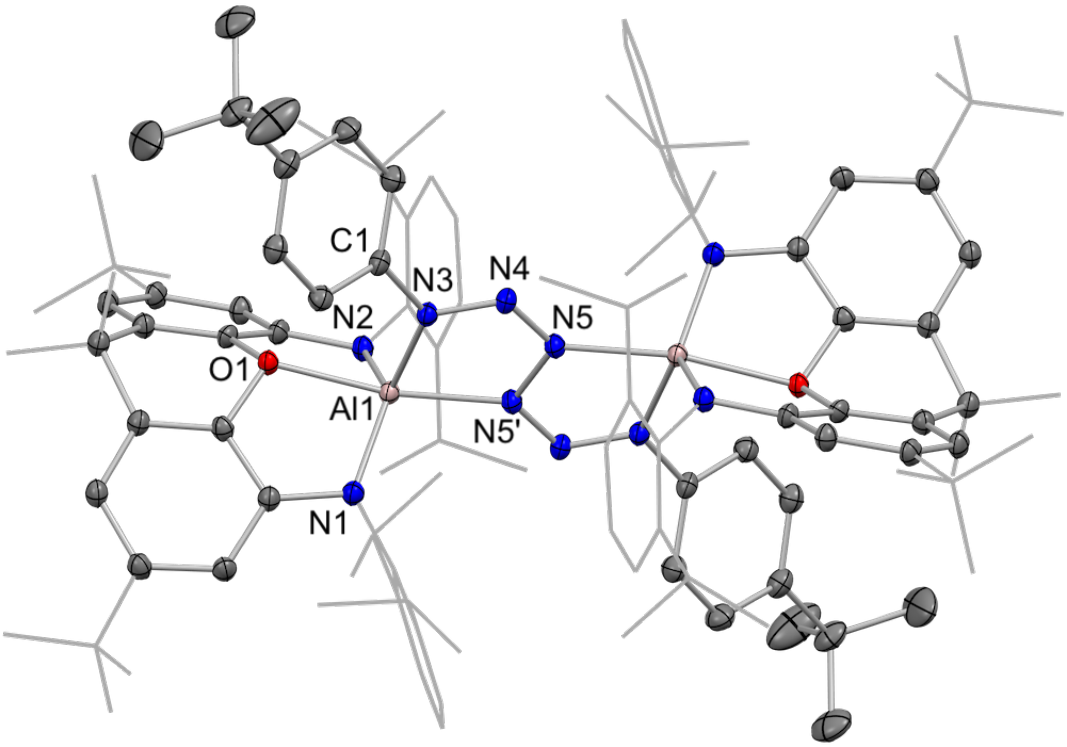

Figure 3.6: Molecular structure of **3.4** as determined by X-ray crystallography. Thermal ellipsoids drawn at 30% probability, H atoms omitted, and selected groups shown in wireframe format for clarity. Key bond lengths (Å): Al1−N3 1.954(2), Al1−N5' 2.000(2), N3−N4 1.312(3), N4−N5 1.298(3), N5−N5' 1.423(4), N3−C1 1.445(3).

In the solid state, **3.4** adopts a centrosymmetric structure. Compared to the above tetrazene complexes the Al–N bond lengths are somewhat longer. In line with other hexazine complexes, the hexazine unit is planar and has four short N–N bonds (1.312(3), 1.298(3) Å) with multiple bond character and a long central N–N single bond (1.423(4) Å).

The reaction of K_2[**NON**Al]$_2$ with $MesN_3$ invariably led to the formation of a mixture of products, which remains unchanged after heating at 80 °C for 1 d, implying that the targeted imide was not among the observed products.

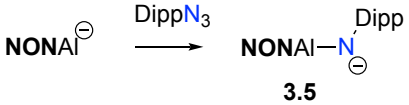

3.5

Scheme 3.6: Synthesis of K_2[**NON**AlNDipp]$_2$. Counter-ions omitted and species shown as monomeric for clarity.

However when $DippN_3$ was reacted with K_2[**NON**Al]$_2$ in benzene, clean conversion to a single new product was observed. ^{1}H NMR spectroscopy shows four resonances in the ^{i}Pr region of the spectrum at δ_H = 4.05, 3.75 (br), 3.63 (br), 2.87 ppm, integrating to a total of 6 H. This

indicates that only one equivalent of $DippN_3$ has been incorporated into the product. Crystals suitable for single crystal X-ray diffraction were obtained from a concentrated toluene solution at room temperature. The molecular structure confirmed the product to be imide K_2[**NON**AlNDipp], K_2[**3.5**]$_2$.

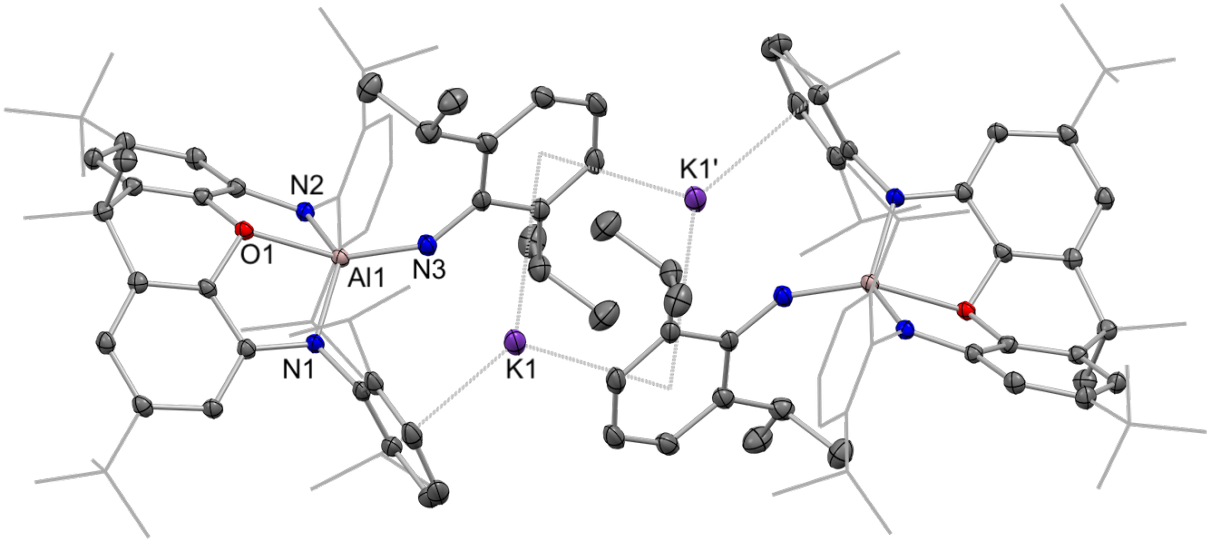

Figure 3.7: Molecular structure of K_2[**3.5**]$_2$ as determined by X-ray crystallography. Thermal ellipsoids drawn at 30% probability, H atoms omitted, and selected groups shown in wireframe format for clarity. Key bond lengths (Å) and angles (°): Al1–N3 1.723(2), N3–C1 1.346(3), N3–K1 2.739(2), Al1–N3–C1 146.43(17).

Addition of $DippN_3$ to a suspension K_2[**NON**Al]$_2$ in pentane at –78 °C does not lead to gas evolution or the disappearance of the yellow colour associated with the aluminyl at low temperatures. However upon warming to room temperature, gas evolution is observed and K_2[**3.5**]$_2$ is formed, which precipitates from solution, and can be isolated by filtration. This synthesis allows the preparation of analytically pure K_2[**3.5**]$_2$ on a gram scale, in up to 90% yield.

In the solid state K_2[**3.5**]$_2$ is a centrosymmetric dimer. Both the Al1–N3 (1.723(2) Å) and N3–C1 (1.346(3) Å) distances are significantly shorter than the corresponding bonds in the tetrazene complex K_2[**3.3**]$_2$. In the case of the N3–C1 bond this implies delocalisation of the N lone pair into the aromatic ring. The Al1–N3 bond length is among the shortest reported, supporting the notion of some degree of multiple bonding. It is, within error, identical to that observed for K_2[**3.VII^{Al}**]$_2$, and is only marginally longer than that observed for **3.V** (1.705(2) Å). The slight

lengthening compared **3.V** is presumably due to the interaction of N3 with the counter-ion. The N3–K1 distance (2.739(2) Å) is approximately equal to the sum of the respective covalent radii (2.74 Å).

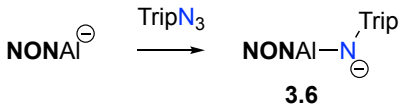

3.6

Scheme 3.7: Synthesis of K[**3.6**]. Counter-ions omitted and species shown as monomeric for clarity.

The reaction of $TripN_3$ with K_2[**NON**Al]$_2$ in benzene affords a product with a ^{1}H NMR spectrum featuring ^{i}Pr resonances at δ_H = 4.08, 3.75 (br), 3.58 (br), 2.93, 2.91 ppm, integrating to 7H. Similar resonances are observed for K_2[**3.5**]$_2$. The remaining resonances however are significantly broadened. The onward reactivity of this product (section 3.2.5) suggests that imide K[**NON**Al(NTrip)], K[**3.6**], was indeed formed.

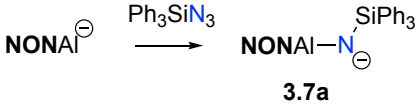

3.7a

Scheme 3.8: Synthesis of K[**3.7a**]. Counter-ions omitted and species shown as monomeric for clarity.

Having demonstrated that isolable imides can be prepared by the use of sufficiently bulky aryl groups, bulky silyl substituents were also investigated. The reaction of Ph_3SiN_3 with K_2[**NON**Al]$_2$ in benzene leads to rapid gas evolution and the disappearance of the orange colour associated with the aluminyl. The ^{1}H NMR spectrum reveals clean conversion to a single new species, and the incorporation of a single equivalent of Ph_3SiN_3 per ligand as indicated by integration of the *ortho* protons of the $SiPh_3$ group at δ_H = 7.90 ppm. Characteristic ligand resonances are observed at δ_H = 6.72, 6.40, 3.92, 2.87 ppm.

Within minutes, the imide product K[**NON**Al($NSiPh_3$)], K[**3.7a**], crystallises from solution as fine needles. These were suitable for single crystal X-ray diffraction, but diffracted only very weakly at high angle. Nonetheless the connectivity could be established unambiguously. Bond lengths and angles should however be interpreted with caution.

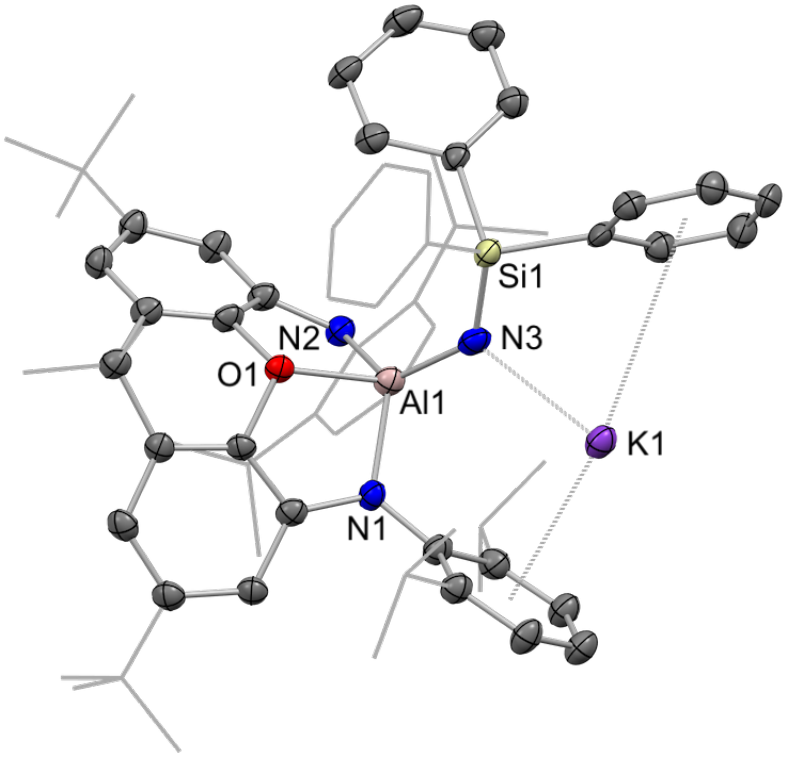

Figure 3.8: Structure of one of the two crystallographically inequivalent molecules of K[**3.7a**] as determined by X-ray crystallography. Both molecules are the same within error. Thermal ellipsoids drawn at 30% probability, H atoms omitted, and selected groups shown in wireframe format for clarity. Key bond lengths (Å) and angles (°) for both molecules: Al1–N3 1.731(6) 1.741(6), N3–Si1 1.657(6) 1.644(5), N3–K1 2.705(5) 2.711(5), Al1–N3-Si1 131.0(3) 130.8(3).

In the solid state K[**3.7a**] adopts a polymeric structure, in which K^+ counter-ions bridge between the imido functionality of one molecule and a phenyl group of the $SiPh_3$ moiety of the neighboring molecule. The asymmetric unit comprises two independent molecules, which (within error) feature identical bond lengths. Compared to K_2[**3.5**]$_2$ the Al1–N3 bond is apparentlyly longer (average 1.736(6) Å), although the difference is not statistically significant. The Al1–N3–R moiety is significantly more bent (average 130.9(3) Å), and the N–K separation is shorter (average 2.708(5) Å) than in K_2[**3.5**]$_2$. The N3–Si1 bond (average 1.651(6) Å) is among the shortest bonds reported for fragments of the type N–$SiAr_3$ and reflects on the ability of the $SiPh_3$ group to act as a π-acceptor substituent.

In an attempt to generate a more soluble imide complex, K_2[**NON**Al]$_2$ was reacted with ^{t}BuPh$_2$SiN$_3$ in pentane. Following the procedure used for K_2[**3.5**]$_2$, allows for the isolation of target imide K[**NON**Al(NSi^{t}BuPh$_2$)], K[**3.7b**], in 38% yield. The ^{1}H NMR spectrum of this

compound shows resonances at δ_H = 7.96, 6.73, 6.38, 3.82, 2.82 ppm, and hence is similar to that of K[**3.7a**]. Integration of the signal associated with the *ortho* C*H* protons confirms the incorporation of only one ^{t}BuPh$_2$Si group per ligand. Although a crystal structure could not be obtained, the onward reactivity of this compound (chapter 5) confirms that it is the targeted imide complex.

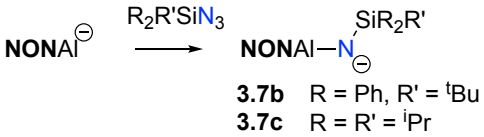

Scheme 3.9: Synthesis of K[**3.7b**] and K[**3.7c**]. Counter-ions omitted and species shown as monomeric for clarity.

Similarly, when K$_2$[**NON**Al]$_2$ is reacted with 1 equivalent of ^{i}Pr$_3$SiN$_3$ per aluminium in benzene, clean conversion to a single new species is observed by ^{1}H NMR spectroscopy. The spectrum shows characteristic resonances at δ_H = 6.66, 6.35, 4.12, 2.73 ppm for the **NON** backbone, which are similar to those observed for K[**3.7a**] and K[**3.7b**] indicating that another imide K[**NON**Al(NSi^{i}Pr$_3$)], K[**3.7c**] has been formed. Although a crystal structure could not be obtained, the onward reactivity of this compound (chapter 5) confirms that it is the desired imide complex.

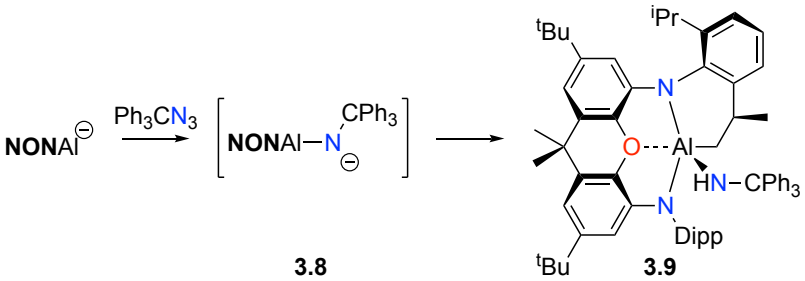

Scheme 3.10: Attempted synthesis of K[**3.8**]. Counter-ions omitted and species shown as monomeric for clarity.

In order to test the synthetic importance of the π-acceptor properties of the SiR$_3$ groups, attempts were made to synthesize an imide with a CPh$_3$ group at N. Such an imide would have a similar steric profile to K[**3.7a**], and while lacking the ability to act as an efficient π-acceptor, might be expected to stabilise the imide through the influence of a more electronegative substituent through the σ framework. Accordingly K$_2$[**NON**Al]$_2$ was reacted with Ph$_3$CN$_3$ in

benzene. The ^{1}H NMR spectrum measured *in situ* shows the formation of a complex mixture of products, including a species featuring a triplet at δ_H = –1.82 ppm with a large coupling constant of $^{n}J_{HH}$ = 13.6 Hz, a doublet of doublets at δ_H = 0.45 ppm with only one resolved coupling of $^{2}J_{HH}$ = 14 Hz, and a 1:3:4:4:3:1 multiplet with an apparent coupling of $^{n}J_{HH}$ = 6.5 Hz corresponding to a doublet of doublet of quartets with one unresolved coupling at δ_H = 3.21 ppm. These signals are likely indicative of decomposition product of the target imide, by ligand activation (Scheme 3.10). Similar signals are observed for crystallographically characterised examples (section 3.2.4 and 3.2.5) and **3.II**. It can therefore be concluded that the π-acceptor capabilities of the SiR_3 groups play an important part in stabilising the imide functional group.

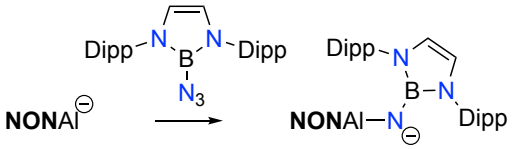

3.10

Scheme 3.11: Synthesis of K[**3.10**]. Counter-ions omitted and species shown as monomeric for clarity.

Given the diagonal relationship between boron and silicon, the possibility of synthesising boryl-substituted imides was also investigated. It was reasoned that the empty *p*-orbital on boron could stabilise the N lone pairs and thereby stabilize the reactive imide functionality both kinetically and thermodynamically. Therefore a bulky azido diazaborole was synthesised and reacted with K_2[**NON**Al]$_2$. The reaction of K_2[**NON**Al]$_2$ with ({HCDippN}$_2$)BN_3 affords the corresponding imide K[**NON**Al(NB{NDippCH}$_2$)], K[**3.10**]. The ^{1}H NMR spectrum of this reaction mixture shows that a number side products are also formed during this reaction. However K[**3.10**] can be purified by recrystallisation from benzene, allowing K[**3.10**] to be characterised by X-ray diffraction.

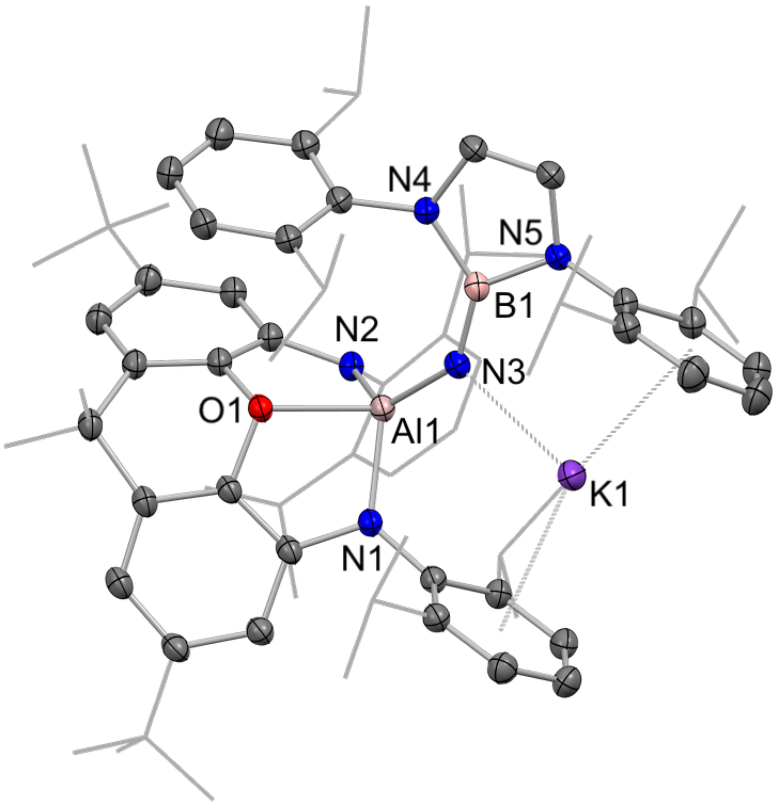

Figure 3.9: Molecular structure of K[**3.10**] as determined by X-ray crystallography. Thermal ellipsoids drawn at 30% probability, H atoms omitted, and selected groups shown in wireframe format for clarity. Key bond lengths (Å) and angles (°): Al1–N3 1.739(2), N3–B1 1.387(4), N3–K1 2.746(3), Al1–N3–B1 136.6(2).

In the solid state K[**3.10**] adopts a monomeric structure. The Al1–N3 bond is significantly longer than in K_2[**3.5**]$_2$ and within error is the same as in K[**3.7a**]. The N3–B1 bond (1.387(4) Å) is very short for a B–N bond (1.363–1.506 Å, for three-coordinate B),[39] and the second shortest example of a N atom bonded to a diazaborole unit. The Al1–N3–B1 angle (136.6(2)°) considerably more bent than in K_2[**3.5**]$_2$ but slightly wider compared to K[**3.7a**]. The N3–K1 separation is larger than in K[**3.7a**] and, within error, the same as in K_2[**3.5**]$_2$.

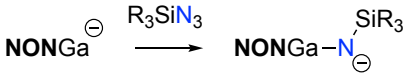

3.11a R = Ph
3.11c R = ^{i}Pr

Scheme 3.12: Synthesis of K[**3.11a**] and K[**3.11c**]. Counter-ions omitted and species shown as monomeric for clarity.

For comparison as a function of the metal, the reactions of K_2[**NON**Ga]$_2$ and similar azides were also investigated. These efforts were complicated by the fact that bulk samples of K_2[**NON**Ga]$_2$ are difficult to obtain free from contamination by a number of species, including

NONGaI, **NON**K_2, THF, and naphthalene. While attempts to react K_2[**NON**Ga]$_2$ with $DippN_3$ leads to a mixture of products, the reaction of K_2[**NON**Ga]$_2$ with excess $^iPr_3SiN_3$ leads to the formation of a single new product, K[**NON**Ga(NSi^{i}Pr$_3$)] (K[**3.11c**]), which exhibits an ^{1}H NMR spectrum is remarkably similar to that observed for K[**3.7c**]. Characteristic resonances are observed in the ^{1}H NMR spectrum at δ_H = 6.69, 6.40, 4.09, 2.73 ppm. The onward reactivity of K_2[**3.7c**]$_2$ (section 5.2.2) suggests that this product is indeed the desired imide complex.

An isolable gallium imide can be obtained from the reaction of K_2[**NON**Ga]$_2$ with Ph_3SiN_3. Carrying out this reaction in hexane allows for the isolation of imide K[**NON**Ga(NSiPh_3)], K[**3.11a**], in moderate yields. The ^{1}H spectrum is remarkably similar to that obtained for K[**3.7a**], and this compound also crystallises from benzene as fine needles, hinting that K[**3.7a**] and K[**3.11a**] are isostructural. Attempts to obtain a crystal structure were unsuccessful as crystals of K[**3.11a**] were found to be very weakly diffracting. This reaction was first performed by Part 2 student Artemis Saddington, however no high quality spectroscopic data could be collected.

3.2.2 Probes of the electronic structure of imide complexes by DFT

The electronic structure of selected imides was investigated by DFT calculations. The full anions [**3.5**]$^-$, [**3.7a**]$^-$, [**3.7c**]$^-$, [**3.8**]$^-$, [**3.10**]$^-$ and [**3.11a**]$^-$ were optimised using the r2scan-3c method, and subsequently analysed using the NBO7 program. Calculated bond lengths are in reasonable agreement with those obtained from single crystal X-ray diffraction experiments, although small deviations in bond angles arise due to the omission of the counter-ions. Upon inclusion of the counter-ions excellent agreement between the calculated and observed structures can be obtained. The results of these efforts are detailed towards the end of this chapter. Here counter-ions are omitted to assess to what extent the various substituents stabilise the imides electronically, without taking into account effects arising from distortions upon binding of the counter-ion. Importantly, inclusion of the counter-ions for selected examples did not significantly change any of the trends discussed in this section.

Table 3.1: Calculated HOMO and HOMO-1 for the imide anions.

	Geometry	HOMO	HOMO-1
[**3.5**]$^-$ [**NON**Al(NDipp)]$^-$	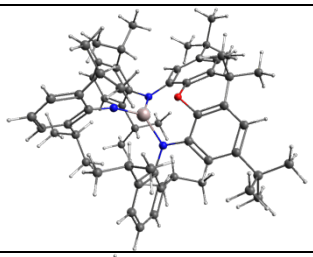	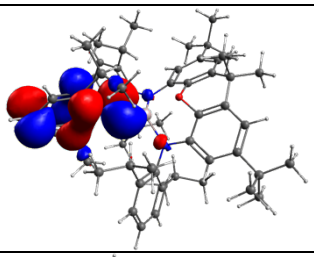	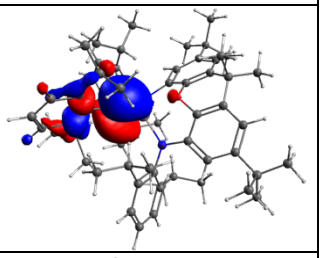
[**3.10**]$^-$ [**NON**Al(NB{NDippCH}$_2$)]$^-$	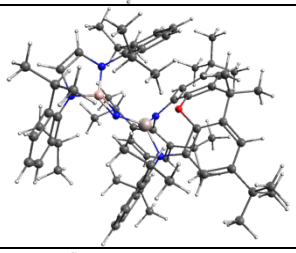	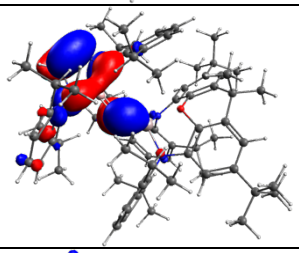	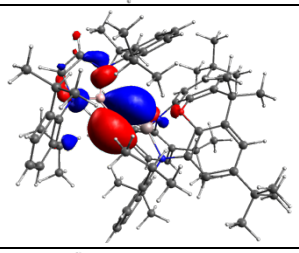
[**3.7c**]$^-$ [**NON**Al(NSi^{i}Pr$_3$)]$^-$	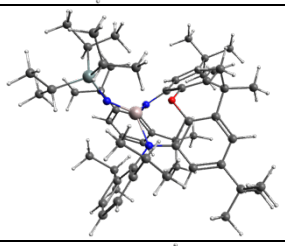	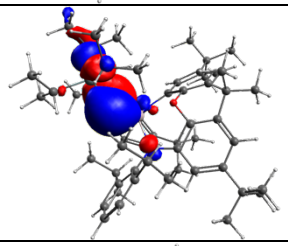	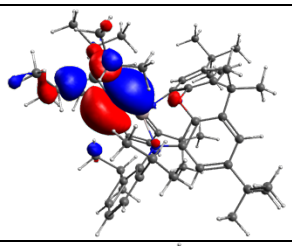
[**3.7a**]$^-$ [**NON**Al(NSiPh$_3$)]$^-$	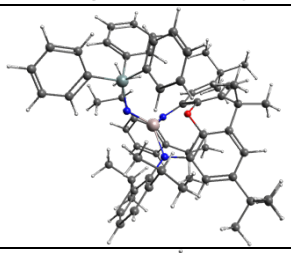	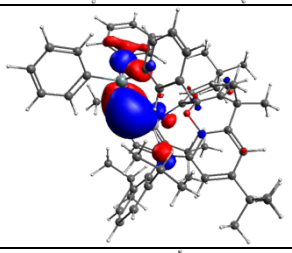	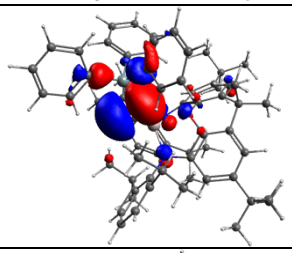
[**3.11a**]$^-$ [**NON**Ga(NSiPh$_3$)]$^-$	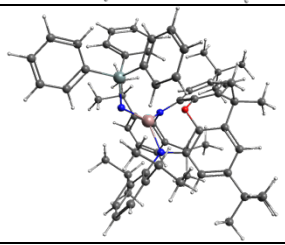	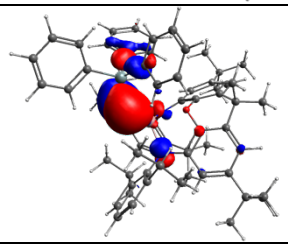	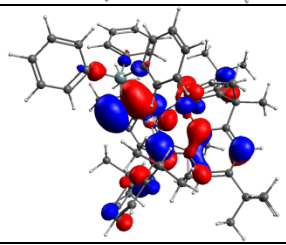
[**3.8**]$^-$ [**NON**Al(NCPh$_3$)]$^-$	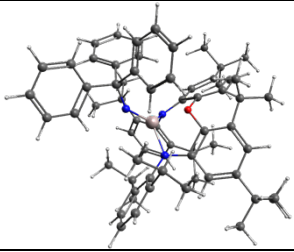	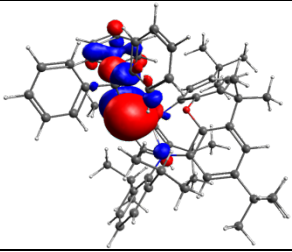	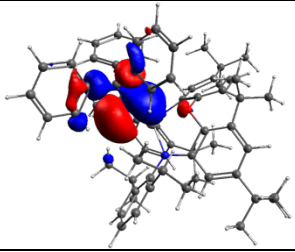

In all cases, the HOMO and HOMO-1 represent a set of orthogonal *p*-orbitals on the imide N atom. The HOMO is aligned parallel the plane of the plane of the NON ligand, while the HOMO-1 is aligned perpendicular to the plane. In the case of [**3.10**]$^-$ however, the orbitals align with the plane of the boryl group. Further, the HOMO of [**3.5**]$^-$ and [**3.10**]$^-$ features additional

contributions from the heterocycles attached to N, and the HOMO-1 of [**3.11a**]$^-$ features additional contributions from the xanthene moiety. Low lying unoccupied orbitals are largely ligand based. Table 3.1 summarises the selected orbital energies, NPA charges, and the Wiberg Bond indices for the M–N_{imide} and N_{imide}–R bonds.

Table 3.2: Selected calculated properties for imide anions in the gas phase.

	Orbital Energies / eV		NPA Charge / e		Wiberg Bond Index	
	HOMO	HOMO -1	N_{imide}	M	M-N	N-R
[**3.5**]$^-$ [**NON**Al(NDipp)]$^-$	-0.5236	-1.2536	-1.2830	1.9989	0.7025	1.3614
[**3.10**]$^-$ [**NON**AlN(B{NDippCH}$_2$)]$^-$	-0.8890	-1.5241	-1.6580	2.0869	0.6265	1.3020
[**3.7c**]$^-$ [**NON**Al(NSi^{i}Pr$_3$)]$^-$	-1.0876	-1.3758	-1.9819	2.0945	0.6399	0.8737
[**3.7a**]$^-$ [**NON**Al(NSiPh$_3$)]$^-$	-1.5483	-1.9747	-1.9191	2.1267	0.5876	0.9568
[**3.11a**]$^-$ [**NON**Ga(NSiPh$_3$)]$^-$	-1.6667	-2.1301	-1.8096	1.9037	0.7356	0.9341
[**3.8**]$^-$ [**NON**Al(NCPh$_3$)]$^-$	-0.7878	-1.1603	-1.4089	2.098	0.6217	1.1208

The Wiberg bond indices are low for the M–N_{imide} bonds, however they are much larger than the indices for the M-N_{ligand} bonds (0.3–0.4). This qualitatively mimics the analysis reported for K[**3.VII^{Al}**]. Calculations of partial charges show considerable negative charge on N_{imide} and a large positive charge on the metal. Similar charges have been reported for **3.V** and K[**3.VII^{Al}**]. This suggests that the M–N_{imide} bonds are best described as highly polarised single bonds, with considerable ionic character, and only a small amount of multiple bond character.

The N-bound substituents have different effects on the electronic structure of the imide complexes. [**3.5**]$^-$ and [**3.10**]$^-$ have HOMOs that are delocalised over the N_{imide} and the attached aromatic ring. This delocalisation is reflected in the larger WBIs for the N–R bonds, and smaller negative charges on N_{imide} compared to the silyl examples. The latter, however, presumably

also reflects on the polarity of the N–Si bond. Despite the delocalisation, the HOMO energies are higher compared to the silyl substituted systems, primarily due to the orbital interactions with filled ring orbitals. The silyl substituted imides cannot stabilise the imide by delocalisation, however Si-C σ* orbitals can act as acceptor orbitals. This is more effective for the $SiPh_3$ groups, where the antibonding orbitals are presumably lower in energy. The negative charge primarily remains on N_{imide}, however the HOMO energies are lower compared to [**3.5**]$^-$ and [**3.10**]$^-$. Further moving from [**3.7a**]$^-$ to its gallium analogue [**3.11a**]$^-$ seems to lead to further stabilisation of the imide, as evidenced by a higher WBI and smaller partial charges. This can be attributed in part to the greater electronegativity of Ga compared to Al, leading to more covalent bonding in this compound.

3.2.3 Stability studies

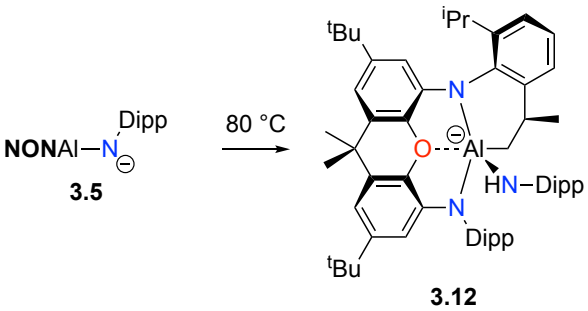

Scheme 3.13: Thermal decomposition of K_2[**3.5**]$_2$. Counter-ions omitted and species shown as monomeric for clarity.

Benzene solutions of K_2[**3.5**]$_2$ do not show signs of decomposition at room temperature over the course of 2 weeks, and this compound is stable in the solid state for at least 1 month. Decomposition is however observed upon heating at 80 °C, and slow formation of a new highly unsymmetrical species is observed by ^{1}H NMR with features a pseudo triplet at $\delta_H = -1.28$ ppm with a coupling constant of $^nJ_{HH} = 13.5$ Hz. This data is consistent with the formation of the self-activation product K[**3.12**]. Although a crystal structure was not be obtained per se, the structure of the closely related derivative [K(crypt)][**3.12**] could be collected. The pseudo triplet at $\delta_H = -1.28$ ppm corresponds the one of the protons of the Al-CH_2 group and has $^2J_{HH}$ and $^3J_{HH}$ coupling of the same magnitude. The $^3J_{HH}$ coupling is large, as the dihedral angle between

the two protons is close to 180° (179.6° for [K(crypt)][**3.12**]). Interestingly ligand activation of the same type is also observed when K_2[**3.5**]$_2$ is heated in toluene. This is a contrast to earlier findings, in which a transient $SiMe_3$ substituted imide gave rise to the toluene activation product K_6[**3.2**]$_6$ in the presence of the same solvent. Presumably the greater steric protection in the case of K_2[**3.5**]$_2$ disfavours an intermolecular reaction. In THF K_2[**3.5**]$_2$ gives rise to a deep blue solution, possibly indicating the formation of a separated ion pair, and after 4 days under these conditions, traces of the ligand activation product are observed. This suggests that the stability of K_2[**3.5**]$_2$ might in part arise from the dimeric nature of this compound. It has previously been shown for K_2[**NON**Al]$_2$ that the dimeric structure is retained in arene solution.

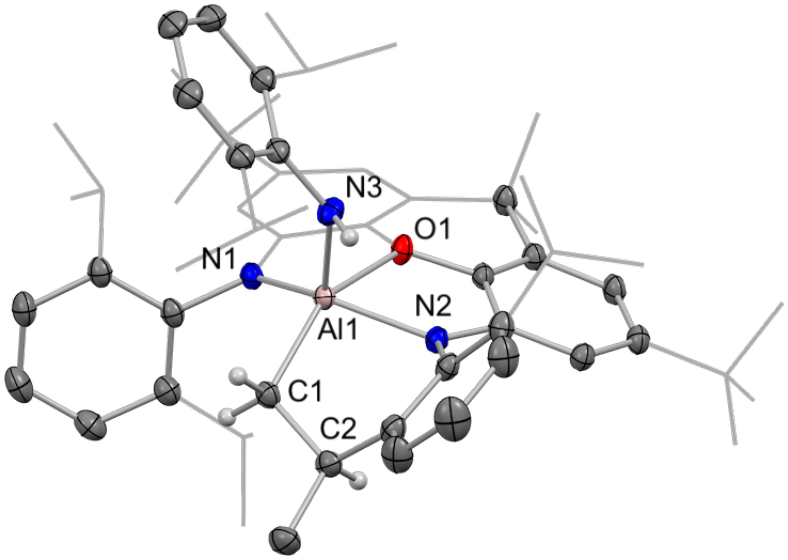

Figure 3.10: Molecular structure of [K(crypt)][**3.12**] as determined by X-ray crystallography. Thermal ellipsoids drawn at 30% probability, selected H atoms and counter-ion omitted, and selected groups shown in wireframe format for clarity. Key bond lengths (Å): Al1–N3 1.8717(14), Al1–C1 2.0145(15).

Unlike K_2[**3.5**]$_2$, spectra of the $SiPh_3$ substituted compound K[**3.7a**] are invariably contaminated with traces of an analogous decomposition product K[**3.13**]. As soon as K[**3.7a**] is dissolved in benzene, a diagnostic pseudo triplet starts to grow in at δ_H = –1.45 ppm ($^nJ_{HH}$ = 13.7 Hz). Similarly K[**3.7a**] undergoes self-activation in the solid state over the course of several months.

Similarly, upon storing a benzene solution of K[**3.8**] overnight at room temperature, a new triplet at $\delta_H = -1.75$ ppm ($^nJ_{HH} = 13.8$ Hz) was observed. After 1 week, approximately 70 % of the starting material has decomposed via self-activation.

Attempts to dissolve K[**3.7a**] in THF lead briefly to the formation of deep green solution, which decolourised quickly. This indicated that a reaction had taken place. Crystals of product reveal it to be the solvent activation product K[**3.14**], formed via formal deprotonation of a THF molecule in the α position.

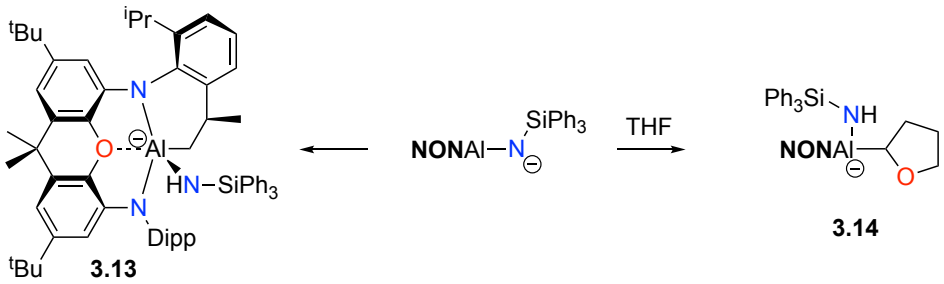

Scheme 3.14: Thermal decomposition of K_2[**3.7a**]$_2$ and reactivity towards THF. Counter-ions omitted and species shown as monomeric for clarity.

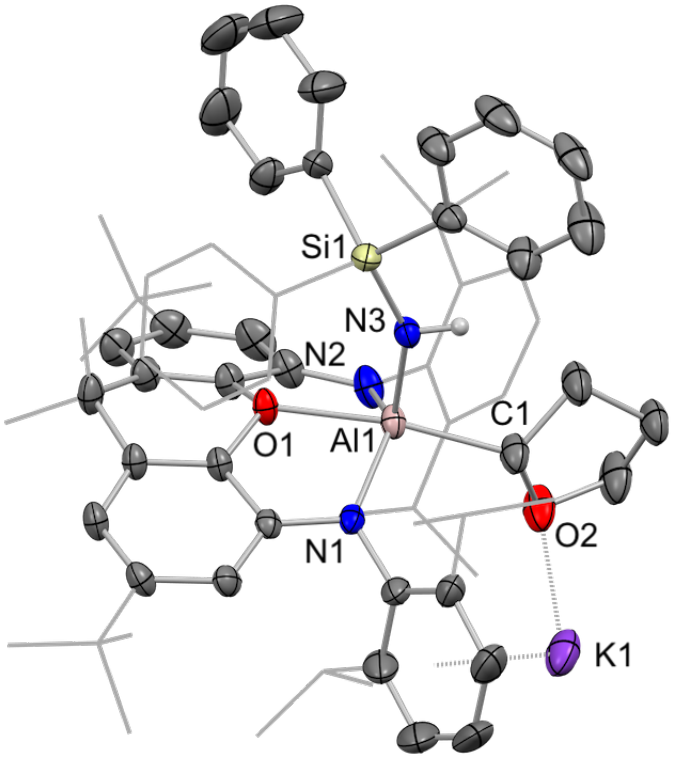

Figure 3.11: Molecular structure of K[**3.14**] as determined by X-ray crystallography. Thermal ellipsoids drawn at 30% probability, selected H atoms and counter-ion omitted, and selected groups shown in wireframe format for clarity. Key bond lengths (Å): Al1–N3 1.871(3), Al1–C1 2.044(4), N3–Si1 1.691(3).

3.2.4 Reaction of imide complexes with 2.2.2-cryptand

Attempts to obtain a "true" terminal imide of the form [K(crypt)][**NON**MNR] (M = Al, Ga) had limited success. The reaction of K_2[**3.5**]$_2$ with 2.2.2-cryptand in a variety of solvents allows for the formation of [K(crypt)][**3.5**]. This compound is blue and stable for at least 12 h at room temperature. Attempts to obtain crystals of this compound, however, were unsuccessful due to its high sensitivity, and a tendency to form oils. Upon standing for several days crystals of the C-H activation product [K(crypt)][**3.10**] formed within the oil.

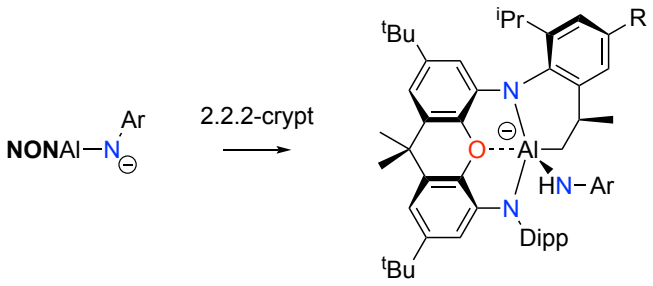

K_2[**3.5**]$_2$ Ar = Dipp
K[**3.6**] Ar = Trip

[K(crypt)][**3.12**] R = H
[K(crypt)][**3.15**] R = ^{i}Pr

Scheme 3.15: Attempted synthesis of [K(crypt)][**3.5**] and [K(crypt)][**3.6**]. Counter-ions omitted and species shown as monomeric for clarity.

To circumvent the problems of the product forming oils, K[**3.6**] was instead reacted with 2.2.2-cryptand in benzene. Unfortunately attempts to obtain crystals of [K(crypt)][**3.6**] only resulted in the isolation of C–H activation product [K(crypt)][**3.15**].

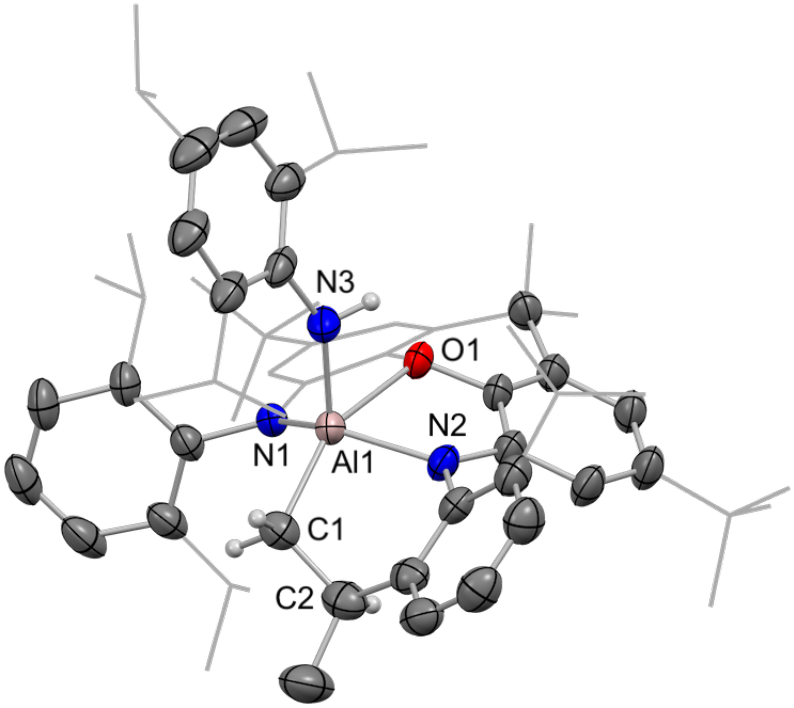

Figure 3.12: Molecular structure of [K(crypt)][**3.15**] as determined by X-ray crystallography. Thermal ellipsoids drawn at 30% probability, selected H atoms and counter-ion omitted, and selected groups shown in wireframe format for clarity. Key bond lengths (Å) and angles (°): Al1–N3 1.889(3), Al1–C1 2.017(4), H–C1–C2–H –171.40 and 70.18.

When K[**3.7a**] was reacted with 2.2.2-cryptand in benzene a mixture of compounds was observed, in addition to a minor resonance at δ_H = –0.33 ppm ($^nJ_{HH}$ = 12.5 Hz). The major species features characteristic peaks at δ_H = 8.19, 6.66, 6.48, 4.67, 3.13, and is assigned [K(crypt)][**3.7a**]. Upon standing overnight the major species oils out of solution. This oil was isolated by decanting and volatiles were removed. Upon dissolution in THF, one major species was observed by ^{1}H NMR spectrum, whose spectrum is consistent with C–H activation product [K(crypt)][**3.13**].

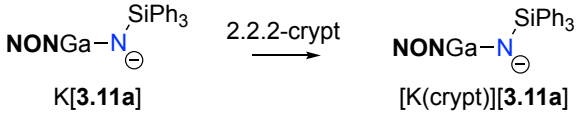

K[**3.11a**] [K(crypt)][**3.11a**]

Scheme 3.16: Synthesis of [K(crypt)][**3.11a**]. Counter-ions omitted and species shown as monomeric for clarity.

Gratifyingly, the reaction of gallium imide K[**3.11a**] reacts cleanly with 2.2.2-cryptand in benzene, to afford [K(crypt)][**3.11a**]. This compound is colourless, stable and remains in solution, exhibiting resonances in the ^{1}H NMR spectrum at δ_H = 7.92, 6.70, 6.38, and 4.01 ppm.

As such the spectra of [K(crypt)][**3.11a**] and [K(crypt)][**3.7a**] are somewhat similar. Another interesting spectroscopic feature of [K(crypt)][**3.11a**] is the $^{13}C\{^{1}H\}$ NMR resonances for the $SiPh_3$ group. These appear at δ_C = 150.6, 136.7, 126.5, 125.6 ppm, and especially the *ipso* carbon resonance is vastly different from the resonances usually observed for $SiPh_3$ groups, while closely resembling the resonances observed for $[Ph_3SiNCa\cdot THF]_4$ (δ_C = 150.6 (*i*), 135.9 (*o*), 128.3 (*m*), 127.7 (*p*)). This provides support for the notion that in these types of compound the M–N bond is highly polarised.

3.2.5 Mechanism of thermal decomposition

Given that the apparent stabilities of the various imides, with regards to self-activation do not correlate well with any of the properties of the free anions in the gas phase, the electronic structures of K[**3.5**], $[K(C_6H_6)]$[**3.7a**], $[K(C_6H_6)]$[**3.8**], and K[**3.10**] were calculated using the r2scan-3c method, and the barrier for decomposition via C–H activation was determined. In the case of K_2[**3.5**]$_2$ only half of the dimer was calculated, resulting a good geometrical agreement with the measured structure. For $[K(C_6H_6)]$[**3.7a**] it was necessary to include a molecule of benzene to match the geometry determined crystallographically. The same geometry was assumed for $[K(C_6H_6)]$[**3.8**].

Compared to the free anions, the morphologies of the HOMOs remain largely unchanged; the orbitals are stabilized as expected by the presence of the counter-cation. As expected the WBIs for the Al–N bonds drop, although not to the same extent for all imides. The HOMO energies and WBIs for the Al–N bond are summarised in Table 3.3.

Table 3.3: HOMO energies and WBIs for selected imides, including counter-ions.

	E (HOMO) / eV	WBI (Al–N)
K[**3.5**], K[**NON**Al(NDipp)]	-3.5505	0.6314
[K(C_6H_6)][**3.7a**], [K(C_6H_6)][**NON**Al($NSiPh_3$)]	-4.2910	0.5518
K[**3.10**], K[**NON**AlN(B{NDippCH}$_2$)]	-3.4069	0.5579
[K(C_6H_6)][**3.8**], [K(C_6H_6)][**NON**Al($NCPh_3$)]	-3.6338	0.5916

For the model systems, the barriers for intramolecular C–H activation were calculated. The results are listed in Table 3.4. The transition states were found to correspond to deprotonation of the methyl group. The calculated values for $\Delta G^{\ddagger}$ fall in the 22–28 kcal mol^{-1} range, and follow the trend observed experimentally. However the difference between the individual barrier heights is perhaps not as pronounced as expected. Comparing $\Delta H^{\ddagger}$ and $\Delta G^{\ddagger}$ it becomes apparent, that the entropy contributions are small, except in the case of K[**3.5**]. This can be traced back to a larger difference in geometry between the reagent and the transition state, compared to the other imides, which can be considered to be preorganised. The lowest energy conformation of K[**3.5**] features the flanking Dipp groups oriented approximately perpendicular to the plane of the xanthene backbone, while for the remaining imides, the flanking Dipp groups are not perpendicular to the plane of the xanthene backbone. This places one ^{i}Pr group in close proximity to the N_{imide}, which is a feature observed in the geometry of the transition states. The different ground state geometries of K[**3.5**] and the remaining imides are primarily a result of the different steric demands of the imide substituents, but are also further enforced by the varying coordination modes of the K^+ counter-ions. As such both the basicity of the imide functionality and the degree of preorganisation together determine the ease with which these compounds decompose.

Table 3.4: Barriers for intramolecular C–H activation of the ligand.

	$\Delta H^{\ddagger}$ / kcal mol^{-1}	$\Delta G^{\ddagger}$ / kcal mol^{-1}
K[**3.5**]	24.7	27.8
[K(C_6H_6)][**3.7a**]	24.7	25.4
K[**3.10**]	24.0	25.4
[K(C_6H_6)][**3.8**]	20.5	22.0
[**3.11a**]$^{-}$	24.8	26.0

3.2.6 Reactions of aluminium imides with H_2

Given the ability of the aluminium imides to activate C–H bonds, their reactivity towards H_2 was also investigated. To this end K_2[**3.5**]$_2$ and K[**3.7a**] were reacted with H_2 in an attempt to synthesise the respective amido complexes. Heating a benzene solution of K_2[**3.5**]$_2$ under H_2 (1 bar) at 80 °C for 16 h leads to complete consumption of K_2[**3.5**]$_2$, and the formation of crystals, in ca 50 % yield. Upon dissolution in THF, ^{1}H NMR spectroscopy confirmed the formation of K_2[**NON**Al(H)NHDipp]$_2$, K_2[**3.16**]$_2$. This compound was previously synthesised from K_2[**NON**Al]$_2$ and the corresponding aniline.

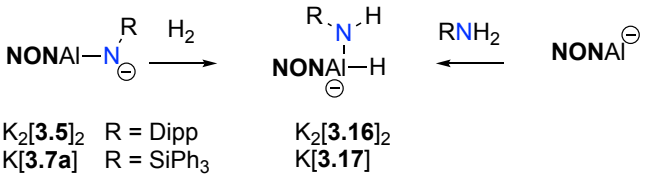

Scheme 3.17: Syntheses of K_2[**3.16**]$_2$ and K[**3.17**].

The reaction of K[**3.7a**] with H_2 (2 bar) in benzene proceeds cleanly in over the course of 1 week at room temperature, to afford K_2[**NON**Al(H)($NHSiPh_3$)]$_2$, K[**3.17**], as the only major product. The same compound is also obtained from the reaction of K_2[**NON**Al]$_2$ and Ph_3SiNH_2 in benzene. As such, H_2 activation by both imide complexes is confirmed.

3.3 Conclusions

The reactions of K_2[**NON**Al]$_2$ and K_2[**NON**Ga]$_2$ with a range of aryl-, silyl-, and boryl- azides were investigated. In the case of azides with small substituents, reactions with two equivalents

of azide afforded tetrazene complexes, while attempts to react the aluminyl precursor with 1 equivalent of Me_3SiN_3 afforded a toluene activation product. Both types of reactions are proposed to proceed via transient imide intermediate. Isolable imides can be obtained when bulky azides are employed. While Dipp-substituted K_2[**3.5**]$_2$ is stable for a least two weeks in benzene solution or the solid state, silyl substituted K[**3.7a**] and trityl-substituted K[**3.8**] undergo decomposition via C–H bond activation of the ligand. Attempts to synthesise stable "free" terminal imides via addition of 2.2.2-cryptand were ultimately only successful for gallium imide [K(crypt)][**3.9a**]. ^{1}H NMR also suggests that [K(crypt)][**3.5**] and [K(crypt)][**3.6**] can be formed cleanly, however these compounds have a tendency to form oils in compatible solvents, and their decomposition could not be monitored by NMR. Unfortunately no crystal structures for any of the cation-sequestered imides could be obtained. The reactions of K_2[**3.5**]$_2$ and K[**3.7a**] with H_2 confirm that the imides are correctly formulated as such, and rules out a possible misidentification of amido hydride complexes, which are the products of the onward reactions with dihydrogen. DFT calculations on selected gas phase anions, show that the HOMO and HOMO-1 orbitals correspond to a set of orthogonal p-orbitals on the imide N atom, while the low-lying unoccupied orbitals are localised on the ligand. NPA analysis reveals significantly positive partial charge on the metal and a very negative partial charge on the imide N atom. The WBI is much less than 1 for all imides, but is still considerably larger (almost double) the WBIs of the M-N_{ligand} bonds. Therefore the M-N_{imide} bond is best described as highly polarised single bond with limited multiple bond character.

3.4 Experimental details

K[NONAl{N_4($SiMe_3$)$_2$}], K[3.1]

To a solution of K_2[(**NON**)Al]$_2$ (200 mg, 0.14 mmol) in toluene (25 mL) was added Me_3SiN_3 (79 μL, 0.59 mmol). This lead immediately to gas evolution and a colour change from yellow to colourless. Yield 100 mg, 40% (>90% by NMR).

^{1}H NMR (500 MHz, THF-d_8): δ -0.75 (s, 9H, Si(CH_3)$_3$), 0.02 (s, 9H, Si(CH_3)$_3$), 0.78 (d, $^{3}J_{HH}$ = 6.8 Hz, 6H, CH(CH_3)$_2$), 0.90 (d, $^{3}J_{HH}$ = 6.8 Hz, 6H, CH(CH_3)$_2$), 0.96 (d, $^{3}J_{HH}$ = 6.8 Hz, 6H, CH(CH_3)$_2$), 1.07 (s, 18H, C(CH_3)$_3$), 1.22 (d, $^{3}J_{HH}$ = 6.8 Hz, 6H, CH(CH_3)$_2$), 1.60 (s, 3H, C(CH_3)$_2$), 1.74 (s, 3H, C(CH_3)$_2$), 3.34 (sept, $^{3}J_{HH}$ = 6.8 Hz, 2H, CHMe$_2$), 3.64 (sept, $^{3}J_{HH}$ = 6.8 Hz, 2H, CHMe$_2$), 5.52 (d, $^{4}J_{HH}$ = 1.9 Hz, 2H, XA-Ar-CH), 6.43 (d, $^{4}J_{HH}$ = 1.9 Hz, 2H, XA-Ar-CH), 6.99 – 7.08 (m, 6H, Dipp-Ar-CH).

^{13}C{^{1}H} NMR (126 MHz, THF-d_8): δ 1.9 (Si(CH$_3$)$_3$), 3.3 (Si(CH$_3$)$_3$), 24.8 (CH(CH$_3$)$_2$), 25.5 (CH(CH$_3$)$_2$), 25.5 (C(CH$_3$)$_2$), 27.2 (CH(CH$_3$)$_2$), 27.2 (CH(CH$_3$)$_2$), 27.9 (CHMe$_2$), 29.5 (CHMe$_2$), 32.2 (C(CH$_3$)$_3$), 33.2 (C(CH$_3$)$_2$), 35.5 (CMe$_3$), 37.3 (CMe$_2$), 104.8 (XA-Ar-CH), 111.1 (XA-Ar-CH), 124.0 (Dipp-*m*-*C*), 124.7 (Dipp-*m*-*C*), 125.2 (Dipp-*p*-*C*), 131.0 (Me$_2$C*C*), 140.0 (*C*O), 145.6 (XA-N*C*), 146.5 (*C*^{t}Bu), 147.0 (Dipp-*i*-*C*), 147.9 (Dipp-*o*-*C*), 149.4 (Dipp-*o*-*C*).

K$_6$[NONAl(NHSiMe$_3$)CH$_2$Ph]$_6$, K$_6$[3.2]$_6$

To a solution of K$_2$[(**NON**)Al]$_2$ (200 mg, 0.27 mmol) in toluene (20 mL) was added Me$_3$SiN$_3$ (36 μL, 0.27 mmol) dropwise at room temperature. The resulting mixture was stirred until no more gas evolution was observed, then concentrated to a quarter of its original volume. Upon standing overnight, colourless crystals of formed. Yield 56 mg, 23%. Anal. Calc. for C 74.70 %, H 8.69 %, N 4.59 %, found: C 74.55 %, H 8.84 %, N 4.44 %.

^{1}H NMR (500 MHz, THF-d_8): δ -0.35 (s, 1H, NH), -0.22 (s, 9H, Si(CH_3)$_3$), 0.84 (d, $^{3}J_{HH}$ = 6.7 Hz, 6H, CH(CH_3)$_2$), 0.90 (d, $^{3}J_{HH}$ = 6.8 Hz, 6H, CH(CH_3)$_2$), 0.91 (d, $^{3}J_{HH}$ = 6.8 Hz, 6H, CH(CH_3)$_2$), 0.96 (s, 2H, CH_2Ph), 1.08 (s, 18H, C(CH_3)$_3$), 1.26 (d, $^{3}J_{HH}$ = 6.9 Hz, 6H, CH(CH_3)$_2$), 1.54 (s, 3H, C(CH_3)$_2$), 1.73 (s, 3H, C(CH_3)$_2$), 3.61 (sept, $^{3}J_{HH}$ = 6.8 Hz, 2H, CHMe$_2$), 4.16 (sept, $^{3}J_{HH}$ = 6.8 Hz, 2H, CHMe$_2$), 5.53 (d, $^{4}J_{HH}$ = 2.0 Hz, 2H, XA-Ar-CH), 5.75 (d, $^{3}J_{HH}$ = 7.2 Hz, 2H, Ph-*o*-CH), 6.18 (t, $^{3}J_{HH}$ = 7.1 Hz, 2H, Ph-*p*-CH), 6.26 (d, $^{4}J_{HH}$ = 2.0 Hz, 2H, XA-Ar-CH), 6.40 (t, $^{3}J_{HH}$ = 7.6 Hz, 2H, Ph-*m*-CH), 6.99 – 7.13 (m, 6H, Dipp-Ar-CH).

$^{13}C\{^{1}H\}$ NMR (126 MHz, THF-d_8): δ 5.2 (*C*Si), 24.5 (C(*C*H$_3$)$_2$), 25.1 (CH(*C*H$_3$)$_2$), 25.7 (CH(*C*H$_3$)$_2$), 26.5 (CH(*C*H$_3$)$_2$), 26.5 (br, *C*Al), 27.3 (*C*H(CH$_3$)$_2$), 27.4 (CH(*C*H$_3$)$_2$), 29.0 (*C*H(CH$_3$)$_2$), 32.5 (C(*C*H$_3$)$_3$), 33.3 (C(*C*H$_3$)$_2$), 35.4 (*C*Me3), 36.9 (*C*Me$_2$), 102.4 (XA-Ar-*C*H), 109.5 (XA-Ar-*C*H), 117.8 (Ph-*p*-*C*), 123.3 (Dipp-*m*-*C*), 124.4 (Dipp-*m*-*C*), 125.3 (Dipp-*p*-*C*), 126.8 (Ph-*m*-*C*), 127.8 (Ph-*o*-*C*), 130.9 (XA-*C*CMe2), 141.0 (*C*O), 145.5 (*C*tBu), 146.8 (XA-N*C*), 148.1 (Dipp-*o*-*C*), 149.0 (Dipp-*i*-*C*), 149.8 (Dipp-*o*-*C*), 155.3 (Ph-*i*-*C*).

K$_2$[NONAl{N$_4$(4-^{t}BuC$_6$H$_4$)$_2$}]$_2$, K$_2$[3.3]$_2$

To a stirred solution of K$_2$[**NON**Al]$_2$ (200 mg, 0.27 mmol) in benzene (15 mL) was added 4-^{t}BuC$_6$H$_4$N$_3$ dropwise at room temperature. After standing for 16 h, the solution was concentrated to a third of its original volume, leading to the formation of large crystals. Yield 100 mg, 35 %.

^{1}H NMR (500 MHz, C_6D_6): δ 1.04 (br d, 6H, CH(C*H*$_3$)$_2$), 1.10 (overlapping s and d, 15H, CH(C*H*$_3$)$_2$ and C(C*H*$_3$)$_3$), 1.20 (br d, 6H, CH(C*H*$_3$)$_2$), 1.26 (s, 18H, C(C*H*$_3$)$_3$), 1.29 (d, $^{3}J_{HH}$ = 7.5 Hz, 6H, CH(C*H*$_3$)$_2$), 1.38 (s, 3H, C(C*H*$_3$)$_2$), 1.65 (s, 3H, C(C*H*$_3$)$_2$), 3.49 (br sept, 2H, C*H*Me$_2$), 4.02 (br sept, 2H, C*H*Me$_2$), 6.04 (br d, 2H, Ar-*o*-C*H*), 6.11 (d, $^{4}J_{HH}$ = 1.8 Hz, 2H, XA-Ar-C*H*), 6.73 (d, $^{4}J_{HH}$ = 1.8 Hz, 2H, XA-Ar-C*H*), 6.84 (d, $^{3}J_{HH}$ = 7.9 Hz, 2H, Ar-*m*-C*H*), 7.06 – 7.14 (m, 4H, Dipp-*o*/*m*-C*H*), 7.19 – 7.33 (m, 6H, Dipp-*m*-C*H* and Ar-*o*/*m*-C*H*).

$^{13}C\{^{1}H\}$ NMR (126 MHz, C_6D_6): δ 23.2 (C(*C*H$_3$)$_2$), 24.4 (CH(*C*H$_3$)$_2$), 25.5 (CH(*C*H$_3$)$_2$), 26.6 (CH(*C*H$_3$)$_2$), 26.6 (CH(*C*H$_3$)$_2$), 27.8 (*C*HMe$_2$), 28.9 (*C*HMe$_2$), 31.5 (C(*C*H$_3$)$_3$), 31.7 (C(*C*H$_3$)$_3$), 31.9 (C(*C*H$_3$)$_3$), 33.3 (C(*C*H$_3$)$_2$), 34.1 (*C*Me$_3$), 34.2 (*C*Me$_3$), 35.2 (*C*Me$_3$), 37.0 (*C*Me$_2$), 106.0 (XA-Ar-*C*H), 110.6 (XA-Ar-*C*H), 119.8 (Ar-*o*-*C*H), 122.3 (Ar-*o*-*C*H), 124.0 (Dipp-*m*-*C*H), 124.3 (Dipp-*m*-*C*H), 125.6 (Dipp-*p*-*C*H), 125.8 (Ar-*m*-*C*H), 126.4 (Ar-*m*-*C*H), 131.8 (*C*CMe$_2$), 139.5 (XA-*C*O), 143.0 (Ar-*p*-*C*), 144.4 (XA-*C*N), 144.6 (Ar-*p*-*C*H), 145.5 (Dipp-*i*-C), 147.0 (Ar-*i*-C), 147.4 (XA-*C*^{t}Bu), 148.3 (Dipp-*o*-C), 148.6 (Dipp-*o*-C), 148.8 (Ar-*i*-C).

K_2[NONAl(NDipp)]$_2$, K_2[3.5]$_2$

To a stirred suspension of K_2[**NON**Al]$_2$ (600 mg, 0.41 mmol) in pentane (5 mL) at –78 °C was added dropwise DippN_3 (150 µL, 0.68 mmol). After stirring for 3 h at room temperature, the off-white solid was isolated, affording K_2[**3.5**]$_2$ in high yields, 550 mg, 89 %. Crystals suitable for X-ray diffraction were obtained from toluene.

Anal. Calc. for $C_{59}H_{79}AlKN_3O$ (%): C 77.67, H 8.73, N 4.61; found C 77.57, H 8.95, N 4.48.

^{1}H NMR (400 MHz, THF-d$_8$): δ 0.34 (d, $^3J_{HH}$ = 6.9 Hz, 6H, CH(CH_3)$_2$), 0.67 (d, $^3J_{HH}$ = 6.7 Hz, 6H, CH(CH_3)$_2$), 0.82 (d, $^3J_{HH}$ = 6.8 Hz, 6H, CH(CH_3)$_2$), 0.98 (d, $^3J_{HH}$ = 6.7 Hz, 6H, CH(CH_3)$_2$), 1.10 (s, 18H, C(CH_3)$_3$), 1.12 (d, $^3J_{HH}$ = 6.8 Hz, 6H, CH(CH_3)$_2$), 1.31 (d, $^3J_{HH}$ = 6.8 Hz, 6H, CH(CH_3)$_2$), 1.69 (s, 3H, C(CH_3)$_2$), 1.82 (s, 3H, C(CH_3)$_2$), 2.69 (sept., $^3J_{HH}$ = 6.8 Hz, 1H, C*H*Me$_2$), 3.59 (sept, $^3J_{HH}$ = 6.8 Hz, 2H, C*H*Me$_2$), 3.66 (sept, $^3J_{HH}$ = 6.8 Hz, 2H, C*H*Me$_2$), 3.84 (sept, $^3J_{HH}$ = 6.8 Hz, 2H, C*H*Me$_2$), 5.61 (t, $^3J_{HH}$ = 7.2 Hz, 1H, Dipp-*p*-C*H*), 5.81 (d, $^4J_{HH}$ = 1.9 Hz, 2H, XA-Ar-C*H*), 6.31 (dd, $^3J_{HH}$ = 7.2, $^4J_{HH}$ = 1.9 Hz, 1H, Dipp-*m*-C*H*), 6.52 (d, $^4J_{HH}$ = 2.0 Hz, 2H, XA-Ar-C*H*), 6.56 (dd, $^3J_{HH}$ = 7.2, $^4J_{HH}$ 1.9 Hz, 1H, Dipp-*m*-C*H*), 6.92 – 7.05 (m, 4H, Dipp-Ar-C*H*), 7.13 (m, 2H, Dipp-Ar-C*H*).

^{13}C{^{1}H} NMR (101 MHz, THF-d$_8$): δ 22.9 (C(*C*H$_3$)$_2$), 23.2 (CH(*C*H$_3$)$_2$, imido), 23.9 (CH(*C*H$_3$)$_2$, imido), 24.7 (CH(*C*H$_3$)$_2$), 25.3 (CH(*C*H$_3$)$_2$), 25.4 (CH(*C*H$_3$)$_2$), 26.4 (CH(*C*H$_3$)$_2$), 27.7 (*C*HMe$_2$, imido), 28.0 (*C*HMe$_2$, imido), 29.0 (*C*HMe$_2$), 29.9 (*C*HMe$_2$), 31.4 (C(*C*H$_3$)$_2$), 32.2 (C(*C*H$_3$)$_3$), 35.6 (*C*Me$_3$), 38.5 (*C*Me$_2$), 103.2 (Dipp-*p*-*C*, imido), 106.1 (XA-Ar-*C*H), 111.6 (XA-Ar-*C*H), 122.2 (Dipp-*m*-*C*, imido), 122.5 (Dipp-*m*-*C*, imido), 123.5 (Dipp-*p*-*C*), 125.4 (Dipp-*m*-*C*), 125.5 (Dipp-*m*-*C*), 135.0 (*C*CMe2), 135.8 (Dipp-*o*-*C*, imido), 136.5 (Dipp-*o*-*C*, imido), 143.0 (*C*O), 145.5 (Dipp-*i*-*C*), 146.6 (*C*^{t}Bu), 147.6 (Dipp-*o*-*C*), 148.2 (*C*NDipp), 148.9 (Dipp-*o*-*C*), 158.2 (Dipp-*i*-*C*, imido).

[K(crypt)][NONAl(NDipp)], [K(crypt)][3.5]

K_2[**3.5**]$_2$ (20 mg, 0.02 mmol) and 2.2.2-cryptand (9 mg, 0.02 mmol) were dissolved in benzene (0.5 mL). ^{1}H NMR shows quantitative conversion to single new species.

^{1}H NMR (400 MHz, C_6D_6): δ 0.94 (d, $^3J_{HH}$ = 6.9 Hz, 6H, CH(CH_3)$_2$), 1.25 (d, $^3J_{HH}$ = 6.9 Hz, 6H, CH(CH_3)$_2$), 1.29 (m, 24H, C(CH_3)$_3$ and , CH(CH_3)$_2$), 1.33 (d, $^3J_{HH}$ = 6.9 Hz, 6H, CH(CH_3)$_2$), 1.54 (d, $^3J_{HH}$ = 6.9 Hz, 6H, CH(CH_3)$_2$), 1.79 (m, 9H, C(CH_3)$_2$ and CH(CH_3)$_2$), 1.84 (s, 3H, C(CH_3)$_2$), 1.99 (m, 12H, NCH_2), 2.96 (m, 12H, NCH$_2$CH_2), 3.03 (s, 12H, OCH_2), 3.39 (sept, $^3J_{HH}$ = 6.9 Hz, 1H, C*H*Me$_2$), 3.97 (sept, $^3J_{HH}$ = 6.9 Hz, 2H, C*H*Me$_2$), 4.53 (sept, $^3J_{HH}$ = 6.9 Hz, 1H, C*H*Me$_2$), 4.63 (sept, $^3J_{HH}$ = 6.9 Hz, 1H, C*H*Me$_2$), 6.04 (t, $^3J_{HH}$ = 7.1 Hz, 1H, Dipp-*p*-C*H*), 6.36 (d, $^4J_{HH}$ = 2.0 Hz, 2H, XA-C*H*), 6.71 (d, $^4J_{HH}$ = 2.0 Hz, 2H, XA-C*H*), 6.82 (dd, $^3J_{HH}$ = 7.1 Hz, $^4J_{HH}$ = 1.9 Hz, 1H, Dipp-*m*-C*H*), 7.08 (dd, $^3J_{HH}$ = 7.1 Hz, $^4J_{HH}$ = 1.9 Hz, 1H, Dipp-*m*-C*H*), 7.27 (t, $^3J_{HH}$ = 7.6 Hz, 2H, Dipp-*p*-C*H*), 7.39 (m, 4H, Dipp-*m*-C*H*).

Due to the low stability of this compounds a ^{13}C NMR spectrum could not be obtained.

K[NONAl(NSiPh$_3$)], K[3.7a]

K_2[**NON**Al]$_2$ (500 mg, 0.68 mmol) and Ph_3SiN_3 (200 mg, 0.68 mmol) were dissolved in Et_2O (10 mL). Upon concentration a small amount of crystals of [**NON**Al]$_2$ formed, and were separated. Pentane (5 mL) was added to the supernatant, causing K[**3.7a**] to precipitate as a white powder. Yield 210 mg, 31 %. Alternatively this reaction can be carried out in benzene or toluene solutions or as a suspension in pentane, and the fractional crystallisation avoided. Clean samples readily crystallise from benzene as thin needles.

^{1}H NMR (400 MHz, C_6D_6): δ 0.71 (d, $^3J_{HH}$ = 6.7, 6H, CH(CH_3)$_2$), 0.87 (d, $^3J_{HH}$ = 6.8, 6H, CH(CH_3)$_2$), 1.01 (d, $^3J_{HH}$ = 6.8, 6H, CH(CH_3)$_2$), 1.03 (d, $^3J_{HH}$ = 6.8, 6H, CH(CH_3)$_2$), 1.22 (s, 18H, C(CH_3)$_3$), 1.70 (s, 3H, C(CH_3)$_2$), 1.78 (s, 3H, C(CH_3)$_2$), 2.87 (sept, $^3J_{HH}$ = 6.7 Hz, 2H, C*H*Me$_2$), 3.92 (sept, $^3J_{HH}$ = 6.7 Hz, 2H, C*H*Me$_2$), 6.40 (d, $^4J_{HH}$ = 1.8, 2H, XA-Ar-C*H*), 6.72 (d,

$^4J_{HH}$ = 1.9, 2H, XA-Ar-C*H*), 6.82 – 6.93 (m, 4H, Ar-C*H*), 7.00 (dd, J=7.1, 2.2, 2H, Ar-C*H*), 7.08 – 7.26 (m, 9H, Ar-C*H*), 7.87 – 7.94 (m, 6H, Ph-*o*-C*H*).

The low solubility of this compounds in compatible solvents prevents the acquisition of meaningful ^{13}C NMR data.

K[NONAl(NSi^{t}BuPh$_2$)], K[3.7b]

To a suspension of K$_2$[**NON**Al]$_2$ (260 mg, 0.35 mmol) in pentane (3 mL) was added ^{t}BuPh$_2$SiN$_3$ (100 µL, 0.35 mmol) dropwise at room temperature. This rapidly leads to gas evolution and tot he formation of a white fluffy precipitate. After standing overnight, the solution was decanted, and the precipitate washed with 5 mL of pentane. Upon removal of volatiles, the product can be obtained as a white solid. Yield 134 mg, 38%. Anal Calc. for $C_{63}H_{81}AlKN_3OSi$ (%): C 76.39 H 8.24 N 4.24; found C 75.10 H 8.18 N 4.29.

^{1}H NMR (400 MHz, C_6D_6): δ 0.65 (br. s, 6H, CH(C*H*$_3$)$_2$), 0.96 (d, $^3J_{HH}$ = 6.8 Hz, 6H, CH(C*H*$_3$)$_2$), 1.00 (d, $^3J_{HH}$ = 6.6 Hz, 6H, CH(C*H*$_3$)$_2$), 1.06 (br. s, 6H, CH(C*H*$_3$)$_2$), 1.21 (s, 18H, XA-C(C*H*$_3$)$_3$), 1.28 (s, 9H, Si-C(C*H*$_3$)$_3$), 1.74 (s, 3H, C(C*H*$_3$)$_2$), 1.95 (s, 3H, C(C*H*$_3$)$_2$), 2.82 (br. s, 2H, C*H*Me$_2$), 3.82 (s, 2H, C*H*Me$_2$), 6.38 (s, 2H, XA-Ar-C*H*), 6.73 (d, $^4J_{HH}$ = 1.9 Hz, 2H, XA-Ar-C*H*), 6.91 (m, 4H, Dipp-Ar-C*H*), 7.03 (m, 2H), 7.22 (m, 6H, Ph-*o/m*-C*H*), 7.92 – 7.99 (m, 4H, Ph-*o*-C*H*).

^{13}C NMR (151 MHz, C_6D_6) δ = 21.3 (Si*C*Me$_3$), 22.7 (C(*C*H$_3$)$_2$), 24.7 (br, CH(*C*H$_3$)$_2$), 25.1 (br, CH(*C*H$_3$)$_2$), 25.3 (CH(*C*H$_3$)$_2$), 26.6 (CH(*C*H$_3$)$_2$), 27.4 (*C*H(CH$_3$)$_2$), 28.5 (*C*H(CH$_3$)$_2$), 29.8 (C(*C*H$_3$)$_2$), 29.8 (SiC(*C*H$_3$)$_3$), 31.8 (CC(*C*H$_3$)$_3$), 35.2 (C*C*Me$_3$), 39.7 (*C*Me$_2$), 107.1 (br, XA-Ar-*C*H), 111.5 (XA-Ar-*C*H), 124.3 (Dipp-Ar-*C*H), 124.5 (Dipp-Ar-*C*H), 124.6 (Dipp-Ar-*C*H), 127.3 (SiPh-*p*-*C*H), 127.5 (SiPh-*m*-*C*H), 136.1 (SiPh-*o*-*C*H), 137.6 (*C*CMe$_2$), 144.6 (*C*N), 145.4 (*C*O), 146.6 (Dipp-*o*-*C*), 147.5 (SiPh-*i*-*C*H), 148.2 (br, Dipp-*o*-*C*), 149.1 (*C*^{t}Bu).

One of the ^{13}C{^{1}H} NMR *C*N resonances was not observed.

K[NONAl(NS^{i}iPr$_3$)], K[3.7c]

A solution of K[**3.7c**] may be prepared *in situ* by combining K_2[**NON**Al]$_2$ (300 mg, 0.40 mmol) with $^{i}Pr_3SiN_3$ (0.1 mL, 0.45 mmol) in benzene (4.5 mL). Carrying out this reaction on an NMR scale in a 1:1 ratio, reveals quantitative conversion to K[**3.7c**]. The isolation of this species was not attempted due to its high reactivity and no ^{13}C NMR data was collected.

^{1}H NMR (400 MHz, C_6D_6): δ 0.62 (s, 6H, CH(C*H*$_3$)$_2$), 0.82 (d, $^3J_{HH}$ = 6.7 Hz, 6H, CH(C*H*$_3$)$_2$), 0.93 (sept, $^3J_{HH}$ = 7.4 Hz, 3H, SiC*H*Me$_2$), 1.18 (s, 18H, C(C*H*$_3$)$_3$), 1.26 – 1.41 (overlapping br s and d, $^3J_{HH}$ = 7.4 Hz, 30H, CH(C*H*$_3$)$_2$), 1.68 (s, 3H, C(C*H*$_3$)$_2$), 1.87 (s, 3H, C(C*H*$_3$)$_2$), 2.73 (br s, 2H, C*H*Me$_2$), 4.13 (br s, 2H, C*H*Me$_2$), 6.36 (d, $^4J_{HH}$ = 1.9 Hz, XA-Ar-C*H*), 6.67 (d, $^4J_{HH}$ = 1.9 Hz, XA-Ar-C*H*), 6.88 – 6.99 (m, 4H, Dipp-C*H*), 7.10 – 7.16 (m, 4H, Dipp-C*H*).

K[NONAlN(B{NDippCH}$_2$)], K[3.10]

Benzene (3 mL) was added to a mixture of K_2[**NON**Al]$_2$ (100 mg, 0.14 mmol) and ({HCDippN}$_2$)BN_3 (50 mg, 0.13 mmol). After the gas evolution ceased, the mixture was concentrated to a third of its original volume. Upon standing over night large colourless crystals of K[**3.8**] were obtained. Samples were however invariably contaminated with a small amount of excess azide.

^{1}H NMR (400 MHz, C_6D_6): δ 0.40 (br s, 6H, CH(C*H*$_3$)$_2$), 0.71 (d, $^3J_{HH}$ = 6.7 Hz, 6H, CH(C*H*$_3$)$_2$), 1.12 (d, $^3J_{HH}$ = 6.7 Hz, 6H, CH(C*H*$_3$)$_2$), 1.17 (s, 18H, C(CH$_3$)$_3$), 1.24 (d, $^3J_{HH}$ = 6.5 Hz, 6H, CH(C*H*$_3$)$_2$), 1.36 (d, $^3J_{HH}$ = 6.7 Hz, 6H, CH(C*H*$_3$)$_2$), 2.50 (br s, 2H, C*H*Me$_2$), 3.81 (br s, 4H, C*H*Me$_2$), 3.99 (br s, 2H, C*H*Me$_2$), 5.96 (d, $^3J_{HH}$ = 2.7 Hz, 1H, NC*H*), 6.14 (d, $^4J_{HH}$ = 1.9Hz, XA-Ar-C*H*), 6.28 (d, $^3J_{HH}$ = 2.7 Hz, 1H, NC*H*), 6.57 (d, $^4J_{HH}$ = 1.9Hz, XA-Ar-C*H*), 6.74 – 7.10 (m, 12H, Ar-C*H*).

The remaining sept. could not be located unambiguously in the ^{1}H NMR spectrum.

Due to the low stability of this compounds a ^{13}C NMR spectrum could not be obtained.

K[NONGa(NSiPh$_3$)], K[3.11a]

K_2[**NON**Ga]$_2$ (500 mg, 70% purity, 0.45 mmol) and Ph_3SiN_3 (190 mg, 0.63 mmol) were suspended in hexane (5 mL) and stirred for 2 h at room temperature. The resulting mixture was allowed to settle, decanted and washed with a further 5 mL of hexane. The product can be obtained as a white powder. Yield 300 mg, 62% based on K_2[**NON**Ga]$_2$ content. The low solubility of this compounds in compatible solvents prevents the collection of meaningful ^{13}C NMR data.

^{1}H NMR (400 MHz, C_6D_6): δ 0.73 (d, $^3J_{HH}$ = 6.7 Hz, 6H, CH(C*H*$_3$)$_2$), 0.92 (d, $^3J_{HH}$ = 6.8 Hz, 6H, CH(C*H*$_3$)$_2$), 0.97 (d, $^3J_{HH}$ = 6.7 Hz, 6H, CH(C*H*$_3$)$_2$), 1.02 (d, $^3J_{HH}$ = 6.7 Hz, 6H, CH(C*H*$_3$)$_2$), 1.22 (s, 18H, C(C*H*$_3$)$_3$), 1.75 (s, 3H, C(C*H*$_3$)$_2$), 1.83 (s, 3H, C(C*H*$_3$)$_2$), 2.94 (sept, $^3J_{HH}$ = 6.8 Hz, 2H, C*H*Me$_2$), 3.77 (sept, $^3J_{HH}$ = 6.8 Hz, 2H, C*H*Me$_2$), 6.39 (d, $^4J_{HH}$ = 1.9 Hz, 2H, XA-Ar-C*H*), 6.75 (d, $^4J_{HH}$ = 1.9 Hz, 2H, XA-Ar-C*H*), 6.83 (t, $^3J_{HH}$ = 7.5 Hz, 2H, Dipp-*p*-C*H*), 6.90 (d, $^3J_{HH}$ = 7.6, 2H, Dipp-*m*-C*H*), 6.95 (d, $^3J_{HH}$ = 7.5, 2H, Dipp-*m*-C*H*), 7.10 – 7.23 (m, 9H, Ph-*m*/*p*-C*H*), 7.84 – 7.91 (m, 6H, Dipp-*o*-C*H*).

[K(crypt)][NONGa(NSiPh$_3$)], [K(crypt)][3.11a]

To a suspension of K[**NON**Ga(NSiPh$_3$)] (20 mg, 0.02 mmol) in benzene (0.5 mL) was added 2.2.2-crypt (7 mg, 0.02 mmol). The solution was briefly warmed, leading to the dissolution of the imide. NMR shows clean conversion to the target compound.

^{1}H NMR (500 MHz, C_6D_6) δ 1.23 (d, $^3J_{HH}$ = 6.7 Hz, 12H, (CH(C*H*$_3$)$_2$)), 1.26 (d, $^3J_{HH}$ = 6.7 Hz, 12H, (CH(C*H*$_3$)$_2$)), 1.27 (s, 18H, (C(C*H*$_3$)$_3$)), 1.88 (s, 6H, (C(C*H*$_3$)$_2$)), 1.90 – 1.96 (m, 12H, crypt), 2.87 – 2.92 (m, 12H, crypt), 2.97 (s, 12H, crypt), 4.01 (s, 4H, (C*H*(CH$_3$)$_2$)), 6.36 (d, J = 1.9 Hz, 2H, XA-Ar-C*H*), 6.70 (d, J = 2.0 Hz, 2H, XA-Ar-C*H*), 7.15 – 7.24 (m, 9H, Ar-C*H*), 7.29 – 7.38 (m, 6H, Ar-C*H*), 7.89 – 7.95 (m, 6H, SiPh-*o*-C*H*).

^{13}C NMR (126 MHz, C6D6) δ = 25.4 (CH(*C*H$_3$)$_2$), 25.6 (CH(*C*H$_3$)$_2$), 28.6 (*C*H(CH$_3$)$_2$), 32.1 (C(*C*H$_3$)$_3$), 35.0 (*C*(CH$_3$)$_3$), 39.2 (*C*(CH$_3$)$_2$), 53.6 (crypt), 67.4 (crypt), 70.3 (crypt), 105.2 (XA-

Ar-*C*H), 111.6 (XA-Ar-*C*H), 124.3 (Dipp-*m*-*C*H), 124.7 (Dipp-*p*-*C*H), 125.6 (SiPh-*p*-*C*H), 126.5 (SiPh-*m*-*C*H), 136.7 (SiPh-*o*-*C*H), 137.3 (*C*CMe$_2$), 144.6 (*C*O), 146.2 (Dipp-*i*-*C*H), 146.5 (XA-*C*N), 146.7 (*C*^{t}Bu), 147.8 (Dipp-*o*-*C*H), 150.6 (SiPh-*i*-*C*).

The resonances associated with the XA-C(*C*H$_3$)$_2$ was not observed, presumably due to rapid inversion of the ligand.

K[NONGa(NSi^{i}Pr$_3$)], K[3.11c]

To a solution of K$_2$[**NON**Ga]$_2$ (35 mg, 0.04 mmol) in benzene (0.5 mL) was added ^{i}Pr$_3$SiN$_3$ (10 µL, 0.04 mmol). After 5 min, quantitative conversion to single species was observed by ^{1}H NMR. The isolation of this compounds was not attempted and no ^{13}C NMR data was collected. ^{1}H NMR (400 MHz, C$_6$D$_6$): δ 0.62 (d, $^3J_{HH}$ = 6.6 Hz, 6H, CH(C*H*$_3$)$_2$), 0.79 (d, $^3J_{HH}$ = 6.6 Hz, 6H, CH(C*H*$_3$)$_2$), 1.01 (m, 3H, SiC*H*Me$_2$), 1.20 (s, 18H, C(C*H*$_3$)$_3$), 1.26 – 1.43 (m, 30H, CH(C*H*$_3$)$_2$), 1.73 (s, 3H, C(C*H*$_3$)$_2$), 1.90 (s, 3H, C(C*H*$_3$)$_2$), 2.74 (s, 2H, C*H*Me$_2$), 4.10 (s, 2H, C*H*Me$_2$), 6.41 (s, 2H, XA-Ar-C*H*), 6.70 (s, 2H, XA-Ar-C*H*), 6.92 (m, 4H, Ar-C*H*), 7.12 (m, 4H, Ar-C*H*).

C–H activation product of K$_2$[3.5]$_2$, K[3.12]

A solution of K$_2$[**3.5**]$_2$ in benzene was heated at 80 °C for 4 d, leading to the near quantitative conversion to K[**3.12**].

^{1}H NMR (400 MHz, C$_6$D$_6$): δ -1.27 (t, $^2J_{HH}$ = $^3J_{HH}$ = 13.6 Hz, 1H, AlC*H*$_2$), 0.03 (d, 3H, $^3J_{HH}$ = 6.9 Hz, CH(C*H*$_3$)$_2$), 0.46 (d, 3H, $^3J_{HH}$ = 6.8 Hz, CH(C*H*$_3$)$_2$), 0.57 (d, $^2J_{HH}$ = 13.6, 1H, AlC*H*$_2$), 1.05 (d, 3H, $^3J_{HH}$ = 6.8 Hz, CH(C*H*$_3$)$_2$), 1.08 (d, 3H, $^3J_{HH}$ = 6.7 Hz, CH(C*H*$_3$)$_2$), 1.15 (m, 7H, NH and CH(C*H*$_3$)$_2$), 1.22 (m, 12H, C(C*H*$_3$)$_3$ and CH(C*H*$_3$)$_2$), 1.27 (m, 15H, C(C*H*$_3$)$_3$ and CH(C*H*$_3$)$_2$), 1.63 (d, 3H, $^3J_{HH}$ = 6.7 Hz, CH(C*H*$_3$)$_2$), 1.70 (d, 3H, $^3J_{HH}$ = 6.7 Hz, CH(C*H*$_3$)$_2$), 1.85 (s, 3H, C(C*H*$_3$)$_2$), 1.94 (s, 3H, C(C*H*$_3$)$_2$), 2.91 (sept, $^3J_{HH}$ = 6.7 Hz, 1H, C*H*Me$_2$), 3.05 (dq, $^3J_{HH}$ = 13.0, 6.7 Hz, 1H, C*H*(CH$_2$Al)Me), 3.43 (sept, $^3J_{HH}$ = 6.7 Hz, 1H, C*H*Me$_2$), 3.60 (sept,

$^{3}J_{HH}$ = 6.7 Hz, 2H, C*H*Me$_2$), 4.43 (sept, $^{3}J_{HH}$ = 6.7 Hz, 1H, C*H*Me$_2$), 6.12 (m, 2H, XA-C*H* and Ar-C*H*), 6.53 (t, $^{3}J_{HH}$ = 7.5 Hz, 1H, Ar-C*H*), 6.56 (d, $^{4}J_{HH}$ = 6.56 Hz, XA-C*H*), 6.67 – 6.76 (m, 4H, XA-C*H* and Ar-C*H*), 6.78 – 6.83 (m, 2H, XA-C*H* and Ar-C*H*), 7.20 (dd, $^{3}J_{HH}$ = 7.6 Hz, $^{4}J_{HH}$ = 1.7 Hz, 1H, Ar-C*H*), 7.31 (t, $^{3}J_{HH}$ = 7.6 Hz, 1H, Ar-C*H*), 7.44 (dd, $^{3}J_{HH}$ = 7.6 Hz, $^{4}J_{HH}$ = 1.7 Hz, 1H, Ar-C*H*).

C–H activation product of K[3.7a], K[3.13]

A solution of K[**3.7a**] in benzene was heated at 80 °C for 4 d, leading to the near quantitative conversion to K[**3.13**].

^{1}H NMR (400 MHz, C_6D_6): δ -1.46 (t, $^{3}J_{HH}$ = $^{2}J_{HH}$ = 13.7 Hz, 1H, AlC*H*$_2$), -0.09 (s, 1H, NH), 0.37 (d, $^{3}J_{HH}$ = 6.6 Hz, 3H, CH(C*H*$_3$)$_2$), 0.50 (d, $^{3}J_{HH}$ = 6.6 Hz, 3H, CH(C*H*$_3$)$_2$), 0.60 (dd, $^{2}J_{HH}$ = 14.1 Hz, $^{3}J_{HH}$ = 2.3, 1H, AlC*H*$_2$), 0.85 (d, $^{3}J_{HH}$ = 6.7 Hz, 3H, CH(C*H*$_3$)$_2$), 1.01 (br s, 3H, CH(C*H*$_3$)$_2$), 1.10 (d, $^{3}J_{HH}$ = 6.6 Hz, 3H, CH(C*H*$_3$)$_2$), 1.13 – 1.19 (m, 9H, CH(C*H*$_3$)$_2$), 1.26 (s, 9H, C(C*H*$_3$)$_3$), 1.29 (d, $^{3}J_{HH}$ = 6.6 Hz, 3H, CH(C*H*$_3$)$_2$), 1.30 – 1.34 (m, 15H, C(C*H*$_3$)$_3$ and CH(C*H*$_3$)$_2$), 1.40 (s, 3H, C(C*H*$_3$)$_2$), 1.84 (s, 3H, C(C*H*$_3$)$_2$), 3.24 (sept, $^{3}J_{HH}$ = 6.6 Hz, 1H, C*H*Me$_2$), 3.35 (ddq, $^{3}J_{HH}$ = 13.7, 2.3, 6.6 Hz, 1H, C*H*(CH$_2$Al)Me), 3.60 (sept, $^{3}J_{HH}$ = 6.7 Hz, 1H, C*H*Me$_2$), 3.69 (sept, $^{3}J_{HH}$ = 6.7 Hz, 1H, C*H*Me$_2$), 6.07 (d, $^{3}J_{HH}$ = 1.9 Hz, 1H, XA-C*H*), 6.66 (t, $^{3}J_{HH}$ = 7.5 Hz, 1H, Ar-C*H*), 6.74 (d, $^{3}J_{HH}$ = 2.0 Hz, 1H, XA-C*H*), 6.78 (d, $^{3}J_{HH}$ = 1.9 Hz, 1H, XA-C*H*), 6.83 (d, $^{3}J_{HH}$ = 1.9 Hz, 1H, XA-C*H*), 6.88 (dd, $^{3}J_{HH}$ = 7.7, 1.6 Hz, 1H, Ar-C*H*), 6.95 (dd, $^{3}J_{HH}$ = 7.5, 1.7 Hz, 1H, Ar-C*H*), 7.00 – 7.16 (m, 9H, Ar-C*H*), 7.26 (m, 3H, Ar-C*H*), 7.61 (m, 6H, Ph-*o*-C*H*).

THF activation product of K[3.7a], K[3.14]

K[**3.7^{a}**] (20 mg) was dissolved in THF-h$_8$ or THF-d$_8$, leading to the formation of a deep green solution. After 2h the colour has disappeared and ^{1}H NMR reveals the quantitative formation of K[**3.14**].

^{1}H NMR (400 MHz, C_6D_6): δ -0.21 (s, 1H, N*H*), 0.76 (m, 4H, C(C*H*$_3$)$_2$ and C$_4$*H*$_7$O), 0.98 (d, $^{3}J_{HH}$ = 6.6, 3H, CH(C*H*$_3$)$_2$), 1.08 (m, 4H, CH(C*H*$_3$)$_2$ and C$_4$*H*$_7$O), 1.15 – 1.22 (m, 9H, CH(C*H*$_3$)$_2$), 1.26 (m, 3H, CH(C*H*$_3$)$_2$), 1.33 (m, 4H, CH(C*H*$_3$)$_2$ and C$_4$*H*$_7$O), 1.35 – 1.40 (m, 12H, CH(C*H*$_3$)$_2$ and C(C*H*$_3$)$_3$), 1.41 (s, 9H, C(C*H*$_3$)$_3$), 1.51 (m, 4H, C(C*H*$_3$)$_2$ and C$_4$*H*$_7$O), 2.13 (m, 1H, C$_4$*H*$_7$O), 2.28 (dd, $^{2}J_{HH}$ = 12.9 Hz, $^{3}J_{HH}$ = 6.6 Hz, C$_4$*H*$_7$O), 2.45 (dt, $^{2}J_{HH}$ = 3.2 Hz, $^{3}J_{HH}$ = 7.7 Hz, C$_4$*H*$_7$O), 3.73 (m, 2H, C*H*Me$_2$), 4.32 (sept, 1H, C*H*Me$_2$), 4.43 (sept, 1H, C*H*Me$_2$), 6.11 (d, $^{4}J_{HH}$ = 1.9 Hz, 1H, XA-C*H*), 6.18 (d, $^{4}J_{HH}$ = 1.9 Hz, 1H, XA-C*H*), 6.60 (m, 2H, XA-C*H*), 6.93 – 7.38 (m, 15H, Ar-C*H*), 7.73 (m, 9H, Ph-*o*-C*H*).

THF-d$_8$ activation product of K[3.7a], K[3.14]-d$_8$

^{1}H NMR (500 MHz, THF-d$_8$): δ = 0.44 (s, 3H, C(C*H*$_3$)$_2$), 0.48 (d, $^{3}J_{HH}$ = 6.8 Hz, 3H, CH(C*H*$_3$)$_2$), 0.51 (d, $^{3}J_{HH}$ = 6.8 Hz, 3H, CH(C*H*$_3$)$_2$), 0.84 (4 d, $^{3}J_{HH}$ = 6.8 Hz, 12H, CH(C*H*$_3$)$_2$), 1.14 (d, $^{3}J_{HH}$ = 6.8 Hz, 3H, CH(C*H*$_3$)$_2$), 1.16 (s, 12H, C(CH$_3$)$_3$), 1.17 (m, 15H, C(CH$_3$)$_3$ and CH(C*H*$_3$)$_2$), 1.57 (s, 3H, C(C*H*$_3$)$_3$), 3.46 (2 sept, $^{3}J_{HH}$ = 6.8 Hz, 2H, C*H*Me$_2$), 4.31 (sept, $^{3}J_{HH}$ = 6.7 Hz, 1H, C*H*Me$_2$), 4.42 (sept, $^{3}J_{HH}$ = 6.7 Hz, 1H, C*H*Me$_2$), 5.64 (d, $^{4}J_{HH}$ = 1.9 Hz, 1H, XA-C*H*), 5.67 (d, $^{4}J_{HH}$ = 1.9 Hz, 1H, XA-C*H*), 6.23 (d, $^{4}J_{HH}$ = 1.9 Hz, 1H, XA-C*H*), 6.23 (d, $^{4}J_{HH}$ = 1.9 Hz, 1H, XA-C*H*), 6.60 – 7.70 (m, 21H ,Ar-C*H*).

^{13}C{^{1}H} NMR (126 MHz, THF-d$_8$): δ 23.9 (CH(*C*H$_3$)$_2$), 24.4 (CH(*C*H$_3$)$_2$), 25.2 (C(*C*H$_3$)$_2$), 26.3 (CH(*C*H$_3$)$_2$), 26.4 (CH(*C*H$_3$)$_2$), 26.9 (CH(*C*H$_3$)$_2$), 27.0 (CH(*C*H$_3$)$_2$), 27.5 (CH(*C*H$_3$)$_2$), 27.9 (*C*HMe$_2$), 28.1 (CH(*C*H$_3$)$_2$), 28.2 (*C*HMe$_2$), 28.9 (*C*HMe$_2$), 28.9 (*C*HMe$_2$), 32.2 (C(*C*H$_3$)$_2$), 32.7 (C(*C*H$_3$)$_3$), 35.6 (*C*Me$_3$), 36.3 (*C*Me$_2$), 102.7 (XA-*C*H), 102.8 (XA-*C*H), 108.3 (XA-*C*H), 108.6 (XA-*C*H), 122.9 (Dipp-*m*-*C*H), 123.8 (Dipp-Ar-*C*H), 123.9 (Dipp-Ar-*C*H), 123.9 (Dipp-Ar-*C*H), 127.3 (Ph-*m*-*C*H), 129.4 (*C*CMe$_2$), 129.5 (*C*CMe$_2$), 136.5 (Ph-*p*-*C*H), 137.3 (Ph-*o*-*C*H), 139.4 (XA-*C*O), 139.4 (XA-*C*O), 144.6 (br, Ph-*i*-*C*), 145.6 (*C*^{t}Bu), 145.7 (*C*^{t}Bu), 146.5 (XA-*C*N), 146.6 (XA-*C*N), 147.7 (Dipp-*o*-*C*), 147.8 (Dipp-*o*-*C*), 148.3 (Dipp-*i*-*C*), 148.3 (Dipp-*i*-*C*), 150.2 (Dipp-*o*-*C*), 150.7 (Dipp-*o*-*C*).

Due to the coupling to D, and resulting lowered peak height, the $^{13}C\{^1H\}$ resonances associated with the C_4D_7O unit could not be identified.

K[NONAl(H)NHSiPh$_3$], K[3.17]

Method 1: A solution of K[**3.7^a**] (20 mg, 0.02 mmol) in benzene (0.5 mL) was exposed to an atmosphere of H_2 (1.5 bar, 3 mL). Upon standing for 1 week, ^1H NMR shows the fairly clean formation of K[**3.15**]. Method 2: K_2[**NON**Al]$_2$ (20 mg, 0.03 mmol) and Ph_3SiNH_2 (8 mg, 0.03 mmol) were dissolved in benzene (0.5 mL). After 5 min, ^1H NMR shows the essentially clean formation of K[**3.17**], which precipitates from solution upon standing over night.

^1H (400 MHz, C_6D_6): δ –0.12 (s, 1H, N*H*), 0.83 (m, 15H, CH(C*H*$_3$)$_2$ and C(C*H*$_3$)$_2$), 1.02 (d, $^3J_{HH}$ = 6.7 Hz, 6H, CH(C*H*$_3$)$_2$), 1.06 (d, $^3J_{HH}$ = 6.7 Hz, 6H, CH(C*H*$_3$)$_2$), 1.33 (s, 18H, C(C*H*$_3$)$_3$), 1.48 (s, 3H, C(C*H*$_3$)$_2$), 2.94 (s, 1H, Al*H*), 3.38 (sept, $^3J_{HH}$ = 6.77 Hz, C*H*Me$_2$), 4.49 (m, 2H, C*H*Me$_2$), 5.93 (s, 2H, XA-C*H*), 6.62 (d, $^3J_{HH}$ = 1.9 Hz, 2H, C*H*Me$_2$), 6.98 – 7.15 (m, 15H, Ar-C*H*), 7.67 (m, 6H, Ph-*o*-C*H*).

$^{13}C\{^1H\}$ NMR (126 MHz, C_6D_6): δ 23.9 (C(*C*H$_3$)$_2$), 25.3 (CH(*C*H$_3$)$_2$), 25.4 (CH(*C*H$_3$)$_2$), 26.8 (CH(*C*H$_3$)$_2$), 26.8 (CH(*C*H$_3$)$_2$), 27.2 (*C*HMe$_2$), 28.3 (*C*HMe$_2$), 31.8 (C(*C*H$_3$)$_2$), 32.2 (C(*C*H$_3$)$_3$), 35.2 (*C*Me$_3$), 36.3 (*C*Me$_2$), 106.3 (XA-Ar-*C*H), 107.8 (XA-Ar-*C*H), 124.1 (Dipp-*m*-*C*H), 125.5 (Dipp-*m*-*C*H), 125.7 (Dipp-*m*-*C*H), 126.0 (Ph-*m*-*C*H), 131.0 (*C*CMe$_2$), 135.6 (Ph-*p*-*C*H), 136.2 (Ph-*o*-*C*H), 139.0 (*C*O), 141.6 (Ph-*i*-*C*), 143.9 (XA-*C*N), 146.6 (Dipp-*i*-*C*), 147.3 (*C*^{t}Bu), 149.5 (Dipp-*o*-*C*), 151.4 (Dipp-*o*-*C*).

3.5 References

[1] D. J. Grant, D. A. Dixon, *J. Phys. Chem. A*, **2005**, *109*, 10138–10147.
[2] H. W. Langmi, G. S. McGrady, *Coord. Chem. Rev.*, **2007**, *251*, 925–935.
[3] T. B. Marder, *Angew. Chem. Int. Ed.*, **2007**, *46*, 8116–8118.
[4] J. A. Jegier, W. L. Gladfelter, *Coord. Chem. Rev.*, **2000**, *206–207*, 631–650.
[5] A. Y. Timoshkin, *Coord. Chem. Rev.*, **2005**, *249*, 2094–2131.
[6] C. J. Carmalt, *Coord. Chem. Rev.*, **2001**, *223*, 217–264.
[7] P. J. Brothers, P. P. Power, *Adv. Organomet. Chem.*, **1996**, *39*, 1–69.
[8] S. J. Schauer, G. H. Robinso, *J. Coord. Chem.*, **1993**, *30*, 197–214.
[9] M. Veith, *Chem. Rev.*, **1990**, *90*, 3–16.

[10] A. W. Laubengayer, J. D. Smith, G. G. Ehrlich, *J. Am. Chem. Soc.*, **1961**, *83*, 542–546.
[11] K. M. Waggoner, P. P. Power, *J. Am. Chem. Soc.*, **1991**, *113*, 3385–3393.
[12] R. J. Wehmschulte, P. P. Power, *J. Am. Chem. Soc.*, **1996**, *118*, 791–796.
[13] M. Cesari, G. Perego, G. del Piero, S. Cucinella, E. Cernia, *J. Organomet. Chem.*, **1974**, *78*, 203–213.
[14] G. del Piero, M. Cesari, G. Dossi, A. Mazzei, *J. Organomet. Chem.*, **1977**, *129*, 281–288.
[15] G. del Piero, M. Cesari, G. Perego, S. Cucinella, E. Cernia, *J. Organomet. Chem.*, **1977**, *129*, 289–298.
[16] T. Belgardt, S. D. Waezsada, H. W. Roesky, H. Gornitzka, L. Häming, D. Stalke, *Inorg. Chem.*, **1994**, *33*, 6247–6251.
[17] N. D. Reddy, H. W. Roesky, M. Noltemeyer, H. G. Schmidt, *Inorg. Chem.*, **2002**, *41*, 2374–2378.
[18] K. M. Waggoner, H. Hope, P. P. Power, *Angew. Chem. Int. Ed.*, **1988**, *27*, 1699–1700.
[19] S. Schulz, A. Voigt, H. W. Roesky, L. Häming, R. Herbst-Irmer, *Organometallics*, **1996**, *15*, 5252–5253.
[20] S. Schulz, L. Häming, R. Herbst-Irmer, H. W. Roesky, G. M. Sheldrick, *Angew. Chem. Int. Ed.*, **1994**, *33*, 969–970.
[21] J. D. Fisher, P. J. Shapiro, G. P. A. Yap, A. L. Rheingold, *Inorg. Chem.*, **1996**, *35*, 271–272.
[22] S. Schulz, F. Thomas, W. M. Priesmann, M. Nieger, *Organometallics*, **2006**, *25*, 1392–1398.
[23] M. D. Anker, M. Lein, M. P. Coles, *Chem. Sci.*, **2019**, *10*, 1212–1218.
[24] H. Zhu, Z. Yang, J. Magull, H. W. Roesky, H. G. Schmidt, M. Noltemeyer, *Organometallics*, **2005**, *24*, 6420–6425.
[25] C. Cui, H. W. Roesky, H.-G. Schmidt, M. Noltemeyer, *Angew. Chem. Int. Ed.*, **2000**, *39*, 4531–4533.
[26] M. D. Anker, Y. Altaf, M. Lein, M. P. Coles, *Dalton Trans.*, **2019**, *48*, 16588–16594.
[27] N. J. Hardman, P. P. Power, *Chem. Commun.*, **2001**, *1*, 1184–1185.
[28] Q. Yu, L. Zhang, Y. He, J. Pan, H. Li, G. Bian, X. Chen, G. Tan, *Chem. Commun.*, **2021**, *57*, 9268–9271.
[29] H. Zhu, J. Chai, V. Chandrasekhar, H. W. Roesky, J. Magull, D. Vidovic, H. G. Schmidt, M. Noltemeyer, P. P. Power, W. A. Merrill, *J. Am. Chem. Soc.*, **2004**, *126*, 9472–9473.
[30] A. Hofmann, T. Tröster, T. Kupfer, H. Braunschweig, *Chem. Sci.*, **2019**, *10*, 3421–3428.
[31] J. D. Queen, S. Irvankoski, J. C. Fettinger, H. M. Tuononen, P. P. Power, *J. Am. Chem. Soc.*, **2021**, *143*, 6351–6356.
[32] J. Li, X. Li, W. Huang, H. Hu, J. Zhang, C. Cui, *Chem. Eur. J.*, **2012**, *18*, 15263–15266.
[33] M. D. Anker, R. J. Schwamm, M. P. Coles, *Chem. Commun.*, **2020**, *56*, 2288–2291.
[34] N. J. Hardman, C. Cui, H. W. Roesky, W. H. Fink, P. P. Power, *Angew. Chem. Int. Ed.*, **2001**, *40*, 2172–2174.
[35] R. J. Wright, M. Brynda, J. C. Fettinger, A. R. Betzer, P. P. Power, *J. Am. Chem. Soc.*, **2006**, *128*, 12498–12509.
[36] R. J. Wright, A. D. Phillips, T. L. Allen, W. H. Fink, P. P. Power, *J. Am. Chem. Soc.*, **2003**, *125*, 1694–1695.
[37] S. L. Zhang, M. C. Yang, M. der Su, *RSC Adv.*, **2019**, *9*, 12195–12208.
[38] A. Y. Timoshkin, H. F. Schaefer, *J. Phys. Chem. A*, **2008**, *112*, 13180–13196.
[39] J. Hicks, A. Heilmann, P. Vasko, J. M. Goicoechea, S. Aldridge, *Angew. Chem. Int. Ed.*, **2019**, *58*, 17265–17268.

[40] M. D. Anker, M. P. Coles, *Angew. Chem. Int. Ed.*, **2019**, *58*, 18261–18265.
[41] M. J. Evans, M. D. Anker, C. L. McMullin, S. E. Neale, N. A. Rajabi, M. P. Coles, *Chem. Sci.*, **2022**, *13*, 4635–4646.
[42] M. J. Evans, M. D. Anker, C. L. McMullin, N. A. Rajabi, M. P. Coles, *Chem. Commun.*, **2021**, *57*, 2673–2676.
[43] 2 sigma range for a bond between N and three coordinate B, taken from the CSD database, version 5.41.
[44] 2 sigma ranges according to: F. H. Allen, O. Kennard, D. G. Watson, L. Brammer, A. G. Orpen, R. Taylor, *J. Chem. Soc., Perkin Trans. 2,* **1987**, S1–S19.
[45] B. Cordero, V. Gómez, A. E. Platero-Prats, M. Revés, J. Echeverría, E. Cremades, F. Barragán, S. Alvarez, *Dalton Trans.*, **2008**, 2832–2838.

Chapter 4. Reactivity of K_2[(**NON**)AlNDipp]$_2$ towards CO_2 and related substrates

4.1 Introduction

Imides are an indispensable class of ligands for the stabilization of high oxidation state early transition metal complexes and have found applications in many areas including inorganic, organic, bioinorganic, medicinal and industrial chemistry.[1–8] Among the most prevalent modes of reactivity of the imide functionality, and relevant to the work presented in this chapter, is cycloaddition chemistry with substrates containing polar bonds, such as CO_2. These reactions are of sustained interest not only from a fundamental perspective, giving rise to a range of different products, but also as they pertain to CO_2 valorisation.[9,10]

The reactivity of metal imides with CO_2 has been reported for metals from the *d*-, *f*-, and *p*-block.[10–31] Among the *d*-block systems the bulk of the investigations have been carried out using titanium imides, although analogous CO_2 chemistry has also been reported for Sc, V, Ni, Mo, W, and Ir. In all cases oxides,[10–14,18,31] carbamates,[23–29] or aminodicarboxylates[19–22] are obtained.

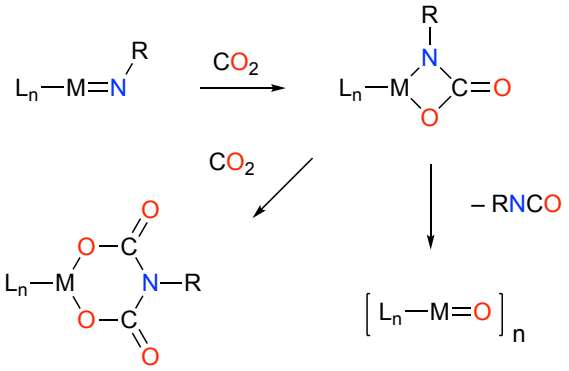

	Element
carbamate	Ti, W, Ir
oxide	Ti, V, Mo, W
aminodicarboxylate	Sc, Ti, Ni

Scheme 4.1: Reactivity of transitionmetal imides with CO_2.

In the case of titanium imides it has been shown that the reactions with CO_2 proceed via initial [2+2] cycloaddition, affording observable (and in some cases isolable) carbamate complexes, which usually undergo either extrusion of an isocyanate molecule to afford an oxide, or

insertion of a second equivalent of CO_2.[13] The energies of the transition states for these two processes can be very similar in some cases. This is perhaps best demonstrated by system **4.I**, where changing the imide substituent from ^{t}Bu to Mes, leads the formation of the aminodicarboxylate **4.III** rather than the oxide product **4.IV** (Scheme 4.2).[13] Analogous reactivity is observed when instead of CO_2, other heteroallenes such as isocyanates or CS_2 are reacted with titanium imides.[21,22,25,32]

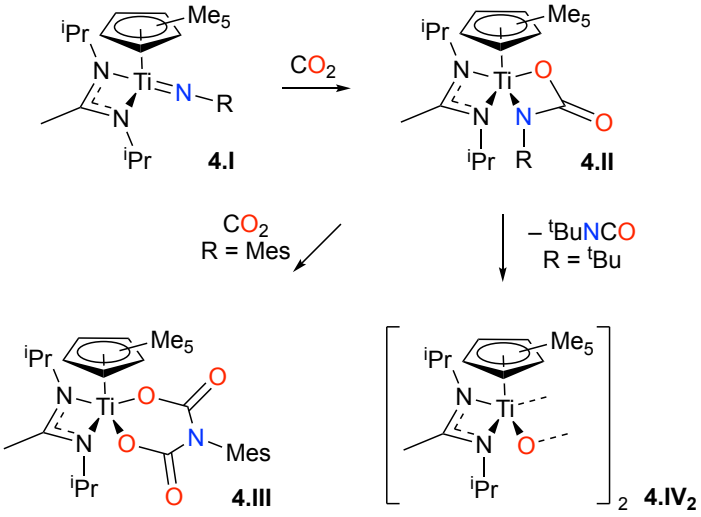

Scheme 4.2: Reactivity of Titanium imides with CO_2.

Also relevant to the work presented in this chapter is the reactivity of metal imides towards organic carbonyl compounds such as benzaldehyde. Such reactions have been reported for a titanium imide and one nickel imide.[28,32] In both cases as simple [2+2] cycloaddition reaction was observed, leading to the formation of a hemi-aminal complex.

Compared to *d*-block metals, monomeric imides of the *p*-block metals and metalloids are rare and their reaction chemistry is less well established. Only limited examples of reactions with CO_2 or other heterocumulenes have been reported.[33–37]

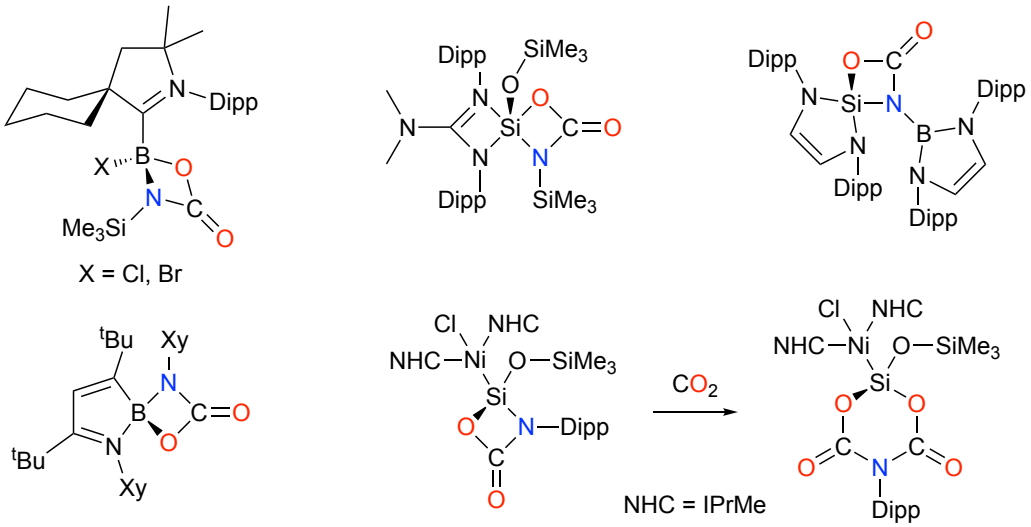

Figure 4.1: Products of the reaction of boron and silicon imides with CO_2.

Boron and silicon imides have been reported to undergo [2+2] cycloadditions with CO_2 to afford carbamates[33–37] and in one instance to uptake a second equivalent of CO_2 was reported, yielding an aminodicarboxylate complex.[37] Concurrent with the work presented in this chapter the Coles group reported on the synthesis of an anionic aluminium imide and its onward reactivity with CO_2.[30] In this case clean conversion to a carbamate complex was reported.

Unlike for transition metal systems, no elimination of an isocyanate from the carbamate species has been reported in the case of the main group systems. This is presumably due to the instability of putative oxide intermediates, arising from a lack of suitable (*d*-) orbitals for efficient π-bonding.

Here we report on the reactivity of aluminium imide K_2[**NON**Al(NDipp)]$_2$, K_2[**3.5**]$_2$, with CO_2, PhCHO, and N_2O, explore its cycloaddition chemistry and demonstrate that K_2[**3.5**]$_2$ acts an efficient transfer reagent for the $[DippN]^{2-}$ group.

4.2 Results and Discussion

4.2.1 Reactivity of K_2[NONAlNDipp]$_2$ towards CO_2 in benzene

Upon exposure of a dilute solution of imide K_2[**NON**Al(NDipp)]$_2$, K_2[**3.5**]$_2$, (10 mg mL^{-1}) in benzene to an atmosphere of CO_2 (1.2 bar, ca. 16 equiv.), clean conversion to a single set of products was observed. A ^{1}H NMR spectrum of the mixture obtained after 1 h, shows the two doublets at δ_H = 6.73 and 6.21 ppm, as well at two septets at δ_H = 3.71 and 3.09 ppm, indicating

the formation of a 1:1 mixture of the previously characterised carbonate K_2[**NON**AlCO_3]$_2$, K_2[**1.44**]$_2$, and DippNCO.

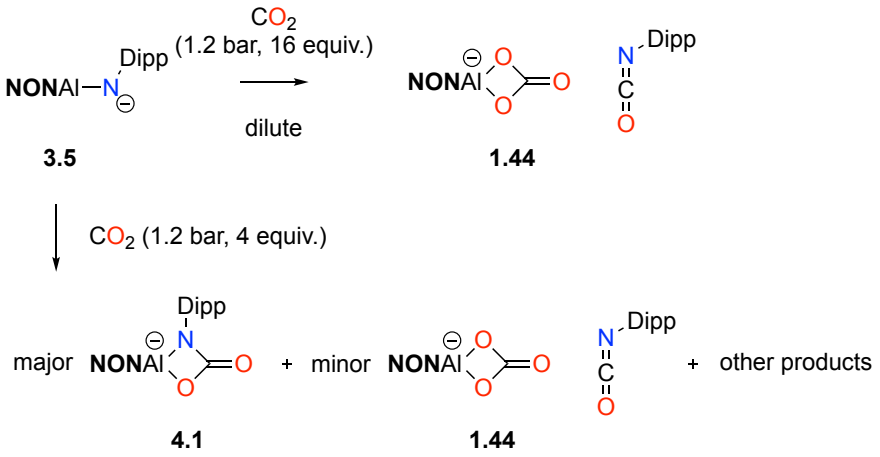

Scheme 4.3: Reactivity of imide K_2[**3.5**]$_2$ towards CO_2. For clarity compounds are shown as monomers and counter-ions are omitted.

When this reaction was repeated with a more concentrated benzene solution of imide K_2[**3.5**]$_2$ (40 mg mL^{-1}) and the same amount of CO_2 (1.2 bar, ca. 4 eqiv.), a mixture of products was formed, as judged by the ^{1}H NMR spectrum after a 10 minutes. Upon standing for one hour, no significant further change to the spectrum is observed. The spectrum shows formation of one major species, with resonances at δ_H = 6.65, 6.35, 3.98, 3.78, 2.60 ppm, corresponding to carbamate K_2[**NON**Al(NDippCO_2)]$_2$, K_2[**4.1**]$_2$, as well as the formation of a number of minor products including carbonate K_2[**1.44**]$_2$, and DippNCO. The former crystallises from the reaction mixture, upon standing overnight. This suggests that the supply of CO_2 and the solubility of the reaction products and intermediates limit the selectivity of this process.

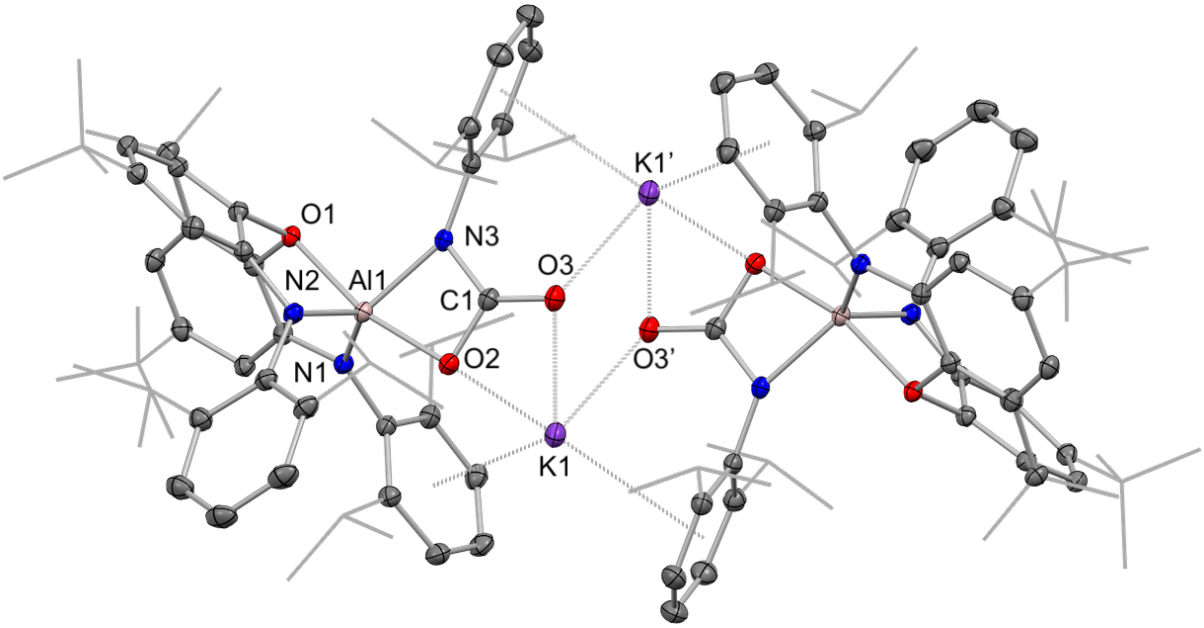

Figure 4.2: Molecular structure of K_2[**4.1**]$_2$ as determined by X-ray crystallography. Thermal ellipsoids drawn at 30% probability, H atoms omitted, and selected groups shown in wireframe format for clarity. Key bond lengths (Å): Al1–N3 1.9202(13), Al1–O2 1.9929(11), C1–N3 1.3660(18), C1–O2 1.3430(19), C1–O3 1.2323(19), O2–C1–N3 107.92(13), O2–C1–O3 122.94(14), O3–C1–N3 129.12(15).

The molecular structure of K_2[**4.1**]$_2$ in the solid state was determined by single crystal X-ray diffraction. K_2[**4.1**]$_2$ adopts a dimeric structure, in which two anionic [**NON**Al(NDippCO$_2$)]$^-$ fragments are bridged by K^+ counter-ions via K···Ar and K···O interactions. The carbamate group is planar and bond lengths and angles fall in the typical range for carbamate groups, i.e. the double bond is mostly localised, in this case on the C(1)–O(3) bond. An IR spectrum of K_2[**4.1**]$_2$ shows a band at ν = 1634 cm^{-1} for the C=O bond stretching mode. This frequency is lower than that observed for free terminal imides, presumably due to interactions with the K^+ counter-ions.

Having isolated carbamate K_2[**4.1**]$_2$ it remained to be shown that it can act as an intermediate in the formation of carbonate K_2[**1.44**]$_2$. To this end K_2[**4.1**]$_2$ was prepared in bulk. This was accomplished by injection of ca. 3 equiv. of gaseous CO_2 into a degassed toluene solution of the imide K_2[**3.5**]$_2$ at –78 °C via syringe and subsequent warming to room temperature. Within one hour precipitation of the targeted product was observed and K_2[**4.1**]$_2$ can be isolated in low to moderate yields upon standing overnight. Better yields are obtained when the headspace of

an ampoule is charged with a stoichiometric amount of CO_2 at elevated pressures (ca. 2 bar) under otherwise identical conditions. In this case a clean second fraction of product can be obtained by concentration of the mother liquor.

Attempts to dissolve isolated samples of K_2[**4.1**]$_2$ in benzene were unsuccessful and attempts to carry out a heterogeneous reaction with CO_2 in suspension were likewise unsuccessful at room temperature. Upon heating a mixture of K_2[**4.1**]$_2$ and CO_2 at 80 °C overnight, fairly clean conversion to one major new product, aminodicarboxylate K[**NON**Al{$(O_2C)_2$NDipp}], K[**4.2**], was observed. A ^{1}H NMR spectrum of the reaction mixture reveals signals at δ_H = 6.72, 6.23, 3.94, 1.98 ppm. Crystals suitable for single crystal X-ray diffraction were obtained from THF solution. During this reaction trace amounts of carbonate K_2[**1.44**]$_2$, DippNCO and the κ^2-O,O' bound isomer of the carbamate complex K[**NON**Al(O_2CNDipp)], K[**4.3**], were also observed.

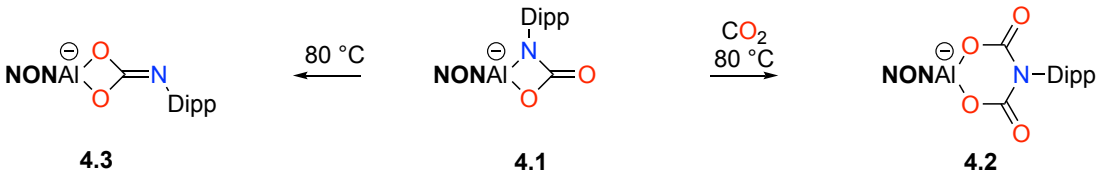

4.3 **4.1** **4.2**

Scheme 4.4: Reactivity of carbamate K_2[**4.1**]$_2$ towards CO_2 and thermal isomerisation. For clarity compounds are shown as monomers and counter-ions are omitted.

As a control experiment, a suspension of K_2[**4.1**]$_2$ (15 mg) in benzene (0.5 mL) was heated at 80 °C for 1 d. A ^{1}H NMR spectrum of the reaction mixture showed a 1:1 mixture of K_2[**4.1**]$_2$ and a new species with characteristic resonances at δ_H = 6.74, 6.12, 3.81, 3.65, 2.59 ppm. This new product was subsequently identified as K[**4.3**], and a crystal structure was obtained for the derivative [K(crypt)][**4.3**] as described in section 4.2.3. Furthermore, given the relative product distributions, it seems likely that K[**4.3**] also reacts with CO_2 to form K[**4.2**].

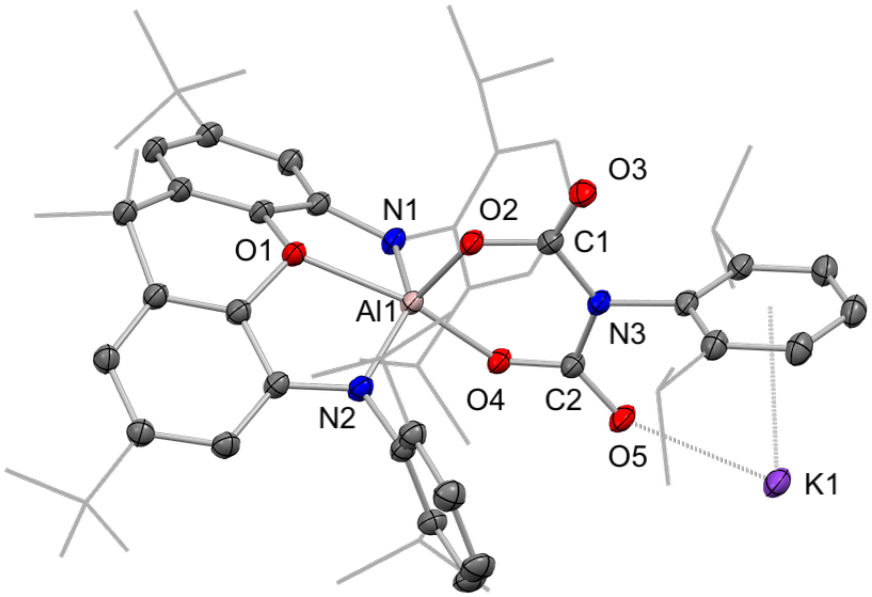

Figure 4.3: Molecular structure of one of the two inequivalent molecules in the asymmetric unit of K[**4.2**] as determined by X-ray crystallography. Thermal ellipsoids drawn at 30% probability, H atoms omitted, and selected groups shown in wireframe format for clarity. Key bond lengths (Å): Al1–O2 1.7909(19), Al1–O4 1.8066(16), O2–C1 1.301(3), O4–C2 1.281(3), C1–O3 1.216(3), C2–O5 1.222(3), C1–N3 1.413(3), C2–N3 1.419(3).

Crystals of [K(THF)$_2$][**4.2**] suitable for single crystal X-ray diffraction could be obtained from a concentrated THF solution. In the solid state the [K(THF)$_2$][**4.2**] forms a coordination polymer. [**NON**Al{(O$_2$C)$_2$NDipp}]$^-$ units are bridged by K$^+$ counter-ions via O(3) and O(5). The K$^+$ ions are each coordinated by two [**NON**Al{(O$_2$C)$_2$NDipp}]$^-$ units via O, one aryl group and two THF molecules (Figure 4.3). The asymmetric unit contains two independent molecules, and structural parameters are in good agreement for both molecules.

The N(CO$_2$)$_2$ unit is close to flat, but the two CO$_2$ units are rotated out of the plane in opposite directions, leading to deviations for up to 0.12 Å from the mean plane, presumably due to the coordination for the exocyclic O atoms to K. The six-membered Al-containing ring features endocyclic single bonds and exocyclic C–O double bonds. Interestingly both the formal C–O single and double bonds are shorter than the respective bonds in K$_2$[**4.1**]$_2$, an observation which presumably reflects the delocalisation of the N lone pair over more atoms, compared to the carbamate case (i.e. resonance structures indicate more double bond character for all bonds). Consistently, the endocyclic C-N bonds are longer than in the carbamate complex. In addition,

compared to K_2[**4.1**]$_2$ and [K(crypt)][**4.3**], [K(THF)$_2$][**4.2**] features shorter Al-O bonds, presumably due to the reduced ring strain. The IR spectrum of [K(THF)$_2$][**4.2**] features two signals associated with CO stretching modes at ν = 1697 and 1640 cm^{-1}. These appear at higher wavenumbers than in K_2[**4.1**]$_2$, presumably due to the delocalisation of the N lone pair over more atoms. Calculations suggest that the latter of the two bands overlaps with a xanthene based vibration.

Selective formation of the carbonate complex under high dilution conditions, and selective aminodicarboxylate formation at elevated temperatures raises the question as to why only traces amounts of the carbonate are formed at elevated temperatures. Based on literature precedent it seems likely that the reaction of the imide with CO_2 affords a carbamate species. Therefore formation of the carbonate likely proceeds via this intermediate. This implies that carbonate formation must have a lower barrier than double insertion. One possible explanation is that the formation of the carbonate is reversible. However in section 4.2.3 it will be shown that [K(crypt)][**NON**Al(CO_3)] is stable in the presence of DippNCO and CO_2 under experimentally relevant conditions.

A more likely explanation is that at higher temperatures K_2[**4.1**]$_2$ dissociates into monomers to a chemically relevant extent, while at lower temperatures it reacts as a dimer. Hence the reactive species are different, and different products are observed. Evidence for the monomerization of K_2[**4.1**]$_2$ at higher temperatures is provided by the thermal isomerisation to κ^2-O,O' K[**NON**Al(O_2CNDipp)], K[**4.3**], which requires the dimer to be broken to some degree. Evidence for a dimeric structure at room temperature comes from the fact that both imine K_2[**3.5**]$_2$ and the carbamate K_2[**4.1**]$_2$ adopt dimeric structures in the solid state. Moreover, it has previously been shown for K_2[**NON**Al]$_2$ that systems of this type retain their dimeric structure at room temperature in arene solution.

4.2.2 Reactivity of K_2[NONAlNDipp]$_2$ towards CO_2 in THF

To overcome the above solubility constraints K_2[**4.1**]$_2$ was dissolved in THF, in an attempt to study its reaction with CO_2 in solution. This however led to near instantaneous isomerisation to the κ^2-O,O' bound isomer, K[**4.3**]. This was demonstrated by dissolving a 1:1 mixture of K_2[**4.1**]$_2$ and K[**4.3**] in THF. A ^{1}H NMR spectrum thus obtained showed a single species in solution. Removal of volatiles *in vacuo* and dissolving the resulting compound in benzene, allowed for the measurement of a further ^{1}H NMR spectrum. It shows formation of a new compound [K(THF)$_2$][**4.3**], with characteristic resonances at δ_H = 6.75, 6.10, 3.80, 3.61, 2.71 ppm, which are similar to those observed for K[**4.3**], with the exception of the septet associated with the carbamate group (δ_H = 2.59 ppm). These signals are significantly different from those observed for the κ^2-N,O bound isomer K_2[**4.1**]$_2$.

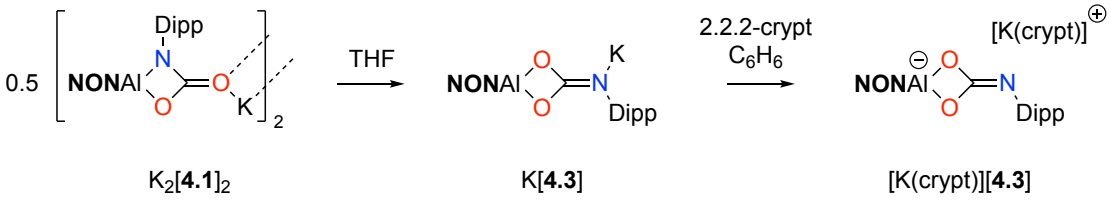

K_2[**4.1**]$_2$ K[**4.3**] [K(crypt)][**4.3**]

Scheme 4.5: Isomerisation of K_2[**4.1**]$_2$ to [K(THF)$_2$][**4.3**] in THF and synthesis of [K(crypt)][**4.3**].

Further evidence for the identity of K[**4.3**] in THF, comes from comparison with the spectra of [K(crypt)][**4.1**] and [K(crypt)][**4.3**], whose chemistry will be described in section 4.2.3. K[**4.3**] exhibits a resonance in the ^{13}C NMR at δ_C = 161.2 ppm in THF-d$_8$ for the carbamate/iminediolate functionality which is close to the resonance observed for the κ^2-O,O' bound isomer of [K(crypt)][**4.3**] (δ_C = 159.8 ppm in C_6D_6) compared to the resonance for the κ^2-N,O isomer [K(crypt)][**4.1**] (δ_C = 165.8 ppm in C_6D_6), the caveat being the different solvents. Furthermore, the xanthene-derived aromatic protons are of interest. K[**4.3**] exhibits resonances at δ_H = 5.71, 6.52 ppm in THF-d$_8$ or δ_H = 6.10, 6.75 ppm in C_6D_6, which are similarly spaced to those observed for κ^2-O,O' [K(crypt)][**4.3**] (δ_H = 6.22, 6.69 in C_6D_6) compared to the significantly more narrow spacing observed for K_2[**4.1**]$_2$ (δ_H = 6.35, 6.65 in C_6D_6) or κ^2-N,O [K(crypt)][**4.1**] (δ_H = 6.46, 6.63 ppm in C_6D_6).

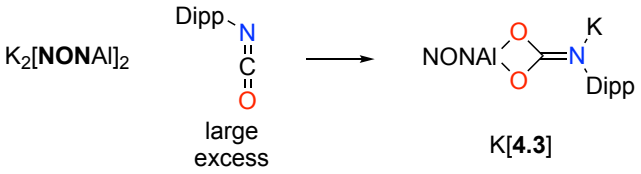

Scheme 4.6: Reaction of K_2[**NON**Al]$_2$ with excess DippNCO.

K[**4.3**] was also obtained from the reaction of K_2[**NON**Al]$_2$ with a large excess of DippNCO. In this case essentially clean conversion to K[**4.3**] and a further Dipp containing species, presumably DippNC, was observed by *in situ* ^{1}H NMR monitoring of the reaction. When a sub-stoiciometric amount of DippNCO was used, a complicated mixture of products is obtained, notably lacking either of the two isomers of the carbamate. Formation of a carbamate during the oxidation of aluminyl K_2[**NON**Al]$_2$ with PhNCO has previously been reported. However in the Ph case, the κ^2-N,O isomer is obtained. It is not obvious why in the case of DippNCO a different isomer would be obtained, although sterics and the excess of isocyanate might play a role. Furthermore, in chapter 5 it will be shown that a mixture of K_2[**NON**Al]$_2$ and DippNCO can act as a source of an aluminium oxide and DippNC.

Definitive proof for the connectivity of [K(THF)$_2$][**4.3**] was obtained by reacting the compound with 2.2.2-cryptand in benzene. This yielded the potassium sequestered compound [K(crypt)][**4.3**] (*vide infra*), which could also prepared via thermal isomerisation of the κ^2-N,O bound carbamate [K(crypt)][**4.1**]. An X-ray crystal structure was obtained to confirm the proposed connectivity.

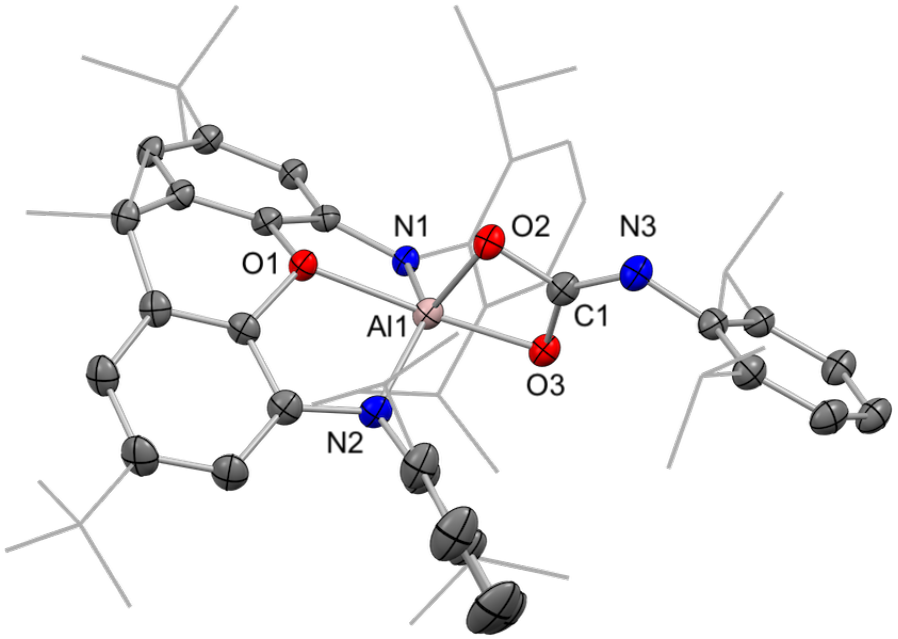

Figure 4.4: Molecular structure of the anion of [K(crypt)][**4.3**] as determined by X-ray crystallography. Thermal ellipsoids drawn at 30% probability, H atoms omitted, and selected groups shown in wireframe format for clarity. Key bond lengths (Å): Al1–O2 1.819(3), Al1–O3 1.850(3), C1–O2 1.353(4), C1–O3 1.335(4), C1–N3 1.279(5), O2–C1–O3 109.2(3), O2–C1–N3 121.5(3), N3–C1–O3 129.3(3).

Crystals of [K(crypt)][**4.3**] suitable for X-ray diffraction were obtained by layering a concentrated benzene solution with pentane. The $[K(crypt)]^+$ and $[\mathbf{NON}Al(O_2CNDipp)]^-$ units are well separated and there are no close contacts between the K^+ ion and the κ^2-O,O' carbamate group. The carbamate group is planar, but unlike for $K_2[\mathbf{4.1}]_2$, the double bond is localised on the C(1)-N(3) bond. This is reflected in the bond lengths and can be rationalised considering the respective resonance structures. Compared to $K_2[\mathbf{4.1}]_2$ the C-N bond is much shorter, while for the C–O bonds one falls into a similar range and one is longer. Further the Al–O bond lengths are shorter than the analogous Al–O and Al–N bonds, and the bite angle for this ligand is slightly wider.

The κ^2-O,O' coordination mode for a carbamate fragment is very rare. Only one example has previously been crystallographically characterised, and a further example was proposed based on NMR data.[38,39] Given that the crystallographically characterised example features silicon,

it comes as no surprise that the bond lengths and angles are comparable to those of [K(crypt)][**4.3**].

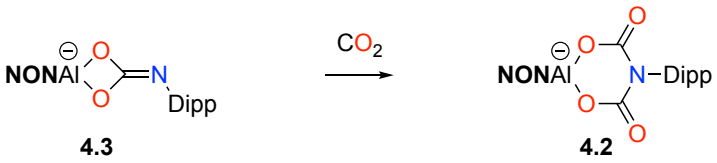

4.3 **4.2**

Scheme 4.7: Reaction of K[**4.3**] with CO_2 in THF.

When K[**4.3**] is reacted with CO_2 in THF, conversion to an aminodicarboxylate complex K[**4.2**] was observed within 2 h, alongside small amounts of carbonate K_2[**1.44**]$_2$ and unreacted K[**4.3**]. This reaction can alternatively be carried out, using the imine K_2[**3.5**]$_2$ as a starting material (in THF). In this case an identical product distribution is obtained.

4.2.3 Reactivity of 2.2.2-cryptand sequestered systems towards CO_2

An alternative approach to overcome the solubility constraints in the reaction of K_2[**4.1**]$_2$ with CO_2 is the utilisation of a sequestering agent, such as 2.2.2-cryptand. Accordingly 2 equiv. of 2.2.2-cryptand were added to K_2[**4.1**]$_2$ in benzene. Upon sonication and gentle warming, the ^{1}H NMR spectrum of the reaction mixture revealed formation a single new species, [K(crypt)][**4.1**]. This compound exhibits a resonance at δ_C = 165.8 ppm in benzene for the carbamate group in the $^{13}C\{^1H\}$ NMR spectrum, and a signal in the IR spectrum at ν = 1644 cm^{-1} for the C=O stretching mode. This frequency is 10 cm^{-1} higher compared to the unsequestered compound K_2[**4.1**]$_2$, and is consistent with the weakening of the C=O···K interaction.

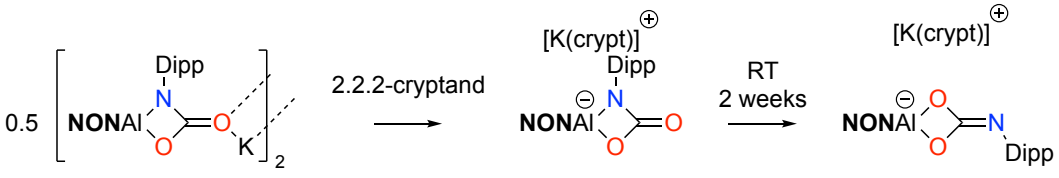

K_2[**4.1**]$_2$ [K(crypt)][**4.1**] [K(crypt)][**4.3**]

Scheme 4.8: Synthesis of [K(crypt)][**4.1**] and [K(crypt)][**4.3**].

Upon standing for 48 h at room temperature however, 30 % of the initial species [K(crypt)][**4.1**] was converted to a second species [K(crypt)][**4.3**]. After two weeks the reaction is mostly

complete (98%, 14 d) and crystals of the new product, suitable for single crystal X-ray diffraction, could be grown by layering a concentrated benzene solution with pentane. The molecular structure determined this way, reveals the second species to be the κ^2-O,O' bound isomer [K(crypt)][**4.3**]. Its molecular structure in the solid state is discussed above. This compound exhibits a resonance in the ^{13}C NMR at δ_C = 159.8 ppm in benzene, which is similar to the analogous resonance for the unsequestered κ^2-O,O' bound isomer K[**4.3**] in THF (δ_C = 161.2 ppm). The IR spectrum of this compound shows a signal at ν = 1621 cm^{-1} with a shoulder. It is assigned to stretching mode for the C=N bond, overlapping with a xanthene based vibration.

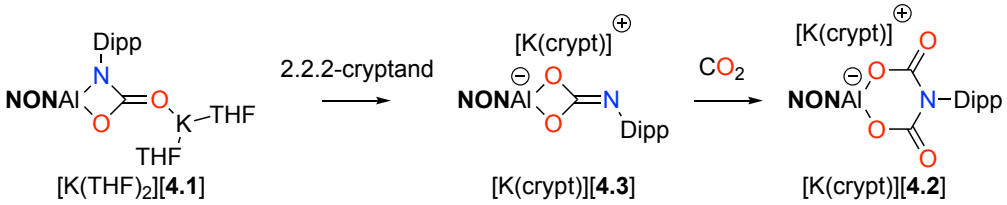

[K(THF)$_2$][**4.1**] [K(crypt)][**4.3**] [K(crypt)][**4.2**]

Scheme 4.9: Alternative synthesis of [K(crypt)][**4.3**] and reactivity towards CO_2.

Alternatively [K(crypt)][**4.3**] may be prepared from [K(THF)$_2$][**4.3**] and 2,2,2-cryptand in benzene. When a mixture of [K(crypt)][**4.3**] and 2 equiv. of THF, prepared in this manner, was exposed to an atmosphere of CO_2, clean conversion to [K(crypt)][**4.2**] was observed within 2 h at room temperature. No further experiments were carried out to determine what effect the residual THF has on the rate of the reaction, if any.

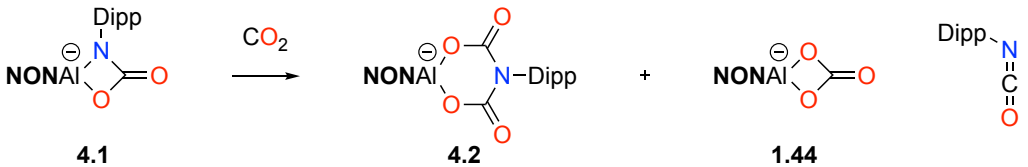

4.1 **4.2** **1.44**

Scheme 4.10: Reactivity of [K(crypt)][**4.1**] towards CO_2.

[K(crypt)][**4.1**] reacts with CO_2 over the course of two days to afford a mixture of carbonate [K(crypt)][**1.44**] and aminodicarboxylate [K(crypt)][**4.2**]. Over the course of the reaction no intermediates are observed by ^1H NMR. After 15 h approximately equal amounts of the carbonate and aminodicarboxylate are present, however when all of the starting material was consumed (after 62 h), the ratio is greater than 3:2 in favour of the aminodicarboxylate.

One possible explanation for these observations is the carbonate and double insertion product are formed at comparable rates, and that carbonate [K(crypt)][**1.44**] is a kinetic product, that might be interconverted to [K(crypt)][**4.2**], which is believed to be the thermodynamic product. To investigate this hypothesis, DippNCO was added to a solution of [K(crypt)][**1.44**] in benzene. Upon standing for three days no conversion to new products was observed by ^{1}H NMR. The mixture was then exposed to CO_2 and after an additional 24 h, still no traces of a reaction could be observed. No attempts were made to leave this mixture for longer, or heat it. It seems likely that formation of the carbonate is irreversible under experimentally relevant conditions. Therefore an alternative explanation for the change in product distribution is necessary.

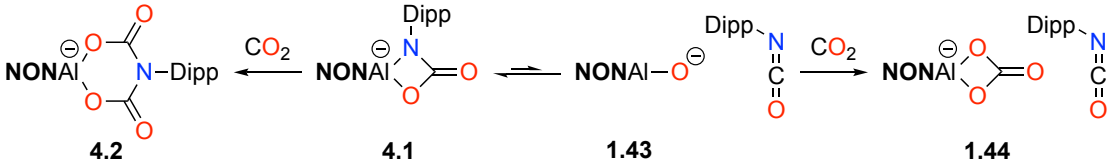

Scheme 4.11: A possible pathway for the formation of **4.2** and **1.44**.

A hypothetical pathway for the formation to the carbonate proceeds via elimination of DippNCO from [K(crypt)][**4.1**] to yield an oxide, which then traps CO_2 to afford the carbonate complex. In that case, as the reaction proceeded, the build-up of DippNCO would accelerate the back reaction to [K(crypt)][**4.1**], in effect slowing down the formation of the carbonate, while leaving the double insertion pathway unaffected. To test whether [K(crypt)][**4.1**] was a source of an oxide intermediate, a benzene solution of [K(crypt)][**4.1**] was exposed to an atmosphere of N_2O. The oxide intermediate has previously been shown to react rapidly with aluminium oxides, to form *cis*-hyponitrites. Over the course of 3 days 66% conversion (complete conversion after 10 days) from [K(crypt)][**4.1**] to [K(crypt)][**4.3**] was observed, but no formation of the hyponitrite complex or DippNCO. During the same timeframe the analogous reaction with CO_2 had gone to completion, indicating that the oxide is not an intermediate in this reaction.

Alternatively, it is conceivable that a pathway for formation of [K(crypt)][**4.2**] via [K(crypt)][**4.3**] is important. The reaction of [K(crypt)][**4.3**] to [K(crypt)][**4.2**] has been shown to procced quickly, albeit in the presence of 2 equiv. of THF. Formation of [K(crypt)][**4.3**] from [K(crypt)][**4.1**] has been shown to proceed in the absence of CO_2, and in the case of the unsequestered system, to happen very quickly in THF. Therefore formation of the aminodicarboxylate via [K(crypt)][**4.3**] is less affected by a decrease in CO_2 concentration, than formation of the carbonate, and in addition might be catalysed by a build-up of DippNCO.

It is the case, however, that other factors, such as changing polarity of the solvent and the interaction of the $[K(crypt)]^+$ counter-ions with the various species may also be important.

Beyond the IR stretching frequencies, potential evidence for the interaction between the $[K(crypt)]^+$ cation and the anions was obtained by comparison of ^{1}H NMR spectra. While the two sets of OC*H*$_2$ signals appear in a similar position for all compounds, the peaks associated with the NC*H*$_2$ groups seem to shift depending on the anion. [K(crypt)][**4.1**] and [K(crypt)][**1.44**], have similar shifts and appear downfield shifted, compared to [K(crypt)][**4.2**] and [K(crypt)][**4.3**] which are also similar. It is conceivable that this shift is a measure for the interaction of the anion with the K^+ ion.

Table 4.1: ^{1}H NMR shift of the NC*H*$_2$ groups

species	δ_H / ppm in C_6D_6
2.2.2-cryptand	2.53
[K(crypt)][**4.1**]	2.14
[K(crypt)][**NON**AlCO$_3$]	2.13
[K(crypt)][**4.2**] + 2 THF	2.05
[K(crypt)][**4.3**]	2.03
[K(crypt)][**NON**AlNDipp]	1.99
[K(crypt)][**NON**Al(κ^2-C$_6$H$_6$)]	1.97

The viability of interactions of the sequestered K^+ ion with the anions, is demonstrated by Coles' [K(crypt)][{O(SiMe$_2$NDipp)$_2$}Al(ONNO)] complex. This complex features a ligand with similar steric profile, and has been shown to feature an interaction between the K atom and the anion via K···N contacts in the solid state.

For completeness is should be noted that [K(crypt)][**1.44**] and [K(crypt)][**4.2**] can be prepared independently via the addition of 2.2.2-cryptand to the carbonate and K_2[**4.2**]$_2$ respectively in benzene. The carbonate has a $^{13}C\{^1H\}$ resonance at δ_C = 163.0 ppm in benzene, which is comparable to the shift for the unsequestered carbonate δ_C = 164.5 ppm in THF. Similarly the [K(crypt)][**4.2**] gives rise to a resonance at δ_C = 153.6 ppm in benzene, which is similar to K[**4.2**], at δ_C = 154.5 ppm in THF.

4.2.4 Computational considerations

With a plethora of experimental observations in hand, we attempted to understand the mechanism better by turning to DFT studies. Calculations were carried out at the B3LYP/def2-SVP level of theory on model systems, where ^{t}Bu and ^{i}Pr groups were replaced with Me groups for computational efficiency. Attempts extend these calculation to the B3LYP/def2-TZVP level were only partially successful, and these results are detailed towards the end of this section.

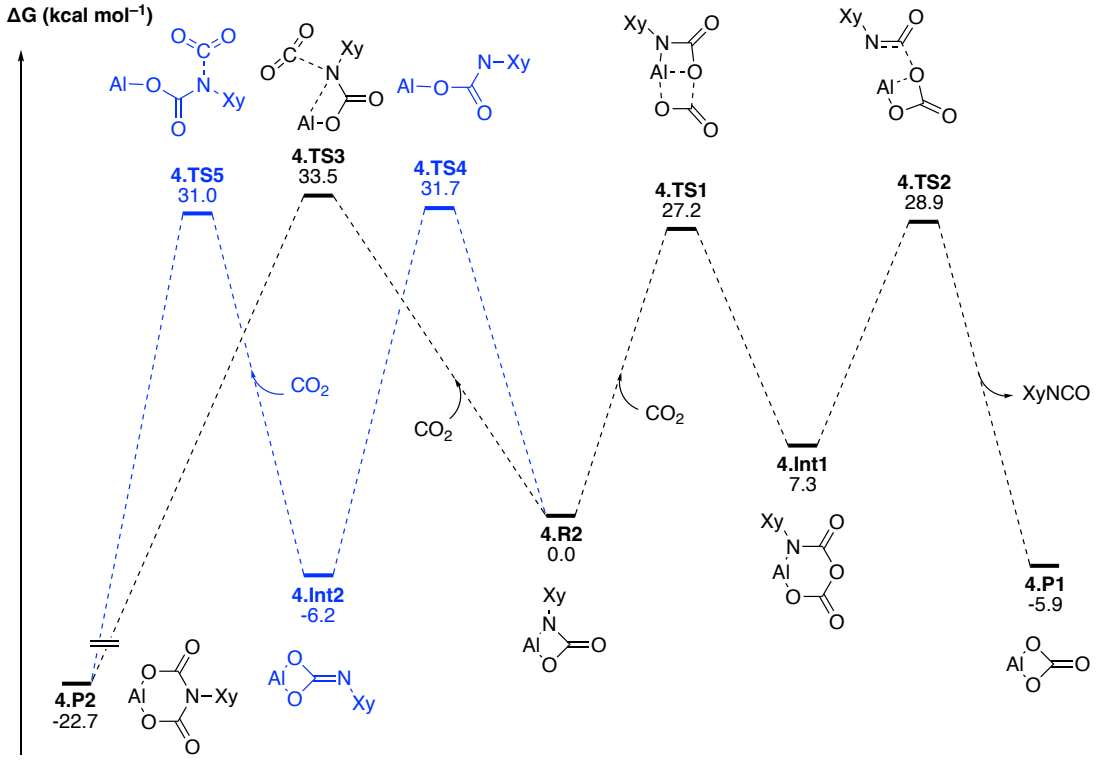

Figure 4.5: Potential energy profile calculated at the B3LYP/def2-SVP level of theory.

The model imide **4.R1** reacts with CO_2 in a barrierless process, to afford carbamate **4.R2**. Figure 4.5 shows how **4.R2** may be converted into the observed products. CO_2 may add to the Al–O bond, via **4.TS1** in a formal [2+2] cycloaddition. In this transition state the Al–O bond is elongated by ca 0.1 Å relative to **4.R2**. The Al–O bond is then further elongated to yield a 6-membered ring, **4.Int1**. Reformation of the Al–O bond then yields **4.TS2**, from which a molecule of isocyanide is lost to afford carbonate **4.P1**. **4.TS1** and **4.TS2** are nearly identical in geometry, only differing significantly in the angle of the [ArNC(O)OCO_2] fragment relative to the plane of the ligand. This raises the question how these transition states are connected. A minimum energy pathway between **4.R2** and **4.P1** obtained via the nudged elastic band (NEB) method only find a single maximum and fails to find **4.Int1**, perhaps due to the insufficient picture density. However following the intrinsic reaction coordinate (IRC) from both **4.TS1** and **4.TS2** shows that **Int1** is an intermediate along the minimum energy pathway. Experimentally there is no evidence for **4.Int1** even if the energy barriers would suggest, that **4.Int1** should be observable.

An alternative pathway for the formation of the carbonate **4.P1** was considered. This involved extrusion of isocyanide from **4.R2**, to yield an oxide intermediate **4.Int4**, which would then trap CO_2. The latter of the two steps has previously been observed experimentally. However the reaction coordinate associated with the oxide intermediate **4.Int4** lies 40.5 kcal mol^{-1} above **4.R2** and can thus be ruled out as an intermediate.

Formation of aminodicarboxylate **4.P2**, via the formal [2+2] cycloaddition of CO_2 across the Al–N bond of **4.R2** has been calculated to proceed via **4.TS3**. This reaction proceeds stepwise via CO_2 assisted breaking of the Al–N bond first, followed by the formation of the N–C bond second, and finally formation of the Al–O. Attempts to confirm the nature of the transition state by IRC were unsuccessful, due to the flatness of the potential energy surface. Similarly attempts to optimise the structure from near the transition state were unsuccessful. In both cases the methods did not converge on a minimum. It can however be shown that formation of **4.P2** (and also **4.Int2**) from this geometry proceeds without a barrier.

Alternatively **4.P2** may be accessed via isomerisation of **4.R1** to κ^2-O,O' bound isomer **4.Int2** via **4.TS4**. As expected the total energy **4.TS4** is higher than that of **4.TS3** due to the lack of a stabilising interaction with CO_2, however the Gibbs free energy is slightly lower. **4.Int2** can then undergo an onward reaction with CO_2. Elongating one of the Al–O bonds leads to enhanced nucleophilicity of the N atom, allowing for the capture of a second molecule of CO_2, and formation of the observed product **4.P2**.

Attempts to calculate this mechanism using the def2-TZVP basis set were complicated by the flatness of the potential energy surface around **4.TS3** and **4.TS4**. Attempts to optimise **4.TS3** freely did not converge. Instead **4.TS3** was located by scanning the potential energy surface along the Al–N bond, taking the maximum, freezing the coordinates of the metal complex and refining the position of the CO_2 molecule only. **4.TS4** was not located and **4.TS5** has a small second imaginary frequency. Results are shown in Figure 4.6.

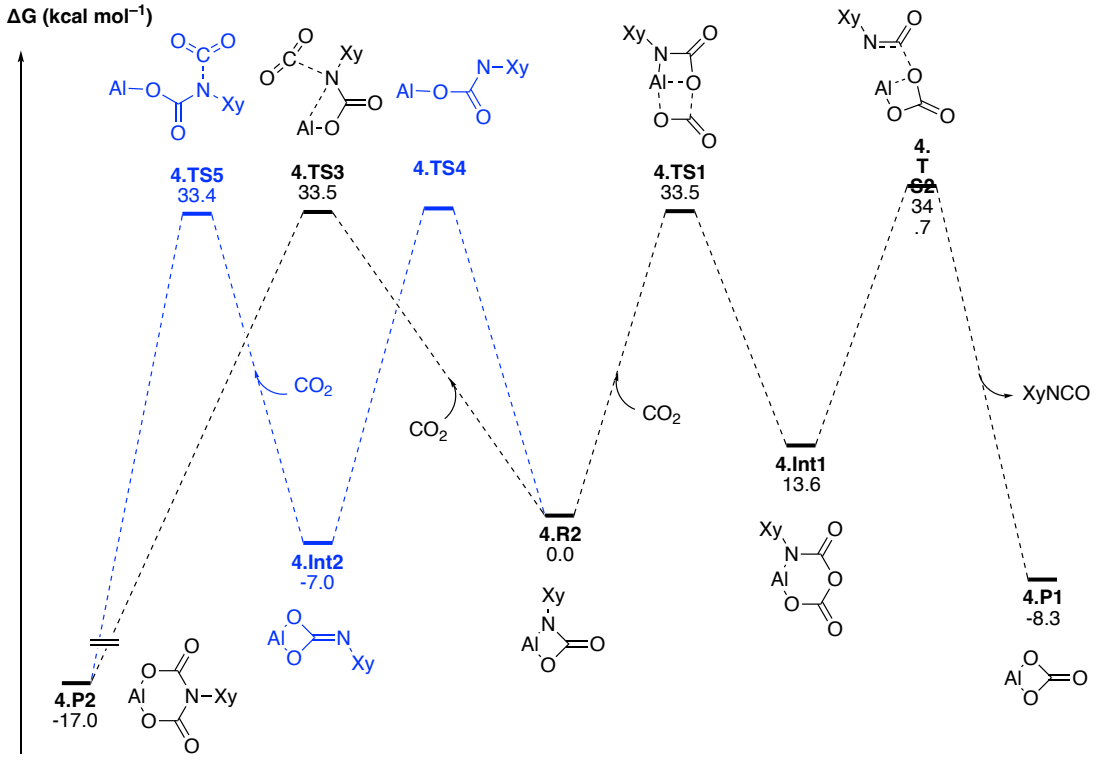

Figure 4.6: Potential energy profile calculated at the B3LYP/def2-TZVP level of theory.

These calculations agree well with most the experimental observations for the crypt-sequestered system. **4.R2**, **4.Int2**, **4.P1** and **4.P2** have sensible energies relative to each other. Furthermore, the calculations suggest that formation of carbonate, aminodicarboxylate, and carbamate isomer products proceed via pathways with similar rate-limiting barriers, and the magnitude of these barriers is consistent with reactions that occur over a timeframe on the order of days.

Where the calculations fall short is explaining the product distribution for the reaction of K_2[**4.1**]$_2$ with CO_2 in benzene or THF. In benzene only the carbonate is observed at low concentrations. The calculations show that formation of the aminodicarboxylate involves elongation of the Al–N bond in either of the transition states. Since the initially formed carbamate is likely a dimer in solution, steric constraints likely raise the energies of **4.TS3** and **4.TS4**. Therefore only formation of the carbonate is observed.

In THF rapid isomerisation of K_2[**4.1**]$_2$ to [K(THF)$_2$][**4.3**] is observed, and the latter undergoes onward reactivity with CO_2 to yield [K(THF)$_2$][**4.2**]. In THF these species are likely monomers. It is conceivable that THF lowers the energies of **4.TS4** and **4.TS5** either on account of the

greater polarity of the solvent, or by stabilisation of the quasi three-coordinate aluminium centre via coordination. Therefore only formation of the aminodicarboxylate is observed.

4.2.5 Reactivity of K_2[(NON)AlNDipp]$_2$ towards benzaldehyde

Having demonstrated that K_2[**3.5**]$_2$ is an effective transfer agent for the [NDipp] functionality towards CO_2, other substrates were explored. It appears that the formation of new Al–O bonds provides a driving force for the above transformations. Benzaldehyde seems like the ideal candidate, as it is a non-enolisable carbonyl compounds with small steric profile, and as such provides the necessary orbitals to undergo cycloadditions, while simultaneously having the ability to form strong Al–O bonds, without having any acidic protons.

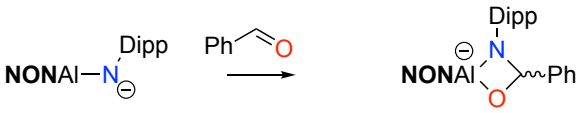

3.5 (+/-) **4.4**

Scheme 4.13: Reaction of K_2[**NON**AlNDipp]$_2$ with PhCHO.

Experimentally, addition of excess benzaldehyde to a benzene solution of K_2[**3.5**]$_2$ leads to the clean formation of the hemi-aminal product K[**4.4**] via formal [2+2] cycloaddition. K[**4.4**] rapidly crystallises as thin hairs. *In situ* monitoring of the reaction by ^{1}H NMR reveals conversion to a single highly asymmetric product. The spectrum of the compound is consistent with the presence of a chiral centre in the molecule, and the incorporation of 1 equiv. of benzaldehyde is further confirmed by an additional singlet in the ^{1}H NMR at 7.06 ppm integrating to 1H with respect to an unsymmetrical ligand backbone. Presumably the two enantiomers of the product are formed racemically.

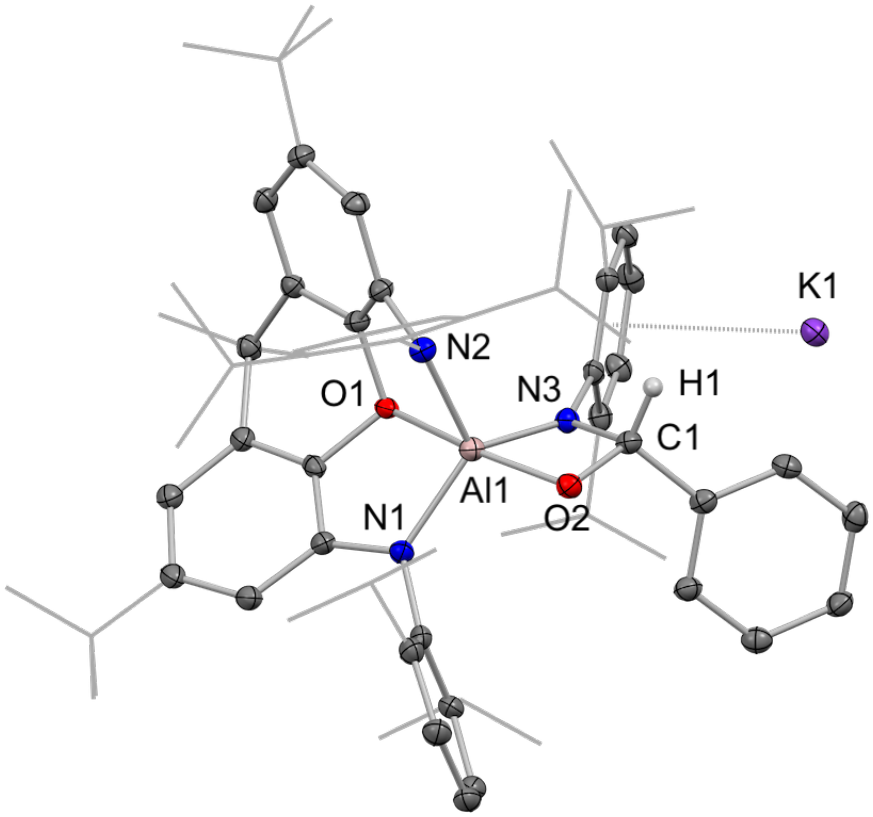

Figure 4.6: Molecular structure of K[**4.4**] as determined by X-ray crystallography. Thermal ellipsoids drawn at 30% probability, H atoms omitted, and selected groups shown in wireframe format for clarity. Key bond lengths (Å): Al1–N3 1.846(4), Al1–O2 1.826(3), N3–C1 1.477(6), O2–C1 1.432(5), N3–C1–O2 99.9(3), N3–C1–C2 111.8(4), O2–C1–C2 113.1(4), H1–C1–C2 110.5(0).

The molecular structure in the solid state could be determined by single crystal X-ray diffraction, and confirms the expected connectivity of the product. K[**4.4**] crystallises in the chiral space group $P3_2$, and contains a single enantiomer. Presumably the other enantiomer gives rise to a second type of crystal in the space group $P3_1$, however this was not measured. In benzene solution, K[**4.4**] forms a coordination polymer, which explains the low solubility.

The C(1)–O(2) and C(1)–N(3) bond lengths are consistent with single bonds and are longer than those in the carbamate complex K_2[**4.1**]$_2$. Al(1)–O(2) and Al(1)–N(3) are shorter than in K_2[**4.1**]$_2$, presumably due to a more localised charge on O(2) and N(3), as well as the greater flexibility of the four membered ring. C(1) is approximately tetrahedral, but N(3)–C(1)–O(2) is significantly smaller than the ideal angle due to ring strain.

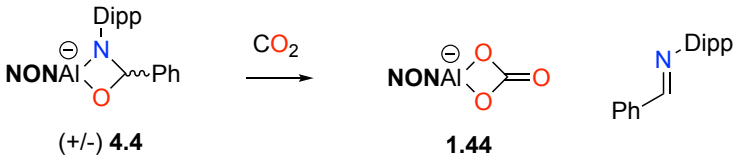

Scheme 4.14: Reaction of K[**4.4**] with CO_2.

Inspired by the reactivity of K_2[**4.1**]$_2$ with CO_2 and a comparable coordination environment around Al, K[**4.4**] was reacted CO_2 in THF. This reaction leads to the formation of PhC(H)NDipp and carbonate K_2[**1.44**]$_2$, over the course of 2 d. A single isomer of the imine, presumably E, is observed in the ^{1}H NMR spectrum. These observations support the mechanism proposed above for the formation of **4.P1** via spectrum **4.TS1**, i.e. the addition of CO_2 across an intact Al–O bond. This once again shows that K_2[**3.5**]$_2$ can be used as a transfer reagent for the [NDipp] fragment.

4.2.6 Reactivity of K_2[(NON)AlNDipp]$_2$ towards N_2O

Upon exposing a benzene solution of K_2[**3.5**]$_2$ to an atmosphere of N_2O, conversion to K_2[**NON**Al(ONNO)]$_2$ (K_2[**1.46**]$_2$) and DippN$_3$ was observed in near quantitative yields within 1 h. A ^{1}H NMR spectrum obtained after 5 min reveals a new set of signals at δ_H = 6.73, 5.97, 3.67, 3.33 ppm, corresponding to the observed products. After 1 h only the product peaks are observable by NMR. No intermediates were observed.

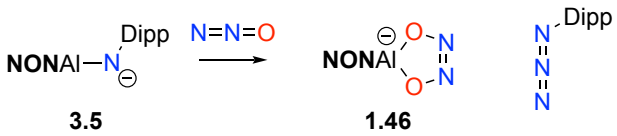

Scheme 4.15: Reactions of K_2[**NON**AlNDipp]$_2$ and [K(crypt)][**NON**AlNDipp] with N_2O.

This reaction presents a further example of an reaction where formation of Al-O bonds is used as a driving force to transfer the [NDipp] fragment. In an attempt to detect potential intermediates, K_2[**3.5**]$_2$ was reacted with a sub-stoichiometric amount of N_2O. Only traces of hyponitrite complex K_2[**1.46**]$_2$ and DippN$_3$ were observed after 5 min by ^{1}H NMR. Upon standing overnight, only the previously observed products, alongside unreacted starting material were observed, indicating that possible intermediates in the reaction are more reactive/have lower barriers towards onward reactivity with N_2O, than the starting imide.

To gain additional insights into the reaction solution of [K(crypt)][**3.5**] was prepared from K_2[**3.5**]$_2$ and 2.2.2-cryptand in benzene, and immediately reacted with N_2O. Interestingly this did not lead immediately to the disappearance of the blue colour associated with [K(crypt)][**3.5**]. A ^{1}H NMR spectrum obtained after 5 min shows complete consumption of starting materials, and formation of one set of major products with signals at δ_H = 6.71, 6.21, 4.05, 3.33 ppm, alongside a minor product (δ_H = 6.75, 6.21). Monitoring this reaction for 2 d, did not lead to a change of the spectrum, however the blue colour disappeared.

The major signals are proposed to correspond to *cis*-hyponitrite [K(crypt)][**1.46**] and $DippN_3$ in a 1:1 ratio. The alternative product [K(crypt)][**NON**AlO] can be ruled out on the basis, that previous attempts to isolate this compound have revealed it to be highly unstable, and an analogous onward reaction of [K(crypt)][{O(SiMe$_2$NDipp)$_2$}AlO] with N_2O has been reported by the Coles group.[40]

The minor product could potentially be the [2+3] addition product [K(crypt)][**NON**Al{N(Dipp)NNO}]. If that were the case, it suggests that the [2+3] addition product would either be in equilibrium with the hyponitrite complex, or not be an intermediate in the formation of the latter. Furthermore, the apparent low selectivity of this reaction could point towards a highly reactive intermediate, such as [K(crypt)][**NON**AlO]. The minor products could then be explained by the decomposition of such an intermediate.

In an attempt to assess the viability of a retro [2+3] addition, a benzene solutions of tetrazene complexes K_2[**NON**Al{N$_4$(R)$_2$}]$_2$ (R = SiMe$_3$, ^{t}BuC$_6$H$_4$), K_2[**3.1**] or K_2[**3.3**]$_2$, were exposed to an atmosphere of N_2O, leading to a slight broadening of the ^{1}H NMR spectra. Upon heating at 80 °C for 1 day, no reaction was observed. These observations suggest that cyclo-reversions from a 5-membered ring of this type are potentially difficult.

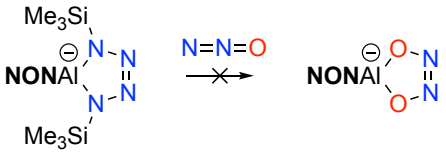

Scheme 4.16: Attempted reaction of K_2[**NON**Al{N_4($SiMe_3$)$_2$}]$_2$ with N_2O.

To shed some light into the reaction mechanism, the reaction of imide K_2[**3.5**]$_2$ and N_2O was investigated by DFT methods.

4.2.7 Computational considerations

The reaction mechanism for the reaction between imide K_2[**3.5**]$_2$ and N_2O was calculated by DFT methods. Calculations were performed at the B3LYP/def2-TZVP level of theory. In the interest of computational efficiency ^{i}Pr and ^{t}Bu groups were replaced by Me, and K^+ counter-ions were omitted. This methodology was chosen to allow for comparison with the CO_2 mechanism (*vide supra*). The results of the calculations are summarised in Scheme 4.17.

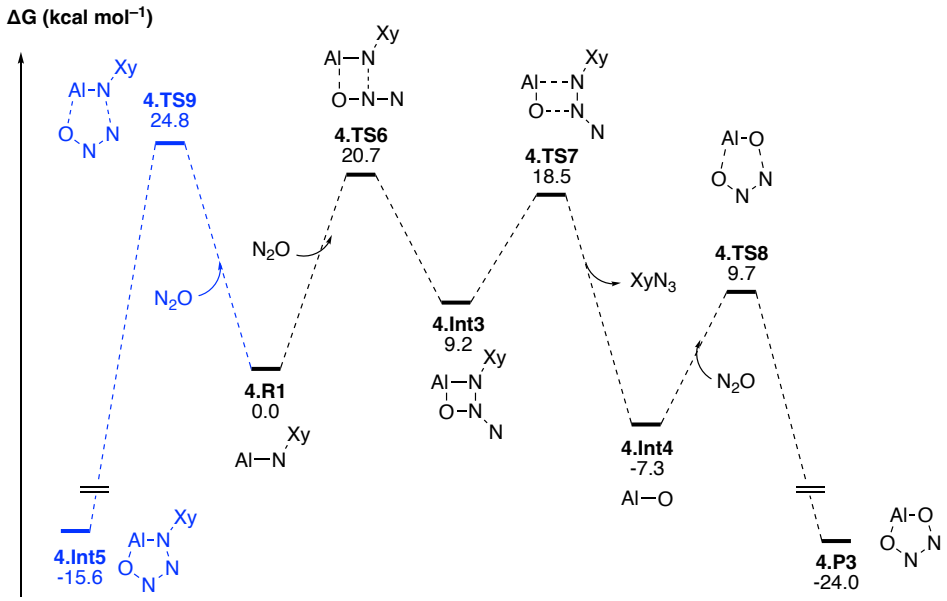

Scheme 4.17: Potential energy profile calculated at the B3LYP/def2-TZVP level of theory.

Different modes of reactivity are conceivable for the initial interaction of the imide with N_2O. Initially a formal [2+3] cycloaddition was considered. This process was found to possess a moderate activation barrier of 24.8 kcal mol^{-1}. The resulting intermediate **4.Int5** is significantly more stable than the starting materials and possesses the expected geometry. For the onward reaction extrusion of XyN_3 to generate **4.Int4** was considered, as well as a further [2+3]

cycloaddition of N_2O across the AlO bond of **4.Int5**. Preliminary work at the B3LYP/def2-SVP level indicated that both pathways occur via transition states high in energy. As such, no low energy pathway connecting **4.Int5** to the product **4.P3** was found, suggesting that **4.Int5** was not an intermediate in the formation of the product. While not observable in the reaction of K_2[**3.5**]$_2$ with N_2O, it might account for the minor product of the analogous reaction in the presence of 2.2.2-cryptand.

Therefore a pathway starting with the [2+2] cycloaddition between N_2O and imide **4.R1** was considered. The activation barrier for this process was found to be 4.1 kcal mol^{-1} lower than for the [2+3] addition. The resulting intermediate **4.Int3** is less stable than the starting materials and can extrude xylylazide to afford the oxide intermediate **4.Int4**. The latter then undergoes a [2+3] cycloaddition with a further molecule of N_2O to afford **4.P3**.

These calculations thus suggest that the reaction of the imide K_2[**3.5**]$_2$ and N_2O proceed via initial [2+2] cycloaddition, rather than [2+3] cycloaddition. Both the overall barrier and all of the individual barriers for the [2+2] pathway have been calculated to be smaller than the barrier the barrier associated with an initial [2+3] addition. To the best of my knowledge [2+2] cycloadditions with N_2O lack literature precedent. However given the isoelectronic relationship between the latter and CO_2 it is conceivable, that both molecules might follow an analogous reaction pathway. Crucially the LUMO of both molecules contain a lobe on the central atom, albeit it not being the dominant feature in the case of N_2O.

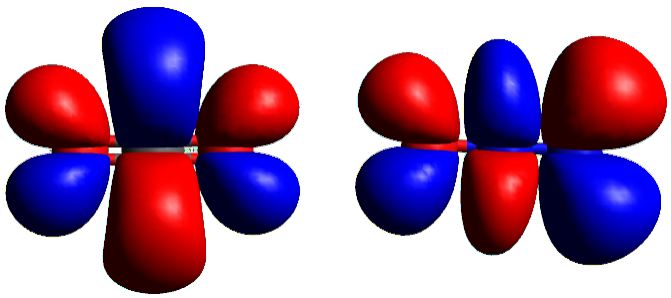

Figure 4.7: LUMO of CO_2 (left) and N_2O (right) calculated at B3LYP/def2-SVP level. Isovalue 0.02.

4.3 Conclusions

The work presented in this chapter describes the reactions of imide K_2[**3.5**]$_2$ with CO_2, PhCHO, and N_2O. It is shown that K_2[**3.5**]$_2$ acts as an efficient transfer reagent for the $[NDipp]^{2-}$ fragment, towards unsaturated oxygen containing substrates. CO_2, PhCHO, and N_2O were converted to DippNCO, PhC(H)NDipp, and $DippN_3$ respectively. These transformations are presumably driven by formation of new Al-O bonds in the aluminium containing side products.

The reaction of K_2[**3.5**]$_2$ with CO_2 produces a wide range of products, depending on conditions. In aromatic solvents this reaction either yields a mixture of the carbonate complex K_2[**1.44**]$_2$ and DippNCO, or the carbamate complex K_2[**4.1**]$_2$. The former is obtained under high dilution conditions in the presence of a large excess of CO_2, while the best yield of the latter are obtained at high concentrations and stoichiometric amounts of CO_2. This suggests that the carbamate is an intermediate in the formation of the carbonate. However, isolated samples of carbamate K_2[**4.1**]$_2$ do not react with CO_2 in arene solutions under ambient conditions, due to very low solubility. Upon heating to 80 °C overnight, conversion to amino dicarboxylate K[**4.2**] was observed.

Dissolution of carbamate K_2[**4.1**]$_2$ in THF leads to the rapid isomerisation to K[**4.3**]. Addition of CO_2 to this isomer leads to the formation of aminodicarboxylate [K(THF)$_2$][**4.2**]. Addition of 2.2.2-cryptand to a benzene solution of K_2[**4.1**]$_2$ leads to the formation of [K(crypt)][**4.1**]. Upon standing for two weeks, isomerisation to [K(crypt)][**4.3**] is observed.

The reaction of carbamate [K(crypt)][**4.1**] with CO_2 in benzene leads to the formation of a mixture of aminodicarboxylate [K(crypt)][**4.2**] and carbonate [K(crypt)][**1.44**] / DippNCO. To probe the reversibility of the carbonate formation, DippNCO was added to [K(crypt)][**1.44**], however no reaction occurred. Addition of CO_2 to this mixture similarly did not lead to a reaction. This suggests that the carbonate formation is irreversible.

Given the literature precedent for oxo species as products in these kinds of reactions in transition metal chemistry, carbamate [K(crypt)][**4.1**] was investigated as a source of an

aluminium oxide. Upon exposure to N_2O no reaction was observed, implying that no oxide intermediate is formed under these conditions.

The mechanism for these reactions was investigated by DFT calculations, and confirms the main features of the reactions, including the relative stabilities of the observed products. Carbonate formation is calculated to occur via [2+2] cycloaddition of CO_2 to the Al–O bond of the carbamate, while formation of the aminodicarboxylate occurs via prior dissociation of the Al–N bonds, with or without the intermediate formation of the carbamate isomer.

This cycloaddition chemistry is not limited to CO_2, and K_2[**3.5**]$_2$ reacts with benzaldehyde via a [2+2] cycloaddition to yield the hemi-aminal complex K[**NON**Al{NDippC(H)(Ph)O}]. This compound can undergo onward reactivity with CO_2 to yield carbonate [K(crypt)][**1.44**] and the organic imine PhCHNDipp.

Imide K_2[**3.5**]$_2$ also reacts cleanly with N_2O to yield K_2[**NON**Al(ONNO)]$_2$ and DippN_3, while [K(crypt)][**3.5**] reacts with N_2O to yield the analogous hyponitrite complex, however an additional side product(s) is observed. DFT investigations of this reaction mechanism suggest, that the reactions proceed via an initial [2+2] cycloaddition between the imine functionality and N_2O. The anticipated [2+3] cycloaddition is found to have a higher barrier.

In summary, the cycloaddition chemistry of K_2[**3.5**]$_2$ with simple unsaturated oxygen containing substrates was explored. Products maximise the formation of new Al-O bonds at the expense of Al-N bonds. This allows the imide to act as an $[NR]^{2-}$ fragment transfer reagent.

4.4 Experimental details

K_2[(NON)Al{κ^2-(N,O)-(NDippCO$_2$)}]$_2$, K_2[4.1]$_2$: A 15 mL reaction bomb, containing a degassed solution of K_2[**3.5**]$_2$ (320 mg, 0.35 mmol) in toluene (11 mL) at -78 °C, was charged with CO_2 (4 mL, 2.2 bar, 0.36 mmol). Upon standing overnight at room temperature, K_2[**4.1**]$_2$ was obtained as a white precipitate. Isolated yield: 123 mg, 37%. Anal. calc. for $C_{120}H_{158}Al_2K_2N_6O_6$: C 75.35, H 8.33, N 4.39, found: C 75.18, H 8.22, N 4.35.

^{1}H NMR (400 MHz, C_6D_6, 298 K): δ 7.18 – 7.27 (m, 2H, Ar*H*), 6.94 – 7.14 (m, 7H, Ar*H*), 6.65 (d, $^{4}J_{HH}$ = 1.9 Hz, 2H, XA-Ar-C*H*), 6.35 (d, $^{4}J_{HH}$ = 1.8 Hz, 2H, XA-Ar-C*H*), 3.97 (sept., $^{3}J_{HH}$ = 7.3 Hz, 2H, C*H*(CH_3)$_2$), 3.78 (m, 2H, C*H*(CH_3)$_2$), 2.60 (m, 2H, C*H*(CH_3)$_2$), 1.65 (s, 3H, C(C*H*$_3$)$_2$), 1.48 (s, 3H, C(C*H*$_3$)$_2$), 1.45 (d, $^{3}J_{HH}$ = 6.7 Hz, 6H, CH(C*H*$_3$)$_2$), 1.30 (d, $^{3}J_{HH}$ = 6.8 Hz, 6H, CH(C*H*$_3$)$_2$), 1.22 (d, $^{3}J_{HH}$ = 6.6 Hz, 6H, CH(C*H*$_3$)$_2$), 1.18 (s, 18H, C(C*H*$_3$)$_3$), 0.95 (br. d, 2H, CH(C*H*$_3$)$_2$), 0.75 (d, $^{3}J_{HH}$ = 6.5 Hz, 6H, CH(C*H*$_3$)$_2$),0.72 (d, $^{3}J_{HH}$ = 6.7 Hz, 6H, CH(C*H*$_3$)$_2$).

Due to the low solubility in compatible solvents no ^{13}C{^{1}H} NMR data could be obtained.

[K(THF)$_2$][NONAl{(CO$_2$)$_2$NDipp}], [K(THF)$_2$][4.2]:

Method 1: CO_2 was bubbled through a solution of K_2[**3.5**]$_2$ (250 mg, 0.14 mmol) in THF (5 ml) for 2 minutes at room temperature, leading to a near colourless solution. Upon standing over night, colourless crystals of [K(THF)$_2$][**4.2**] formed. Yield 200 mg, 64 %. Method 2: Same as method 1, but using K_2[**4.1**]$_2$ instead of K_2[**3.5**]$_2$. Method 3: A suspension of K_2[**4.1**]$_2$ (20 mg, 0.02 mmol) in C_6D_6 (0.5 mL) was exposed to CO_2 (1.2 bar, 3 ml). Upon heating the mixture at 80 °C for 16 h, K[**4.2**] was observed as the only major product by ^{1}H NMR. Anal. calc. for $C_{61}H_{79}AlKN_3O_5$ + 2 THF: C 72.41 H 8.37 N 3.67, found: C 72.36 H 8.20 N 3.75.

^{1}H NMR (THF-d$_8$, 500 MHz, 298 K): δ 7.15 – 7.09 (m, 6H, Dipp-Ar-C*H*), 7.02 (t, $^{3}J_{HH}$ = 7.7 Hz, 1 H, Dipp-p-C*H*), 6.89 (d, $^{3}J_{HH}$ = 7.7 Hz, 2 H, Dipp-m-C*H*), 6.53 (d, $^{4}J_{HH}$ = 2.0 Hz, 2 H, XA-Ar-C*H*), 5.82 (d, $^{4}J_{HH}$ = 2.0 Hz, 2 H, XA-Ar-C*H*), 3.62 (m, 8 H, THF), 3.67 (sept., $^{3}J_{HH}$ = 6.8 Hz, 4 H, C*H*Me$_2$), 1.78 (m, 8 H, THF), 1.99 (sept., $^{3}J_{HH}$ = 6.7 Hz, 2H, C*H*Me$_2$), 1.71 (s, 6 H, C(C*H*$_3$)$_2$), 1.30 (d, $^{3}J_{HH}$ = 6.8 Hz, 12H, CH(C*H*$_3$)$_2$), 1.12 (s, 18 H, C(C*H*$_3$)$_3$), 0.94 (d, $^{3}J_{HH}$ = 6.8 Hz, 12H, CH(C*H*$_3$)$_2$), 0.75 (d, $^{3}J_{HH}$ = 6.7 Hz, 12H, CH(C*H*$_3$)$_2$).

^{13}C{^{1}H} NMR (THF-d$_8$, 126 MHz, 298 K): δ 154.5 (N*C*O$_2$), 148.7 (Dipp-*o*-*C*), 148.0 (Dipp-*o*-*C*), 147.4 (*C*^{t}Bu), 146.2 (XA-*C*N), 144.5 (Dipp-*i*-*C*), 141.3 (XA-*C*O), 138.6 (Dipp-*i*-*C*), 133.2 (*C*CMe$_2$), 127.5 (Dipp-*p*-*C*), 126.0 (Dipp-*p*-*C*), 124.5 (Dipp-*m*-*C*), 123.8 (Dipp-*m*-*C*), 111.7

(XA-Ar-*C*H), 68.4 (THF), 105.9 (XA-Ar-*C*H), 37.5 (*C*Me$_2$), 35.6 (*C*Me$_3$), 32.2 (C(*C*H$_3$)$_3$), 29.1 (*C*HMe$_2$), 28.3 (*C*HMe$_2$), 28.1 (C(*C*H$_3$)$_2$), 27.0 (CH(*C*H$_3$)$_2$), 26.6 (THF), 25.5 (CH(*C*H$_3$)$_2$),25.0 (CH(*C*H$_3$)$_2$).

K[(NON)Al{κ^2-(O,O')-(NDippCO$_2$)}], K[4.3]: Method 1: K$_2$[**4.1**]$_2$ (40 mg, 0.04 mmol) was dissolved in THF (0.8 mL). After 1 h, volatiles were removed, affording [K(THF)$_2$][4.**3**] as a white powder. Yield 41 mg, 89%. Method 2: K$_2$[**4.1**]$_2$ (20 mg, 0.02 mmol) was suspended in 0.5 ml C$_6$D$_6$ and heated at 80 °C for 24 h. A ^{1}H NMR revealed a 1:1 mixture between K[4.**3**] and K$_2$[**4.1**]$_2$.

^{1}H NMR(THF-d$_8$, 500 MHz, 298 K): δ 7.14 (dd, 2 H, $^3J_{HH}$ = 7.5 Hz, $^4J_{HH}$ = 1.9 Hz, Dipp-*p*-C*H*), 7.09 (t, 2 H, $^3J_{HH}$ = 7.5 Hz, Dipp-*m*-C*H*), 7.04 (dd, 2 H, $^3J_{HH}$ = 7.5 Hz, $^4J_{HH}$ = 1.9 Hz, Dipp-*p*-C*H*), 6.60 (d, 2 H, $^3J_{HH}$ = 7.3 Hz, Dipp-*m*-C*H*), 6.52 (d, 2 H, $^4J_{HH}$ = 2.0 Hz, XA-Ar-C*H*), 6.51 (t, 1 H, $^3J_{HH}$ = 7.3 Hz, Dipp-*p*-C*H*), 5.71 (d, 2 H, $^4J_{HH}$ = 2 Hz, XA-Ar-C*H*), 3.63 (sept., 2 H, $^3J_{HH}$ = 6.9 Hz, C*H*Me$_2$), 3.43 (sept., 2 H, $^3J_{HH}$ = 6.9 Hz, C*H*Me$_2$), 2.36 (sep.t, 2 H, $^3J_{HH}$ = 6.9 Hz, C*H*Me$_2$), 1.80 (s, 3 H, C(C*H*$_3$)$_2$), 1.58 (s, 3 H, C(C*H*$_3$)$_2$), 1.36 (d, 6 H, $^3J_{HH}$ = 6.9 Hz, CH(C*H*$_3$)$_2$), 1.08 (s, 18 H, C(CH$_3$)$_3$), 1.00 (d, 6 H, $^3J_{HH}$ = 6.9 Hz, CH(C*H*$_3$)$_2$), 0.93 (2 overlapping d, 6 H and 6 H, $^3J_{HH}$ = 6.9 Hz and $^3J_{HH}$ = 6.9 Hz, CH(C*H*$_3$)$_2$), 0.77 (br s, 12 H, CH(C*H*$_3$)$_2$).

^{13}C{^{1}H} NMR(THF-d$_8$, 126 MHz, 298 K): δ 161.2 (N*C*O2), 148.2 (Dipp-*o*-*C*), 148.2 (*C*CMe3), 146.9 (Dipp-*o*-*C*), 146.6 (XA-*C*N), 145.7 (Dipp-*i*-*C*), 144.9 (Dipp-*i*-*C*), 142.0 (XA-*C*O), 141.8 (Dipp-*o*-*C*), 133.7 (*C*CMe2), 126.0 (Dipp-*p*-*C*), 125.2 (Dipp-*m*-*C*), 124.0 (Dipp-*m*-*C*), 122.0 (Dipp-*m*-*C*), 121.2 (Dipp-*p*-*C*), 111.8 (XA-Ar-*C*H), 106.2 (XA-Ar-*C*H), 37.7 (*C*Me$_2$), 35.6 (*C*Me$_3$), 32.4 (C(*C*H$_3$)$_2$), 32.2 (C(*C*H$_3$)$_3$), 29.2 (*C*HMe$_2$), 28.9 (*C*HMe$_2$), 28.2 (*C*HMe$_2$), 26.3 (CH(*C*H$_3$)$_2$), 26.1 (CH(*C*H$_3$)$_2$), 25.1 (CH(*C*H$_3$)$_2$), 24.7 (br, CH(*C*H$_3$)$_2$), 24.4 (CH(*C*H$_3$)$_2$),23.3 (C(*C*H$_3$)$_2$).

[K(crypt)][NONAlCO$_3$], [K(crypt)][1.44]:

K_2[**1.44**]$_2$ (20 mg, 0.03 mmol) and 2.2.2-cryptand (9 mg, 0.03 mmol) were suspended in C_6D_6. After briefly heating to reflux, quantitative conversion to [K(crypt)][**1.44**] was observed by NMR.

^{1}H NMR (600 MHz, C_6D_6) δ 7.23 (d, $^3J_{HH}$ = 7.6 Hz, 4H, Dipp-*m*-C*H*), 7.09 (t, $^3J_{HH}$ = 7.6 Hz, 2H, Dipp-*p*-C*H*), 6.73 (d, $^4J_{HH}$ = 2.0 Hz, 2H, XA-Ar-C*H*), 6.33 (d, $^4J_{HH}$ = 2.0 Hz, 2H, XA-Ar-C*H*), 4.01 (sept., $^3J_{HH}$ = 6.8 Hz, 4H, C*H*(CH$_3$)$_2$), 3.22 (s, 12H, OC*H*$_2$), 3.16 (t, $^3J_{HH}$ = 4.7 Hz, 12H, NCH$_2$C*H*$_2$), 2.13 (t, $^3J_{HH}$ = 4.7 Hz, 12H, NC*H*$_2$), 1.63 (s, 6H, C(C*H*$_3$)$_2$), 1.47 (d, $^3J_{HH}$ = 6.8 Hz, 12H, CH(C*H*$_3$)$_2$), 1.33 (s, 18H, C(C*H*$_3$)$_3$),1.28 (d, $^3J_{HH}$ = 6.8 Hz, 12H, CH(C*H*$_3$)$_2$).

^{13}C NMR (150 MHz, C_6D_6) δ 163.0 (*C*O$_3$), 147.9 (Dipp-*o*-*C*), 147.7 (*C*^{t}Bu), 145.7 (XA-N*C*), 145.1 (Dipp-*i*-*C*), 141.0 (XA-*C*O), 132.7 (*C*CMe$_2$), 124.6 (Dipp-*p*-*C*), 123.6 (Dipp-*m*-*C*), 110.5 (XA-Ar-*C*H), 105.7 (XA-Ar-*C*H), 70.5 (O*C*H$_2$), 67.8 (NCH$_2$*C*H$_2$), 55.0 (N*C*H$_2$), 37.1 (*C*(CH$_3$)$_2$), 35.2 (*C*(CH$_3$)$_3$), 32.1 (C(*C*H$_3$)$_3$), 28.7 (*C*H(CH$_3$)$_2$), 27.8 (C(*C*H$_3$)$_2$), 26.0 (CH(*C*H$_3$)$_2$), 25.2 (CH(*C*H$_3$)$_2$).

[K(crypt)][(NON)Al{κ^2-(N,O)-(NDippCO$_2$)}], [K(crypt)][4.1]: K_2[**4.1**]$_2$ (30 mg, 0.04 mmol) and 2.2.2-cryptand (11 mg, 0.04 mmol) were suspended in C_6D_6. After briefly heating to reflux, quantitative conversion to [K(crypt)][**4.1**] was observed by NMR.

^{1}H NMR (400 MHz, C_6D_6) δ 7.36 (t, $^3J_{HH}$ = 4.7 Hz, 1H, Dipp-*p*-C*H*), 7.15 – 7.21 (m, 7H, Dipp-Ar-C*H*), 7.12 (dd, $^3J_{HH}$ = 8.6, 6.4 Hz, 1H, Dipp-*p*-C*H*), 6.63 (d, $^3J_{HH}$ = 1.9 Hz, 2H, XA-Ar-C*H*), 6.46 (d, $^3J_{HH}$ = 1.8 Hz, 2H, XA-Ar-C*H*), 4.42 (s, 2H, C*H*(CH$_3$)$_2$), 4.37 (s, 2H, C*H*(CH$_3$)$_2$), 3.12 (s, 12H, OC*H*$_2$), 3.09 (m, 12H, NCH$_2$C*H*$_2$), 2.60 (br s, 2H, C*H*(CH$_3$)$_2$), 2.14 (m, 12H, NC*H*$_2$), 1.70 (s, 3H, C(C*H*$_3$)$_2$), 1.66 (d, $^3J_{HH}$ = 6.7 Hz, 6H, CH(C*H*$_3$)$_2$), 1.61 (d, $^3J_{HH}$ = 6.7 Hz, 6H, CH(C*H*$_3$)$_2$), 1.54 (s, 3H, C(C*H*$_3$)$_2$), 1.44 (br s, 12H, CH(C*H*$_3$)$_2$), 1.24 (s, 18H, C(C*H*$_3$)$_3$), 0.89 (d, $^3J_{HH}$ = 6.6 Hz, 6H, CH(C*H*$_3$)$_2$), 0.78 (br s, 6H, CH(C*H*$_3$)$_2$).

^{13}C NMR (151 MHz, C_6D_6) δ 165.8 (N*C*O$_2$), 148.2 (XA-*C*N, Dipp-*o*-*C*), 147.7 (Dipp-*o*-*C*), 147.5 (*C*^{t}Bu), 147.3 (Dipp-*i*-*C*), 145.8 (Dipp-*i*-*C*), 142.3, 144.2 (XA-*C*O), 135.3 (*C*CMe$_2$), 124.8 (Dipp-Ar-*C*H), 124.1 (Dipp-Ar-*C*H), 123.8 (Dipp-Ar-*C*H), 122.5 (Dipp-Ar-*C*H), 112.4 (XA-Ar-*C*H), 106.2 (XA-Ar-*C*H), 70.4 (O*C*H$_2$), 67.9 (NCH$_2$*C*H$_2$), 55.0 (N*C*H$_2$), 39.0 (*C*Me$_2$), 35.1 (*C*Me$_3$), 32.0 (C(*C*H$_3$)$_3$), 30.4 (C(*C*H$_3$)$_2$), 28.7 (*C*HMe$_2$), 28.5 (*C*HMe$_2$), 28.0 (*C*HMe$_2$), 26.8 (CH(*C*H$_3$)$_2$), 26.6 (CH(*C*H$_3$)$_2$), 26.0 (CH(*C*H$_3$)$_2$), 25.7 (CH(*C*H$_3$)$_2$), 24.9 (CH(*C*H$_3$)$_2$), 23.4 (C(*C*H$_3$)$_2$).

[K(crypt)][NONAl{(CO$_2$)$_2$NDipp}], [K(crypt)][4.2]: Method 1: To a solution of [K(THF)$_2$][**4.2**] (10 mg, 0.01 mmol) in benzene (0.5 ml), was added 2.2.2-cryptand (1.1 eqiv, 4 mg, 0.01 mmol). Upon shaking for 1 minute quantitative conversion to the product was observed by NMR. Method 2: A solution of [K(crypt)][**4.3**] (25 mg, 0.01 mmol) and 2 equiv. THF in C_6D_6 (0.5 mL) was exposed to CO_2 (1.2 bar, 3 mL). Within 2 h, [K(crypt)][**4.2**] was observed as the only major product by NMR.

^{1}H NMR (400 MHz, C_6D_6) δ 7.46 (d, $^3J_{HH}$ = 7.6 Hz, 4H, NON Dipp-*m*-C*H*), 7.36 (m, 2H, Dipp-*p*-C*H*), 7.11 (m, 3H, Dipp-Ar-C*H*), 6.73 (d, $^4J_{HH}$ = 2.0 Hz, 2H, XA-Ar-C*H*), 6.35 (d, $^4J_{HH}$ = 1.9 Hz, 2H, XA-Ar-C*H*), 4.25 (sept., $^3J_{HH}$ = 6.9 Hz, 4H, C*H*Me$_2$), 3.06 (s, 12H, crypt OC*H*$_2$), 3.00 (br., 12H, crypt NCH$_2$C*H*$_2$), 2.52 (sept., $^3J_{HH}$ = 6.6 Hz, 2H, C*H*Me$_2$), 2.05 (br., 12H, crypt NC*H*$_2$), 1.74 (d, *J* = 6.9 Hz, 12H, CH(C*H*$_2$)$_2$), 1.71 (s, 6H, C(C*H*$_3$)$_2$), 1.38 (d, $^3J_{HH}$ = 6.9 Hz, 12H, NON CH(C*H*$_2$)$_2$), 1.32 (s, 18H, C(C*H*$_3$)$_3$),1.19 (d, $^3J_{HH}$ = 6.6 Hz, 12H, CH(C*H*$_2$)$_2$).

^{13}C NMR (126 MHz, C_6D_6) δ 153.6 (N(*C*O$_2$)$_2$), 148.4 (Dipp-*o*-*C*), 147.5 (Dipp-*o*-*C*), 146.9 (*C*^{t}Bu), 146.0 (OC*C*N), 144.5 (Dipp-*i*-*C*), 140.9 (XA-O*C*), 138.9 (Dipp-*i*-*C*), 132.6 (*C*CMe$_2$), 126.2 (Dipp-*p*-*C*H), 125.5 (NON Dipp-*p*-*C*H), 124.1 (NON Dipp-*m*-*C*H), 122.8 (Dipp-*m*-*C*H), 111.1 (XA-*C*H), 53.7, 67.6, 70.4, 105.3 (XA-*C*H), 36.9 (*C*Me$_2$), 35.1 (*C*Me$_3$), 32.1

(C(CH_3)$_3$), 28.8 (NON $CHMe_2$), 28.1 (NON CH(CH_3)$_2$), 28.0 ($CHMe_2$), 27.1 (NON CH(CH_3)$_2$), 25.8 (CH(CH_3)$_2$),25.1 (XA-C(CH_3)$_2$).

[K(crypt)][(NON)Al{κ^2-(O,O')-(NDippCO$_2$)}], [K(crypt)][4.3]: Method 1: A solution of [K(crypt)][**4.1**] (40 mg, 0.02 mmol) in benzene (0.5 ml) was allowed at room temperature for 2 week. This led to quantitative isomerisation as judged by NMR. Method 2: [K(THF)$_2$][**4.3**] (22 mg, 0.02 mmol) and 2.2.2-cryptand (7 mg, 0.02 mmol) were suspended in C_6D_6. After briefly heating to reflux, quantitative conversion to [K(crypt)][**4.3**] was observed by NMR.

^{1}H NMR (600 MHz, C_6D_6) δ 7.50 – 7.30 (br s, 4H, Dipp-*m*-C*H*), 7.34 (t, $^3J_{HH}$ = 7.4 Hz, 2H, Dipp-*p*-C*H*), 7.08 (d, $^3J_{HH}$ = 7.5 Hz, 2H, Dipp-*m*-C*H*), 6.85 (t, $^3J_{HH}$ = 7.5 Hz, 1H, Dipp-*p*-C*H*), 6.69 (d, $^4J_{HH}$ = 2.0 Hz, 2H, XA-Ar-C*H*), 6.22 (d, $^4J_{HH}$ = 2.0 Hz, 2H, XA-Ar-C*H*), 4.12 (br s, 2H, C*H*Me$_2$), 4.01 (br s, 2H, C*H*Me$_2$), 3.12 (overlapping s and sept, 14H, OCH_2 and C*H*Me$_2$), 3.03 (m, 12H, NCH$_2$CH_2), 2.03 (m, 12H, NCH_2),1.60 – 1.90 (2 overlapping broad s, 18H, C(CH_3)$_2$ and CH(CH_3)$_2$), 1.25 – 1.45 (br s, 12H, CH(CH_3)$_2$), 1.27 (s, 18H, C(CH$_3$)$_3$), 1.21 (d, $^3J_{HH}$ = 6.7 Hz, 12H, CH(CH_3)$_2$).

^{13}C NMR (151 MHz, C_6D_6) δ 159.8 (N*C*O$_2$), 148.4 (Dipp-*i*-*C*), 147.5 (br, Dipp-*o*-*C*), 147.4 (*C*^{t}Bu), 146.7 (XA-*C*N), 145.4 (Dipp-*i*-*C*), 141.7 (XA-*C*O), 141.7 (Dipp-*o*-*C*H), 133.0 (*C*CMe$_2$), 125.2 (Dipp-*p*-*C*H), 123.7 (v. br, Dipp-*m*-*C*H), 121.6 (Dipp-*m*-*C*H), 119.2 (Dipp-*p*-*C*H), 111.2 (XA-Ar-*C*H), 105.2 (XA-Ar-*C*H), 70.5 (O*C*H$_2$), 67.5 (NCH$_2$*C*H$_2$), 53.7 (N*C*H$_2$), 37.2 (*C*(CH$_3$)$_3$), 35.1 (*C*(CH$_3$)$_3$), 32.1 (C(*C*H$_3$)$_3$), 28.8 (br, *C*H(CH$_3$)$_2$), 27.8 (*C*H(CH$_3$)$_2$), 26.0 (br, CH(*C*H$_3$)$_2$),= 25.1 (CH(*C*H$_3$)$_2$).

Missing XA-C*Me*$_2$ ^{13}C resonance likely associated with broadness between 24 and 27 ppm.

K[NONAl(NDippOCHPh)], K[4.4]: To a solution of K$_2$[**NON**AlNDipp]$_2$ (200 mg, 0.22 mmol) in benzene (5 ml) was added benzaldehyde (24 µl, 0.23 mmol, 1.05 eq). Upon standing over night, hairy white precipitate formed. The solution was decanted and the residue washed

with pentane (2 x 5ml) and dried under vacuum. The product was obtained as a fluffy white powder. Yield 95 mg, 43%. Anal. calc. for $C_{66}H_{85}AlKN_3O_2$: C 77.83, H 8.41, N 4.13; found: C 77.80, H 8.31, N 4.09.

^{1}H NMR (600 MHz, THF) δ 7.31 (d, $^3J_{HH}$ = 7.1 Hz, 1H, Dipp-*m*-C*H*), 7.05 – 7.12 (m, 2H, Dipp-*m*-C*H*), 7.02 (d, $^3J_{HH}$ = 7.1 Hz, 1H, Dipp-*m*-C*H*), 6.81 – 6.96 (m, 7H, Ph-C*H* and Dipp-C*H*), 6.71 (d, $^3J_{HH}$ = 7.3 Hz, 1H, Dipp-*m*-C*H*), 6.66 (dd, $^nJ_{HH}$ = 7.6, 1.9 Hz, 1H, Dipp-*m*-C*H*), 6.61 (t, $^3J_{HH}$ = 7.5 Hz, 1H, Dipp-*p*-C*H*), 6.37 (d, $^4J_{HH}$ = 1.9 Hz, 1H, XA-Ar-C*H*), 6.24 (d, $^4J_{HH}$ = 1.9 Hz, 1H, XA-Ar-C*H*), 6.07 (s, 1H, C*H*Ph), 5.97 (overlapping d, $^4J_{HH}$ = 1.9 Hz, 2H, XA-Ar-C*H*), 4.74 (sept., $^3J_{HH}$ = 6.9 Hz, 1H, C*H*(CH$_3$)$_2$), 4.52 (sept., $^3J_{HH}$ = 6.9 Hz, 1H, C*H*(CH$_3$)$_2$), 3.82 (sept., $^3J_{HH}$ = 6.8 Hz, 1H, C*H*(CH$_3$)$_2$), 3.63 (sept., $^3J_{HH}$ = 7.6 Hz, 1H, C*H*(CH$_3$)$_2$), 3.00 (sept., $^3J_{HH}$ = 7.7 Hz, 1H, C*H*(CH$_3$)$_2$), 1.60 (m, 4H, C(C*H*$_3$)$_2$ and C*H*(CH$_3$)$_2$), 1.46 (d, $^3J_{HH}$ = 6.8 Hz, 3H, CH(C*H*$_3$)$_2$), 1.41 (overlapping d, $^3J_{HH}$ = 6.8 Hz, 6H, 2x CH(C*H*$_3$)$_2$), 1.36 (d, $^3J_{HH}$ = 6.6 Hz, 3H, CH(C*H*$_3$)$_2$), 1.26 (s, 3H, C(C*H*$_3$)$_2$), 1.10 (apparent s, 12H, , C(C*H*$_3$)$_3$ and CH(C*H*$_3$)$_2$), 1.06 (s, 9H, C(C*H*$_3$)$_3$), 0.92 (d, $^3J_{HH}$ = 6.7 Hz, 3H, CH(C*H*$_3$)$_2$), 0.79 (d, $^3J_{HH}$ = 6.5 Hz, 3H, CH(C*H*$_3$)$_2$), 0.74 (d, $^3J_{HH}$ = 6.6 Hz, 3H, CH(C*H*$_3$)$_2$), 0.48 (d, $^3J_{HH}$ = 6.6 Hz, 3H, CH(C*H*$_3$)$_2$), 0.41 (d, $^3J_{HH}$ = 6.7 Hz, 3H, CH(C*H*$_3$)$_2$), 0.22 (d, $^3J_{HH}$ = 6.8 Hz, 3H, CH(C*H*$_3$)$_2$),0.02 (d, $^3J_{HH}$ = 6.6 Hz, 3H, CH(C*H*$_3$)$_2$).

^{13}C NMR (151 MHz, THF) δ 152.0 (Ph-*i*-*C*), 151.0 (XA-*C*N), 150.4 (Dipp-*o*-*C*), 149.7 (Dipp-*o*-*C*), 149.0 (Dipp-*o*-*C*), 148.8 (XA-*C*N), 148.7 (Dipp-*o*-*C*), 148.7 (Dipp-*o*-*C*), 147.5 (*C*^{t}Bu), 148.4 (Dipp-*o*-*C*), 146.8 (XA-*C*O), 146.5 (Dipp-*i*-*C*), 146.4 (Dipp-*i*-*C*), 146.3 (*C*^{t}Bu), 145.9 (Dipp-*i*-*C*), 144.0 (XA-*C*O), 138.1 (*C*CMe$_2$), 134.8 (*C*CMe$_2$), 128.5 (Ph-*m*-*C*), 127.2 (Ph-*o*-*C*), 126.4 (Ph-*p*-*C*), 125.5 (Dipp-*m*-*C*), 125.1 (Dipp-*m*-*C*), 124.5 (Dipp-*p*-*C*), 124.1 (Dipp-*m*-*C*), 124.0 (Dipp-*p*-*C*), 123.5 (Dipp-*m*-*C*), 123.4 (Dipp-*m*-*C*), 123.2 (Dipp-*m*-*C*), 122.2 (Dipp-*p*-*C*), 113.1 (XA-Ar-*C*H), 112.0 (XA-Ar-*C*H), 106.3 (XA-Ar-*C*H), 105.4 (XA-Ar-*C*H), 90.3 (*C*HPh), 39.5 (*C*Me$_2$), 35.6 (*C*Me$_3$), 35.4 (*C*Me$_3$), 32.4 (C(*C*H$_3$)$_3$), 32.1 (C(*C*H$_3$)$_3$), 30.5 (C(*C*H$_3$)$_2$), 29.0 (*C*H(CH$_3$)$_2$), 29.0 (*C*H(CH$_3$)$_2$), 28.8 (*C*H(CH$_3$)$_2$), 28.7 (CH(*C*H$_3$)$_2$), 28.6 (CH(*C*H$_3$)$_2$), 28.6

(*C*H(CH$_3$)$_2$), 28.0 (*C*H(CH$_3$)$_2$), 27.7 (CH(*C*H$_3$)$_2$), 27.5 (*C*H(CH$_3$)$_2$), 27.3 (CH(*C*H$_3$)$_2$), 27.2 (CH(*C*H$_3$)$_2$), 26.5 (CH(*C*H$_3$)$_2$), 26.3 (CH(*C*H$_3$)$_2$), 26.2 (CH(*C*H$_3$)$_2$), 26.0 (CH(*C*H$_3$)$_2$), 24.7 (CH(*C*H$_3$)$_2$), 24.5 (CH(*C*H$_3$)$_2$), 24.0 (CH(*C*H$_3$)$_2$), 23.8 (C(*C*H$_3$)$_2$).

Reaction of [K(crypt)][4.1] with CO_2: A solution of [K(crypt)][**4.1**] (30 mg, 0.02 mmol) in C_6D_6 (0.5 mL) was exposed to CO_2 (1.2 bar, 3 mL). Over the course of 2 days gradual conversion to [K(crypt)][**4.2**] and [K(crypt)][**1.44**] was observed by ^{1}H NMR. No intermediates were observed.

Reaction of K[4.4] with CO_2: A solution of K[**4.4**] (20 mg, 0.02 mmol) in THF-d_8 was exposed to an atmosphere of CO_2 (1.2 bar, 3 mL). Over the course of 2 days gradual conversion to K$_2$[**1.44**]$_2$ and PhCHNDipp was observed.

PhCHNDipp: ^{1}H NMR (400 MHz, THF) δ = 8.22 (s, 1H, C*H*Ph), 7.96 – 7.89 (m, 2H, Ar*H*), 7.52 – 7.44 (m, 3H, Ar*H*), 7.12 – 7.09 (m, 2H, Ar*H*), 7.02 (dd, J = 8.4, 6.9 Hz, 1H, Ar*H*), 2.97 (sept., $^3J_{HH}$ = 6.9 Hz, 2H, C*H*(CH$_3$)$_2$), 1.14 (d, $^3J_{HH}$ = 6.9, 12H, CH(C*H*$_3$)$_2$).

4.5 References

[1] A. L. Odom, *Dalton Trans.*, **2005**, 225–233.
[2] P. Mountford, *Chem. Commun.*, **1997**, 2127–2134.
[3] N. Hazari, P. Mountford, *Acc. Chem. Res.*, **2005**, *38*, 839–849.
[4] D. E. Wigley, *Progress in Inorganic Chemistry,* **2007**, *42*, 239–482.
[5] K. J. Weller, P. A. Fox, S. D. Gray, D. E. Wigley, *Polyhedron*, **1997**, *16*, 3139–3163.
[6] W. A. Nugent, B. L. Haymore, *Coord. Chem. Rev.*, **1980**, *31*, 123–175.
[7] A. R. Fout, U. J. Kilgore, D. J. Mindiola, *Chem. Eur. J.* **2007**, *13*, 9428–9440.
[8] E. Lu, J. Chu, Y. Chen, *Acc. Chem. Res.*, **2018**, *51*, 557–566.
[9] U. J. Kilgore, F. Basuli, J. C. Huffman, D. J. Mindiola, *Inorg. Chem.*, **2006**, *45*, 487–489.
[10] A. E. Guiducci, C. L. Boyd, E. Clot, P. Mountford, *Dalton Trans.*, **2009**, 5960–5979.
[11] C. L. Boyd, T. Toupance, B. R. Tyrrell, B. D. Ward, C. R. Wilson, A. R. Cowley, P. Mountford, *Organometallics*, **2005**, *24*, 309–330.
[12] C. L. Boyd, E. Clot, A. E. Guiducci, P. Mountford, *Organometallics*, **2005**, *24*, 2347–2367.
[13] A. E. Guiducci, A. R. Cowley, M. E. G. Skinner, P. Mountford, *Dalton Trans.*, **2001**, 1392–1394.
[14] S. R. Dubberley, A. Friedrich, D. A. Willman, P. Mountford, U. Radius, *Chem. Eur. J.*, **2003**, *9*, 3634–3654.

[15] S. C. Bart, C. Anthon, F. W. Heinemann, E. Bill, N. M. Edelstein, K. Meyer, *J. Am. Chem. Soc.*, **2008**, *130*, 12536–12546.
[16] A. C. Schmidt, F. W. Heinemann, L. Maron, K. Meyer, *Inorg. Chem.*, **2014**, *53*, 13142–13153.
[17] A. C. Schmidt, F. W. Heinemann, W. W. Lukens, K. Meyer, *J. Am. Chem. Soc.*, **2014**, *136*, 11980–11993.
[18] A. J. Keane, W. S. Farrell, B. L. Yonke, P. Y. Zavalij, L. R. Sita, *Angew. Chem. Int. Ed.*, **2015**, *54*, 10220–10224.
[19] P. J. Tiong, L. R. Groom, E. Clot, P. Mountford, *Chem. Eur. J.*, **2013**, *19*, 4198–4216.
[20] J. Chu, E. Lu, Z. Liu, Y. Chen, X. Leng, H. Song, J. X. Chu, E. L. Lu, Z. X. Liu, Y. F. Chen, X. B. Leng, H. B. Song, *Angew. Chem. Int. Ed.*, **2011**, *50*, 7677–7680.
[21] P. J. Tiong, A. Nova, L. R. Groom, A. D. Schwarz, J. D. Selby, A. D. Schofield, E. Clot, P. Mountford, *Organometallics*, **2011**, *30*, 1182–1201.
[22] P. J. Tiong, A. D. Schofield, J. D. Selby, A. Nova, E. Clot, P. Mountford, *Chem. Commun.*, **2010**, *46*, 85–87.
[23] D. S. Glueck, F. J. Hollander, R. G. Bergman, *J. Am. Chem. Soc.* **1989**, *111*, 2719–2721.
[24] D. S. Glueck, J. Wu, F. J. Hollander, R. G. Bergman, *J. Am. Chem. Soc.*, **1991**, *113*, 2041–2054.
[25] A. J. Blake, J. M. McInnes, P. Mountford, G. I. Nikonov, D. Swallow, D. J. Watkin, *Dalton Trans.*, **1999**, 379–392.
[26] B. D. Ward, E. Clot, S. R. Dubberley, L. H. Gade, P. Mountford, *Chem. Commun.*, **2002**, *2*, 2618–2619.
[27] Z. J. Tonzetich, R. R. Schrock, P. Müller, *Organometallics*, **2006**, *25*, 4301–4306.
[28] D. J. Mindiola, R. Waterman, V. M. Iluc, T. R. Cundari, G. L. Hillhouse, *Inorg. Chem.*, **2014**, *53*, 13227–13238.
[29] M. Kinauer, M. Diefenbach, H. Bamberger, S. Demeshko, E. J. Reijerse, C. Volkmann, C. Würtele, J. van Slageren, B. de Bruin, M. C. Holthausen, S. Schneider, *Chem. Sci.*, **2018**, *9*, 4325–4332.
[30] M. D. Anker, R. J. Schwamm, M. P. Coles, *Chem. Commun.*, **2020**, *56*, 2288–2291.
[31] L. Suresh, J. Finnstad, K. W. Törnroos, E. le Roux, *Inorg. Chim. Acta.*, **2021**, *521*, 120301.
[32] A. E. Guiducci, C. L. Boyd, P. Mountford, *Organometallics*, **2006**, *25*, 1167–1187.
[33] F. Dahcheh, D. W. Stephan, G. Bertrand, *Chem. Eur. J.*, **2015**, *21*, 199–204.
[34] L. Xie, J. Zhang, H. Hu, C. Cui, *Organometallics*, **2013**, *32*, 6875–6878.
[35] F. M. Mück, J. A. Baus, A. Ulmer, C. Burschka, R. Tacke, *Eur. J. Inorg. Chem.*, **2016**, *2016*, 1660–1670.
[36] K. Yuvaraj, C. Jones, *Dalton Trans.*, **2019**, *48*, 11961–11965.
[37] T. J. Hadlington, T. Szilvási, M. Driess, *Chem. Commun.*, **2018**, *54*, 9352–9355.
[38] X. Liu, X.-Q. Xiao, Z. Xu, X. Yang, Z. Li, Z. Dong, C. Yan, G. Lai, M. Kira, *Organometallics*, **2014**, *33*, 5434–5439.
[39] J. F. Hartwig, R. G. Bergman, R. A. Andersen, *Organometallics*, **1991**, *10*, 3344–3362.
[40] M. D. Anker, M. P. Coles, *Angew. Chem. Int. Ed.*, **2019**, *58*, 18261–18265.

Chapter 5. Reactivity of aluminium and gallium imides towards CO and N_2O

5.1 Introduction

CO has become an important C_1 feedstock material, which is functionalised on an industrial scale.[1] Its most significant applications are in the Monsanto and Cativa processes,[2] in which methanol is carbonylated to acetic acid, and in Fischer-Tropsch chemistry where CO and H_2 are converted to hydrocarbons and water.[3] CO is also used in the synthesis of fine chemicals, and many different catalysts have been devised for its incorporation into useful compounds.[1,4,5] The chemistry of CO is dominated by interactions with transition metals.[1,4,5] This can be attributed to the availability of partially filled *d*-orbitals, particularly for those complexes with empty σ-symmetry orbitals suitable for CO coordination and filled π-symmetry *d*-orbitals necessary for efficient back-bonding.[1] In recent years a number of main group systems have been developed that mimic transition metals, and a growing number of reactions between main group systems and CO have been reported. These have been reviewed recently.[6] Generally either coordination of CO, homologation via C–C bond formation,[7,8] or C–O bond cleavage is observed.[9,10] Systems capable of both C–C bond formation and C–O bond cleavage remain rare (Scheme 5.1).[11–13]

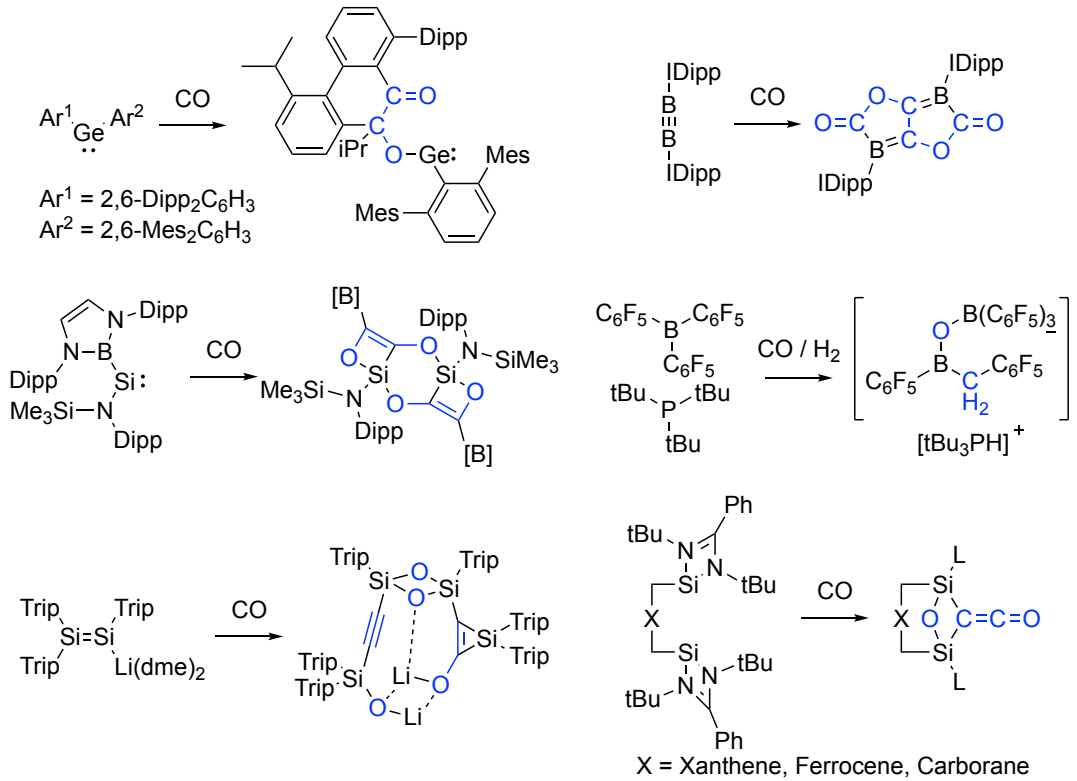

Scheme 5.1: Selected reactions of main group species with CO leading to either C–C coupling and/or C–O cleavage.

Of particular relevance to the work presented in this chapter are the reactions of non-metal anions with alkali metal counter-ions, the majority of which have been published concurrently with the investigations presented in this chapter.[14–18]

The reactions of lithium alkyl and amide reagents with CO have been known for a long time, but have received little attention.[19–26] These processed typically lead to the formation of acyl and carbamoyl anions, which have been trapped by organic electrophiles. Recently this chemistry has been reinvestigated in the context of FLP chemistry.[14–17]

The reactions of benzyl potassium with CO leads to the formation of carbene like intermediates which, depending on steric bulk, either undergo dimerization, ligand activation, or reactions with a second equivalent of CO.[14]

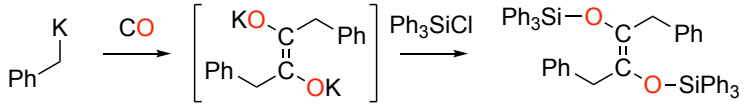

Scheme 5.2: Reaction of benzyl potassium with CO.

The reaction of phosphide [K(18-c-6)][P^{t}Bu$_2$] ([K(18-c-6)][**5.I**]) with CO proceeds under ambient conditions and leads to insertion of CO into the P-C bonds in the presence of light.[15] This reaction is thought to proceed via a carbene intermediate, which upon photochemical promotion to the triplet state affords the observed product [K(THF)$_2$(18-c-6)][**5.II**]. Evidence for the carbene intermediate comes from the observation of its dimerized form as a side product, i.e. [K$_6$(18-c-6)][**5.III**]$_3$.

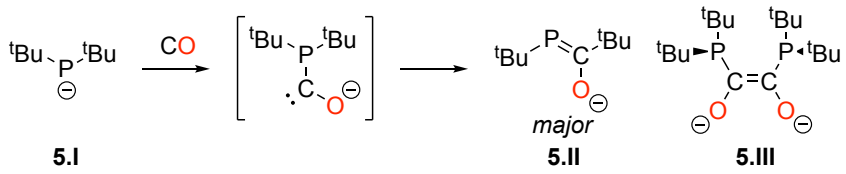

5.I **5.II** **5.III**

Scheme 5.3: Reaction of [K(18-c-6)][**5.I**] with CO. Counter-ions omitted for clarity.

Concurrent with the work presented in this chapter, the Stephan group reported on the reactions of lithium alkyl- or silylamide reagents with CO.[16,17] The reaction of lithium dicyclohexylamide with CO leads to the formation of CO homologation products. Depending on conditions, compounds derived from the incorporation of either three or four molecules of CO are the major product, although species with up to seven CO units can be observed by mass spectrometry.

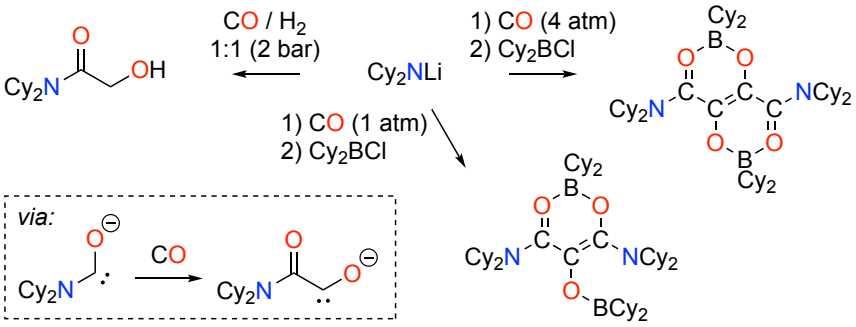

Scheme 5.4: Reactions of Cy$_2$NLi with CO.

When one or both of the N-bound alkyl groups are replaced with silyl groups, the formation of isonitriles or metal cyanides can be observed, instead of CO homologation.[17] Upon formation of the initial carbene intermediate, **5.IV**, 1,3-silyl migration from nitrogen to oxygen takes place to yield **5.V**. Elimination of the metal siloxide, ultimately leads to the formation of the observed products (Scheme 5.5).

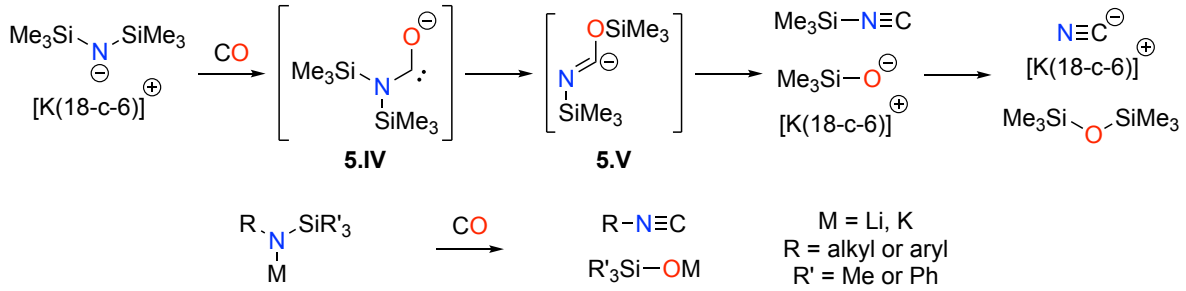

Scheme 5.5: Reactions of silylated amides with CO.

The reaction of aluminium oxide species $K_2[\{O(SiMe_2NDipp)_2\}AlO]_2$ with CO has also been reported.[18] In this case the product of this reaction is ethenetetraolate complex K_2[**5.VI**]$_2$. DFT suggests that this reaction proceeds via initial [2+2] cycloaddition of CO across the Al–O bond, followed by addition of a second molecule of CO to the resulting carbene centre, leading to the formation of K_2[**5.VI**]$_2$ (Scheme 5.6).

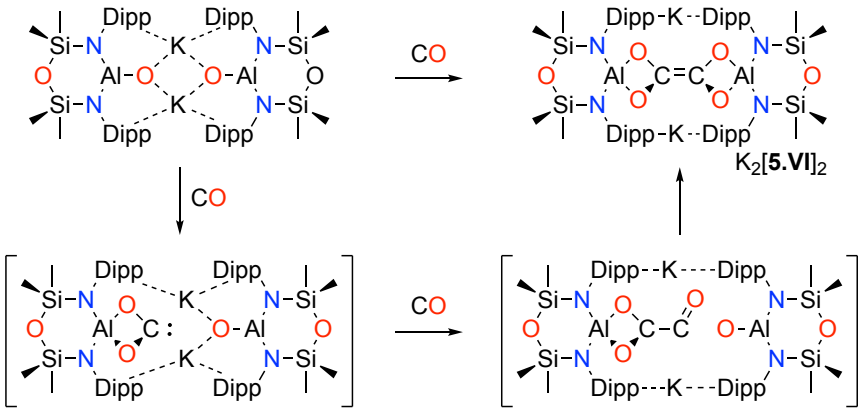

Scheme 5.6: Reaction of $K_2[\{O(SiMe_2NDipp)_2\}AlO]_2$ with CO.

The (NON)-supported aluminium and gallium imides, described in chapter 3, superficially resemble simple alkali metal amides. The latter have shown interesting reactivity towards CO, leading to a range of different products, depending on the substituents on nitrogen. The imides described in chapter 3 also span a range of substitution patterns and might show interesting reactivity towards CO. Here the reactions of these imides towards CO and N_2O are reported.

5.2 Results and discussion

5.2.1 Reactivity of K_2[(NON)AlNDipp]$_2$ towards CO

Upon exposure of solution of K_2[**NON**Al(NDipp)]$_2$, K_2[**3.5**]$_2$, in benzene to an atmosphere of CO, a colour change from colourless to orange was observed. A ^{1}H NMR spectrum obtained

after 5 min reveals quantitative conversion to a single new species with signals at δ_H = 6.78, 6.06, 3.86, 3.80 ppm. In addition to the resonances associated with the ligand, the $^{13}C\{^1H\}$ NMR spectrum shows two signals at δ_C = 171.8 and 211.6 ppm, indicating incorporation of at least two molecules of CO into the product.

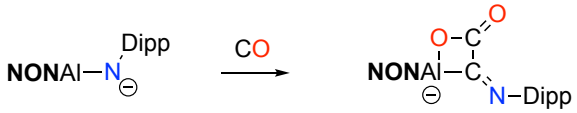

5.1

Scheme 5.7: Reactivity of imide K_2[**3.5**]$_2$ towards CO. Counter-ions omitted and species shown as monomeric for clarity.

Single crystals suitable for X-ray diffraction could be obtained from concentrated benzene solutions. The molecular structure thus obtained reveals the product to be K_2[**NON**Al{C(NDipp)CO_2}]$_2$, K_2[**5.1**]$_2$.

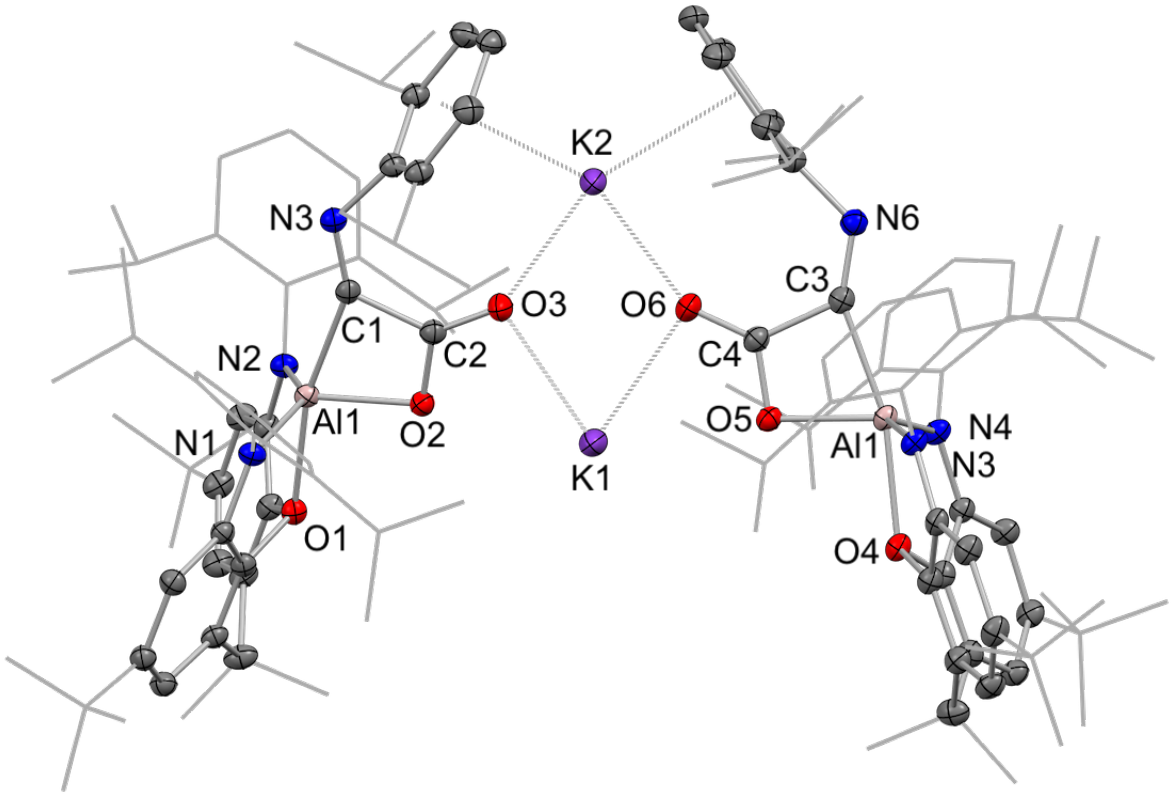

Figure 5.1: Molecular structure of K_2[**5.1**]$_2$. Thermal ellipsoids set at 30 % probability. Hydrogens omitted and selected groups shown in wireframe format for clarity. Key bond lengths (Å): Al1−C1 2.034(3), Al2−C3 2.045(3), Al1−O2 1.9006(18), Al2−O5 1.9042(18), C1−C2 1.536(3), C3−C4 1.535(4), C1−N3 1.282(3), C3−N6 1.279(4), C2−O2 1.306(3), C4−O5 1.310(3), C2−O3 1.233(3), C4−O6 1.225(3), K1−O3 2.718(2), K1−O6 2.714(2), K2−O3 2.556(2), K2−O6 2.603(2).

The molecular structure of K_2[**5.1**]$_2$ in the solid state comprises two crystallographically inequivalent [**NON**Al{C(NDipp)CO_2}]$^-$ units, featuring κ^2-C,O [C(NDipp)CO_2]$^{2-}$ fragments, which are bridged by K^+ counter-ions via K···Ar and K···O interactions. The key bond lengths for the two units are in good agreement, hence only one set will be discussed. The Al1–O2 (1.9006(18) Å) and Al1–C1 (2.034(3) Å) bond lengths fall in the expected range for single bonds. The C2–O2 (1.306(3) Å) and C2–O3 (1.233(3) Å) bond lengths fall in the range of other carboxylate groups (1.308(19), 1.250(17) Å).[27] The C1–C2 (1.536(3) Å) bond length is consistent with a single bond (1.530 Å), and the C1–N3 (1.282(3) Å) bond length is indicative of a double bond (1.279 Å).[27] Further the K2–O3 (2.556(2) Å) and K2–O6 (2.603(2) Å) separations are significantly shorter than the sum of covalent radii (2.69 Å) indicating a strong interaction.[28]

It is evident that the [C(NDipp)CO_2]$^{2-}$ fragments are derived from the imido group and two equivalents of CO. Interestingly the C–O bond of one molecule of CO was completely cleaved, and the carbon atoms of the two CO molecules have formed a bond. As such K_2[**3.5**]$_2$ is a rare example of a main group compound capable of C–C bond formation and C–O cleavage in reactions with CO.

To gain a better understanding of the mechanism, investigations were carried out by DFT at the PBE0 D3BJ/def2-TZVP level of theory. This work was carried out in collaboration with Dr. Petra Vasko (Aldridge group). For computational efficiency ^{t}Bu groups were replaced with Me groups and only the anionic unit was modelled. The results of these efforts are summarised in scheme 5.8. in which **5.R** and **5.P** correspond to the cut down [**3.5**]$^-$ and [**5.1**]$^-$ anions respectively.

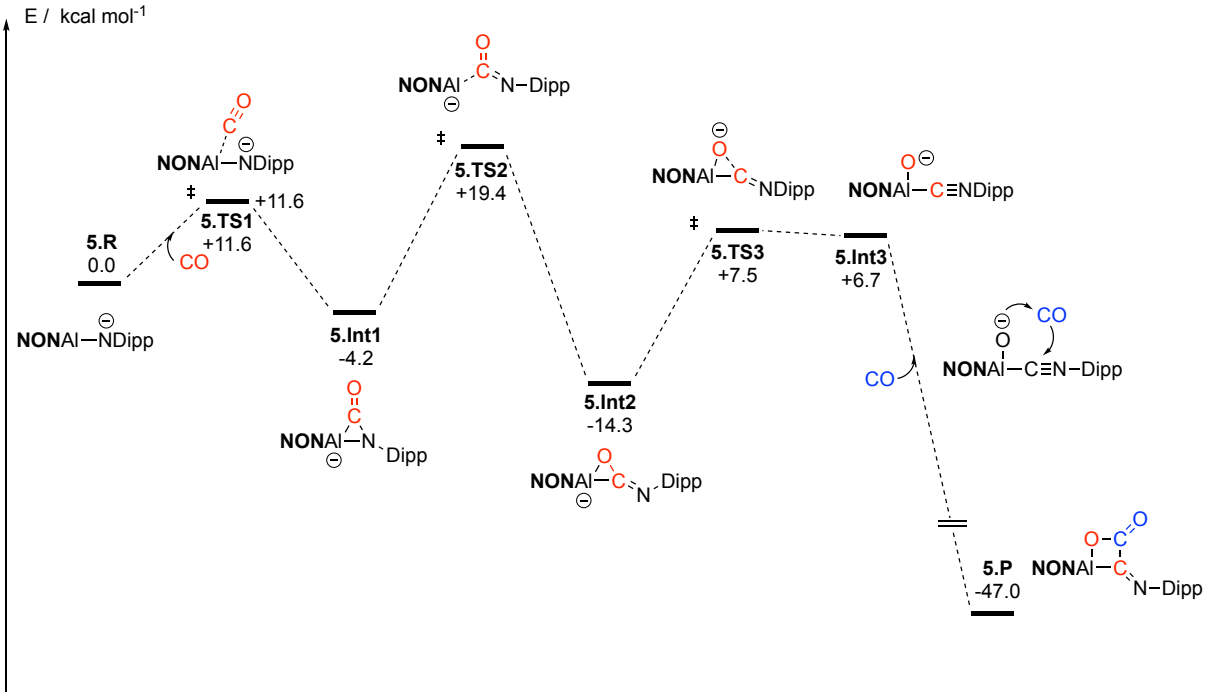

Scheme 5.8: Proposed reaction mechanism for the reaction of anionic **5.R** with CO, calculated at the PBE0 D3BJ/def2-SVP level of theory.

This reaction has been calculated to proceed via initial end on coordination of CO to Al on the convex face of the ligand. This is followed by C–N bond formation to afford a side-on bound isocyanate complex, **5.Int1**. The rate determining step is then the isomerisation from the κ^2-C,N to κ^2-C,O mode of coordination (**5.TS2**). **5.Int2** features a three membered ring, which can open and can act as a source of an isocyanide stabilised oxide (**5.Int3**). **5.Int3** can then take up a further equivalent of CO in an essentially barrierless process to yield the observed product **5.P**. For the initial reaction between **5.R** and CO, a [2+2] cycloaddition was also considered. The associated transition state was found at 25.8 kcal mol^{-1}, and is hence higher than the highest energy transition state in the above mechanism.

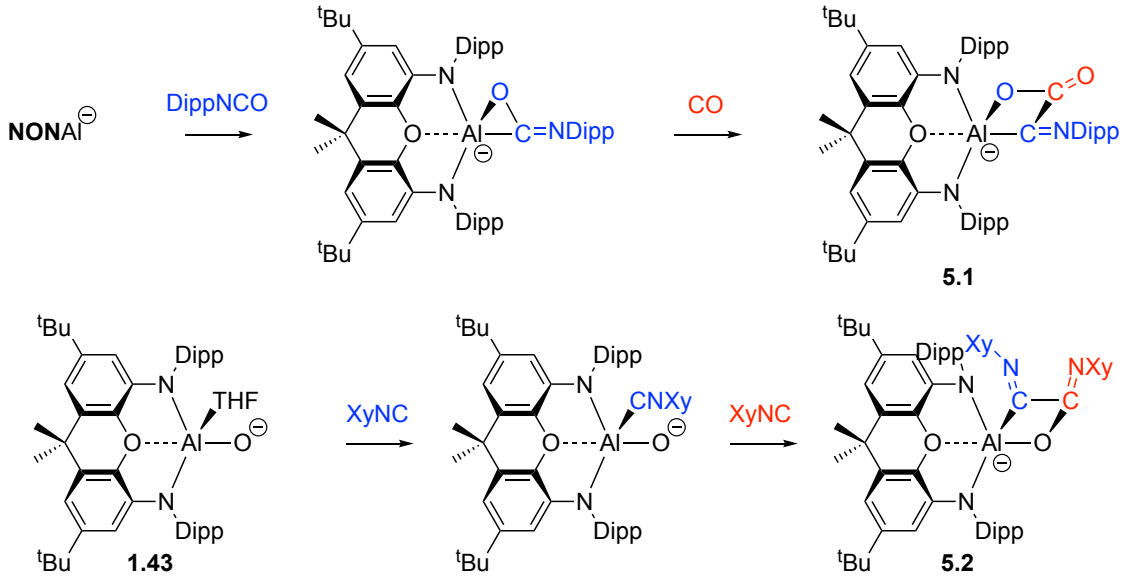

Scheme 5.9: Experiments carried out in support of the mechanism. Counter-ions omitted for clarity.

To provide further evidence for this mechanism, further experiments were carried out (Scheme 5.9). K_2[**NON**Al]$_2$ was dissolved in THF and 1 equiv. DippNCO was added at –78 °C, leading to the immediate decolourisation of the solution. CO was added and the mixture allowed to warm to room temperature. Upon removal of volatiles ^{1}H NMR spectroscopy shows formation of K_2[**5.1**]$_2$ as the only major product. This suggests that the reaction manifold can be entered from an isocyanate complex intermediate akin to **5.Int1** or **5.Int2**. Attempts to observe this intermediate are complicated by the high reactivity of this compound. To offer additional evidence the isocyanide stabilised oxide was targeted. Accordingly a solution of aluminium oxide K_2[**1.43**]$_2$ was prepared from K_2[**NON**Al]$_2$ and N_2O in THF at –78 °C. Addition of XyNC at low temperature gave a mixture of products, from which crystals of [K(THF)$_n$][**NON**Al{C(NXy)C(NXy)O}], [K(THF)$_n$][**5.2**], could be obtained. This compound features a κ^2-C,O [C(NXy)C(NXy)O]$^{2-}$ fragment, which is analogous to the κ^2-C,O [C(NDipp)CO$_2$]$^{2-}$ fragment observed in K_2[**5.1**]$_2$. However the spatial orientation of the κ^2-C,O [C(NXy)C(NXy)O]$^{2-}$ fragment relative to the **NON** ligand is different, i.e. the C donor position (at aluminium) of one compound is occupied by the O donor in the other and vice versa. It should however be noted, that the barrier for ligand inversion is likely to be low, such that

interconversion between the two isomers is a facile process. Evidence for this idea comes from the ^{1}H NMR spectra of aluminyl [K(crypt)][**NON**Al] and carbonate [K(crypt)][**NON**Al(CO$_3$)], which show only one resonance of the methyl groups of the xanthene backbone, suggesting that ligand inversion is a facile process. This is also supported by DFT calculations: the barrier for inversion for a model [**NON**Al(CO$_3$)]$^-$ ion, with ^{i}Pr and ^{t}Bu groups replaced by Me for computational efficiency, was found to be $\Delta G^{\ddagger}$ = 7.5 kcal mol^{-1} at the r2scan-3c / def2-SVP level of theory.

The molecular structure of [K(THF)$_n$][**5.2**] could be determined by single crystal X-ray diffraction. However due to the poor quality of crystals and initially wrongly determined symmetry, the diffraction data are weak and not entirely complete. As such exact bond metrics are subject to some uncertainty.

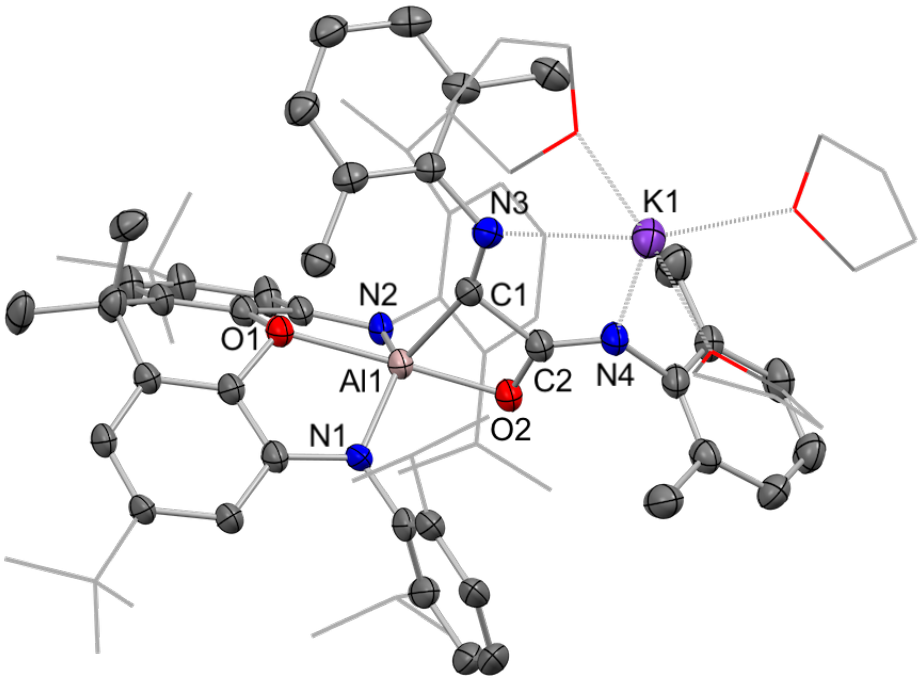

Figure 5.2: Molecular structure of [K(THF)$_3$][**5.2**]. One of the two inequivalent molecules in the asymmetric unit shown. Thermal ellipsoids set at 30 % probability. Hydrogen omitted and selected groups shown in wireframe format for clarity. Key bond lengths (Å): Al1–O2 1.839(4), Al1–C1 2.053(7), C2–O2 1.325(8), C2–N4 1.277(8), C1–N3 1.290(8), C1–C2 1.518(8).

Unlike K$_2$[**5.1**]$_2$, [K(THF)$_n$][**5.2**] adopts a monomeric form in the solid state, presumably due to the presence of THF, and the greater steric demands of the additional aryl group. Two

independent molecules are found in the asymmetric unit. Each molecule is comprised of an $[XyNCCNXyO]^{2-}$ unit, coordinated to aluminium via carbon and oxygen, and to potassium via both nitrogen atoms. The K^+ counter-ions are further coordinated to three or two THF molecules. In the case where only two THF molecules are coordinated, these are disordered over several sites. In the absence of reliable diffraction data, a detailed discussion of bond lengths will be omitted. However the available data suggest that the key bond metrics are similar for the two inequivalent molecules in the unit cell and that the bonding situation is similar to that observed in K_2[**5.1**]$_2$.

5.2.2 Reactivity of silyl substituted imides towards CO

Intrigued by the different products observed for simple disilyl amides compared to the monosilyl amides (Scheme 5.5), the reactivity of CO towards **NON**-supported aluminium and gallium imides bearing silyl or boryl groups was investigated, with the hypothesis that these reactions might proceed via N–Si or N–B bond cleavage.

When K[**NON**Al(NSiPh$_3$)], K[**3.7a**], is reacted with CO in benzene, initially a deep purple solution is obtained, and the sparingly soluble imide dissolves. The colour however fades within 3 min at room temperature. ^{1}H NMR spectroscopy reveals the formation of a complicated mixture of products. After standing for 3 d at room temperature no further change was observed by ^{1}H NMR spectroscopy. Concentrating this mixture afforded crystals suitable for single crystal X-ray diffraction. The structure so obtained revealed a 3:1 co-crystal of silylcarboxylate-cyanide complex K_2[**NON**Al{O$_2$C(SiPh$_3$)}(CN)], K_2[**5.3a**]$_2$ and siloxy-cyanide complex K_2[**NON**Al(OSiPh$_3$)(CN)], K_2[**5.4a**]. Structural parameters will be discussed below.

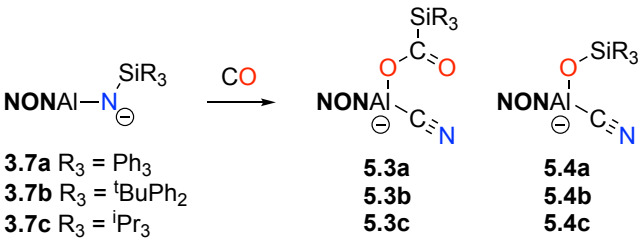

3.7a R_3 = Ph_3 **5.3a** **5.4a**
3.7b R_3 = ^{t}BuPh$_2$ **5.3b** **5.4b**
3.7c R_3 = ^{i}Pr$_3$ **5.3c** **5.4c**

Scheme 5.10: Reactivity of silyl imides K[**3.7a,b,c**] with CO. Counter-ions omitted and products shown as monomeric for clarity.

Carrying out this reaction at low temperatures prolonged the existence of the coloured intermediate(s). *In situ* monitoring of the reaction at –78 °C in toluene showed formation of one major product upon mixing. After 12 h at –78 °C the colour and ^{1}H NMR spectrum of the mixture remained unchanged, however an intensely blue waxy solid precipitated from solution. The supernatant was decanted and the residue taken into THF. The solid exhibited limited solubility, but the ^{1}H NMR spectrum showed essentially one clean compound, with resonances for one $SiPh_3$ group per NON ligand (characteristic resonances: δ_H = 7.86, 6.70, 5.81, 3.49, 2.98 ppm). This compound is thermally unstable, and application of a slight amount of heat to redissolve it led to its decomposition. Unfortunately, the identity of this compound or the decomposition products could not be established. A ^{1}H NMR spectrum of the supernatant showed a mixture of compounds upon standing at room temperature for 1 h, from which crystals of hexaphenyldisiloxane, $Ph_3Si–O–SiPh_3$, could be obtained.

To overcome problems with the solubility and selectivity of the $SiPh_3$ substituted system, the Si^tBuPh_2 substituted imide system was tested. Upon exposing a solution of K[**NON**Al(NSi^{t}BuPh$_2$)], K[**3.7b**], prepared *in situ*, to an atmosphere of CO, a colour change from colourless to deep blue was observed. This blue colour persisted longer than in the case of K[**3.7a**] but disappeared within 5 min.

Monitoring this reaction by ^{1}H NMR reveals a less complex mixture of products compared to the analogous $SiPh_3$ reaction. Over the course of two weeks, the formation of a single major species was observed, via a number of intermediates. Upon concentration of the reaction mixture crystals of carboxylate-cyanide complex K_2[**NON**Al{$O_2C(Si^tBuPh_2)$}(CN)]$_2$, K_2[**5.3b**]$_2$ suitable for single crystal X-ray diffraction could be obtained. It should be noted that K_2[**5.3b**]$_2$ just like the parent imide K[**3.7b**] is highly soluble, resulting in low isolated yields.

When this reaction is repeated with isolated samples of K[**3.7b**] the coloured intermediate persisted for at least 4 h, and a ^{1}H NMR spectrum shows only one major and one minor species. Over the course of two weeks, formation of a number of species (including K_2[**5.3b**]$_2$ as the

major product) was observed. Upon addition of CO to a solution of K[**3.7b**] in toluene at –78 °C, and the removal of excess CO, followed by warming to room temperature, a complex mixture of **NON**-containing products, but only one major silyl species, was observed.

In an attempt to find a happy medium between crystallinity and solubility, the Si^iPr_3 substituted imide K[**NON**Al(NSi^iPr_3)], K[**3.7c**], was tested. Upon addition of CO to a solution of K[**3.7c**], a brief colour change to an intense purple colour was observed. The colour, however, faded within 20 s. A ^1H NMR spectrum of the mixture obtained after 2 min reveals a mixture of only two compounds. After 30 min a single major species remained in the mixture, as judged by ^1H NMR spectroscopy. Crystals suitable for single crystal X-ray diffraction could be grown by slow evaporation from benzene, revealing the product to be the carboxylate-cyanide complex K_2[**NON**Al{$O_2C(Si^iPr_3)$}(CN)]$_2$, K_2[**5.3c**]$_2$, obtained in 34% yield.

An IR spectrum of K_2[**5.3c**]$_2$ shows absorption bands at ν = 2126, 1640, 1587, 1486, and 1417 cm^{-1}. The band at 2126 cm^{-1} is weak and corresponds to the C–N stretching mode; the remaining four bands are stronger and correspond to the symmetric and asymmetric stretching modes of the carboxylate C–O bonds, and two vibrations of the ligand backbone.

The molecular structures of the various silylcarboxylate-cyanide complexes K_2[**5.3a**,**b**,**c**]$_2$ could be determined by single crystal X-ray diffraction and their structures are shown in Figure 5.3.

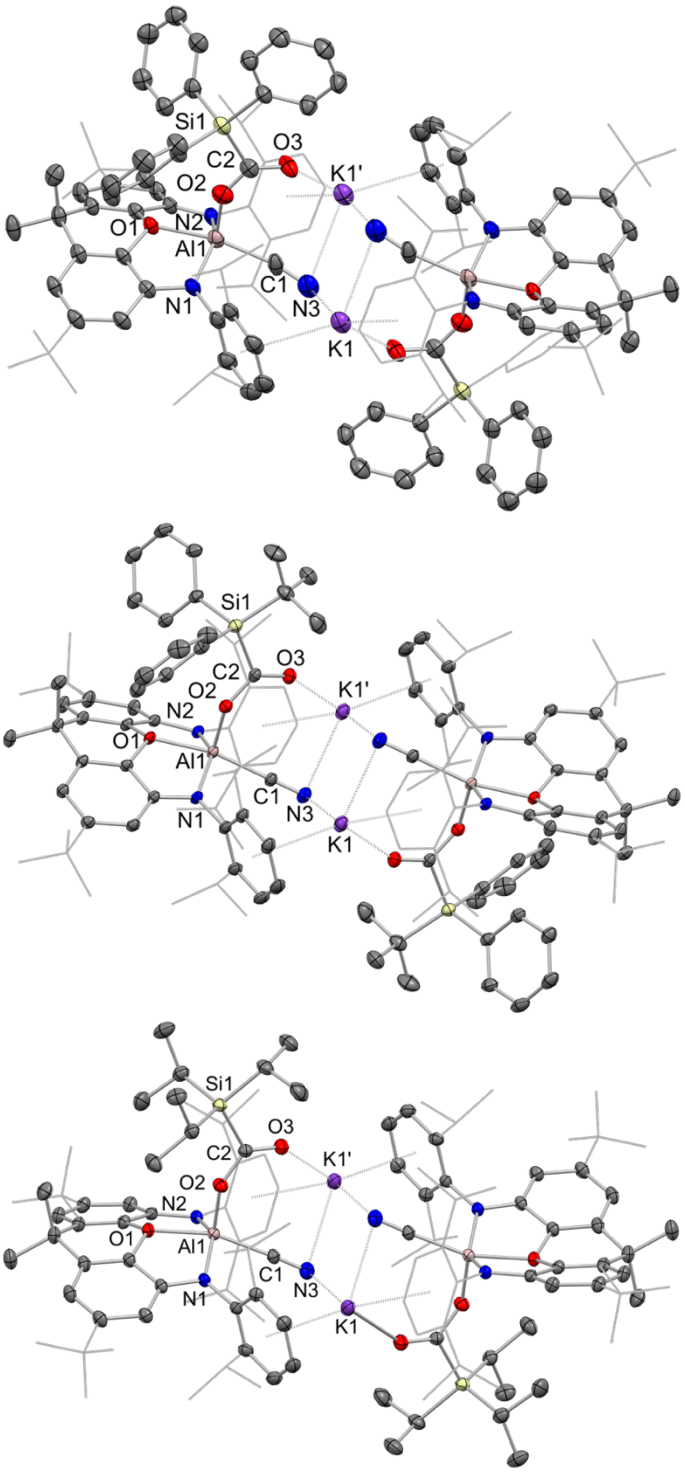

Figure 5.3: Molecular structures of K_2[**5.3a**]$_2$ (top), K_2[**5.3b**]$_2$ (middle), K_2[**5.3c**]$_2$ (bottom). The structure of K_2[**5.3a**]$_2$ corresponds to the major component (74 %) of a co-crystal with K_2[**5.4a**]$_2$. Thermal ellipsoids set at 30 % probability. Hydrogens omitted and selected groups shown in wireframe format for clarity. Key bond lengths (Å): K_2[**5.3a**]$_2$: Al1–C1 1.981(3), Al1–O2 1.784(3), C1–N3 1.193(6), C2–O2 1.207(5), C2–O3 1.235(5), C2–Si1 1.924(5), N3–K1 2.738(8), N3–K1' 2.998(9), O3–K1' 2.598(4); K_2[**5.3b**]$_2$: Al1–C1 2.0263(18), Al1–O2 1.7891(14), C1–N3 1.148(2), C2–O2 1.293(2), C2–O3 1.225(2), C2–Si1 2.0263(18), N3–K1 2.8009(19), N3–K1' 2.846(2), O3–K1' 2.6178(15); K_2[**5.3c**]$_2$: Al1–C1 2.0141(18), Al1–O2 1.7788(13), C1–N3 1.152(3), C2–O2 1.298(2), C2–O3 1.226(2), C2–Si1 1.9356(18), N3–K1 2.779(2), N3–K1' 2.840(2), O3–K1' 2.6153(16).

In the solid state all three compounds have the same connectivity. They adopt centrosymmetric dimeric structures, in which two anionic [**NON**Al{$O_2C(SiR_3)$}(CN)]$^-$ units are bridged by K^+ counter-ions. The cyanide moieties bridge between aluminium and both potassium ions, while the carboxylate groups bridge between aluminium and only one potassium cation. Bonding parameters for K_2[**5.3b**]$_2$ and K_2[**5.3c**]$_2$ are near identical. The parameters for K_2[**5.3a**]$_2$ are unreliable due to being derived from a co-crystal. All bond lengths fall into the expected ranges.

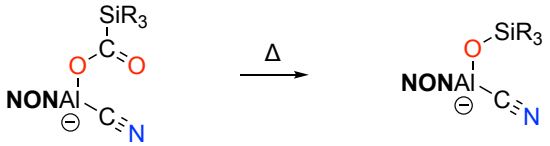

5.3b R_3 = ^{t}BuPh$_2$
5.3c R_3 = ^{i}Pr$_3$

5.4b
5.4c

Scheme 5.11: Thermal decarbonylation of K[**5.3b,c**]. Counter-ions omitted and products shown as monomeric for clarity.

Given the observation of K_2[**5.4a**]$_2$ as minor component in a co-crystal obtained from a reaction between K[**3.7a**] and CO, and the well-known thermal instability of silylcarboxylic acids, the thermal stabilities of K_2[**5.3b**,**c**]$_2$ were assessed. Upon heating a benzene solution of K_2[**5.3b**]$_2$ (in the presence of ^{i}PrCl) at 80 °C for 4 h, ca. 20% conversion to a single new species was observed. Upon heating for a week at 80 °C and concentration of the resulting solution, crystals of the decarbonylation product, K_2[**NON**Al(OSi^{t}BuPh$_2$)(CN)]$_2$, K_2[**5.4b**]$_2$ could be obtained. Similarly, complete thermal decarbonylation is observed upon heating a THF solution of K[**5.3c**] at 65 °C overnight. In this case formation of a major and a minor species are observed, which exhibit near identical ^{1}H NMR shift, with all peaks shifted by less than 0.04 ppm. It is proposed that the second species corresponds to either a different solvate, or the isocyanide analogue of [K(THF)]$_2$[**NON**Al(OSi^{i}Pr$_3$)(CN)]$_2$, [K(THF)]$_2$[**5.4c**]$_2$. Crystals of [K(THF)]$_2$[**5.4c**]$_2$ could be obtained upon concentration of a concentrated THF solution.

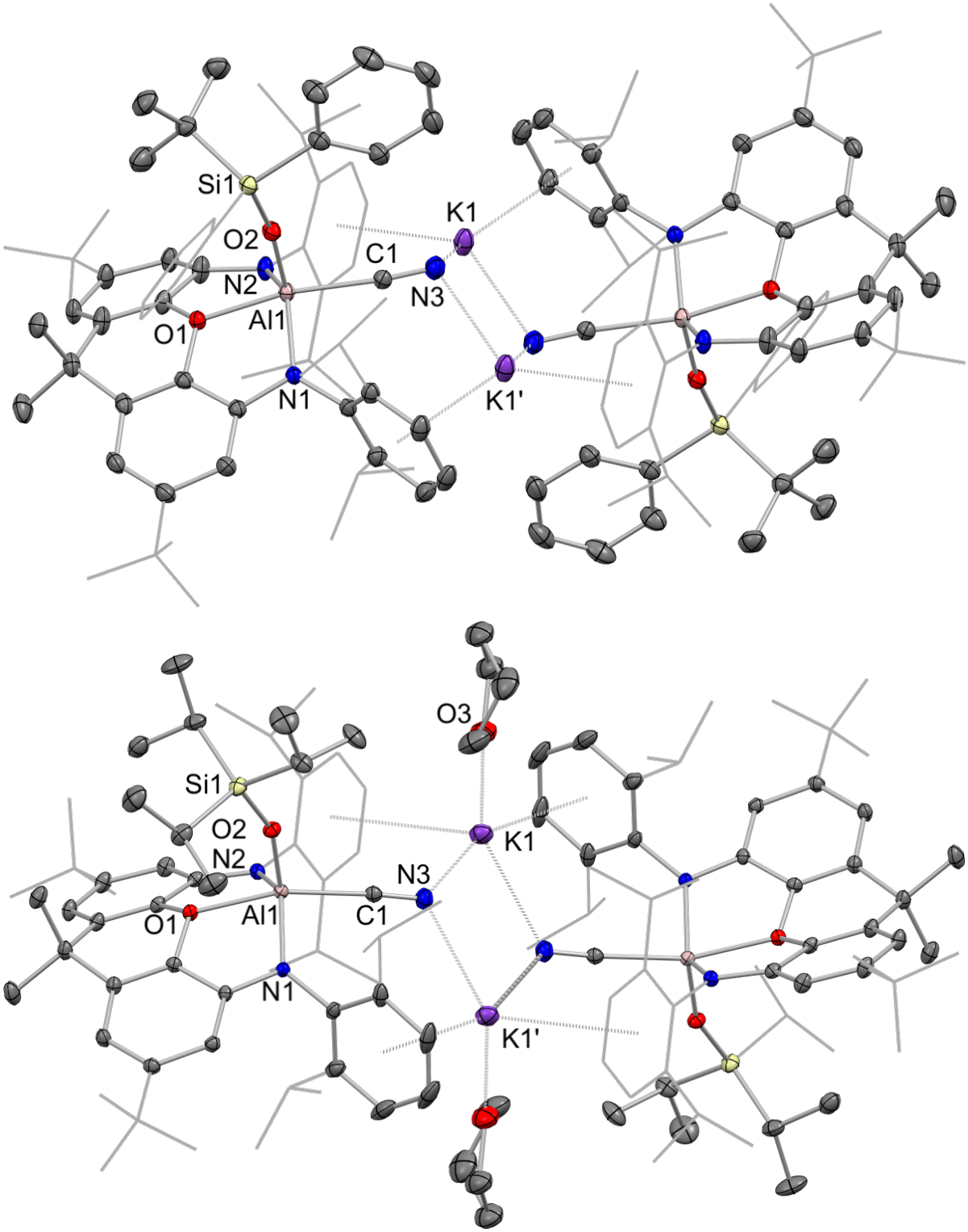

Figure 5.4: Molecular structures of K_2[**5.4b**]$_2$ (top) and [K(THF)]$_2$[**5.4c**]$_2$ (bottom). Thermal ellipsoids set at 30 % probability. Hydrogens omitted and selected groups shown in wireframe format for clarity. Key bond lengths (Å): K_2[**5.4b**]$_2$: Al1–C1 2.0541(18), Al1–O2 1.7390(13), C2–N3 1.137(2), O2–Si1 1.6067(13), N3–K1 2.7410(18), N3–K1' 2.8100(18); [K(THF)]$_2$[**5.4c**]$_2$: Al1–C1 2.0594(14), Al1–O2 1.7292(10), C2–N3 1.1490(19), N3–K1 2.8227(13), N3–K1' 2.8719(14).

In the solid state K_2[**5.4b**]$_2$ and [K(THF)]$_2$[**5.4c**]$_2$ adopt structures analogous to those of the parent carboxylates. The structures comprise two anionic [**NON**Al(CN)(OSiR$_3$)]$^-$ units bridged by K$^+$ counter-ions, via interactions with the flanking Dipp groups and the cyanide groups. The structure of [K(THF)]$_2$[**5.4c**]$_2$ features additional coordination of one molecule of THF to each potassium. All bond lengths fall into the expected ranges and are similar to those observed for the carboxylate complexes K_2[**5.3b**]$_2$ and K_2[**5.3c**]$_2$

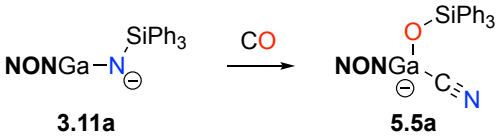

3.11a **5.5a**

Scheme 5.12: Reactivity of gallium imides K[**3.11a**] with CO. Counter-ions omitted and products shown as monomeric for clarity.

The corresponding chemistry of related gallium imides was also investigated. When the K[**NON**Ga(NSiPh$_3$)] , K[**3.11a**], is reacted with CO, clean conversion to a single new product is observed over the course of 3 d. Monitoring the reaction by ^{1}H NMR spectroscopy suggest that the reaction is more than 80% complete within 2 h, however as the reaction proceeded more of the poorly soluble imide starting material was dragged into solution. No intermediates were observed. Crystals of the final product could be obtained from a concentrated benzene solution. Diffraction experiments reveal the product to be siloxy-cyanide complex K_2[**NON**Ga(OSiPh$_3$)(CN)], K_2[**5.5a**]$_2$.

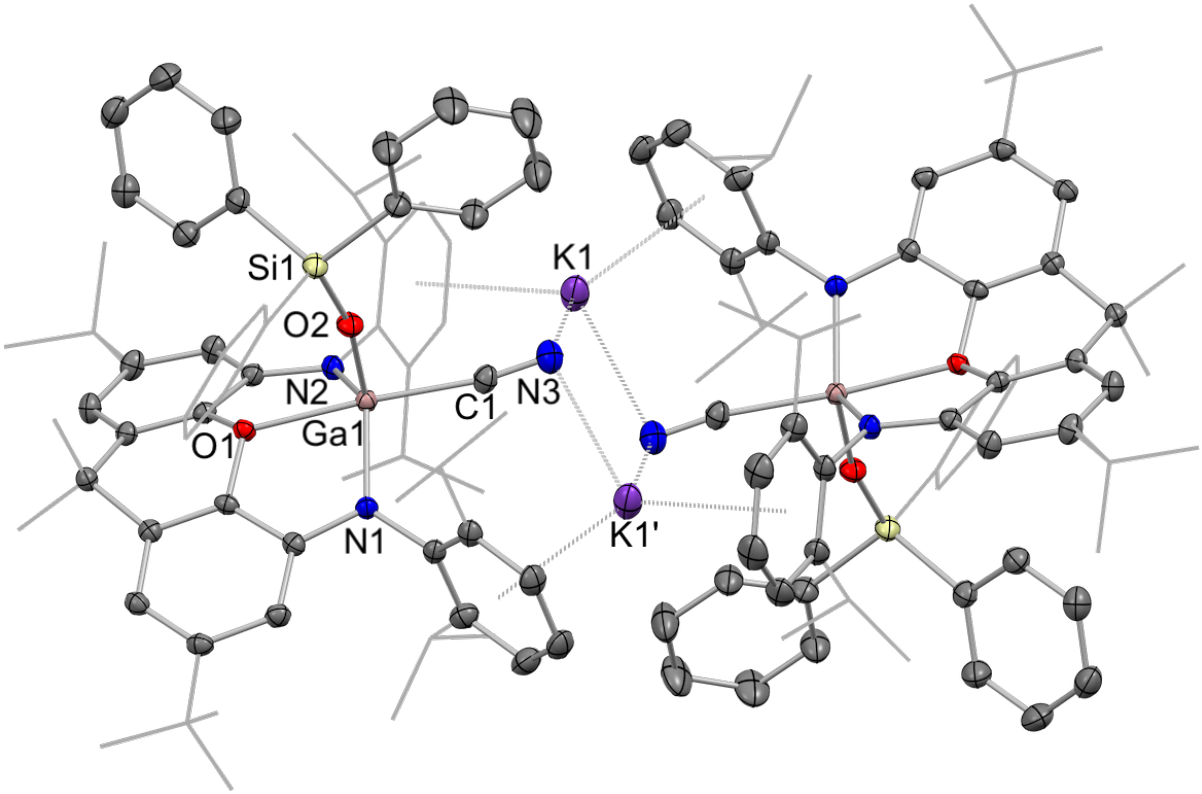

Figure 5.5: Molecular structures of K_2[**5.5a**]$_2$. Thermal ellipsoids set at 30 % probability. Hydrogens omitted and selected groups shown in wireframe format for clarity. Key bond lengths (Å): Ga1–C1 2.0463(18), Ga1–O1 1.8312(12), C1–N3 1.148(2), Si1–O2 1.5956(12), N3–K1 2.8201(19), N3–K1' 2.8174(18).

In the solid state K_2[**5.5a**]$_2$ adopts a structure analogous to the aluminium siloxy-cyanide complexes K_2[**5.4b**]$_2$ and [K(THF)]$_2$[**5.4c**]$_2$. The C1–N3 bond length (1.148(2) Å) is comparable to those observed in the aluminium examples, as are the Si1–O2 (1.5956(12) Å), N3–K1 (2.8201(19) Å) and N3–K1' (2.8174(18) Å) distances.

When the related cation sequestered imide [K(crypt)][**3.11a**] is reacted with CO, a complex mixture of products is obtained after 2 h as judged by ^{1}H NMR spectroscopy. Upon standing for another day, no further reaction takes place. From this mixture crystals of $Ph_3SiOSiPh_3$ could be grown. ^{1}H NMR spectroscopy suggests that ca. 20 % of the silyl groups are converted to the siloxide. The identity of the **NON**-containing products could not be determined.

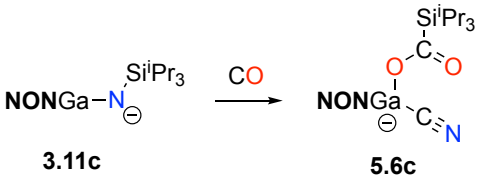

3.11c **5.6c**

Scheme 5.13: Reactivity of gallium imides K[**3.11c**] with CO. Counter-ions omitted and compounds shown as monomeric for clarity.

When CO was added to a solution of K[**NON**Ga(NSi^{i}Pr$_3$)], K[**3.11c**] prepared *in situ* from K$_2$[**NON**Ga]$_2$ and ^{i}Pr$_3$SiN$_3$, the ^{1}H NMR spectrum of the reaction mixture remained unchanged upon standing overnight at room temperature. However, a small amount of precipitate was observed. Warming the mixture to 45 °C for 16 h leads to the formation of more precipitate, and the complete consumption of the starting material as judged by ^{1}H NMR spectroscopy. The spectrum shows the formation of two major products, one of which exhibits signals nearly identical in shift and shape to those observed for carboxylate-cyanide complex K$_2$[**5.3c**]$_2$. It is therefore postulated that the analogous gallium complex, K$_2$[**5.6c**]$_2$, is one of the products of the reaction. Upon standing at room temperature for several days, no further reaction was observed. Attempts to analyse the precipitate were unsuccessful due to the low solubility of the solid.

5.2.3 Reactivity of K[(NON)Al(NB{NDippCH}$_2$)] with CO

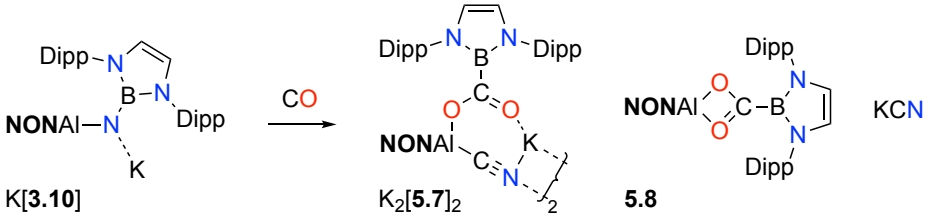

K[**3.10**] K$_2$[**5.7**]$_2$ **5.8**

Scheme 5.14: Reaction of K[**3.10**] with CO.

Addition of CO to a solution of (in situ generated) boryl-substituted aluminium imide K[**NON**Al(NB{NDippCH}$_2$)], K[**3.10**] in benzene leads to a slight colour change from light brown to light yellow. Following the reaction by ^{1}H NMR spectroscopy shows the formation of a complex mixture of products within 5 min via one major intermediate. After 16 h, the majority of the starting material and the intermediate have been consumed, and the ^{1}H NMR spectrum reveals the formation of two products, K[**NON**Al(CN)(O$_2$CB{NDippCH}$_2$)]

(K_2[**5.7**]$_2$) and **NON**Al(O_2CB{NDippCH}$_2$) (**5.8**), in approximately equal amounts. Simultaneously, over the same timeframe half of the excess boryl azide, ({CHNDipp}$_2$B)N_3, **5.9** starting material (ca. 0.3 eqiv, left over from the synthesis of imide K[**3.10**]) is converted to the corresponding cyanide, ({CHNDipp}$_2$B)CN, **5.10**. After three weeks the majority of K_2[**5.7**]$_2$ has been converted to **5.8** and small amounts of **5.9** and **5.10** remain visible in the ^{1}H spectra, indicating that the loss of KCN is independent of the onward reaction with the borole species.

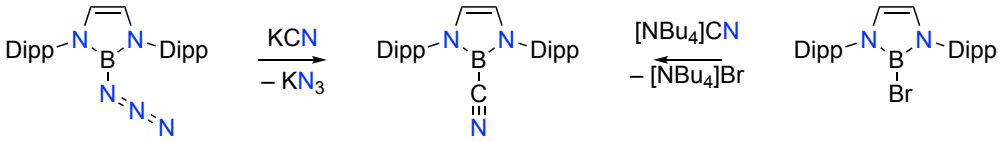

5.9 **5.10** **5.11**

Scheme 5.15: Syntheses of boryl cyanide **5.10**.

Cyanide **5.10** has not been reported previously in literature. Therefore for comparison **5.10** was synthesised independently from bromo-borane **5.11** and [^{n}Bu$_4$N]CN in benzene. This afforded cyanide **5.10** as the major species, and peaks are identical to those observed in the imide reaction above.

Concentrating a reaction mixture of K[**3.10**] and CO after 6 h led to the formation of two types of crystal, and the structures of both K_2[**5.7**]$_2$ and **5.8** could be determined by single crystal X-ray diffraction.

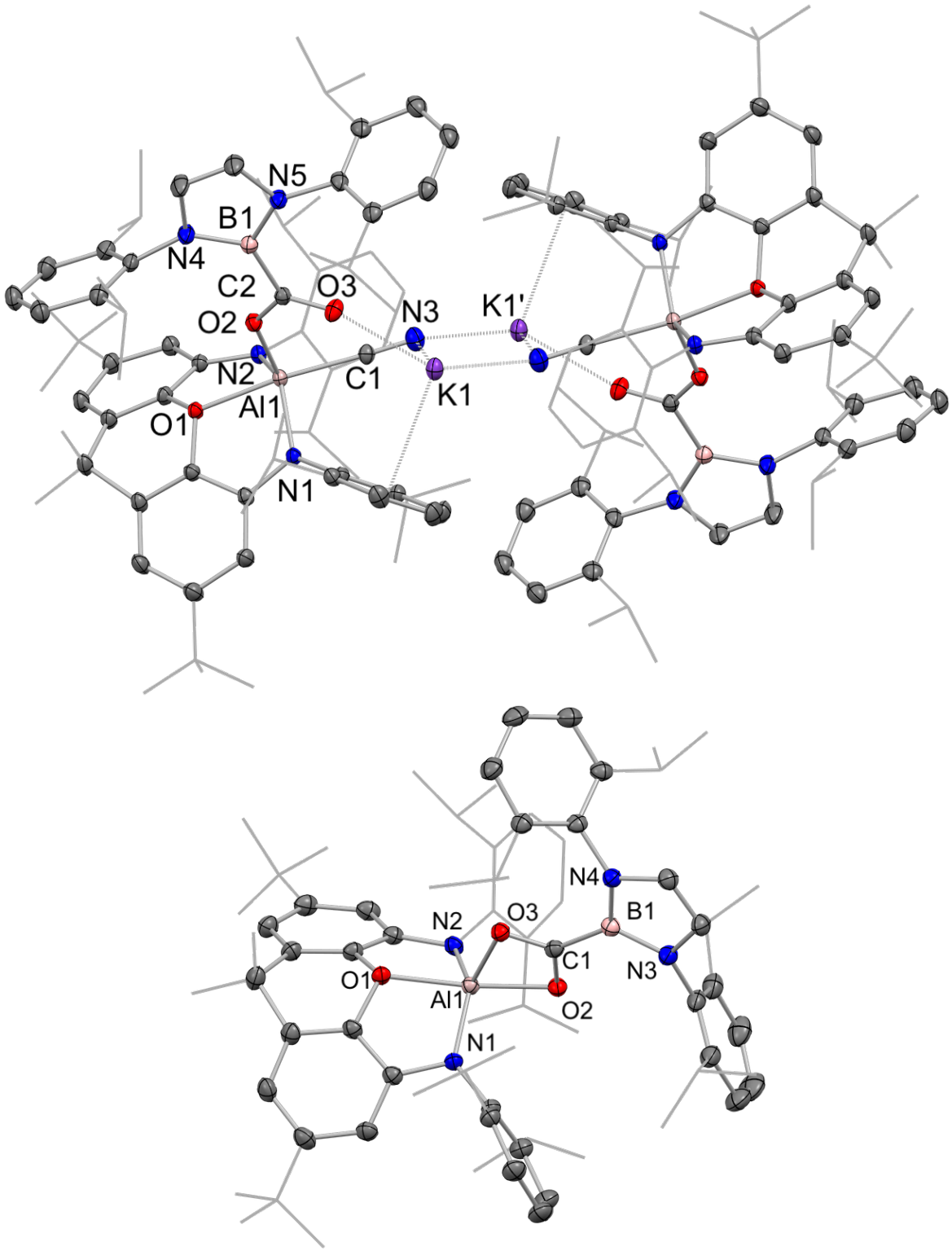

Figure 5.6: Molecular structures of K_2[**5.7**]$_2$ (top) and **5.8** (bottom). Thermal ellipsoids set at 30 % probability. Hydrogens omitted and selected groups shown in wireframe format for clarity. Key bond lengths (Å) and angles (°): K_2[**5.7**]$_2$: Al1–C1 2.0163(15), Al1–O2 1.8155(11), C1–N3 1.147(2), C2–O2 1.3108(17), C2–O3 1.2330(18), C2–B1 1.595(2), N3–K1 2.9961(14), N3–K1' 2.7182(15), K1–O3 2.5988(11), O2–C1–O3 122.64(13), O2–C2–B1–N4 24.7; **5.8**: Al1–O2 1.9376(10), Al1–O3 1.8895(10), C1–O2 1.2803(17), C1–O3 1.2903(17), C1–B1 1.5925(19), O2–C1–O3 114.33(11), O2–C1–B1–N3 17.7(2).

In the solid state K_2[**5.7**]$_2$ is a centrosymmetric dimer. Two anionic [**NON**Al(O_2CB{NDippCH}$_2$)(CN)]$^-$ units are bridged by K^+ counter-ions via K···Ar and K···N interactions. Unlike in the case of the siliyl-carboxylate-cyanide complexes K_2[**5.3a**,**b**,**c**]$_2$, each K^+ interacts with only one flanking Dipp group. The structure can thus be described as a "slipped" dimer. The cyanide group has a C–N bond length that, within error, is identical to those observed in the silyl substituted systems. The carboxylate bridges between aluminium and one potassium centre. Compared to the silyl compounds, the Al1–O2 bond (1.8155(11) Å) is marginally longer and the K1–O3 interaction is identical within error. Within the carboxylate group the C–O bond lengths are less similar compared to the silyl case.

5.8 adopts a monomeric structure in the solid state. The Al–O bond lengths are longer than in K_2[**5.7**]$_2$, presumably due to ring strain, and this is reflected in the O2–C1–O3 angles. The C1–O2 and C1–O3 bond lengths are nearly identical, and the C1–B1 bond length is comparable to that in K_2[**5.7**]$_2$.

Analysing the isolated crystals by NMR spectroscopy confirms that the two compounds correspond to the two major products of this reaction. This creates some ambiguity as the direct link between a crystal structure and clean NMR spectra of a single compound was not established. Assignment of the spectra to the compounds is based on the assumption that in benzene solution the loss of KCN is irreversible, and that therefore the signals associated with the final product of the reaction correspond to **5.8**.

Although approximately (by eye) equal amounts of crystals of K_2[**5.7**]$_2$ and **5.8** were present in the sample, a ^{1}H NMR spectrum of the mixture shows a 4:1 ratio of products, however some solid remained undissolved. This suggests that K_2[**5.7**]$_2$ and **5.8** have very different solubilities, potentially allowing for the separation of these species.

Repeating this reaction in toluene, and storing a concentrated reaction mixture in a freezer at –30 °C after one day, allows for the clean isolation of **5.8**.

In an attempt to isolate the intermediate en route to the formation of K_2[**5.7**]$_2$ and **5.8**, a solution of K[**3.10**] in benzene was exposed to an atmosphere of CO (1.2 bar) and, after shaking for a few seconds, immediately degassed via two freeze-pump-thaw cycles. A ^{1}H NMR spectrum of this mixture reveals ca. 20 % conversion to an intermediate species characterised by very sharp signals at δ_H = 5.90, 3.03, 1.30 ppm. These signals persist for several days without decaying. This pattern of resonances implies that the boryl group is likely further away from the **NON** ligand, and hence able to rotate freely. This scenario could potenially be achieved by inserting CO into the Al–N bond of K[**3.10**]. As such the proposed intermediate would be a side on bound isocyanate, K[**5.12**].

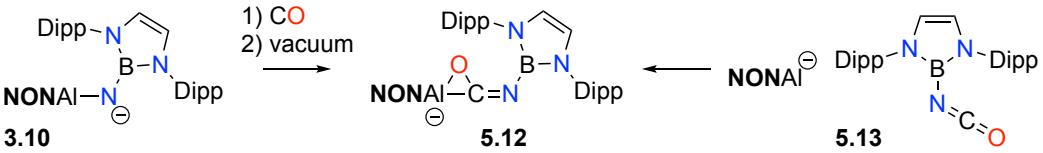

Scheme 5.16: Reactions leading to postulated intermediate K[**5.12**]. Counter-ions omitted and compounds shown as monomeric for clarity.

To test this hypothesis, K_2[**NON**Al]$_2$ was reacted with a stoichiometric amount of isocyanate **5.13**, and indeed formation of the same intermediate species, K[**5.12**], was observed. Unfortunately, attempts to crystallise K[**5.12**] were unsuccessful, and the clean isolation or the structural characterisation of this compound was not accomplished.

Although **5.13** has been reported in literature, an improved synthesis was desirable. **5.13** can be conveniently accessed via the addition of a stoichiometric amount of PMe_3 in THF to a solution of azide **5.9** in benzene, leading to the formation of the iminophosphorane over the course of 16 h. Addition of CO_2 then converted the iminophosphorane to **5.13** and Me_3PO over the course of another 16 h. The phosphine oxide by-product can be removed by sublimation at 60 °C affording **5.13** cleanly.

5.2.4 Mechanistic postulates

The mechanism for these transformations is clearly of some interest. The main features of the reaction that need to be explained are the formation of the silyl or boryl carboxylate and cyanide

moieties, and why the introduction of a hetero substituent on the imide leads to different products compared to the product obtained from the reaction of K_2[**3.5**]$_2$ with CO. A proposed mechanism is outlined in scheme 5.17.

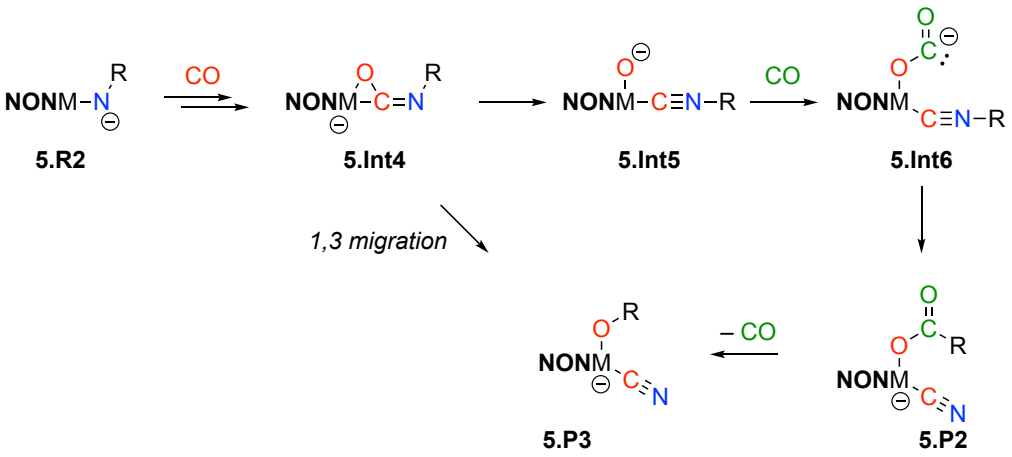

Scheme 5.17: Proposed mechanism for the formation of siloxied-cyanide and carboxylate-cyanide complexes.

The reactions of the imides, **5.R2**, with CO are proposed to proceed via formation of a side-on bound isocyanate (**5.Int4**). In the case of K[**3.7a**] and K[**3.11a**], 1,3-silyl-migration from nitrogen to oxygen leads to the formation of the siloxide-cyanide products **5.P3**. A similar mechanism has been proposed by the Stephan group for the reaction of $K_2[N(SiMe_3)_2]_2$ with CO.[17] Alternatively **5.Int4** may ring open to yield oxide intermediate **5.Int5**. This oxide intermediate then traps a further molecule of CO generating a carbene like species **5.Int6**, which can abstract the heteroatom imide substituent via a six membered transition state.

5.2.5 Reactions of aluminium and gallium imides with N_2O

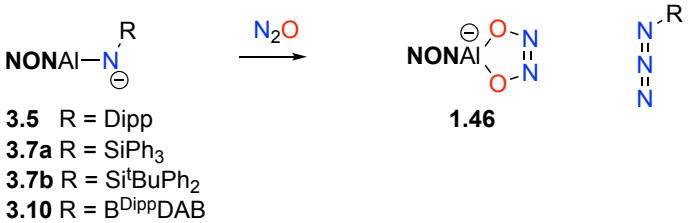

Scheme 5.18: Reactions of aluminium imides with N_2O. Counter-ions omitted and compounds shown as monomeric for clarity.

As discussed in chapter 4, the reaction of K_2[**3.5**]$_2$ reacts cleanly with N_2O to afford a *cis*-hyponitrite complex K_2[**NON**Al(ONNO)]$_2$ (K_2[**1.46**]$_2$) and $DippN_3$. The corresponding reactions of imides K[**3.7a,b,c**] and K[**3.10**] also lead to the clean formation of the cis-

hyponitrite complex K_2[**1.46**]$_2$ and the corresponding azide. However, when gallium imide K[**3.11a**] is reacted with N_2O, no reaction is observed at room temperature. Upon heating at 80 °C for 3 d, the formation of a large amount of microcrystalline precipitate K_2[**NON**Ga(OSiPh$_3$)(N$_3$)]$_2$, K_2[**5.14**]$_2$, was observed, which could be isolated in 61% yield. The IR spectrum of this compound shows a strong band ν = 2127 cm^{-1}, which is indicative of a metal bound azide group. On one occasion a few crystals suitable for single crystal X-ray diffraction formed over the course of the reaction, and the molecular structure confirms the formation of a siloxy-azide complex K_2[**NON**Ga(N$_3$)OSiPh$_3$], K_2[**5.14**]$_2$.

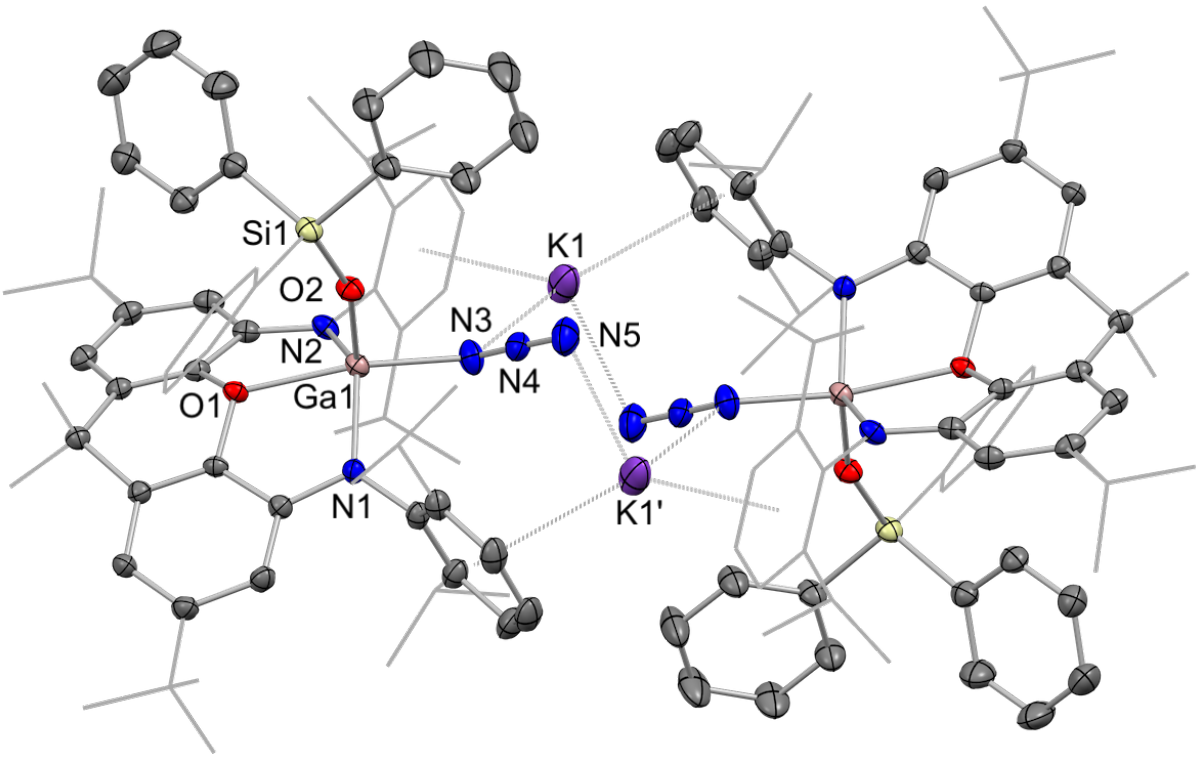

Figure 5.7: Molecular structures of K_2[**5.14**]$_2$. Thermal ellipsoids set at 30 % probability. Hydrogens omitted and selected groups shown in wireframe format for clarity. Key bond lengths (Å): K_2[**5.4b**]$_2$: Ga1–N3 1.989(2), Ga1–O2 1.8345(16), N3–N4 1.182(3), N4–N5 1.152(3), O2–Si1 1.6079(17), N3–K1 2.834(2), N5–K1' 2.686(3).

In the solid state K_2[**5.14**]$_2$ forms a centrosymmetric dimer, in which two formally anionic [**NON**Ga(OSiPh$_3$)(N$_3$)]$^-$ units are bridged by K$^+$ counter-ions via K···Ar and K···N interactions. The azide group features N–N bond lengths of 1.182(3) Å and 1.152(3) Å which fall into the range of other metal bound azides. The azide group is coordinated to Ga1 via N3

and features N3–K1 (2.834(2) Å) and N5–K1' (2.686(3) Å) contacts which are comparable to the sum of the covalent radii for these elements (2.74 Å).

By analogy to the mechanism described in chapter 4 (scheme 4.17) for aluminium, it is proposed that the reaction proceeds via either [2+2] or [2+3] cycloaddition, followed by cycloreversion to afford a gallium oxide and one equivalent of Ph_3SiN_3. The observed product is then obtained via coordination of the azide to gallium and migration of the silyl group to oxygen. A similar mechanism has been proposed for the reaction of a transient aluminium imide with Me_3SiN_3. Previous work in our group suggested, that the putative gallium oxide K_2[**NON**GaO]$_2$ does not react with N_2O to form a *cis*-hyponitrite complex.

5.3 Conclusions

The reactions of aluminium and gallium imides towards CO have been investigated. In the case of Dipp-substituted imide K_2[**3.5**]$_2$ uptake of two molecules of CO per aluminium centre is observed, and the product arises from the CO insertion into the Al–N bond, C–O cleavage, and trapping of a second molecule of CO via C–C bond formation.

The reactions of silyl substituted aluminium imides afford complexes featuring a cyanide and a hetero-carboxylate ligand. Heating these compounds leads to the decarbonylation and the formation of silyloxy-cyanide complexes. Attempts to characterise further intermediates in these transformations were ultimately unsuccessful.

In the case of gallium imides the $SiPh_3$-substituted system exclusively affords a siloxide cyanide complex on reaction with CO, while the Si^iPr_3-substituted system proved unreactive towards CO at room temperature. Upon warming, a mixture of products is formed, including a species with very similar NMR shift compared to the aluminium silyl-carboxylate-cyanide complex K_2[**5.3c**]. A crypt-sequestered gallium silyl imide also reacts rapidly with CO, however a wide product distribution is obtained. This shows that these compounds do not require the potassium counter-ion to react, contrasting with the findings of the Stephan group. Potassium does however appear to aid the selectivity.

Boryl-substituted aluminium imide K[**3.10**] reacts with CO to afford a cyanide carboxylate complex, analogous to those observed with silyl substituted imides. This complex is also shown to slowly lose KCN. Monitoring the initial stages of the reaction by NMR shows the formation of a stable intermediate. This can be trapped by the removal of excess CO, or can be synthesised independently from the reaction of aluminyl and ({HCNDipp}$_2$B)NCO. Therefore the intermediate is proposed to be a side on bound isocyanate complex.

Mechanistically these reactions are proposed to proceed along an analogous path as for the Dipp imide. Insertion of one molecule of CO into the Al–N bond followed by C–O cleavage gives rise to an isocyanate stabilised oxide, which reacts with a further molecule CO via C–O bond formation to generate a species with a nucleophilic carbon centre. This is trapped via migration of the silyl or boryl groups, rather than by the π* orbitals of the isocyanide fragment, as in the case of the Dipp imide.

The reaction of hetero substituted imides towards N_2O was described. In the case of aluminium imides, formation of a *cis*-hyponitrite complex was observed. The analogous reaction with gallium imide does not proceed at room temperature, but upon heating affords a siloxide azide complex.

Thus it has been shown that the hetero atom substituted imides can act as either $[NR]^{2-}$ or $[N]^{3-}$ transfer reagents, converting CO and N_2O into CN^-, RN_3 and N_3^- respectively.

5.3 Experimental details

K_2[NONAl{C(NDipp)CO_2}]$_2$, K_2[5.1]$_2$

Method A: A solution of K_2[**NON**Al(NDipp)]$_2$ (140 mg, 0.07 mmol) in benzene (10 mL) was exposed to an atmosphere of CO (1.2 bar, 50 mL), leading to an immediate colour change from colourless to orange. After 1 h volatiles were removed, affording the product as an orange powder. Yield 80 mg, 54%.

Method B: To a solution of K_2[(**NON**)Al]$_2$ (300mg, 0.2 mmol) in THF (3 mL) at -78 °C was added DippNCO (78 μL, 0.37 mmol), which immediately caused the solution to decolourise.

The reaction mixture was removed from the cold bath and CO was bubbled through the solution for 5 min, resulting in an orange solution. After 2 h volatiles were removed affording the product. Yield 300 mg, 77%. Anal. Calc. for $C_{61}H_{79}AlKN_3O_3$ (%): C 74.66, H 8.22, N 4.34; found: C 74.34, H 8.40, N 4.71.

^{1}H NMR (500 MHz, C_6D_6): δ 0.57 (d, 6H, $^3J_{HH}$ = 6.8 Hz, CH(CH_3)$_2$), 0.78 (d, 6H, $^3J_{HH}$ = 6.8 Hz, CH(CH_3)$_2$), 0.90 (d, 6H, $^3J_{HH}$ = 6.8 Hz, CH(CH_3)$_2$), 1.16 (d, 6H, $^3J_{HH}$ = 6.8 Hz, CH(CH_3)$_2$), 1.21 (sept, 2H, $^3J_{HH}$ = 6.8 Hz, C*H*Me$_2$), 1.25 (s, 18H, C(CH_3)$_3$), 1.30 (d, 6H, $^3J_{HH}$ = 6.8 Hz, CH(CH_3)$_2$), 1.46 (d, 6H, $^3J_{HH}$ = 6.8 Hz, CH(CH_3)$_2$), 1.70 (s, 3H, C(CH_3)$_2$), 1.80 (s, 3H, C(CH_3)$_2$), 3.80 (sept, 2H, $^3J_{HH}$ = 6.8 Hz, C*H*Me$_2$), 3.86 (sept, 2H, $^3J_{HH}$ = 6.8 Hz, C*H*Me$_2$), 6.06 (d, 2H, $^4J_{HH}$ = 2.0 Hz, XA-Ar-C*H*), 6.56 – 6.66 (m, 3H, Dipp-Ar-C*H*), 6.78 (d, 2H, $^4J_{HH}$ = 2.0 Hz, XA-Ar-C*H*), 7.13 (dd, 2H, J = 7.6 Hz, J = 1.7 Hz, Dipp-*m*-C*H*), 7.17 (t, 2H, $^3J_{HH}$ = 7.6 Hz, Dipp-*p*-C*H*), 7.26 (dd, 2H, J = 7.6 Hz, J = 1.7 Hz, Dipp-*m*-C*H*).

^{13}C{^{1}H} NMR (126 MHz, C_6D_6): δ 23.4 (C(*C*H$_3$)$_2$), 23.9 (CH(*C*H$_3$)$_2$), 24.2 (CH(*C*H$_3$)$_2$), 25.1 (CH(*C*H$_3$)$_2$), 25.3 (CH(*C*H$_3$)$_2$), 25.9 (CH(*C*H$_3$)$_2$), 26.1 (CH(*C*H$_3$)$_2$), 26.8 (*C*HMe$_2$), 27.9 (*C*HMe$_2$), 29.4 (*C*HMe$_2$), 31.9 (C(*C*H$_3$)$_3$), 32.9 (C(*C*H$_3$)$_2$), 35.1 (*C*Me$_3$), 37.0 (*C*Me$_2$), 106.8 (XA-Ar-*C*H), 111.3 (XA-Ar-*C*H), 122.0 (Dipp-*p*-*C*), 122.4 (Dipp-*m*-*C*), 124.7 (Dipp-*m*-*C*), 124.9 (Dipp-*m*-*C*), 126.0 (Dipp-*p*-*C*), 132.7 (*C*CMe$_2$), 135.8 (Dipp-*m*-*C*), 140.9 (XA-*C*O), 143.3 (Dipp-*i*-*C*), 145.4 (XA-*C*N), 145.7 (Dipp-*o*-*C*), 148.1 (*C*^{t}Bu), 148.1 (Dipp-*o*-*C*), 152.3 (Dipp-*i*-*C*), 171.8 (*C*O$_2$), 211.6 (Al*C*NDipp).

[K(THF)$_n$][NONAlC(NXy)CNXyO], [K(THF)$_n$][5.2]

A solution of K_2[(**NON**)Al]$_2$ (250 mg, 0.17 mmol) in THF (3 mL) at -78 °C was exposed to N_2O (1 bar, 150 mL). After 5 min excess N_2O was removed under a dynamic vacuum for 10 min at -78 °C. A pre-cooled solution Xylyl isonitrile (111 mg, 0.85 mmol) in thf (5 mL). The resulting mixture was allowed to warm to room temperature and concentrated to approximately 1 mL. Storage at -30 °C overnight afforded a small quantity of yellow crystals of the product

covered in a thick layer of a sticky oil. Separation of the crystalline material from the oil was unsuccessful.

Reaction of K[3.7a] with CO

A solution of K[**NON**AlNSiPh$_3$] (20 mg, 0.02 mmol) in benzene (0.5 mL) was exposed to an atmosphere of CO (1.5 bar, 3 mL), leading to an immediate colour change from colourless to deep purple. This colour fades within minutes. An NMR obtained after 20 minutes, shows formation of a complicated mixture of products, which remains unchanged upon standing for 3 days at room temperature. Concentrating this mixture to a quarter of its original volume, lead to the formation of co-crystals of K$_2$[**5.3a**]$_2$ and K$_2$[**5.4a**]$_2$.

Reaction of K[3.7a] with CO at –78 °C

A solution of K[**NON**AlNSiPh$_3$] (20 mg, 0.02 mmol) in toluene (0.5 mL) was exposed to an atmosphere of CO (1.5 bar, 3 mL) at –78 °C, leading to an immediate colour change from colourless to deep purple. A ^{1}H NMR spectrum shows formation of two species. After 12 h at –78 °C the ^{1}H NMR spectrum appears sharper and a blue oil precipitated from solution. After 2 h at –10 °C the oil was isolated and dissolved in THF at room temperature, yielding a royal blue solution. A ^{1}H NMR spectrum of this mixture shows one major species.

^{1}H NMR (400 MHz, THF-d$_8$): δ 0.28 (d, $^3J_{HH}$ = 6.6 Hz, 6H, CH(C*H*$_3$)$_2$), 0.49 (d, $^3J_{HH}$ = 6.6 Hz, 6H, CH(C*H*$_3$)$_2$), 0.96 (d, $^3J_{HH}$ = 6.4 Hz, 6H, CH(C*H*$_3$)$_2$), 1.19 (s, 18H, C(C*H*$_3$)$_3$), 1.24 (d, $^3J_{HH}$ = 6.9 Hz, 6H, CH(C*H*$_3$)$_2$), 1.43 (s, 3H, C(C*H*$_3$)$_2$), 1.83 (s, 3H, C(C*H*$_3$)$_2$), 2.98 (sept, $^3J_{HH}$ = 6.7, 1H, C*H*Me$_2$), 3.49 (sept, $^3J_{HH}$ = 6.7, 1H, C*H*Me$_2$), 5.81 (d, $^4J_{HH}$ = 1.8, 2H, XA-Ar-C*H*), 6.70 (d, $^4J_{HH}$ = 1.9, 2H, XA-Ar-C*H*), 6.80 – 7.20 (Ar-C*H*), 7.85 (m, 6H, Ph-*o*-C*H*).

The low solubility of this compound prevents the collections of meaningful ^{13}C NMR data.

Reaction of K[3.7a] with CO at 7 °C

A solution of K[**NON**AlNSiPh$_3$] (20 mg, 0.02 mmol) in benzene (0.5 mL) was exposed to an atmosphere of CO (1.5 bar, 3 mL) at 7 °C, vigorously shaken until completely purple. The solution was exposed to vacuum causing an instant colour change from purple to blue. Volatiles were removed and the residue taken into THF affording a purple suspension. A ^{1}H NMR spectrum shows a mixture of products, including the above species, the spectrum is however very weak. Upon standing overnight a large amount of purple precipitate is formed and a ^{1}H NMR spectrum shows new signals, corresponding to an asymmetric species, as would be expected for a solvent activation product. This suggests that the intense colours might be associated with a paramagnetic species.

The low solubility of this compound prevents the collection of meaningful NMR data. Characteristic peaks for asymmetric species:

^{1}H NMR (400 MHz, THF-d$_8$): δ 3.25 (sept, $^3J_{HH}$ = 6.9 Hz, 1H), 3.35 (sept, $^3J_{HH}$ = 6.9 Hz, 1H), 3.42 (sept, $^3J_{HH}$ = 6.9 Hz, 1H), 3.74(sept, $^3J_{HH}$ = 6.9 Hz, 1H), 5.68 (d, $^4J_{HH}$ = 1.9 Hz, 1H), 5.76 (d, $^4J_{HH}$ = 1.9 Hz, 1H), 6.52 (d, $^4J_{HH}$ = 1.9 Hz, 1H), 6.66 (d, $^4J_{HH}$ = 1.9 Hz, 1H).

K$_2$[NONAl{O$_2$C(Si^{t}BuPh$_2$)}(CN)]$_2$, K$_2$[5.3b]$_2$

A solution of K[**NON**Al(NSi^{t}BuPh$_2$)] (200 mg, 0.20 mmol) in toluene (3 mL) was exposed to an atmosphere of CO (1.5 bar, 25 mL), leading to a colour change from colourless to deep blue. Upon standing overnight the solution turned orange. After 2 d, pentane (10 mL) was added. After two additional days, the mixture was concentrated to ca. 1 mL, leading to the formation of a fine precipitate. Benzene (3 mL) was added, and the resulting solution concentrated to the point of cloudiness. Upon standing overnight, crystals of the product were obtained. Crystals suitable for X-ray diffraction were obtained by carrying out the entire reaction in benzene, however yields are much lower. Yield 27 mg, 13 %. Anal. Calc. for $C_{65}H_{81}AlKN_3O_3Si$ (%): C 74.60 H 7.86 N 4.02; found C 73.72 H 7.86 N 3.72.

^{1}H NMR (600 MHz, C_6D_6): δ 0.91 (d, $^{3}J_{HH}$ = 6.5 Hz, 6H, CH(CH_3)$_2$), 1.01 (d, $^{3}J_{HH}$ = 6.9 Hz, 6H, CH(CH_3)$_2$), 1.06 (d, $^{3}J_{HH}$ = 6.7 Hz, 6H, CH(CH_3)$_2$), 1.25 (d, $^{3}J_{HH}$ = 6.7 Hz, 6H, CH(CH_3)$_2$), 1.28 (s, 18H, XA-C(CH_3)$_3$), 1.30 (s, 9H, Si-C(CH_3)$_3$), 1.63 (s, 3H, C(CH_3)$_2$), 1.68 (s, 3H, C(CH_3)$_2$), 3.50 (sept, $^{3}J_{HH}$ = 7.6 Hz, 2H, C*H*Me$_2$), 3.57 (sept, $^{3}J_{HH}$ = 7.6 Hz, 2H, C*H*Me$_2$), 6.08 (s, 2H, XA-Ar-C*H*), 6.77 (d, $^{3}J_{HH}$ = 1.9 Hz, XA-Ar-C*H*), 6.97 – 7.05 (m, 4H, Ph-*m*-C*H*), 7.09 – 7.21 (m, 8H, Ph-*p*-C*H* and Dipp-Ar-C*H*), 8.03 (d, $^{3}J_{HH}$ = 7.4 Hz, 4H, Ph-*o*-C*H*).

^{13}C NMR (151 MHz, C_6D_6): δ 18.6 (Si*C*Me$_3$), 23.3 (C(*C*H$_3$)$_2$), 24.9 (CH(*C*H$_3$)$_2$), 25.7 (2x CH(*C*H$_3$)$_2$, overlapping), 26.0 (CH(*C*H$_3$)$_2$), 27.8 (*C*H(CH$_3$)$_2$), 28.1 (SiC(*C*H$_3$)$_3$), 28.8 (*C*H(CH$_3$)$_2$), 31.9 (XA-C(*C*H$_3$)$_3$), 33.6 (C(*C*H$_3$)$_2$), 35.2 (XA-*C*Me$_3$), 36.8 (*C*Me$_2$), 106.6 (XA-Ar-*C*H), 110.1 (XA-Ar-*C*H), 124.1 (Dipp-*m*-*C*H), 124.2 (Dipp-*m*-*C*H), 125.7 (Dipp-*p*-*C*H), 128.6 (Ph-*m*-*C*H), 129.6 (Ph-*p*-*C*H), 130.8 (*C*CMe$_2$), 133.4 (Ph-*i*-*C*), 137.0 (Ph-*o*-*C*H), 138.6 (XA-*C*O), 143.9 (^{Ar}*C*N), 147.8 (*C*^{t}Bu), 149.3 (Dipp-*o*-*C*), 150.0 (Dipp-*o*-*C*), 187.7 (Si*C*O$_2$).

One ^{Ar}*C*N and Al*C*N were not observed in the ^{13}C{^{1}H} NMR spectrum.

K$_2$[NONAl{O$_2$C(Si^{i}Pr$_3$)}(CN)]$_2$, K$_2$[5.3c]$_2$

K$_2$[**NON**Al]$_2$ (300 mg) was dissolved in benzene (4.5 mL) and ^{i}Pr$_3$SiN$_3$ (0.1 mL) was added, leading to rapid gas evolution. The mixture was sonicated briefly and left to stand for 1 h at room temperature. The resulting solution was degassed and the headspace replaced with CO (1.5 bar, 20 mL). Upon shaking vigorously, the mixture turned purple, and the colour faded after 20 s. Upon standing overnight, colourless crystals of the product form in a yellow solution. A second crop was obtained after concentrating the solution to a quarter of its original volume. The crystals were washed with pentane and dried to yield a white powder. Yield 132 mg, 34 %. Anal. Calc. for $C_{58}H_{83}AlKN_3O_3Si$ (%): C 72.23 H 8.67 N 4.36; found C 72.28 H 8.79 N 4.22. IR (nujol): 2126.4 (CN), 1639.9, 1586.6, 1486.1, 1417.4 cm^{-1}.

^{1}H NMR (600 MHz, THF-d$_8$): δ 0.82 (d, $^{3}J_{HH}$ = 6.7 Hz, 6H, CH(CH_3)$_2$), 1.00 (d, $^{3}J_{HH}$ = 6.7 Hz, 6H, CH(CH_3)$_2$), 1.09 (s, 18H, C(CH_3)$_3$), 1.14 (apparent d, $^{3}J_{HH}$ = 7.2 Hz, 21H, Si(C*H*(CH_3)$_2$)),

1.18 (d, $^{3}J_{HH}$ = 6.9 Hz, 6H, CH(CH_3)$_2$), 1.22 (d, $^{3}J_{HH}$ = 6.9 Hz, 6H, CH(CH_3)$_2$), 1.56 (s, 3H, C(CH_3)$_2$), 1.77 (s, 3H, C(CH_3)$_2$), 3.34 (sept, $^{3}J_{HH}$ = 6.8 Hz, 2H, CH(CH_3)$_2$), 3.65 (sept, $^{3}J_{HH}$ = 6.8 Hz, 2H, CH(CH_3)$_2$), 5.66 (d, $^{4}J_{HH}$ = 1.8 Hz, 2H, XA-Ar-CH), 6.50 (d, $^{4}J_{HH}$ = 1.8 Hz, 2H, XA-Ar-CH), 7.08 – 7.14 (m, 2H, Dipp-*p*-CH), 7.14 – 7.20 (m, 4H, Dipp-*m*-CH).

^{13}C NMR (151 MHz, THF-d$_8$): δ 12.5 (SiCHMe$_2$), 19.4 (SiCH(CH$_3$)$_2$), 23.9 (C(CH$_3$)$_2$), 25.3 (CH(CH$_3$)$_2$), 26.3 (CH(CH$_3$)$_2$), 26.4 (CH(CH$_3$)$_2$), 26.4 (CH(CH$_3$)$_2$), 28.2 (CH(CH$_3$)$_2$), 29.2 (CH(CH$_3$)$_2$), 32.2 (C(CH$_3$)$_3$), 33.7 (C(CH$_3$)$_2$), 35.6 (C(CH$_3$)$_3$), 37.1 (C(CH$_3$)$_2$), 105.6 (XA-CH), 110.5 (XA-CH), 124.4 (Dipp-*m*-CH), 124.4 (Dipp-*m*-CH), 125.6 (Dipp-*p*-CH), 130.9 (CCMe$_2$), 139.4 (XA-CO), 144.6 (Dipp-*i*-C), 145.1 (XA-CN), 147.2 (C^{t}Bu), 149.0 (Dipp-*o*-C), 149.2 (Dipp-*o*-C), 189.6 (O$_2C$Si).

Due to quadrupolar broadening, the Al-CN resonance was not observed.

K$_2$[NONAl(OSi^{t}BuPh$_2$)(CN)]$_2$, K$_2$[5.4b]$_2$

A sample of K$_2$[**NON**Al{O$_2$C(Si^{t}BuPh$_2$)}(CN)]$_2$ (15 mg, 0.02 mmol) in benzene (0.5 mL) was heated at 80 °C for 5 d, in the presence of ^{i}PrCl (2 eq). The latter is just a spectator in the reaction. ^{1}H NMR shows essentially clean conversion to a single species, with broad resonances. Crystals of the product can be obtained by concentrating this mixture.

^{1}H NMR (400 MHz, C$_6$D$_6$): δ 0.89 – 1.08 (br m, 18H, CH(CH_3)$_2$), 1.21 – 1.32 (m, 24H, CH(CH_3)$_2$ and C(CH_3)$_3$), 1.70 (s, 3H, C(CH_3)$_2$), 1.90 (s, 3H, C(CH_3)$_2$), 3.25 (s, 2H, CHMe$_2$), 4.47 (br s, 2H, CHMe$_2$), 5.79 (br s, 2H, XA-Ar-CH), 6.80 (br s, 2H, XA-Ar-CH), 6.87 – 7.40 (m, 12H, Ar-CH), 7.87 – 8.43 (s, 4H, Ph-*o*-CH).

Due to the broadness of the spectrum the resonance for the Si^{t}Bu group could not be found.

[K(THF)]$_2$[NONAl(OSi^{i}Pr$_3$)(CN)]$_2$, [K(THF)]$_2$[5.3c]$_2$

A solution of K$_2$[**NON**Al{O$_2$C(Si^{i}Pr$_3$)}(CN)]$_2$ (15 mg, 0.02 mmol) in THF (0.5 mL) was heated at 65 °C for 1 d. ^{1}H NMR shows the quantitative conversion to two new species in a 4:1 ratio.

Interestingly, all peaks associated with the minor species appear in the same places as the signals associated with the major component, but are shifted by no more than 0.04 ppm.

^{1}H NMR (400 MHz, THF-d_8): δ 0.70 (d, $^{3}J_{HH}$ = 6.7 Hz, 6H, CH(CH_3)$_2$), 0.99 (s, 21H, SiCH(CH_3)$_2$), 1.03 (d, $^{3}J_{HH}$ = 6.7 Hz, 6H, CH(CH_3)$_2$), 1.07 (m, 24H, C(CH_3)$_3$ and CH(CH_3)$_2$), 1.29 (d, $^{3}J_{HH}$ = 6.7 Hz, 6H, CH(CH_3)$_2$), 1.59 (s, 3H, C(CH_3)$_2$), 1.71 (s, 3H, C(CH_3)$_2$), 3.21 (sept, $^{3}J_{HH}$ = 6.7 Hz, 2H, CHMe$_2$), 4.03 (sept, $^{3}J_{HH}$ = 6.7 Hz, 2H, CHMe$_2$), 5.53 (d, $^{4}J_{HH}$ = 1.9 Hz, 2H, XA-Ar-CH), 6.42 (d, $^{4}J_{HH}$ = 1.9 Hz, 2H, XA-Ar-CH), 6.98 – 7.09 (m, 4H, Ar-CH), 7.11 – 7.19 (m, 2H, Ar-CH).

K_2[NONAl(CN)(O_2CB{NDippCH}$_2$)]$_2$, K_2[5.7]$_2$

A solution of imide K[**3.10**] in benzene (3 mL) was prepared *in situ* from K_2[**NON**Al] (100 mg, 0.2 mmol) and azide **5.9** (55 mg, 0.2 mmol). The mixture was placed under CO (1.2 bar) for 5 h. The mixture was concentrated until the formation of crystals was observed (ca. 1 mL). These were isolated after 2 d. K_2[**5.7**]$_2$ formed rod shaped crystals while **5.8** formed cubes. These could not be separated. Recovered mass 55 mg. Suspending a mixture of both types of crystals (ca. 35 mg) in C_6D_6 allows for the measurement of NMR spectra with K_2[**5.7**]$_2$ is the major species (ca. 80%).

^{1}H NMR (400 MHz, C_6D_6): δ 0.92 (overlapping d, 12H, CH(CH_3)$_2$), 1.07–1.12 (m, 42H, CH(CH_3)$_2$ and C(CH_3)$_3$), 1.65 (s, 3H, C(CH_3)$_2$), 1.67 (s, 3H, C(CH_3)$_2$), 2.90 (br s, 4H, CHMe$_2$), 3.41 (d, $^{3}J_{HH}$ = 6.7 Hz, 2H, CHMe$_2$), 3.52 (d, $^{3}J_{HH}$ = 6.7 Hz, 2H, CHMe$_2$), 5.93 (d, $^{4}J_{HH}$ = 1.9 Hz, XA-Ar-CH), 6.10 (s, 2H, NCH), 6.69 (d, $^{4}J_{HH}$ = 1.9 Hz, XA-Ar-CH), 7.06 (m, 4H, Ar-CH), 7.12–7.16 (m, 8H, Ar-CH).

The remaining ^{i}Pr resonances are presumably very broad.

^{13}C NMR (101 MHz, C_6D_6): δ 22.3 (C(CH_3)$_2$), 23.3, 23.7, 24.6, 25.7, 26.5, 26.5, 27.9, 28.6, 29.1 (9x ^{i}Pr), 31.1 (C(*C*H$_3$)$_2$), 31.6 (C(*C*H$_3$)$_3$), 35.0 (*C*Me$_3$), 37.6 (*C*Me$_2$), 107.5 (XA-Ar-*C*H),

112.4 (XA-Ar-*C*H), 123.7, 123.9, 125.5, 126.1 (4x Ar-*C*H), 134.1 (*C*CMe$_2$), 137.8, 142.1 (XA-*C*O), 142.9, 145.4, 145.6, 146.8, 148.5 (*C*^{t}Bu).

Not all peaks observed due to a weak $^{13}C\{^1H\}$ spectrum with insufficient number of scans.

NONAl(O$_2$CB{NDippCH}$_2$), 5.8

A solution of imide K[**3.10**] in toluene (5 mL) was prepared *in situ* from K$_2$[**NON**Al] (190 mg, 0.2 mmol) and azide **5.9** (90 mg, 0.2 mmol). The mixture placed under CO (1.2 bar). After 1 d the solution was concentrated to half of its original volume and was stored at –30 °C leading to the formation of crystals of **5.8**. Yield 32 mg, 10%. A second fraction (20 mg) was obtained after 5 d at room temperature containing a mixture of **5.8** and K$_2$[**5.7**]$_2$.

^{1}H NMR (500 MHz, THF-d$_8$): δ 0.64 (d, $^3J_{HH}$ = 6.7 Hz, 6H, CH(C*H*$_3$)$_2$), 0.94 (d, $^3J_{HH}$ = 6.7 Hz, 6H), 1.06 (m, 30 H, CH(C*H*$_3$)$_2$ and C(C*H*$_3$)$_3$), 1.08 (d, $^3J_{HH}$ = 7.1 Hz, 12H, CH(C*H*$_3$)$_2$), 1.12 (d, $^3J_{HH}$ = 6.7 Hz, 6H), 1.14 (s, 3H, C(C*H*$_3$)$_2$), 1.17 (d, $^3J_{HH}$ = 6.8 Hz, 6H, CH(C*H*$_3$)$_2$), 1.68 (s, 3H, C(C*H*$_3$)$_2$), 3.13 (sept, $^3J_{HH}$ = 6.8 Hz, 4H, C*H*Me$_2$), 3.32 (overlapping sept, $^3J_{HH}$ = 6.8 Hz, 4H, C*H*Me$_2$), 5.65 (d, $^4J_{HH}$ = 1.9 Hz, 2H, XA-Ar-C*H*), 6.11 (s, 2H, NC*H*), 6.40 (d, $^4J_{HH}$ = 1.9 Hz, 2H, XA-Ar-C*H*), 7.00 – 7.16 (m, 12H, Dipp-Ar-C*H*).

^{13}C NMR (126 MHz, THF-d$_8$): δ 23.1 (C(*C*H$_3$)$_2$), 24.0 (DAB-CH(*C*H$_3$)$_2$), 24.4 (CH(*C*H$_3$)$_2$), 26.2 (CH(*C*H$_3$)$_2$), 26.6 (DAB-CH(*C*H$_3$)$_2$), 26.7 (CH(*C*H$_3$)$_2$), 27.6 (CH(*C*H$_3$)$_2$), 28.1 (*C*HMe$_2$), 29.2 (DAB-*C*HMe$_2$), 29.4 (*C*HMe$_2$), 32.2 (C(*C*H$_3$)$_3$), 33.9 (C(*C*H$_3$)$_2$), 35.5 (*C*Me$_3$), 37.4 (*C*Me$_2$), 105.5 (XA-Ar-*C*H), 110.9 (XA-Ar-*C*H), 122.2 (N*C*H), 123.7 (Dipp-*m*-*C*H), 124.1 (DAB-Dipp-*m*-*C*H), 124.4 (Dipp-*m*-*C*H), 125.4 (Dipp-*p*-*C*H), 127.8 (DAB-Dipp-*p*-*C*H), 132.4 (*C*CMe$_2$), 140.9 (XA-*C*O), 141.5 (DAB-Dipp-*i*-*C*), 145.0 (Dipp-*i*-*C*), 145.3 (OC*C*N), 146.9 (*C*^{t}Bu), 147.0 (DAB-Dipp-*o*-*C*), 149.0 (Dipp-*o*-*C*), 149.8 (Dipp-*o*-*C*).

^{11}B NMR (128 MHz, C$_6$D$_6$): δ 15.2.

(HCNDipp)$_2$BCN, 5.10

Bromoborane (HCNDipp)$_2$BBr (42 mg, 0.09 mmol) and [^{n}Bu$_4$N][CN] (30 mg, 0.11 mmol), were dissolved in benzene (0.5 mL). After 1 h ^{1}H NMR shows the formation of one major product.

^{1}H (400 MHz, C_6D_6): δ 1.16 (d, $^3J_{HH}$ = 6.9 Hz, 12H, CH(CH_3)$_2$), 1.17 (d, $^3J_{HH}$ = 6.9 Hz, 12H, CH(CH_3)$_2$), 2.99 (sept, $^3J_{HH}$ = 6.9 Hz, 4H, CHMe$_2$), 5.99 (s, 2H, NCH), 7.10 – 7.20 (m, 6H, Ar-CH).

^{11}B (128 MHz, C_6D_6): δ 14.7.

(HCNDipp)$_2$BNCO, 5.13

To a solution of (HCNDipp)$_2$BN$_3$ (20 mg, 0.05 mmol) in benzene (0.5 mL) was added PMe$_3$ (0.05 mL, 1 M in THF). After 16 h the solution was degassed and CO_2 (1.2 bar, 3 mL) was added. After another 16 h, volatiles were removed and Me$_3$PO was sublimed from the mixture at 60 °C under a dynamic vacuum. ^{1}H NMR shows essentially clean formation of the desired product. NMR data matches literature values.[29]

K$_2$[NONGa(OSiPh$_3$)(CN)]$_2$, K$_2$[5.5a]$_2$

K[**NON**Ga(NSiPh$_3$)] (80 mg) was suspended in benzene (20 mL) and exposed to an atmosphere of CO (1.5 bar, 35 mL) and allowed to stand at room temperature for 6 d. The solution was then filtered and concentrated to a quarter of its original volume. Upon standing over night microcrystalline precipitate of the product formed. Yield 71 mg of K$_2$[**5.5a**]$_2$ + 4 C_6H_6, 79%. Anal Calc for $C_{66}H_{77}GaKN_3O_2Si$ +1.8 C_6H_6 (%): C 75.49 H 7.24 N 3.44; found: C 75.54 H 7.28 N 3.40. IR: vw 2080, 2071 cm^{-1}

^{1}H NMR (600 MHz, C_6D_6): δ 0.75 (d, $^3J_{HH}$ = 6.6 Hz, 6H, CH(CH_3)$_2$), 0.84 – 0.90 (m, 6H, CH(CH_3)$_2$), 1.00 (d, $^3J_{HH}$ = 6.2 Hz, 6H, CH(CH_3)$_2$), 1.09 (d, $^3J_{HH}$ = 7.0 Hz, 6H, CH(CH_3)$_2$) 1.10 (s, 3H, C(CH_3)$_2$), 1.31 (s, 18H, C(CH_3)$_3$), 1.54 (s, 3H, C(CH_3)$_2$), 3.19 – 3.43 (sept, $^3J_{HH}$ = 6.9

Hz, 2H, C*H*(CH_3)$_2$), 4.25 (sept, $^3J_{HH}$ = 6.9 Hz, 2H, C*H*(CH_3)$_2$), 5.98 (d, $^3J_{HH}$ = 1.9 Hz, 2H, XA-Ar-C*H*), 6.73 (d, $^3J_{HH}$ = 1.9 Hz, 2H, XA-Ar-C*H*), 6.90 – 7.40 (m, 15H, Ar-C*H*), 7.60 – 8.20 (m, 6H, SiPh-*o*-C*H*).

^{13}C NMR (151 MHz, C_6D_6): δ 23.1 (C(*C*H_3)$_2$), 24.8 (CH(*C*H_3)$_2$), 25.1 (CH(*C*H_3)$_2$), 26.2 (CH(*C*H_3)$_2$), 26.9 (CH(*C*H_3)$_2$), 27.6 (*C*H(CH_3)$_2$), 28.2 (*C*H(CH_3)$_2$), 32.1 (C(*C*H_3)$_3$), 35.2 (*C*Me_3), 37.4 (*C*Me_2), 106.9 (XA-*C*H), 108.7 (XA-*C*H), 123.4 (Dipp-*m*-*C*H), 124.6 (Dipp-*m*-*C*H), 125.4 (Dipp-*p*-*C*H), 127.5 (Si*Ph*), 128.6 (Si*Ph*), 132.2 (*C*CMe_2), 135.7 (Si*Ph*), 136.1 (Si*Ph*), 138.4 (XA-*C*O), 142.2 (XA-*C*N), 145.5 (Dipp-*i*-*C*), 147.0 (C^{t}Bu), 150.7 (Dipp-*o*-*C*), 153.6 (Dipp-*o*-*C*).

The Ga*C*N signal could not be assigned in the ^{13}C{^{1}H} NMR spectrum.

K_2[NONGa{O_2C(Si^{i}Pr$_3$)}(CN)]$_2$, K_2[5.6c]$_2$

To a solution of K_2[**NON**Ga]$_2$ (35 mg, 0.04 mmol) in benzene (0.5 mL) was added ^{i}Pr$_3$SiN$_3$ (10 µL, 0.04 mmol). After 30 min, the mixture was placed under an atmosphere of CO (1.2 bar, 3 mL). Upon standing overnight, precipitate (presumably of the imide) formed and no new peaks were observed in the ^{1}H NMR spectrum. Upon heating to 45 °C for 16 h, conversion to two major species was observed. Species 1 has a spectrum that is nearly identical to that of K_2[**NON**Al{O_2C(Si^{i}Pr$_3$)}(CN)]$_2$ and is proposed to be the analogous Ga compound. Separation of products was unsuccessful, therefore not all signals of the major products could be identified unambiguously. Characteristic peaks:

Species 1: ^{1}H NMR (400 MHz, C_6D_6): δ 1.23, 3.46, 3.77 (br), 6.10 (br), 6.74.

Species 2: ^{1}H NMR (400 MHz, C_6D_6): δ 3.51 (br), 6.27, 6.76.

K_2[NONGa(OSiPh$_3$)(N_3)]$_2$, K_2[5.14]$_2$

K[**NON**Ga($NSiPh_3$)] (200 mg) was suspended in benzene (4 mL) and placed under an atmosphere of N_2O (1 bar, 100 ml). The mixture was then heated to 80 C for 3 d. This initially

leads to the dissolution of all reagents, followed by precipitation of the product. The mixture was then allowed to cool to room temperature. After two days the liquid was decanted and the residue washed with pentane. Upon drying K_2[**5.14**]$_2$ was obtained as a white powder. Yield 128 mg, 61%. Anal. Calc for $C_{65}H_{77}GaKN_3O_2Si$ (%): C 71.15 H 7.07 N 6.38; found C 70.79 H 6.52 N 6.00. IR: 2127.6 (azide), 1624, 1579 cm^{-1}.

^{1}H NMR (600 MHz, THF-d_8): δ 0.30 (d, $^3J_{HH}$ = 6.7 Hz, 6H, CH(CH_3)$_2$), 0.65 (d, $^3J_{HH}$ = 6.7 Hz, 6H, CH(CH_3)$_2$), 0.86 (d, $^3J_{HH}$ = 6.7 Hz, 6H, CH(CH_3)$_2$), 1.09 (s, 3H, C(CH_3)$_2$), 1.14 (apparent s, 24H, C(CH_3)$_3$ and CH(CH_3)$_2$), 1.74 (s, 3H, C(CH_3)$_2$), 3.31 (sept, $^3J_{HH}$ = 6.8 Hz, 2H, CH(CH-$_3$)$_2$), 3.84 (sept, $^3J_{HH}$ = 6.8 Hz, 2H, CH(CH$_3$)$_2$), 5.67 (d, $^4J_{HH}$ = 1.9 Hz, 2H, XA-Ar-CH), 6.47 (d, $^4J_{HH}$ = 1.9 Hz, 2H, XA-Ar-CH), 6.90 (m, 6H), 6.94 – 7.07 (m, 9H), 7.66 (m, 6H).

^{13}C NMR (151 MHz, THF-d_8): δ 23.9 (C(CH$_3$)$_2$), 25.4 (CH(CH$_3$)$_2$), 26.1 (CH(CH$_3$)$_2$), 26.3 (CH(CH$_3$)$_2$), 26.7 (CH(CH$_3$)$_2$), 27.9 (CH(CH$_3$)$_2$), 28.9 (CH(CH$_3$)$_2$), 32.3 (C(CH$_3$)$_2$), 32.5 (C(CH$_3$)$_3$), 35.6 (CMe$_3$), 37.8 (C(CH$_3$)$_2$), 104.7 (XA-Ar-CH), 109.4 (XA-Ar-CH), 123.7 (Dipp-*m*-CH), 124.6 (Dipp-*m*-CH), 125.1 (Dipp-*p*-CH), 127.4 (SiPh-*m*-CH), 128.2 (SiPh-*p*-CH), 132.3 (CCMe$_2$), 136.7 (SiPh-*o*-CH), 139.6 (XA-CO), 142.9 (SiPh-*i*-C), 144.7 (XA-CN), 145.1 (Dipp-*i*-C), 146.4 (C^{t}Bu), 148.6 (Dipp-*o*-C), 150.8 (Dipp-*o*-C).

5.5 References

[1] J. B. Peng, H. Q. Geng, X. F. Wu, *Chem.*, **2019**, *5*, 526–552.
[2] C. le Berre, P. Serp, P. Kalck, G. P. Torrence, in *Ullmann's Encyclopedia of Industrial Chemistry*, Wiley-VCH Verlag, Weinheim, Germany, **2014**, 1–34.
[3] H. Schulz, *Appl. Catal. A: Gen.*, **1999**, *186*, 3–12.
[4] H. Werner, *Angew. Chem. Int. Ed.*, **1990**, *29*, 1077–1089.
[5] W. A. Herrmann, *J. Organomet. Chem.*, **1990**, *383*, 21–44.
[6] S. Fujimori, S. Inoue, *J. Am. Chem. Soc.*, **2022**, *144*, 2034–2050.
[7] X. Wang, Z. Zhu, Y. Peng, H. Lei, J. C. Fettinger, P. P. Power, *J. Am. Chem. Soc.*, **2009**, *131*, 6912–6913.
[8] A. v. Protchenko, P. Vasko, D. C. H. Do, J. Hicks, M. Á. Fuentes, C. Jones, S. Aldridge, *Angew. Chem. Int. Ed.*, **2019**, *58*, 1808–1812.
[9] H. Braunschweig, T. Dellermann, R. D. Dewhurst, W. C. Ewing, K. Hammond, J. O. C. Jimenez-Halla, T. Kramer, I. Krummenacher, J. Mies, A. K. Phukan, A. Vargas, *Nature Chem.*, **2013**, *5*, 1025–1028.
[10] R. Dobrovetsky, D. W. Stephan, *J. Am. Chem. Soc.*, **2013**, *135*, 4974–4977.
[11] Y. Xiong, S. Yao, T. Szilvási, A. Ruzicka, M. Driess, *Chem. Commun.*, **2020**, *56*, 747–750.

[12] Y. Wang, A. Kostenko, T. J. Hadlington, M. P. Luecke, S. Yao, M. Driess, *J. Am. Chem. Soc.*, **2019**, *141*, 626–634.
[13] M. Majumdar, I. Omlor, C. B. Yildiz, A. Azizoglu, V. Huch, D. Scheschkewitz, *Angew. Chem. Int. Ed.*, **2015**, *54*, 8746–8750.
[14] T. Wang, M. Xu, A. R. Jupp, Z.-W. Qu, S. Grimme, D. W. Stephan,] T Wang, M. Xu, A. R. Jupp, D. W. Stephan, Z.-W. Qu, S. Grimme, *Chem. Asian J.*, **2021**, *16*, 3640–3644.
[15] M. Xu, A. R. Jupp, D. W. Stephan, M. Xu, A. R. Jupp, D. W. Stephan, *Angew. Chem. Int. Ed.*, **2019**, *58*, 3548–3552.
[16] M. Xu, Z. W. Qu, S. Grimme, D. W. Stephan, *J. Am. Chem. Soc.*, **2021**, *143*, 634–638.
[17] M. Xu, B. Kooij, T. Wang, J. H. Lin, Z. W. Qu, S. Grimme, D. W. Stephan, *Angew. Chem. Int. Ed.*, **2021**, *60*, 16965–16969.
[18] M. D. Anker, C. L. McMullin, N. A. Rajabi, M. P. Coles, *Angew. Chem. Int. Ed.*, **2020**, *59*, 12806–12810.
[19] P. Jutzi, F. -W Schröder, *Angew. Chem. Int. Ed.*, **1971**, *10*, 339–339.
[20] A. Orita, M. Fukudome, K. Ohe, S. Murai, *J. Org. Chem.*, **1994**, *59*, 477–481.
[21] H. Kai, M. Yamauchi, S. Murai, *Tetrahedron Lett.*, **1997**, *38*, 9027–9030.
[22] H. Kai, A. Orita, S. Murai, *Synth. Commun.*, **2006**, *28*, 1989–2000.
[23] P. Jutzi, F. W. Schröder, *J. Organomet. Chem.*, **1970**, *24*, 1–5.
[24] D. Seyferth, R. M. Weinstein, *J. Am. Chem. Soc.*, **1982**, *104*, 5534–5535.
[25] S. Murai, I. Ryu, J. Iriguchi, N. Sonoda, *J. Am. Chem. Soc.*, **1984**, *106*, 2440–2442.
[26] I. Ryu, Y. Hayama, A. Hirai, N. Sonoda, A. Orita, K. Ohe, S. Murai, *J. Am. Chem. Soc.*, **1990**, *112*, 7061–7063.
[27] F. H. Allen, O. Kennard, D. G. Watson, L. Brammer, A. G. Orpen, R. Taylor, *J. Chem. Soc, Perkin Trans. 2*, **1987**, S1.
[28] B. Cordero, V. Gómez, A. E. Platero-Prats, M. Revés, J. Echeverría, E. Cremades, F. Barragán, S. Alvarez, *Dalton Trans.,* **2008**, 2832.
[29] K. Yuvaraj, C. Jones, *Dalton Trans*., **2019**, 48, 11961–11965.

Chapter 6: Coordination and homologation of CO by aluminyl complexes

6.1 Introduction

The utilization of CO and CO_2 as synthons for the construction of complex molecules is a highly topical area of chemistry, both from a fundamental perspective, and in light of climate change and the Earth's limited hydrocarbon supply.[1] Within this context the Fischer-Tropsch (F-T) process is of sustained interest. This process is employed on an industrial scale to convert syngas, a mixture of CO and H_2, to short-to-medium length hydrocarbons using heterogeneous transition metals catalysts with main group activators.[2] Although syngas is traditionally derived from coal, today a variety of feedstocks can be used including biomass or methane.[3,4] Even the direct hydrogenation of CO_2 to synthetic fuels has been demonstrated.[5]

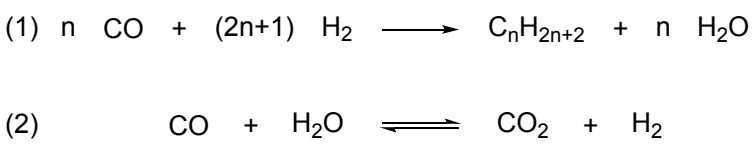

Scheme 6.1: Equations for (1) Fischer-Tropsch reaction and (2) water-gas shift reaction, employed to adjust the CO:H_2 ratio.

Despite being nearly a century old, little is known about mechanism of the F-T process.[6] Therefore homogeneous organometallic systems have been studied as model compounds, since they are amenable to small molecule and solution state characterization techniques.[7] Compounds capable of CO homologation include *s*-,[8–10] *d*-[11–13] and *f*-block[14–19] hydride and alkyl compounds, low-valent compounds from the *s*-,[20–24] *p*-,[25–30] *d*-[31–38] and *f*-blocks,[39–48] as well systems that activate CO cooperatively using *p*- and *d*-block metals.[49–51] Commonly the 2-electron reduction of CO is observed, leading to the formation of compounds containing cyclic systems of the type $[C_nO_n]^{2-}$ (n = 3–6) or the related linear ethynediolate dianions, $[C_2O_2]^{2-}$. A number of open chains, as well as more (or less) highly reduced fragments have also been reported.

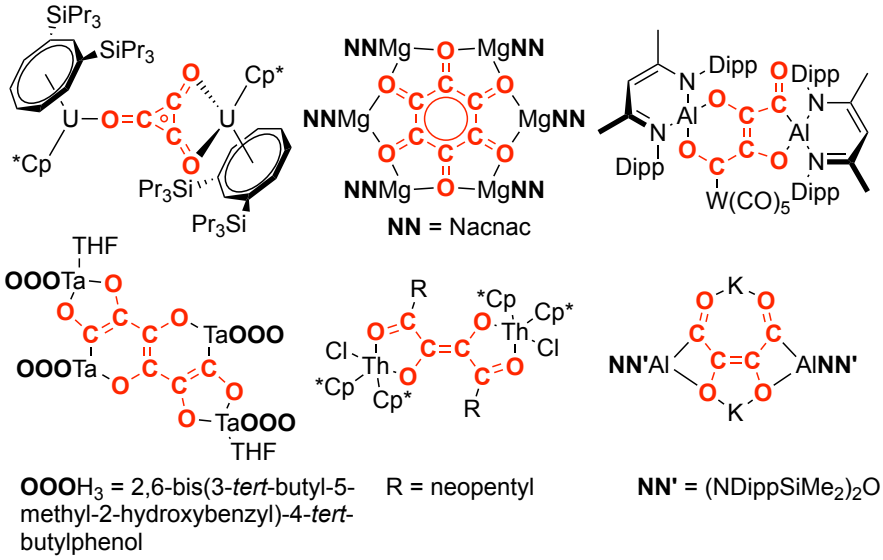

Figure 6.1: Selected CO homologation products.

Systems through which the degree of homologation can be influenced have also been reported. These include Mg(I) and U(III) complexes, in which the extent of CO homologation is determined by the steric bulk of the supporting ligands.[21,22,45–48] More recently, Crimmin reported on the cooperative activation of CO using a transition metal carbonyl compounds in conjunction with Al(I) reducing agents.[49–51] Using these systems, stepwise chain growth can be demonstrated, as well as partial hydrogenation or incorporation of organic molecules. Concurrent with our own investigations, Coles reported the reactivity of aluminyl $K_2[(O\{SiMe_2NDipp\}_2)Al]_2$, K_2[**1.22**]$_2$, with CO under various conditions leading to compounds featuring $[C_4O_4]^{4-}$ and $[C_5O_5]^{5-}$ fragments.[52]

Aluminyl systems have demonstrated high reactivity towards a range of small molecules, and have shown novel reactivity, e.g. in the reactions with N_2O. Therefore these systems might show interesting reactivity towards CO. Here the reactivity of aluminyl reagents K_2[**NON**Al]$_2$ and $[Li(OEt_2)_2]$[**NON**Al] towards CO is described.

6.2 Results and discussion

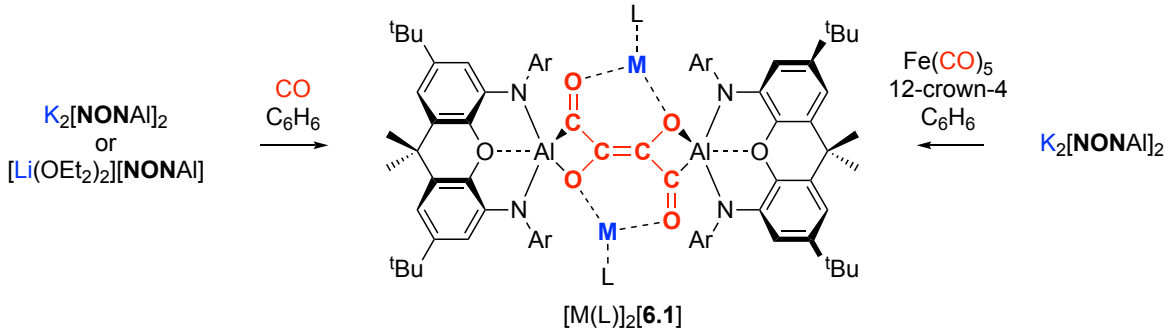

Scheme 6.2: Syntheses of complexes of the type $[M(L)]_2$[**6.1**] (M = Li, K; L = C_6H_6, C_7H_8, Et_2O, 12-crown-4).

Rapid mixing of a solution of K_2[**NON**Al]$_2$ in benzene with CO (1.3 bar, ca. 4 equiv per Al) at 34 °C leads to an immediate colour change from yellow to deep red. Upon standing undisturbed for 16 h at this temperature small orange crystals of the CO homologation product $[K(C_6H_6)]_2$[**6.1**] are obtained. Dried samples of this compound are invariably contaminated with small amounts of (**NON**)H_2, potentially arising from the decomposition of the compound under vacuum. Furthermore, powders are prone to develop electrostatic charge, making them difficult to handle. Therefore crystals of $[K(C_6H_6)]_2$[**6.1**] were isolated by decanting the mother liquor, and without prior drying were recrystallised from toluene. This leads to the formation of large crystals of $[K(C_7H_8)]_2$[**6.1**], which can be isolated cleanly in up to 11% yield, although typically yields fall into the 4–7% range.

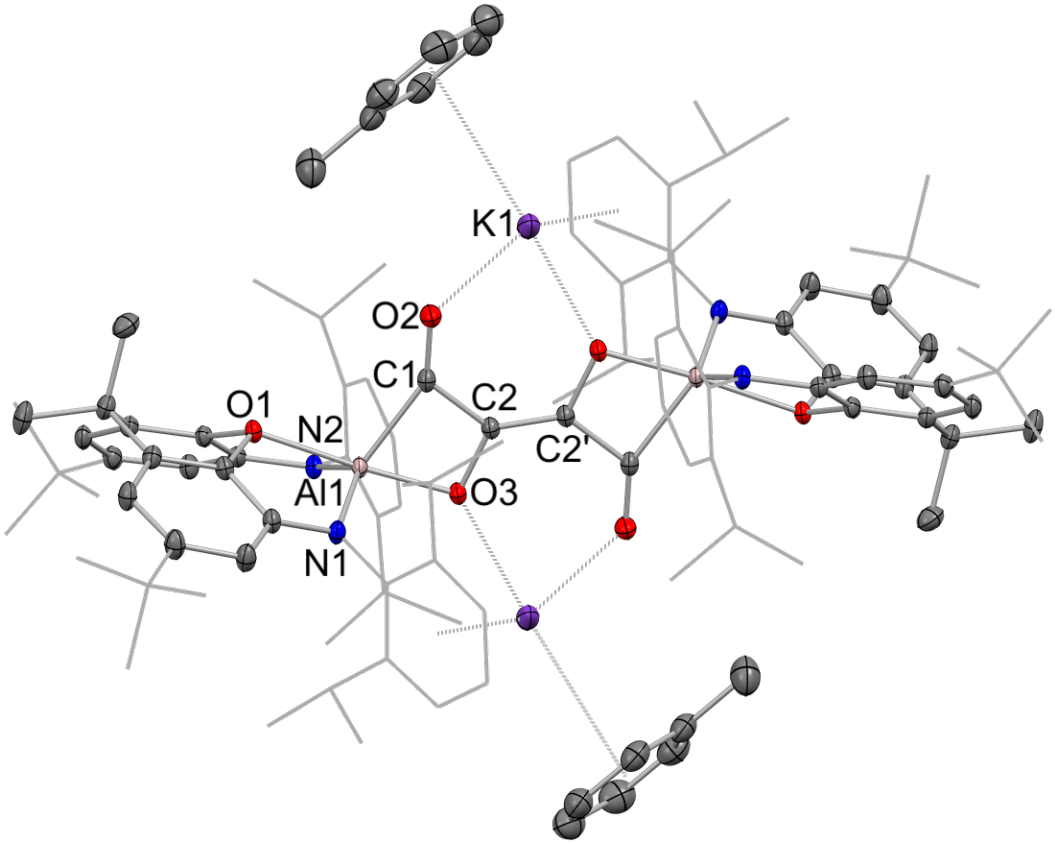

Figure 6.2: Molecular structure of $[K(C_7H_8)]_2$[**6.1**] as determined by X-ray crystallography. Thermal ellipsoids drawn at 30% probability, H atoms omitted, and selected groups shown in wireframe format for clarity. Key bond lengths (Å): Al1–C1 2.0936(8), Al1–O3 1.8709(8), C1–C2 1.5072(14), C2–C2' 1.373(2), C1–O2 1.2329(14), C2–O3 1.3826(13).

In the solid state $[K(C_7H_8)]_2$[**6.1**] adopts a centrosymmetric structure, containing two aluminium centres and a linear $[C_4O_4]^{4-}$ fragment, derived from the 4-electron reduction and C–C coupling of four molecules of CO. Two K^+ counter-ions are present in the structure, and are each coordinated by two oxygen atoms, one flanking Dipp group and one molecule of toluene. The formal charge on the $[C_4O_4]^{4-}$ is indicated by the overall charge balance, and is also reflected in the bond lengths. The outer C–C bonds lengths (1.5072(14) Å) fall in the range of single bonds, while the central C–C bond is a double bond (1.373(2) Å). Similarly, the outer C–O bond lengths (1.2329(14) Å) fall in the range of double bonds, while the central C–O bond lengths (1.3826(13) Å) are consistent with single bonds.

Monitoring the reaction of K_2[**NON**Al]$_2$ with CO in benzene by ^{1}H NMR spectroscopy, shows the complete consumption of starting materials immediately upon mixing, however the resulting spectrum shows very few well-defined signals of meaningful intensity other than those

associated with impurities present in the starting material. Possible explanations include the formation of a wide product distribution or the formation of paramagnetic products.

Analogous observations are made when the reaction is carried under alternative conditions, such as different pressures, concentrations, temperatures, stoichiometries, in the solid state, or without rapid mixing, however in these cases no crystals of $[K(C_6H_6)]_2$[**6.1**] could be obtained. Similarly the Coles group reports the observation of very broad signals upon mixing aluminyl K_2[**1.22**]$_2$ and CO.

In an attempt to gain further understanding of the homologation process, the use of transition metal carbonyl compounds as an alternative source of CO has been investigated. This strategy has previously enabled the isolation of a number of CO homologation products, and has enabled the selective chain growth in presence of CO. Therefore the reaction of K_2[**NON**Al]$_2$ with $M(CO)_6$ (M = Cr, Mo, W) was investigated. These reactions however afforded complicated mixtures of products. Liam Griffin in the Aldridge group attempted the reaction of $Fe(CO)_5$ with K_2[**NON**Al]$_2$ and 12-crown-4 in benzene. This reaction afforded two products in a 3:1 ratio as judged by ^{1}H NMR spectroscopy, the minor of which could be crystallised and was shown to be [K(12-c-4)]$_2$[**6.1**] by means of single crystal X-ray diffraction. This method did not allow for the clean isolation of bulk samples of [K(12-c-4)]$_2$[**6.1**]. Therefore [K(12-c-4)]$_2$[**6.1**] was prepared from $[K(C_6H_6)]_2$[**6.1**] and 12-crown-4 in benzene to aid spectroscopic characterisation.

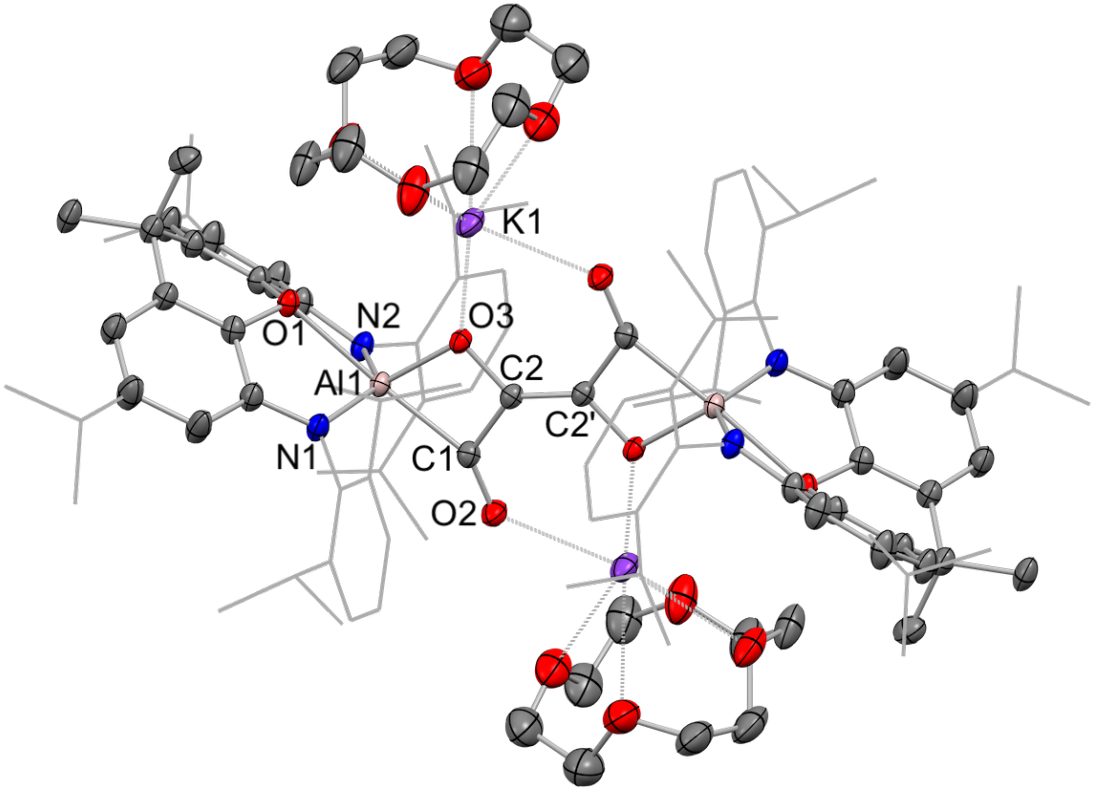

Figure 6.3: Molecular structure of [K(12-crown-4)]$_2$[**6.1**] as determined by X-ray crystallography. Thermal ellipsoids drawn at 30% probability, H atoms omitted, and selected groups shown in wireframe format for clarity. Key bond lengths (Å): Al1–C1 2.054(2), Al1–O3 1.8394(13), C1–C2 1.509(2), C2–C2' 1.364(4), C1–O2 1.230(2), C2–O3 1.386(2).

In the solid state [K(12-c-4)]$_2$[**6.1**] adopts a structure that is similar to that observed for [K(C$_6$H$_7$)]$_2$[**6.1**]. The **NON** ligands however appear to have undergone inversion, i.e. O3 occupies the equatorial position at aluminium in the former but the axial position in the latter, assuming trigonal bipyramidal geometry around aluminium. As outlined in chapter 5 inversion of the ligand is thought to be a relatively facile process, and in this case is presumably driven by the steric bulk of the 12-crown-4 ligands. Although the coordination geometry is different for [K(12-c-4)]$_2$[**6.1**] and [K(C$_6$H$_7$)]$_2$[**6.1**], resulting in slightly different Al–C and Al–O bond lengths, the corresponding C–C and C–O bond lengths within the [C$_4$O$_4$]$^{4-}$ fragments are identical within error.

An alternative approach to gain a better understanding of the homologation reaction was to study the reaction of alternative aluminyl reagents with CO. Given the similar structures of K$_2$[**NON**Al]$_2$ and [K(C$_6$H$_7$)]$_2$[**6.1**], one key question was whether the nuclearity of the aluminyl

reagent influenced the degree homologation via a template effect. Therefore the reaction between [Li(OEt$_2$)]$_2$[**NON**Al] and CO was investigated, which was carried out by Dr. Matthew Roy (Aldridge group). In this case formation of at least three species could be observed by ^{1}H NMR spectroscopy. From this mixture crystals of [Li(OEt$_2$)]$_2$[**6.1**] could be obtained. To aid spectroscopic characterisation, [Li(OEt$_2$)]$_2$[**6.1**] was prepared from [K(C$_7$H$_8$)]$_2$[**6.1**] and LiI in Et$_2$O. Isolation of clean samples was however complicated by decomposition of this compound in solution, presumably via the loss of Et$_2$O and the formation of higher aggregates. Therefore [Li(OEt$_2$)$_2$][**6.1**] was dissolved in THF, leading to the formation of one major species, [Li(THF)]$_2$[**6.1**]. An analytically pure sample of [Li(THF)]$_2$[**6.1**] can be obtained by addition of a THF solution of Li[^{s}Bu$_3$BH] to a crude reaction mixture containing [K(C$_6$H$_6$)][**6.1**], prepared from K$_2$[**NON**Al]$_2$ and CO in benzene as described above, in ca. 4% yield.

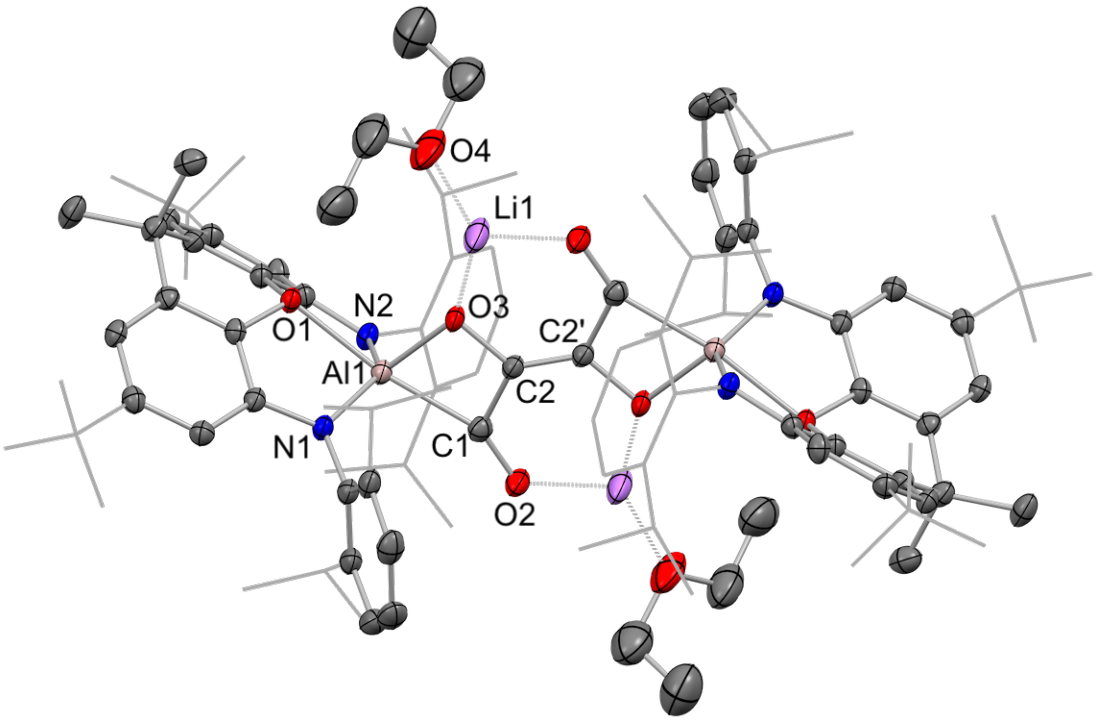

Figure 6.4: Molecular structure of [Li(OEt$_2$)]$_2$[**6.1**] as determined by X-ray crystallography. Thermal ellipsoids drawn at 30% probability, H atoms omitted, and selected groups shown in wireframe format for clarity. Key bond lengths (Å): Al1–C1 2.064(3), Al1–O3 1.877(2), C1–C2 1.482(5), C2–C2' 1.358(7), C1–O2 1.246(4), C2–O3 1.391(4).

In the solid state [Li(OEt$_2$)]$_2$[**6.1**] and [Li(THF)]$_2$[**6.1**] adopt structures analogous to that observed for [K(12-c-4)]$_2$[**6.1**]. The key bond lengths for [Li(OEt$_2$)]$_2$[**6.1**] and [Li(THF)]$_2$[**6.1**]

are identical within error. As for [K(12-c-4)]$_2$[**6.1**], the central C–C and outer C–O bonds of [Li(OEt$_2$)]$_2$[**6.1**] fall in the range expected for double bonds (1.358(7), 1.246(4) Å), while the outer C–C bonds and central C–O bonds fall in the range of single bonds (1.482(5), 1.391(4) Å). Compared to [K(12-c-4)]$_2$[**6.1**], the $[C_4O_4]^{4-}$ fragment of the lithiate features C1–O2 bonds that are slightly longer, and C1–C2 bond lengths that are somewhat shorter, while the remaining bond lengths are very similar. This presumably reflects on the fact that lithium cations are typically more polarising than K^+.

It has previously been shown by DOSY NMR experiments, that K$_2$[**NON**Al]$_2$ retains its dimeric structure in arene solutions, while [Li(OEt$_2$)]$_2$[**6.1**] is a monomeric species in the solid state, with a long Al–Li interaction (>2.7 Å), and presumably does not dimerise in solution. Considering monomeric and dimeric reagents afford compounds of the type [M(L)][**6.1**], it is proposed that formation of the $[\mathbf{6.1}]^{2-}$ unit proceeds via dimerisation of two identical [**NON**Al(C$_2$O$_2$)]$^-$ fragments. With this in mind, a mechanism was investigated by DFT methods at the B3LYP/def2-TZVP//B3LYP/def2-SVP level of theory, using CPCM solvent model for benzene. Counter-ions were omitted and ^{t}Bu and ^{i}Pr groups were replaced with Me groups for computational efficiency. This work was carried out by Agamemnon Crumpton (Aldridge group).

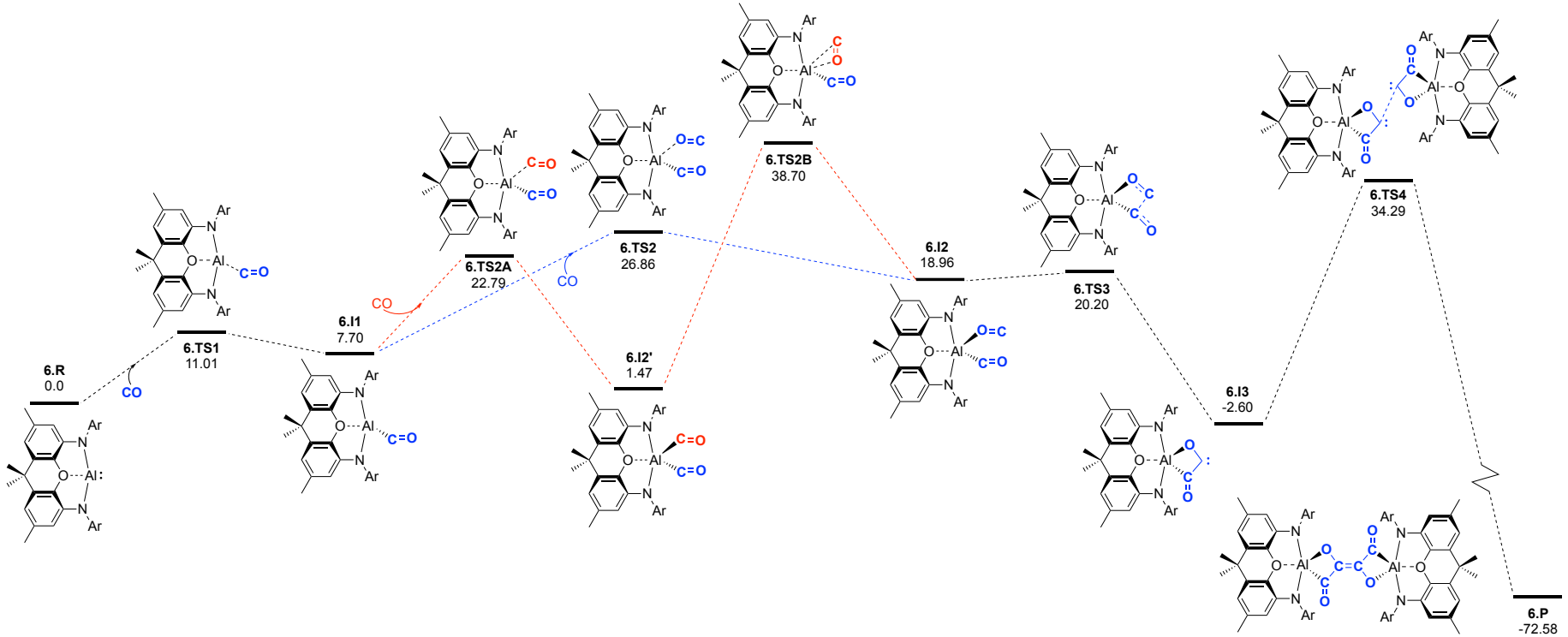

Scheme 6.3: Free energy profile (ΔG / kcal mol^{-1}) for the proposed reaction mechanism for the reaction of **6.R** with CO (B3LYP/def2-TZVP//B3LYP/def2-SVP) on the singlet surface.

The minimum energy conformation for the binding of one CO at the aluminium centre features a bent geometry (**6.I1**), indicating that the primary interaction between aluminium and CO is the donation of the aluminium lone pair into an empty π* orbital of CO. Thus it is different from the linear end-on coordination of CO that has been reported for silylenes[53–55] and mononuclear transition metal complexes, presumably reflecting the nucleophilic nature of the aluminium centre. Coordination of a second molecule of CO occurs similarly in a bent fashion, affording **6.I2'**. The HOMO of this species comprises the aluminium lone pair and CO π* orbitals of both CO molecules, and is thus indicative of a 3-centre-2-electron bond. Extended transition state with natural orbitals for chemical valence (ETS-NOCV) analysis of **6.I2'** was used to estimate the components of the orbital interaction energy, ΔE_{orb}. The three-centre "back-bonding" interaction is found to account for the majority of ΔE_{orb} (261 kcal mol^{-1}), while the interaction of the CO lone pairs with the empty p-orbital on aluminium is significantly weaker (25 kcal mol^{-1}). The corresponding deformation density plots are shown in Figure 6.5. For comparison an ETS-NOCV analysis of the bonding of CO to a cationic borole, in which CO acts primarily as a σ-donor ligand, estimates the back-bonding interaction as 26 kcal mol^{-1} and the σ-donor interaction as 106 kcal mol^{-1}. It is therefore concluded that in **6.I2'** the two CO molecules primarily act as rare examples of Z-type ligand.

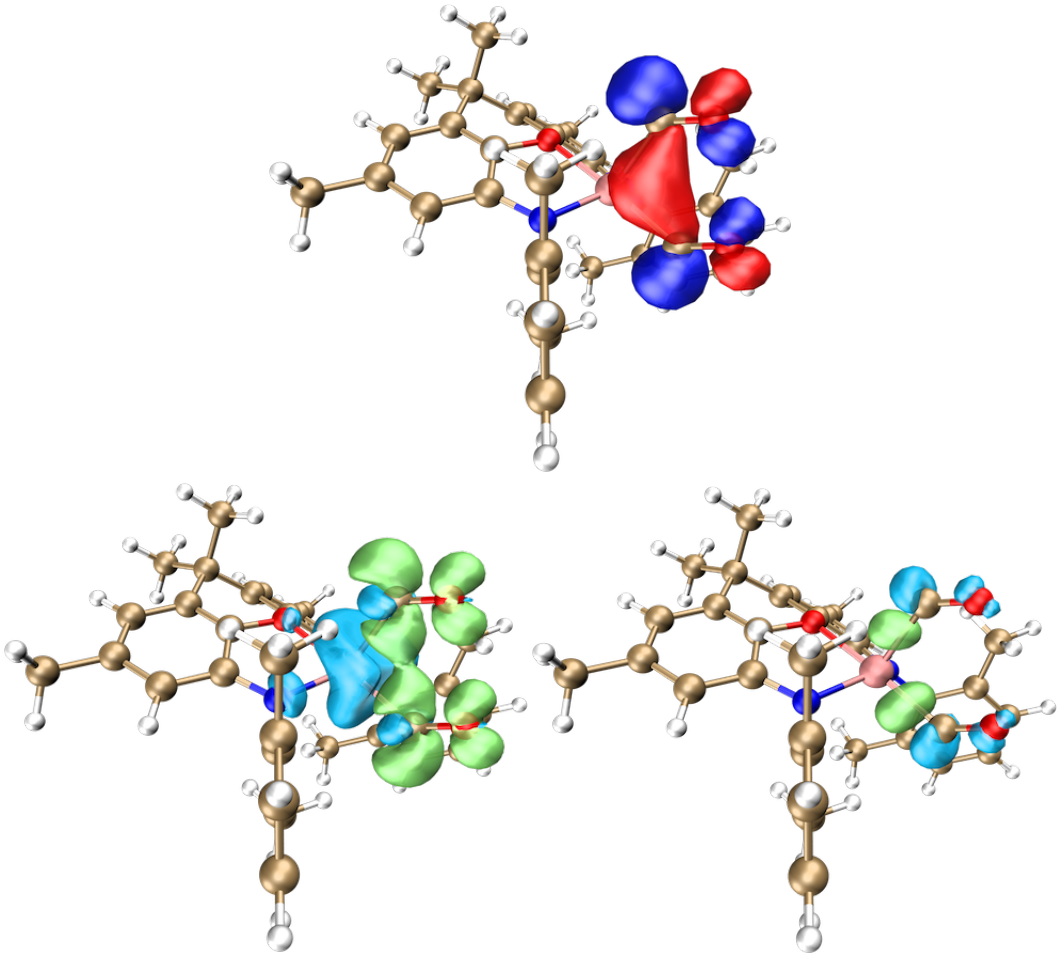

Figure 6.5: HOMO of **6.I2'** (shading denotes phasing of the wavefunction) (top) and deformation densities for the dominant orbital interactions as determined by ETS-NOCV (shading denotes deformation densities: blue/green – depletion/enhancement of electron density) (bottom).

Conversion of **6.I2'** to **6.I2** likely occurs via dissociation of one CO molecule and binding as an isocarbonyl in a bent fashion. **6.I2** subsequently forms carbene intermediate **6.I3**, which can dimerise to give the observed product **6.P**. The barrier for dimerisation is rate determining, and relatively high, presumably due to the omission of the counter-ions, and hence effectively constituting the combination of two anionic fragments. Alternatively, the promotion of **6.I3** to a triplet state was considered. The singlet-triplet gap for this carbene was found to be 1.74 eV (40.1 kcal mol^{-1}) which corresponds to the energy of a photon in the red range of the visible spectrum. Thus the triplet state can feasibly be accessed, when exposed to ambient light. When the combination of two triplet state carbene fragments is considered, **6.TS4** is lowered to $\Delta G^{\ddagger}$ = 26 kcal mol^{-1} (B3LYP/def2-SVP). Thus the involvement of the triplet state seems feasible.

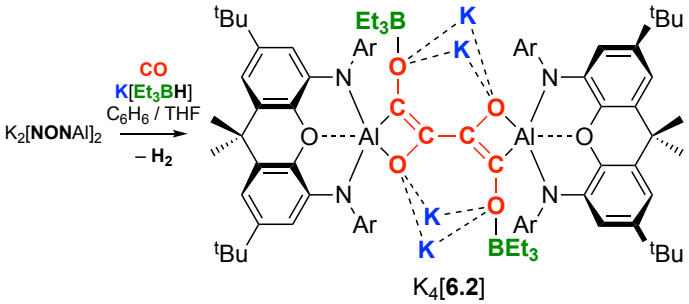

Scheme 6.4: Synthesis of K_4[**6.2**].

In an attempt to gather evidence for the involvement of (di)radical species, the reaction of K_2[**NON**Al]$_2$ with CO was investigated in the presence of trapping reagents. Carrying out the CO reduction in the presence of Et_3SiH, or via sequential addition of CO and H_2 to a solution of K_2[**NON**Al]$_2$ did not lead to the formation of alternative products. However reacting a benzene solution of aluminyl sequentially with CO and a solution of K[Et_3BH] in THF leads to the evolution of H_2 as judged by ^{1}H NMR spectroscopy over the course of 1 day. Upon standing for 2 weeks at room temperature, crystals of a new species were observed. Single crystal X-ray diffraction reveals the formation of the more highly reduced species K_4[(**NON**Al)$_2$(C_4O_4)(BEt_3)$_2$], K_4[**6.2**] (Scheme 6.4).

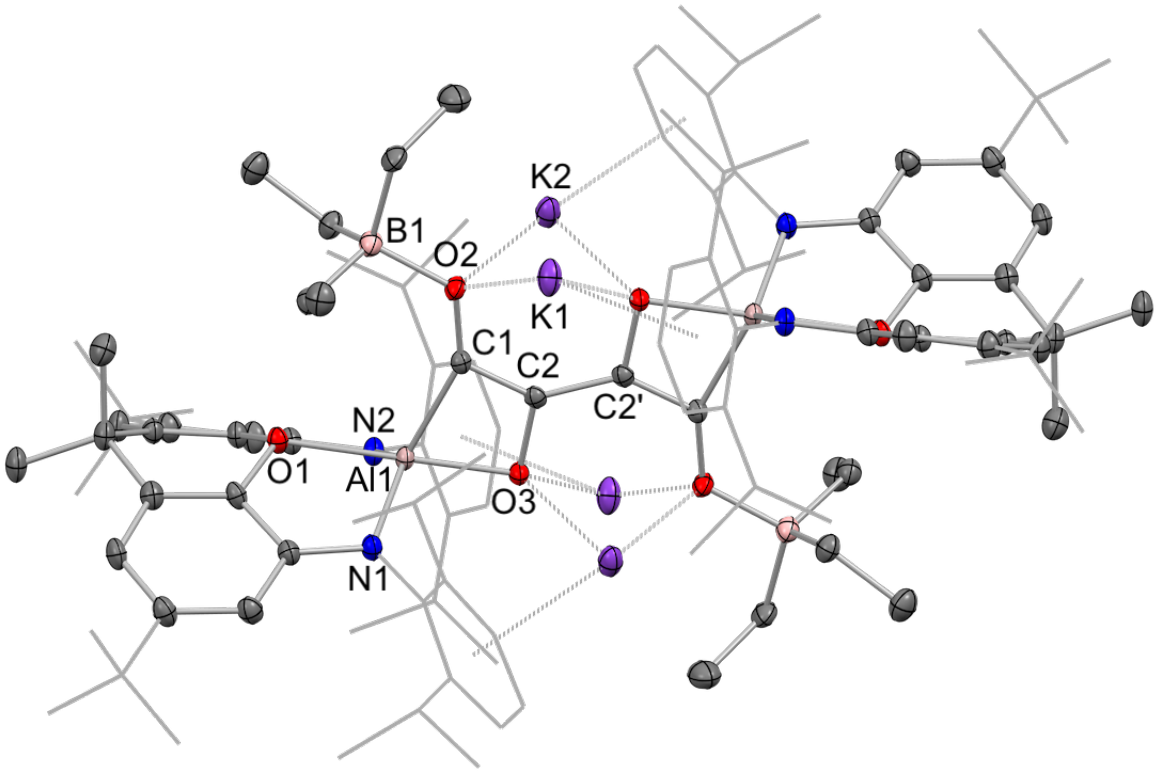

Figure 6.6: Molecular structure of K_4[**6.2**] as determined by X-ray crystallography. Thermal ellipsoids drawn at 30% probability, H atoms omitted, and selected groups shown in wireframe format for clarity. Key bond lengths (Å): Al1–C1 2.008(3), Al1–O3 1.8741(18), C1–C2 1.378(3), C2–C2' 1.481(5), C1–O2 1.382(3), C2–O3 1.440(3).

In the solid state K_4**[6.2]** adopts a centrosymmetric structure similar to that of $[K(C_7H_8)]_2$[**6.1**]. The structure however incorporates a total of four K^+ counter-ions, each coordinated to two oxygen atoms and one flanking Dipp group. Furthermore, O2 (and O2') are coordinated by BEt_3 groups. Charge balance suggests that the $[C_4O_4]^{6-}$ fragment has been formed, featuring a 6– charge. This is reflected in the key bond length of this fragment. The C–O bond lengths fall in the range of single bonds (1.382(3), 1.440(3) Å), the C1–C2 bond length (1.378(3) Å) is consistent with a double bond, while the central C2–C2' bond (1.481(5) Å) falls in the range of a single bond.

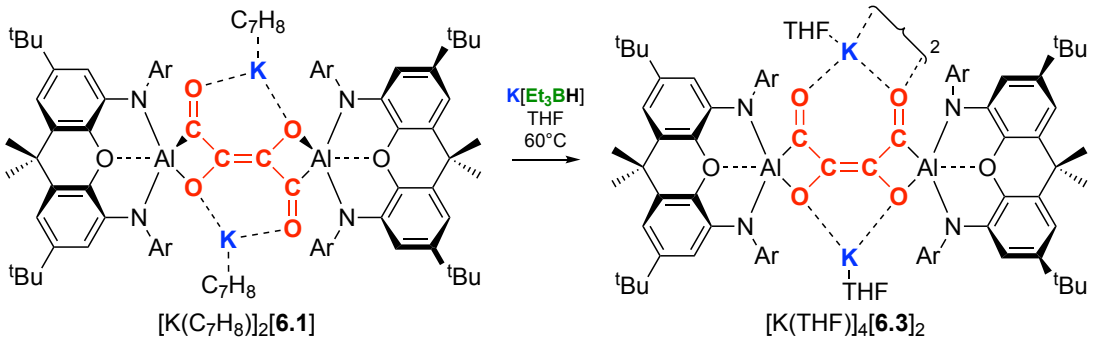

Scheme 6.5: Synthesis of [K(THF)]$_4$[**6.3**]$_2$.

Attempts to react *isolated* samples of [K(C$_7$H$_8$)]$_2$[**6.1**] with K[Et$_3$BH] in THF at room were unsuccessful. Upon heating at 62 °C for two weeks, slow conversion to one major **NON**-containing product is observed by ^{1}H NMR spectroscopy and retention of the [Et$_3$BH]$^-$ ion. From this reaction mixture, a large amount of dichroic crystals were obtained. Single X-ray diffraction reveals to product to be [K(THF)]$_4$[**6.3**]$_2$ (Scheme 6.5). Heating THF solutions of [K(C$_7$H$_8$)]$_2$[**6.1**] in the absence of K[Et$_3$BH], did not lead to an observable reaction.

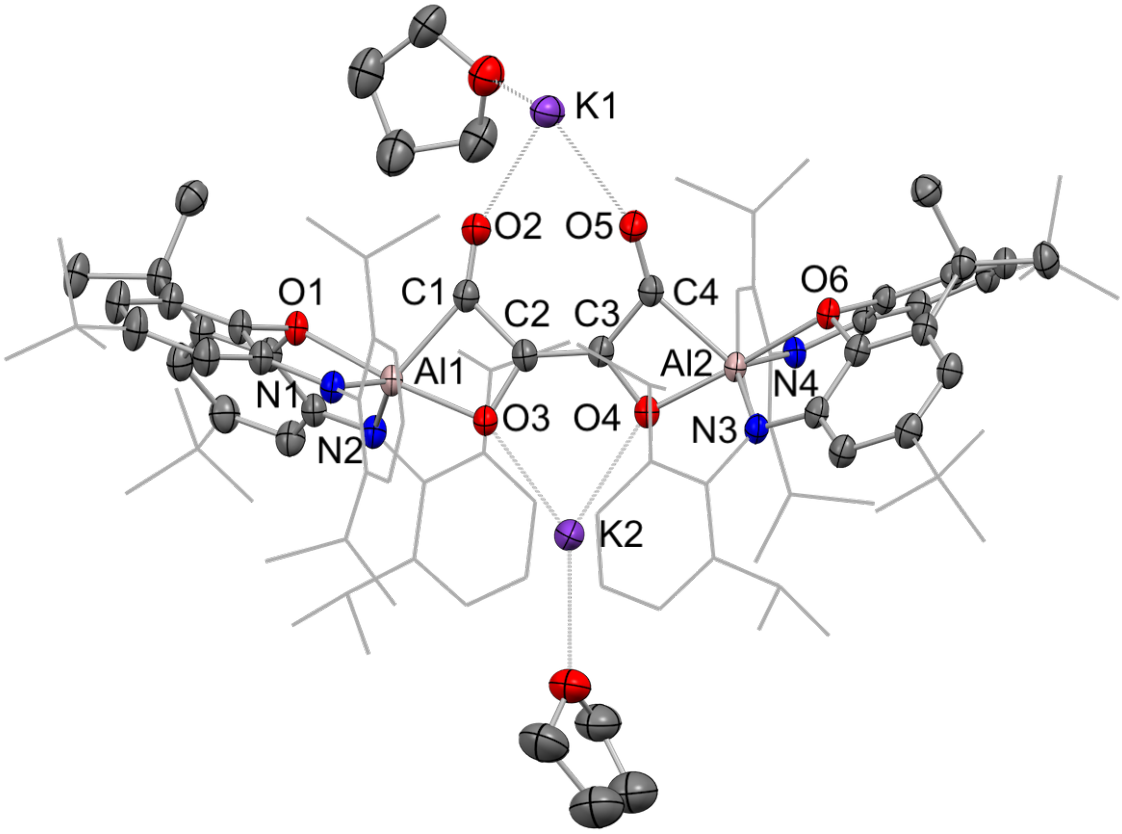

Figure 6.7: Molecular structure of [K(THF)]$_4$[**6.3**]$_2$ as determined by X-ray crystallography. One half of the dimer is shown. Thermal ellipsoids drawn at 30% probability, H atoms omitted, and selected groups shown in wireframe format for clarity. Key bond lengths (Å): Al1–C1 2.041(3), Al2–C4 2.053(3), Al1–O3 1.8721(18), Al2–O4 1.8603(17), C1–C2

1.525(4), C2–C3 1.376(3), C3–C4 1.489(4), C1–O2 1.213(4), C2–O3 1.373(3), C3–O4 1.381(3), C4–O5 1.247(3).

In the solid state [K(THF)]$_4$[**6.3**]$_2$ adopts a centrosymmetric, dimeric structure. Two monomeric units each comprising two aluminium centres and a $[C_4O_4]^{4-}$ fragment dimerise via bridging K^+ counter-ions. As in the case of [K(C$_7$H$_8$)]$_2$[**6.1**], the outer C–C bond lengths (1.525(4), 1.489(4) Å) of the $[C_4O_4]^{4-}$ fragment fall in the range of single bonds, while the C2–C3 bond lengths (1.376(3) Å) is consistent with a double bond. Similarly, the outer C–O bond lengths fall in the range of double bonds (1.213(4), 1.247(3) Å), while the inner C–O bond lengths are indicative of single bonds (1.373(3), 1.381(3) Å). Unlike for [K(C$_7$H$_8$)]$_2$[**6.1**] however, the $[C_4O_4]^{4-}$ fragment is not completely planar, and the central C–C bond adopts a *cis*-configuration. Presumably this isomerisation, and distortion of the $[C_4O_4]^{4-}$ from planarity is driven by the formation of new potassium–oxygen interactions.

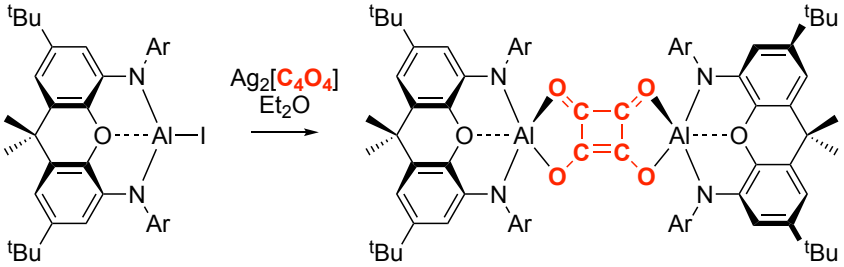

Scheme 6.6: Synthesis of **6.4**.

Having achieved the 4- and 6-electron reduction of four CO molecules, an analogous compound featuring a squarate ($[C_4O_4]^{2-}$) fragment was targeted. Attempts to synthesise such a compound from CO were unsuccessful. Reactions of aluminium(II) compound [**NON**Al]$_2$ with CO did not lead to the incorporation of CO into the final product. Similarly attempts to reduce **NON**AlI over sodium under an atmosphere of CO, only lead to the formation of [**NON**Al]$_2$. Therefore the metathesis reaction between **NON**AlI and silver squarate, $Ag_2[C_4O_4]$, was investigated. This reaction leads to the formation of **6.4**, and crystals suitable for single crystal X-ray diffraction could be obtained from benzene.

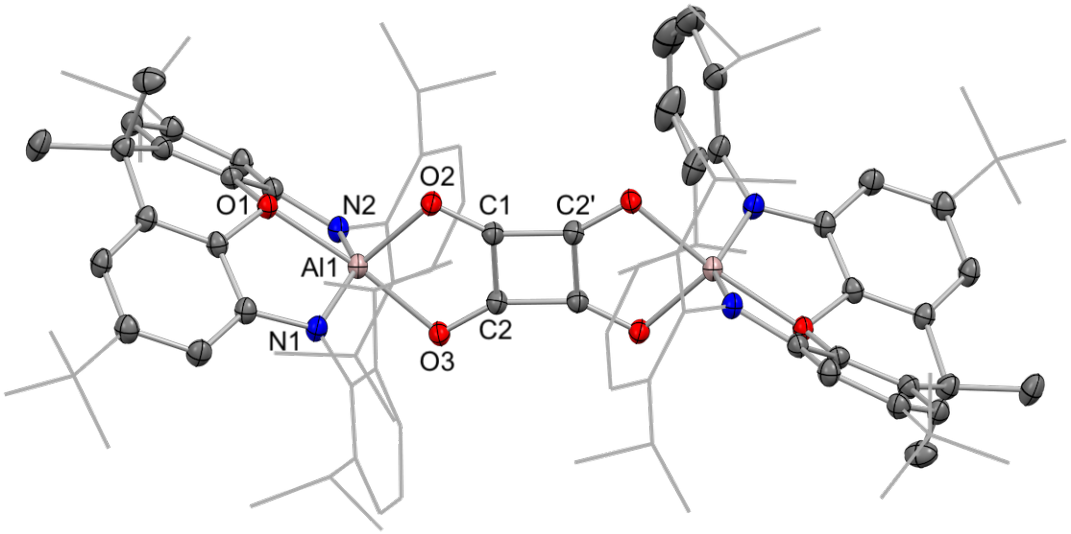

Figure 6.8: Molecular structure of **6.4** as determined by X-ray crystallography. Thermal ellipsoids drawn at 30% probability, H atoms omitted, and selected groups shown in wireframe format for clarity. Key bond lengths (Å): Al1–O2 1.9324(10), Al1–O3 1.9941(10), C1–C2 1.4379(18), C1–C2' 1.4614(18), C1–O2 1.2646(17), C2–O3 1.2575(17).

In the solid state **6.4** adopts a centrosymmetric structure. The cyclic $[C_4O_4]^{2-}$ squarate ion is planar, and bound to each aluminium centres via two oxygen atoms. The C–O bond lengths and C–C bond lengths fall between the values expected for single and double bonds, and are indicative of a high degree of delocalisation within the squarate unit.

With the molecular structures of compounds containing the $[C_4O_4]^{n-}$ (n = 2, 4, 6) in hand their electronic structures were investigated in collaboration with Agamemnon Crumpton. Selected molecular orbitals are shown in Figure 6.9.

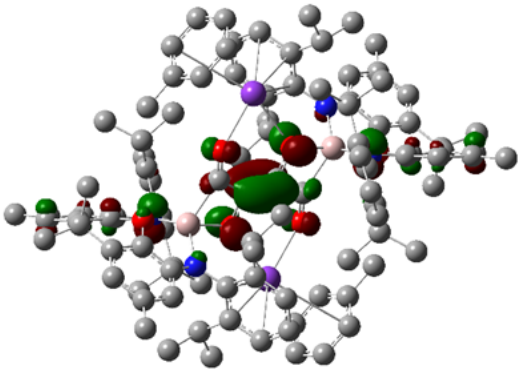

[K(C7H8)]2[**6.1**] HOMO-1

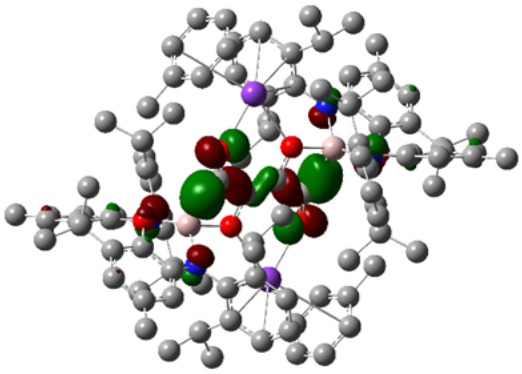

[K(C7H8)]2[**6.1**] HOMO

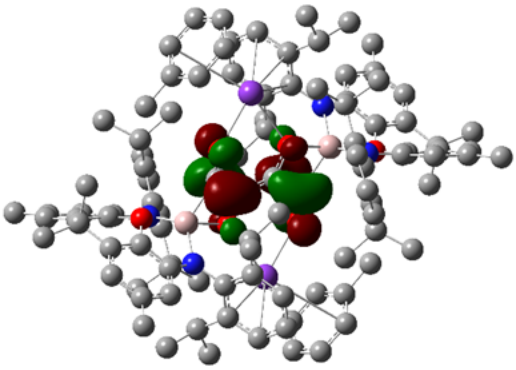

[K(C7H8)]2[**6.1**] LUMO

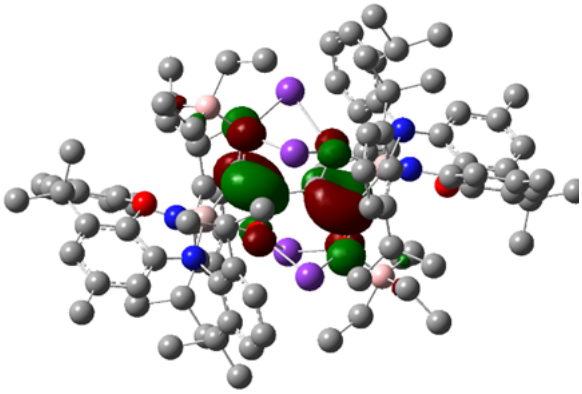

K4[**6.2**] HOMO

Figure 6.9: Selected molecular orbitals: [K(C7H8)]2[**6.1**] HOMO-1 (top left), HOMO (top right), LUMO (bottom left) and K4[**6.2**] HOMO (bottom right).

For [K(C7H8)]2[**6.1**] the HOMO corresponds to the in-phase combination of in-plane CO π* orbitals of the outer CO units, which possesses Al–C and C–C bonding character. The HOMO-1 corresponds to the in phase combination of out-of-plane CO π* orbitals of the central CO units. This orbital possesses C–C π-bonding character and C–O π-antibonding character. The LUMO involves the out-of-plane π-orbitals of all CO units, and possesses π-bonding character for the outer C–C bonds, and π-antibonding character for the central C–C bond, as well as all C–O bonds. Thus it is expected that the 2-electron reduction of [K(C7H8)]2[**6.1**], i.e. the filling of the LUMO would lead to a $[C_4O_4]^{6-}$ fragment with a bond distribution analogous to that observed for K4[**6.2**]. Indeed the HOMO of K4[**6.2**] is found to have the same morphology as the LUMO

of $[K(C_7H_8)]_2$[**6.1**]. Furthermore, the possibility of a 2-electron oxidation was assessed, i.e. formation of [**6.1**]$^{+0}$. In line with the depopulation of the HOMO, [**6.1**]$^{+0}$ was found to not correspond to a minimum on the potential energy surface, and instead optimisation of the structure leads to formation of an ethynediolate, which the molecules of CO coordinated to aluminium. The enthalpy of formation of which was found to be ca 11 kcal mol^{-1} higher than that of **6.4**. For completeness the enthalpy of formation was also computed for a hypothetical reduction product of the squarate, K_2[**6.4**]. This was found to be ca. 51 kcal mol^{-1} higher, compared to that of $[K(C_7H_8)]_2$[**6.1**].

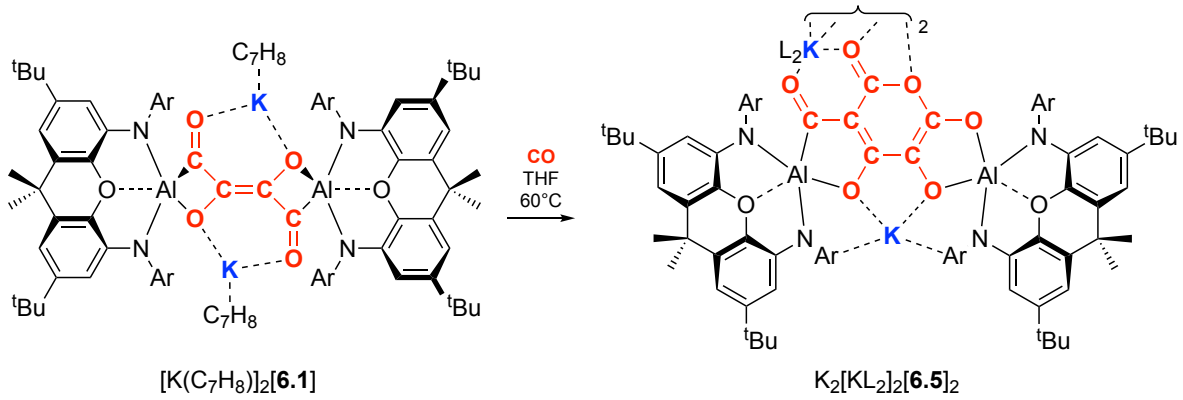

Scheme 6.7: Synthesis of $K_2[K(THF)]_2$[**6.5**]$_2$.

In an attempt to obtain higher C–C homologues, more forcing conditions were employed. While the reaction of K_2[**NON**Al]$_2$ with 2.5 bar CO or at 80 °C ultimately did not lead to separable products, the reaction of isolated samples of $[K(C_7H_8)]_2$[**6.1**] and CO (2 bar, 7 equiv. per aluminium) in THF at 66 °C led to the formation the quantitative conversion to a single new species over the course of 4 days as judged by ^{1}H NMR spectroscopy. From this mixture crystals of the product suitable for single crystal X-ray diffraction could be obtained upon concentration of the solution. The structure thus obtains reveals formation of $K_2[K(THF)_2]_2$[**6.5**]$_2$. Better quality crystals are obtained upon recrystallisation from Et_2O, affording $K_2[K(Et_2O)_2]_2$[**6.5**]$_2$.

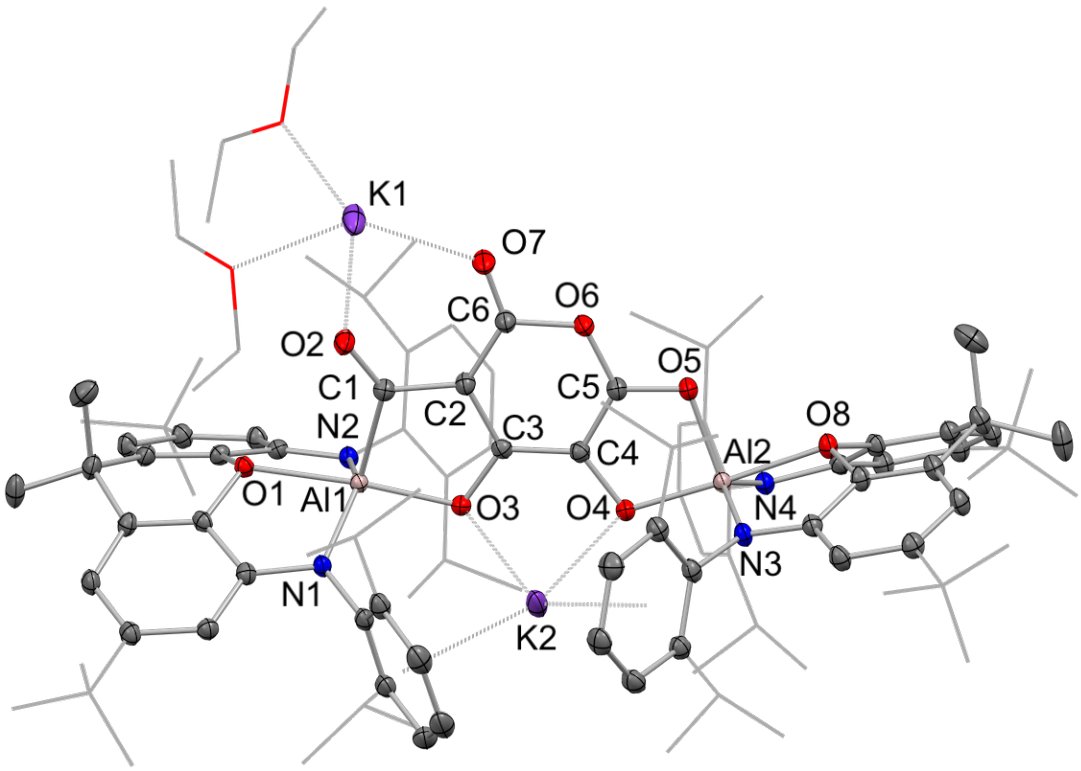

Figure 6.10: Molecular structure of $K_2[K(OEt_2)]_2$[**6.5**]$_2$ as determined by X-ray crystallography. Thermal ellipsoids drawn at 30% probability, H atoms omitted, and selected groups shown in wireframe format for clarity. Key bond lengths (Å): Al1–C1 2.018(2), Al–O3 1.8955(15), Al2–O4 1.8456(14), Al2–O5 1.8509(16), C1–C2 1.471(3), C2–C3 1.436(3), C3–C4 1.412(3), C4–C5 1.383(3), C2–C6 1.411(3), C1–O2 1.243(3), C3–O3 1.329(2), C4–O4 1.370(2), C5–O5 1.292(2), C5–O6 1.343(3), C6–O6 1.421(2), C6–O7 1.220(3).

In the solid state $K_2[K(Et_2O)_2]_2$[**6.5**]$_2$ adopts a dimeric structure. Two monomeric units each comprising two aluminium centres and a $[C_6O_6]^{4-}$ fragment dimerise via bridging potassium counter-ions. The $[C_6O_6]^{4-}$ fragment features a mono-branched six-carbon chain with a pyran core. C2 is only bonded to other carbon atoms, implying that formation of the $[C_6O_6]^{4-}$ fragment proceeds via cleavage of a robust C–O bond. While the formation of homologation products featuring linear or cyclic carbon chains is well established, the formation of branched carbon chains in a homologation reaction, in the absence of additional reagents is, to the best of our knowledge, unprecedented.

6.3 Conclusions

The work presented in this chapter describes the CO homologation chemistry of aluminyl reagents. The reactions of K_2[**NON**Al]$_2$ with CO led to the four electron reduction of CO to

afford K_2[**6.1**], while under more reducing conditions a six-electron reduction can be achieved, leading to the formation of K_4[**6.2**]. Isolated samples of K_2[**6.1**] undergo (i) chain growth to afford K_2[**6.5**], bringing about chain branching via C–O bond cleavage in a homogeneous system for the first time in the absence of additional reagents; or (ii) thermal isomerisation in the presence of excess potassium, yielding K_2[**6.3**]. Use of either monomeric [Li(OEt_2)$_2$][**NON**Al] or dimeric K_2[**NON**Al]$_2$ aluminyl reagents led to the formation of M_2[**6.1**] (M = Li, K), suggesting that M_2[**6.1**] is formed via dimerisation of two carbene fragments. This hypothesis is confirmed computationally, and is found to be the rate determining step. Furthermore, the initial interactions of the aluminyl reagents with CO proceed via an usual coordination mode in which CO acts primarily as a Z-type ligand.

6.4 Experimental details

[K(C_7H_8)]$_2$[6.1], [K(C_7H_8)]$_2$[(NONAl)$_2C_4O_4$]

To a 25 mL reaction bomb was added K_2[**NON**Al]$_2$ (250 mg, 0.34 mmol) and benzene (7.5 mL). The resulting mixture was degassed twice using the freeze-pump-thaw method, and sealed under vacuum. The bomb was then warmed to 34 °C in an oil bath, and after a few minutes the headspace was charged with CO (1.5 bar, ca 1.2 mmol). After sealing the vessel, the mixture was vigorously shaken for 30 s, and subsequently allowed to stand undisturbed at 34 °C for 16 h, leading to the formation of small orange crystals of the product. The supernatant was decanted and the crystal were regrown from toluene. Yield 37 mg, 10%. Anal. Calc. for $C_{98}H_{124}Al_2K_2N_4O_6$ + 1.5 toluene (%): C 75.57, H 7.95, N 3.25; found: C 75.52, H 8.04, N 3.22. ^{1}H NMR (400 MHz, THF-d_8): δ 0.43 (d, $^3J_{HH}$ = 6.8 Hz, 6H, CH(CH_3)$_2$), 0.68 (d, $^3J_{HH}$ = 6.8 Hz, 6H, CH(CH_3)$_2$), 0.86 (d, $^3J_{HH}$ = 6.8 Hz, 6H, CH(CH_3)$_2$), 1.04 (s, 18H, C(CH_3)$_3$), 1.11 (d, $^3J_{HH}$ = 6.8 Hz, 6H, CH(CH_3)$_2$), 1.56 (s, 3H, C(CH_3)$_2$), 1.73 (s, 3H, C(CH_3)$_2$), 3.14 – 3.30 (m, 4H, C*H*Me$_2$), 5.62 (d, $^4J_{HH}$ = 1.9 Hz, 2H, XA-C*H*), 6.42 (d, $^4J_{HH}$ = 1.9 Hz, 2H, XA-C*H*), 6.95 – 7.07 (m, 6H, Dipp-Ar-C*H*).

^{13}C NMR (126 MHz, THF-d$_8$): δ 23.8 (C(*C*H$_3$)$_2$), 24.5 (CH(*C*H$_3$)$_2$), 24.7 (CH(*C*H$_3$)$_2$), 25.5 (CH(*C*H$_3$)$_2$), 26.3 (CH(*C*H$_3$)$_2$), 28.5 (*C*H(CH$_3$)$_2$), 29.1 (*C*H(CH$_3$)$_2$), 32.2 (C(*C*H$_3$)$_3$), 32.6 (C(*C*H$_3$)$_2$), 35.5 (*C*Me$_3$), 37.9 (*C*CMe$_2$), 105.3 (XA-*C*H), 111.0 (XA-*C*H), 123.6 (Dipp-*m*-*C*H), 125.2 (Dipp-Ar-*C*H), 125.4 (Dipp-Ar-*C*H), 133.8 (*C*CMe$_2$), 131.3 (C(=O)*C*O), 129.2 (C$_6$H$_6$), 142.5 (XA-*C*O), 144.8 (Dipp-*i*-*C*), 146.8 (XA-*C*N), 147.6 (Dipp-*o*-*C*), 147.8 (*C*^{t}Bu), 148.2 (Dipp-*o*-*C*).

[K(12-c-4)]$_2$[6.1], [K(12-c-4)]$_2$[(NONAl)$_2$C$_4$O$_4$]

Method 1: To a suspension of [K(C$_6$H$_6$)]$_2$[(**NON**Al)$_2$(C$_4$O$_4$)] (15 mg, 0.009 mmol) in C$_6$D$_6$ (0.5 ml) was added a solution of 12-crown-4 in toluene (0.18 ml, 0.1 M, 0.018 mmol, 2.05 equiv.) and the reaction heated at 85 °C for 2 h. Volatiles were under vacuum and the product was obtained as an orange powder. Yield 13 mg, 80 % (quantitative by NMR). Method 2: To a solution of K$_2$[**NON**Al]$_2$ (120 mg, 0.163 mmol) in toluene (5 mL) was added a solution of 12-crown-4 in toluene (3.2 mL, 0.1M, 0.320 mmol). The resulting red solution was stirred at room temperature for 5 minutes, before addition of Fe(CO)$_5$ (22 μL, 0.161 mmol). The resulting dark red solution was stirred overnight. ^{1}H NMR spectroscopy shows complete conversion to two new products, of which the minor is [K(12-c-4)]$_2$[**6.1**]. Removal of volatiles yields a yellow oil which can be dissolved in minimal benzene and stored at room temperature overnight to yield single crystals suitable for X-ray crystallography. Yield >5 mg, (24% by NMR)

^{1}H NMR (600 MHz, THF-d$_8$): δ 0.33 (d, $^3J_{HH}$ = 6.8 Hz, 6H, CH(C*H*$_3$)$_2$), 0.77 (d, $^3J_{HH}$ = 6.8 Hz, 6H, CH(C*H*$_3$)$_2$), 0.79 (d, $^3J_{HH}$ = 6.8 Hz, 6H, CH(C*H*$_3$)$_2$), 1.03 (s, 18H, C(C*H*$_3$)$_3$), 1.24 (d, $^3J_{HH}$ = 6.7 Hz, 6H, CH(C*H*$_3$)$_2$), 1.58 (s, 3H, C(C*H*$_3$)$_2$), 1.73 (s, 3H, C(C*H*$_3$)$_2$), 3.14 (sept, $^3J_{HH}$ = 6.9 Hz, 2H, C*H*Me$_2$), 3.34 – 3.42 (m, 2H, C*H*Me$_2$), 3.60 (s, 16H, 12-crown-4), 5.59 (d, $^4J_{HH}$ = 1.9 Hz, 2H, XA-C*H*), 6.40 (d, $^4J_{HH}$ = 2.0 Hz, 2H, XA-C*H*), 6.96 (d, $^3J_{HH}$ = 7.0 Hz, 4H, Dipp-*m*-C*H*), 7.01 (t, $^3J_{HH}$ = 7.0 Hz, 2H, Dipp-*p*-C*H*).

^{13}C NMR (151 MHz, THF-d_8): δ 23.6 (C(*C*H$_3$)$_2$), 24.3 (CH(*C*H$_3$)$_2$), 24.6 (CH(*C*H$_3$)$_2$), 25.0 (CH(*C*H$_3$)$_2$), 26.5 (CH(*C*H$_3$)$_2$), 28.7 (*C*HMe$_2$), 29.4 (*C*HMe$_2$), 32.0 (C(*C*H$_3$)$_2$), 32.2 (C(*C*H$_3$)$_3$), 35.4 (*C*(CH$_3$)$_3$), 37.8 (*C*Me$_2$), 70.5 (O*C*H$_2$), 105.3 (XA-*C*H), 111.4 (XA-*C*H), 123.1 (Dipp-*m*-*C*H), 125.1 (Dipp-*p*-*C*H), 125.9 (Dipp-*m*-*C*H), 130.8 (C(=O)*C*O), 134.1 (*C*CMe$_2$), 142.7 (XA-*C*O), 145.2 (Dipp-*i*-*C*), 146.9 (XA-*C*N), 147.4 (*C*^{t}Bu), 147.5 (Dipp-*o*-*C*), 147.7 (Dipp-*o*-*C*), 296.2 (Al*C*O).

[Li(OEt$_2$)]$_2$[6.1], [Li(OEt$_2$)]$_2$[6.1]$_2$[(NONAl)$_2$C$_4$O$_4$]

Method 1: A solution of [Li(OEt$_2$)$_2$][**NON**Al] (15 mg, 0.017 mmol) in C_6D_6 (0.5 mL) was exposed to CO (2 bar) and briefly shaken. ^{1}H NMR spectroscopy reveals the formation of a mixture of products, including [Li(OEt$_2$)]$_2$[**6.1**] in ca. 40% yield. Upon concentration (to ca. 1/3 volume) and standing for 2 days, X-ray quality crystals of [Li(OEt$_2$)]$_2$[**6.1**] formed. Method 2: [K(C$_7$H$_8$)][**6.1**] (30 mg, 0.018 mmol) and LiI (5 mg, 2.1 equiv) were dissolved in Et$_2$O (15 mL) and briefly warmed to 318 K in a sealed ampoule, leading to a colour change from orange to yellow. Upon cooling to room temperature the mixture was filtered onto benzene (8 mL), and subsequently concentrated to ca. 5 mL. At this point, a sample (0.2 mL) was diluted with C_6D_6 (0.3 mL), and a ^{1}H NMR spectrum was measured. The resulting spectrum shows the presence of a single species, which has the same spectroscopic signals as those obtained using method 1 in a J. Young's NMR tube. ^{1}H NMR (400 MHz, C_6D_6): δ 0.36 (d, $^3J_{HH}$ = 6.9 Hz, 6H, CH(C*H*$_3$)$_2$), 1.19 (s, 18H, C(C*H*$_3$)$_3$), 1.52 (d, $^3J_{HH}$ = 6.9 Hz, 6H, CH(C*H*$_3$)$_2$), 1.61 (s, 3H, C(C*H*$_3$)$_2$), 1.70 (s, 3H, C(C*H*$_3$)$_2$), 3.72 (sept, $^3J_{HH}$ = 6.9 Hz, 2H), 6.00 (d, $^4J_{HH}$ = 2.0 Hz, 2H, XA-C*H*), 6.67 (d, $^4J_{HH}$ = 2.0 Hz, 2H, XA-C*H*).Samples of [Li(OEt$_2$)]$_2$[**6.1**] lose Et$_2$O under continuous vacuum. Dissolution in THF-d_8, however, yields spectroscopic signals indistinguishable from samples of [Li(OEt$_2$)]$_2$[**6.1**] prepared as set out below.

[Li(THF)]$_2$[6.1], [Li(THF)]$_2$[6.1]$_2$[(NONAl)$_2$C$_4$O$_4$]

A solution containing [K(C$_6$H$_6$)]$_2$[(**NON**Al)$_2$(C$_4$O$_4$)] (ca. 20 mg) was prepared as described above and Li[HBsBu3] (1 ml, 1M solution in THF) was added. The mixture was heated at 34 °C for 16 h affording small yellow crystals. Analytically pure samples were obtained by recrystalising from benzene or THF and washing with THF. Yield 7 mg, 30% over last step. Anal. Calc. (%) for: C$_{106}$H$_{140}$Al$_2$Li$_2$N$_4$O$_8$ + 1.74 THF: C 75.73, H 8.66, N 3.13; found: C 75.13, H 8.66, N 3.21.

^{1}H NMR (400 MHz, C$_6$D$_6$): δ 0.36 (d, $^3J_{HH}$ = 6.9 Hz, 6H, CH(C*H*$_3$)$_2$), 1.15 (overlapping d, $^3J_{HH}$ = 6.9 Hz, 12H, CH(C*H*$_3$)$_2$), 1.21 (s, 18H, C(C*H*$_3$)$_3$), 1.32 (m, 4H, THF), 1.58 (d, $^3J_{HH}$ = 6.9 Hz, 6H, CH(C*H*$_3$)$_2$), 1.60 (s, 3H, C(C*H*$_3$)$_2$), 1.69 (s, 3H, C(C*H*$_3$)$_2$), 3.41 (sept, $^3J_{HH}$ = 6.9 Hz, 2H, C*H*Me$_2$), 3.70 (s, m, 4H, THF), 3.77 (sept, $^3J_{HH}$ = 6.9 Hz, 2H, C*H*Me$_2$), 6.05 (d, $^4J_{HH}$ = 2.0 Hz, 2H, XA-C*H*), 6.70 (d, $^4J_{HH}$ = 2.0 Hz, 2H, XA-C*H*), 7.25 (m, 6H, Dipp-Ar-C*H*).

^{13}C NMR (151 MHz, C$_6$D$_6$): δ 23.2(CH(*C*H$_3$)$_2$), 23.2 (C(*C*H$_3$)$_2$), 23.9(CH(*C*H$_3$)$_2$), 24.1(CH(*C*H$_3$)$_2$), 25.4 (THF), 26.3 (CH(*C*H$_3$)$_2$), 28.2 (*C*HMe$_2$), 29.5 (*C*HMe$_2$), 31.9 (C(*C*H$_3$)$_3$), 32.1 (C(*C*H$_3$)$_2$), 35.0 (*C*Me$_3$), 37.0 (*C*Me$_2$), 68.6 (THF-*C*O), 106.4 (XA-*C*H), 111.3 (XA-*C*H), 123.0 (Dipp-*m*-*C*), 125.8 (Dipp-*p*-*C* and Dipp-*m*-*C*), 133.1 (*C*CMe$_2$), 141.4 (XA-*C*O), 143.6 (Dipp-*i*-*C*), 145.7 (XA-*C*^{4}), 146.3 (Dipp-*o*-*C*), 147.2 (Dipp-*o*-*C*), 147.8 (*C*^{t}Bu).

^{7}Li NMR (156 MHz, C$_6$D$_6$): δ = 0.61.

K$_4$[(NONAl)$_2$C$_4$O$_4$], K$_4$[6.2]

A solution containing [K(C$_6$H$_6$)]$_2$[**6.1**] was prepared from K$_2$[**NON**Al]$_2$ (220 mg, 0.3 mmol), benzene (6.6 ml), and CO (1.3 bar) in a 25 ml reaction bomb as described above. Upon standing overnight, K[HBEt$_3$] (1.5 ml, 1M in THF) as added. After 1 d, the solution was concentrated to a fifth of its original volume under reduced pressure. Upon prolonged standing colourless crystals of K$_4$[**6.2**] were obtained. Yield 12 mg, 4%.

^{1}H NMR (400 MHz, THF-d_8): δ 0.06 (q, $^{3}J_{HH}$ = 7.7 Hz, 6H, BCH_2CH$_3$), 0.57 (t, $^{3}J_{HH}$ = 7.7 Hz, 9H, BCH$_2$CH_3), 0.80 (d, $^{3}J_{HH}$ = 6.6 Hz, 13H), 1.00 (s, 18H, C(CH_3)$_3$), 1.28 (br s, 6H, CH(CH_3)$_2$), 1.68 (s, 6H, C(CH_3)$_2$), 3.47 (sept, $^{3}J_{HH}$ = 6.6 Hz, 2H, CHMe$_2$), 3.79 (br s, 2H, CHMe$_2$), 5.28 (s, 2H, XA-CH), 6.36 (br s, 2H, XA-CH), 7.27 (br s, 6H, Dipp-Ar-CH). The remaining 6H did not give rise to a crosspeaks in the COSY, HSQC or HMBC and could not be located unambiguously.

Due to the low solubility and stability of this compound in solution, no satisfactory ^{11}B and ^{13}C spectra could be obtained.

[K(THF)]$_4$[6.3]$_2$, [K(THF)]$_4$[6.3]$_2$

[K(C$_7$H$_8$)]$_2$[**6.1**] (26 mg) and K[HBEt$_3$] (6 mg, solid, 1.5 eq) were dissolved in THF (0.5 ml) and heated at 62 °C. After 2 weeks ^{1}H NMR spectroscopy reveals 70% conversion to [K(THF)]$_4$[**6.3**]$_2$. Concentration of this mixture to 0.05 mL leads to the formation of yellow-blue X-ray quality crystals of [K(THF)]$_4$[**6.3**]$_2$.

^{1}H NMR (400 MHz, THF-d_8): δ 0.71 (d, $^{3}J_{HH}$ = 7 Hz, 6H, CH(CH_3)$_2$), 0.87 (d, $^{3}J_{HH}$ = 6.1 Hz, 6H, CH(CH_3)$_2$), 1.02 (s, 18H, C(CH)$_3$), 1.09 (br s, 6H, CH(CH_3)$_2$), 1.56 (s, 3H, C(CH_3)$_2$), 1.68 (s, 3H, C(CH_3)$_2$), 3.11 (br s, 2H, CHMe$_2$), 3.45 (br s, 2H, CHMe$_2$), 5.51 (br, s, 2H, XA-CH), 6.39 (d, $^{4}J_{HH}$ = 1.9 Hz, 2H, XA-CH), 7.25 – 6.94 (m, 6H, Ar-H). The remaining 6H did not give rise to a crosspeak in the COSY and could not be located unambiguously.

(NONAl)$_2$C$_4$O$_4$, 6.4

NONAlI (500 mg, 0.60 mmol) and Ag$_2$(C$_4$O$_4$) (110 mg, 0.33 mmol) were suspended in Et$_2$O (10 mL) and refluxed at 35 °C for 48 h in the dark. Volatiles were removed and the reside extracted into toluene (15 ml), filtered, and layered with hexane (15 ml). Upon standing for several days, crystals suitable for single crystal X-ray diffraction were obtained. Yield 180 mg, 39%.

^{1}H NMR (400 MHz, C_6D_6): δ 0.83 – 0.91 (br s, 12H, CH(CH_3)$_2$), 1.06 (d, $^{3}J_{HH}$ = 6.8 Hz, 12H, CH(CH_3)$_2$), 1.15 (s, 18H, C(CH_3)$_3$), 1.58 (s, 6H, C(CH_3)$_2$), 3.54 (sept, $^{3}J_{HH}$ = 6.8 Hz, 4H, C*H*Me$_2$), 5.98 (d, $^{4}J_{HH}$ = 1.9 Hz, 2H, XA-C*H*), 6.72 (d, $^{4}J_{HH}$ = 1.9 Hz, 2H, XA-C*H*), 7.14 (m, 4H, Dipp-*p*-C*H*), 7.20 (m, 2H, Dipp-*p*-C*H*).

^{13}C NMR (126 MHz, C_6D_6): δ 24.7(CH(*C*H$_3$)$_2$), 25.4 (CH(*C*H$_3$)$_2$), 26.4 (br, C(*C*H$_3$)$_2$), 28.4 (*C*HMe$_2$), 31.7 (C(*C*H$_3$)$_3$), 35.1(*C*Me$_3$), 37.2 (*C*Me$_2$), 108.2 (XA-*C*^{1}H), 112.1 (XA-*C*^{3}H), 125.1 (Dipp-*m*-*C*), 127.0 (Dipp-*p*-*C*), 133.3 (*C*CMe$_2$), 141.0, 140.8 (Dipp-*i*-*C*, XA-*C*O), 144.4 (XA-*C*N), 147.0 (Dipp-*o*-*C*), 148.9 (*C*^{t}Bu), 194.0 (*C*$_4$O$_4$).

K$_2$[K(THF)$_2$]$_2$[6.2]$_2$, K$_2$[K(THF)$_2$]$_2$[(NONAl)$_2$C$_6$O$_6$]$_2$

[K(C_6H_6)][**6.1**] (25 mg, 0.015 mmol) was suspended in THF-d$_8$ (0.5 mL) in a J. Young's NMR tube (3.5 mL) and degassed twice using the freeze–pump–thaw method. The headspace was then charged with CO (2 atm) and subsequently heated at 66 °C K for 4 d. ^{1}H NMR spectroscopy monitoring shows quantitative conversion to a single product, K$_2$[K(THF)$_2$]$_2$[**6.2**]$_2$. After concentrating the solution to a quarter of its original, small pale orange plates formed at the surface of the solution. Anal. Calc. for $C_{108}H_{140}Al_2K_2N_4O_{10}$ + 2 THF (%): C 72.16; H, 8.14; N, 2.90; found: C, 72.13; H, 8.06; N, 2.55.

^{1}H NMR (600 MHz, THF-d$_8$): δ 0.51 (d, $^{3}J_{HH}$ = 6.8 Hz, 6H, CH(CH_3)$_2$), 0.68 (d, $^{3}J_{HH}$ = 6.8 Hz, 6H, CH(CH_3)$_2$), 0.73 (d, $^{3}J_{HH}$ = 6.7 Hz, 6H, CH(CH_3)$_2$), 0.80 (d, $^{3}J_{HH}$ = 6.7 Hz, 6H, CH(CH_3)$_2$), 0.83 (d, $^{3}J_{HH}$ = 6.8 Hz, 6H, CH(CH_3)$_2$), 0.87 (d, $^{3}J_{HH}$ = 6.7 Hz, 6H, CH(CH_3)$_2$), 0.95 (d, $^{3}J_{HH}$ = 6.9 Hz, 6H, CH(CH_3)$_2$), 1.00 (s, 18H, C(CH_3)$_3$), 1.03 (s, 18H, C(CH_3)$_3$), 1.20 (d, $^{3}J_{HH}$ = 7.0 Hz, 6H, CH(CH_3)$_2$), 1.54 (s, 3H, C(CH_3)$_2$), 1.57 (s, 3H, C(CH_3)$_2$), 1.73 (s, 3H, C(CH_3)$_2$), 1.75 (s, 3H, C(CH_3)$_2$), 3.16 (sept, $^{3}J_{HH}$ = 6.9 Hz, 2H, C*H*Me$_2$), 3.32 (sept, $^{3}J_{HH}$ = 7.2 Hz, 2H, C*H*Me$_2$), 3.36–3.46 (overlapping sept, 4H, C*H*Me$_2$), 5.34 (d, $^{4}J_{HH}$ = 1.9 Hz, 2H, XA-C*H*), 5.36 (d, $^{4}J_{HH}$ = 1.9 Hz, 2H, XA-C*H*), 6.42 (d, $^{4}J_{HH}$ = 1.9 Hz, 2H, XA-C*H*), 6.49 (d, $^{4}J_{HH}$ = 1.9 Hz, 2H, XA-C*H*), 7.00 (dd, $^{n}J_{HH}$ = 7.7, 1.6 Hz, 2H, Dipp-*m*-C*H*), 7.09 (dd, $^{n}J_{HH}$ = 7.8, 1.6 Hz, 2H, Dipp-*m*-

C*H*), 7.16 (dd, $^{n}J_{HH}$ = 7.6, 1.6 Hz, 2H, Dipp-*m*-C*H*), 7.25 (dd, $^{n}J_{HH}$ = 7.8, 1.6 Hz, 2H, Dipp-*m*-C*H*), 7.32 (t, $^{3}J_{HH}$ = 7.6 Hz, 2H, Dipp-*p*-C*H*), 7.43 (t, $^{3}J_{HH}$ = 7.6 Hz, 2H, Dipp-*p*-C*H*). ^{13}C NMR (151 MHz, THF-d_8): δ 22.9 (C(*C*H$_3$)$_2$), 22.9 (C(*C*H$_3$)$_2$), 24.9 (CH(*C*H$_3$)$_2$), 25.2 (CH(*C*H$_3$)$_2$), 25.3 (CH(*C*H$_3$)$_2$), 26.0 (CH(*C*H$_3$)$_2$), 26.1 (CH(*C*H$_3$)$_2$), 26.2 (CH(*C*H$_3$)$_2$), 28.0 (*C*HMe$_2$), 28.1 (*C*HMe$_2$), 28.8 (*C*HMe$_2$), 29.2 (*C*HMe$_2$), 32.0 (C(*C*H$_3$)$_2$), 32.1 (C(*C*H$_3$)$_2$), 32.1 (C(*C*H$_3$)$_3$), 32.2 (C(*C*H$_3$)$_3$), 35.4 (*C*Me$_3$), 35.5 (*C*Me$_3$), 37.8 (*C*Me$_2$), 37.9 (*C*Me$_2$), 105.9 (XA-*C*^{1}H), 106.5 (XA-*C*^{1}H), 110.5 (C_6O_6), 111.3 (XA-*C*^{3}H), 118.2 (C_6O_6), 123.8 (Dipp-*m*-*C*H), 124.4 (Dipp-*m*-*C*H), 126.2 (Dipp-*m*-*C*H), 127.2 (Dipp-*m*-*C*H), 127.3 (Dipp-*p*-*C*H), 127.4 (Dipp-*p*-*C*H), 133.3 (*C*CMe$_2$), 133.7 (*C*CMe$_2$), 141.5 (XA-*C*O), 145.6 (XA-*C*^{4}), 142.7 (XA-*C*O), 145.7 (Dipp-*i*-*C*), 145.8 (Dipp-*i*-*C*), 146.1 (XA-*C*^{4}), 147.3 (*C*^{t}Bu), 147.5 (Dipp-*o*-*C*), 147.6 (*C*^{t}Bu), 148.0 (Dipp-*o*-*C*), 149.1 (Dipp-*o*-*C*), 149.4 (Dipp-*o*-*C*), 156.2 (C_6O_6), 169.0 (C_6O_6), 173.5 (C_6O_6), 258.6 (C_6O_6).

6.5 References

[1] W. Zhou, K. Cheng, J. Kang, C. Zhou, V. Subramanian, Q. Zhang, Y. Wang, *Chem. Soc. Rev.*, **2019**, *48*, 3193–3228.
[2] H. Schulz, *Appl. Catal. A: Gen.*, **1999**, *186*, 3–12.
[3] S. S. Ail, S. Dasappa, *Renewable and Sustainable Energy Reviews*, **2016**, *58*, 267–286.
[4] A. J. Ragauskas, C. K. Williams, B. H. Davison, G. Britovsek, J. Cairney, C. A. Eckert, W. J. Frederick, J. P. Hallett, D. J. Leak, C. L. Liotta, J. R. Mielenz, R. Murphy, R. Templer, T. Tschaplinski, *Science*, **2006**, *311*, 484–489.
[5] J. Wei, Q. Ge, R. Yao, Z. Wen, C. Fang, L. Guo, H. Xu, J. Sun, *Nat. Commun.*, **2017**, *8*, 1–9.
[6] R. A. van Santen, I. M. Ciobîcâ, E. van Steen, M. M. Ghouri, *Adv. Catal.*, **2011**, *54*, 127–187.
[7] R. Li, R. Y. Kong, M. R. Crimmin, *Dalton Trans.*, **2020**, *49*, 16587–16597.
[8] M. D. Anker, M. S. Hill, J. P. Lowe, M. F. Mahon, *Angew. Chem. Int. Ed.*, **2015**, *54*, 10009–10011.
[9] R. Lalrempuia, C. E. Kefalidis, S. J. Bonyhady, B. Schwarze, L. Maron, A. Stasch, C. Jones, *J. Am. Chem. Soc.*, **2015**, *137*, 8944–8947.
[10] M. Xu, Z. W. Qu, S. Grimme, D. W. Stephan, *J. Am. Chem. Soc.*, **2021**, *143*, 634–638.
[11] J. M. Manriquez, D. R. McAlister, R. D. Sanner, J. E. Bercaw, *J. Am. Chem. Soc.*, **1978**, *100*, 2716–2724.
[12] C. C. Cummins, G. D. van Duyne, C. P. Schaller, P. T. Wolczanski, *Organometallics*, **1991**, *10*, 164–170.
[13] T. Watanabe, Y. Ishida, T. Matsuo, H. Kawaguchi, *J. Am. Chem. Soc.*, **2009**, *131*, 3474–3475.
[14] G. M. Ferrence, R. McDonald, J. Takats, *Angew. Chem. Int. Ed.*, **1999**, *38*, 2233–2237.
[15] P. J. Fagan, K. G. Moloy, T. J. Marks, *J. Am. Chem. Soc.*, **1981**, *103*, 6959–6962.

[16] P. J. Fagan, J. M. Manriquez, T. J. Marks, V. W. Day, S. H. Vollmer, C. S. Day, *J. Am. Chem. Soc.*, **1980**, *102*, 5393–5396.
[17] E. L. Werkema, L. Maron, O. Eisenstein, R. A. Andersen, *J. Am. Chem. Soc.*, **2007**, *129*, 2529–2541.
[18] W. J. Evans, A. L. Wayda, W. E. Hunter, J. L. Atwood, *J. Chem. Soc. Chem. Commun.*, **1981**, 706–708.
[19] N. S. Radu, M. P. Engeler, C. P. Gerlach, T. D. Tilley, A. L. Rheingold, *J. Am. Chem. Soc.*, **1995**, *117*, 3621–3622.
[20] A. Paparo, K. Yuvaraj, A. J. R. Matthews, I. Douair, L. Maron, C. Jones, *Angew. Chem. Int. Ed.*, **2021**, *60*, 630–634.
[21] K. Yuvaraj, I. Douair, D. D. L. Jones, L. Maron, C. Jones, *Chem. Sci.*, **2020**, *11*, 3516–3522.
[22] K. Yuvaraj, I. Douair, A. Paparo, L. Maron, C. Jones, *J. Am. Chem. Soc.*, **2019**, *141*, 8764–8768.
[23] X. Shi, C. Hou, C. Zhou, Y. Song, J. Cheng, *Angew. Chem. Int. Ed.*, **2017**, *56*, 16650–16653.
[24] K. Yuvaraj, C. Jones, *Chem. Commun.*, **2021**, *57*, 9224–9227.
[25] X. Wang, Z. Zhu, Y. Peng, H. Lei, J. C. Fettinger, P. P. Power, *J. Am. Chem. Soc.*, **2009**, *131*, 6912–6913.
[26] H. Braunschweig, T. Dellermann, R. D. Dewhurst, W. C. Ewing, K. Hammond, J. O. C. Jimenez-Halla, T. Kramer, I. Krummenacher, J. Mies, A. K. Phukan, A. Vargas, *Nat. Chem.*, **2013**, *5*, 1025–1028.
[27] M. Majumdar, I. Omlor, C. B. Yildiz, A. Azizoglu, V. Huch, D. Scheschkewitz, *Angew. Chem. Int. Ed.*, **2015**, *54*, 8746–8750.
[28] A. v. Protchenko, P. Vasko, D. C. H. Do, J. Hicks, M. Á. Fuentes, C. Jones, S. Aldridge, *Angew. Chem. Int. Ed.*, **2019**, *58*, 1808–1812.
[29] Y. Wang, A. Kostenko, T. J. Hadlington, M. P. Luecke, S. Yao, M. Driess, *J. Am. Chem. Soc.*, **2019**, *141*, 626–634.
[30] M. J. Evans, M. G. Gardiner, M. D. Anker, M. P. Coles, *Chem. Commun.*, **2022**, 58, 5833–6836.
[31] H. R. Sharpe, A. M. Geer, L. J. Taylor, B. M. Gridley, T. J. Blundell, A. J. Blake, E. S. Davies, W. Lewis, J. McMaster, D. Robinson, D. L. Kays, *Nat. Commun.*, **2018**, *9*, 3757.
[32] J. A. Buss, T. Agapie, *Nature*, **2016**, *529*, 72–75.
[33] B. B. Wayland, A. E. Sherry, V. L. Coffin, *J. Chem. Soc. Chem. Commun.*, **1989**, 662–663.
[34] J. D. Protasiewicz, S. J. Lippard, *J. Am. Chem. Soc.*, **1991**, *113*, 6564–6570.
[35] P. A. Bianconi, I. D. Williams, M. P. Engeler, S. J. Lippard, *J. Am. Chem. Soc.*, **1986**, *108*, 311–313.
[36] A. J. M. Miller, J. A. Labinger, J. E. Bercaw, *J. Am. Chem. Soc.*, **2008**, *130*, 11874–11875.
[37] R. N. Vrtis, C. P. Rao, S. G. Bott, S. J. Lippard, *J. Am. Chem. Soc.*, **1988**, *110*, 7564–7566.
[38] V. L. Coffin, W. Brennen, B. B. Wayland, *J. Am. Chem. Soc.*, **1988**, *110*, 6063–6069.
[39] W. J. Evans, J. W. Grate, L. A. Hughes, H. Zhang, J. L. Atwood, *J. Am. Chem. Soc.*, **1985**, *107*, 3728–3730.
[40] W. J. Evans, D. S. Lee, J. W. Ziller, N. Kaltsoyannis, *J. Am. Chem. Soc.*, **2006**, *128*, 14176–14184.
[41] P. L. Arnold, Z. R. Turner, R. M. Bellabarba, R. P. Tooze, *Chem. Sci.*, **2011**, *2*, 77–79.
[42] S. M. Mansell, N. Kaltsoyannis, P. L. Arnold, *J. Am. Chem. Soc.*, **2011**, *133*, 9036–9051.

[43] B. M. Gardner, J. C. Stewart, A. L. Davis, J. McMaster, W. Lewis, A. J. Blake, S. T. Liddle, *Proc. Natl. Acad. Sci. USA*, **2012**, *109*, 9265–9270.
[44] B. Wang, G. Luo, M. Nishiura, Y. Luo, Z. Hou, *J. Am. Chem. Soc.*, **2017**, *139*, 16967–16973.
[45] A. S. Frey, F. G. N. Cloke, P. B. Hitchcock, I. J. Day, J. C. Green, G. Aitken, *J. Am. Chem. Soc.*, **2008**, *130*, 13816–13817.
[46] O. T. Summerscales, F. G. N. Cloke, P. B. Hitchcock, J. C. Green, N. Hazari, *Science*, **2006**, *311*, 829–831.
[47] O. T. Summerscales, F. G. N. Cloke, P. B. Hitchcock, J. C. Green, N. Hazari, *J. Am. Chem. Soc.*, **2006**, *128*, 9602–9603.
[48] N. Tsoureas, O. T. Summerscales, F. G. N. Cloke, S. M. Roe, *Organometallics*, **2013**, *32*, 1353–1362.
[49] R. Y. Kong, M. R. Crimmin, *J. Am. Chem. Soc.*, **2018**, *140*, 13614–13617.
[50] R. Y. Kong, M. Batuecas, M. R. Crimmin, *Chem. Sci.*, **2021**, *12*, 14845–14854.
[51] M. Batuecas, R. Y. Kong, A. J. P. White, M. R. Crimmin, *Angew. Chem. Int. Ed.*, **2022**, *61*, e202202241.
[52] M. J. Evans, M. G. Gardiner, M. D. Anker, M. P. Coles, *Chem. Commun.*, **2022**, *58*, 5833–5836.
[53] C. Ganesamoorthy, J. Schoening, C. Wölper, L. Song, P. R. Schreiner, S. Schulz, *Nat. Chem.*, **2020**, *12*, 608–614.
[54] J. Schoening, C. Ganesamoorthy, C. Wölper, E. Solel, P. R. Schreiner, S. Schulz, *Dalton Trans.*, **2022**, *51*, 8249–8257.
[55] D. Reiter, R. Holzner, A. Porzelt, P. Frisch, S. Inoue, *Nat. Chem.*, **2020**, *12*, 1131–1135.

Conclusions

This thesis examines the reactivity of a range of terminal aluminium and gallium imides towards small molecules, as well as the reactions of aluminyl reagents towards CO.

The reactions of K_2[**NON**Al]$_2$ with sterically unencumbered organoazides leads to the formation of tetrazene complexes, K_2[**NON**Al(N_4R_2)]$_2$. By contrast, terminal aluminium and gallium imides could be synthesised from aluminyl and gallyl reagents by the use of more bulky organic azides. Single crystal X-ray diffraction experiments reveal very short aluminium–nitrogen bonds and DFT calculations show that the metal imide bonds are highly polarised, but possess only limited multiple bond character. Nonetheless their reactivity is reminiscent of multiply bonded species, undergoing hydrogenation reactions with H_2 and a number of 1,2-addition reactions.

K_2[**NON**Al(NDipp)]$_2$ reacts with CO_2 or benzaldehyde to initially afford isolable [2+2] cycloaddition products, K_2[**NON**Al(NDippCO_2)]$_2$ and K[**NON**Al(NDippOCHPh)]. Both species undergo further reaction with CO_2, ultimately yielding products such as carbonate K_2[**NON**Al(CO_3)]$_2$ or aminodicarboxylate [K(THF)$_2$][**NON**Al{$(O_2C)_2$NDipp}], as well as isocyanate DippNCO or imine PhC(H)NDipp. Mechanistically, the onwards reactions are proposed to proceed initially via further cycloaddition reactions to yield intermediates featuring six membered rings. Furthermore aluminium imides of this type are shown to react with N_2O to afford the *cis*-hyponitrite K_2[**NON**Al(ONNO)]$_2$ and the corresponding organoazide. Calculations suggest that this reaction proceeds via an initial [2+2] cycloaddition, and an aluminium oxide intermediate. By contrast, the analogous reaction of the gallium imide K[**NON**Ga($NSiPh_3$)] proceeds slowly at elevated temperatures, leading to the formation of azido complex K_2[**NON**Ga(N_3)($OSiPh_3$)]$_2$.

The reaction of K_2[**NON**Al(NDipp)]$_2$ with CO affords K_2[**NON**Al{C(=NDipp)CO_2}]$_2$, while the reactions of hetero-substituted imides lead to formation of complexes of the type

K_2[**NON**M(O_2CR)(CN)]$_2$ or K_2[**NON**M(OR)(CN)]$_2$ featuring a cyanide moiety, with the difference in reactivity thought to arise from the ability of silyl- and boryl- groups to migrate. Thus it has been shown that group 13 imides can act as transfer reagents for imido, $[NR]^{2-}$, or nitride $[N]^{3-}$ groups towards oxygenated unsaturated substrates, leading to the conversion of CO_2, N_2O, PhCHO, and CO to isocyanates, organic and inorganic azides, organic imines and cyanides (as well as other products), depending on conditions.

Finally the reactivity of aluminyl reagents towards CO was investigated. The reactions K_2[**NON**Al]$_2$ and [Li(OEt_2)$_2$][**NON**Al] with CO lead to the formation of mixture of products from which compounds of the type [M(L)]$_2$[(**NON**Al)$_2$(C_4O_4)] (M = K, Li; L = C_7H_8, Et_2O) could be isolated. The mechanism for the formation of the $[C_4O_4]^{4-}$ unit is proposed to proceed via sequential coordination of two CO molecules with in an unusual bent geometry. ETS-NOCV analysis reveals that in these intermediates CO primarily acts as a Z-type ligand. C–C coupling of two CO molecules leads to the formation of a carbene intermediate, whose dimerisation is the rate limiting step in this mechanism. When this reaction is carried out under more reducing conditions crystals of K_4[(**NON**Al)$_2$(C_4O_4)(BEt_3)$_2$] could be obtained, featuring a $[C_4O_4]^{6-}$ unit. Further isolated samples of [K(C_6H_6)]$_2$[(**NON**Al)$_2$(C_4O_4)] were shown to undergo chain growth with further equivalents of CO under more forcing conditions affording K_2[K(THF)]$_2$[(**NON**Al)$_2$(C_6O_6)]$_2$. The latter features the first example of a branched carbon chain obtained from a solution state homologation reaction of CO in the absence of additional reagents. Thus, the four- or six-electron reduction of CO and the formation of topologically linear or branched C_4 and C_6 chains has been demonstrated utilising aluminyl reagents.